Assessment of $CaCO_3$ surface deposition mechanisms and kinetics in low supersaturation environments.

By

Alagbalawura Eniola Fujah-Sanni

Submitted in accordance with the requirement for the degree of

Doctor of Philosophy

Institute of Functional Surfaces
School of Mechanical Engineering
University of Leeds, UK

February, 2023

The candidate confirms that the work submitted is her own, except where work which has formed part of jointly authored publications has been included. The contribution of the candidate and the other authors to this work has been explicitly indicated below. The candidate confirms that appropriate credit has been given within the thesis where reference has been made to the work of others.

In the papers contributed to this thesis, the candidate (first author) carried out all the experiments, analysis and preparation of the manuscripts. All other authors contributed by proof reading and providing insight on the discussions.

Acknowledgements

I would like to express my sincere appreciation to Professor Anne Neville, although she is no longer with us, she had a monumental impact to my study, she was always willing to go above and beyond her call of duty to ensure I achieved my optimum potential, words are not enough to express my gratitude to her.

I would also like to thank my academic supervisors, Professor Richard Barker, Professor Nik Kapur, Dr Olujide Sanni and Dr Thibaut Charpentier for their relentless support, guidance, patience and understanding throughout this journey, the completion of this work would not be possible without their support.

I want to appreciate my sponsors Hugh Bourne and Nikos Diamantonis, their outstanding advice, encouragement, understanding and motivation throughout the course of this study is invaluable. I am also grateful to bp for providing funding throughout the course of my research.

Very special thanks to the technical and administrative staff at the University of Leeds, Institute of Function Surfaces (iFS) for their support and assistance; Fiona Slade, Judith Schneider, Simon Lloyds, Tom, Mick, Ryan, Paul, and particularly Jordan for being incredibly patient and helpful through the 4-year duration of my study especially at the early stage of my research. I am thankful to the members of my research group for making the experience enjoyable and their willingness of offer help; Frederick, Kabir, Ogbemi, Yasmin, Amthal, Alex, Wang, Qingyang, Ryan, Frank, Joseph.

My deepest appreciation to my amazing Mother and my Father for their sacrifices, unconditional love, constant encouragement, prayers and guidance. I would also like to thank my siblings Damilola, Abimbola, and Oyinkan, my friends Sue, Stuart, Clementina, Fadzai, Nima, Dorothy, Getrude and Miriam. The members of TREM Leeds, and Gateway church; Kemi Ope, Aderonke, Fola, Ebere, John, Lesley, Anna for always praying for me and encouraging me when I had challenges.

May God bless you all.

All glory to God, I am what I am by the grace of God.

‘Fear not, for I am with you; be not dismayed, for I am your God. I will strengthen you, yes, I will help you, I will uphold you with My righteous right hand.’ – Isaiah 41:10

Abstract

Mineral scale formation is the deposition of unwanted materials on solid surfaces to the detriment of their function. Scale deposition can have a significant impact on operations. Scale restrictions can reduce flow capacity, hinder the correct operation of valves and other safety critical equipment. Removing this scale, which in some forms can be radioactive, and performing preventative treatments can run into tens of millions of dollars per well per event especially in subsea deep-water production.

Calcium carbonate ($CaCO_3$) scale is one of the most common mineral scaling types found in the oil and gas industry. $CaCO_3$ formation at low saturation ratio (SR) is particularly challenging because its deposition progresses slowly until triggering catastrophic event. A reliable scale prediction tool is crucial to reduce the uncertainties associated with scale prediction. This requires a suitable methodology for generating reproducible data on the kinetics of $CaCO_3$ deposition. The common techniques used for studying $CaCO_3$ deposition such as the dynamic tube blocking rig and static jar setup are not suitable for generating measurable data at low SR within an acceptable time frame in the laboratory.

This research focuses on understanding the mechanisms of bulk precipitation and surface deposition at low SRs (2 -10) and mid-range temperatures (50^oC - 90^oC). Static jar tests were carried out to follow the kinetics of bulk precipitation. An *in-situ* visualisation flow set-up was also used to follow the build-up of scale on surfaces as a function of SR and flowrate. The results showed evidence of nucleation and crystal growth. Finally, a newly developed beadpack technique, which has shown huge potential to accurately quantify scaling kinetics at low SR. The sensitivity of the beadpack to parameters such as area-to-volume ratio, surface roughness and flowrate was also evaluated.

In contrast to previous studies, this study has demonstrated that bulk precipitation can occur at very low SR over a sufficient time. The beadpack design was effective for quantifying the kinetics of $CaCO_3$ deposition on the surface at low SR due to the presence of a high area-to-volume (A/V) ratio in the pack. The results from the *in-situ* visualisation cell demonstrated that an increase in SR and flowrate led to an increase in the growth-rate of $CaCO_3$ on the surface at low SR. In addition, the growth-rate of $CaCO_3$ was 10 times faster at SR 10 on the surface compared to the bulk and 5 times faster for SR 5. This result indicates the role of surface deposition should be seriously considered in the development of a reliable scale prediction model.

The three techniques employed have shown to be complementary and provide insight into different aspects of the crystallisation process. The understanding and results generated in this study can serve as the building blocks for the development of a reliable kinetic model for predicting scale deposition at low SR in the oil and gas industry.

Table of Contents

Chapter 1- Introduction 1
1.1 Oil and gas formation and production 2
1.1.1 Mineral scale formation and its economic implications 4
1.2 Research background 6
1.3 Research aims and objectives. 8
1.4 Thesis Outline 9
Chapter 2 - Literature review 11
2.1 Introduction to scale formation 11
2.1.1 Process of scale formation 11
2.2 Scale formation in the bulk solution 20
2.2.1 Factors affecting scale formation in the bulk solution 21
2.2.2 Experimental studies of the bulk scaling phenomenon 28
2.3 Scale formation on solid surfaces 32
2.3.1 Factors affecting scale formation on surfaces 33
2.3.2 Laboratory studies of surface scaling phenomenon 40
2.4 Limitations and gaps in literature 48
Chapter 3 - Experimental Methodology 50
3.1 Brine Composition 50
3.2 Bulk precipitation method 51
3.2.1 Calcium combination ion selective electrode 53
3.3 Surface deposition study 54
3.4 Set-up for surface deposition test 54
3.5 Methodology for *in-situ* visualisation tests 54
3.5.1 Experimental procedure for surface deposition test 55
3.5.2 Computational protocol for Image capture and processing 56
3.5.3 Reproducibility for the *in-situ* visualisation cell 59
3.6 Bead pack method 62
3.6.1 Introduction 62
3.6.2 Characterisation for the beadpack parameters 66
3.7 Post experimental analysis 69
3.7.1 Atomic Absorption Spectroscopy (AAS) technique 69
3.7.2 SEM and EDX spectroscopy 70
Chapter 4 - Factors influencing $CaCO_3$ formation in the bulk solution and on steel surfaces at low SR 72
4.1 Kinetics of $CaCO_3$ formation in the bulk: 72

4.1.1 Effect of SR on bulk precipitation kinetics 72
4.1.2 Effect of temperature on bulk precipitation kinetics 74
4.2 Factors influencing $CaCO_3$ deposition on the surface 75
4.2.1 Introduction 75
4.2.2 Effect of SR on the surface deposition $CaCO_3$ at 50^oC 75
4.2.3 Effect of SR on the quantification of $CaCO_3$ growth on the surface at 79^oC 82
4.2.4 Effect of flowrate on surface deposition of $CaCO_3$ at 50^oC 89
Chapter 5 - Comparing the kinetics of bulk precipitation to surface deposition at low SR 105
5.1 Introduction 105
5.2 Bead pack method 106
5.2.1 Theoretical calculation for change in calcium ion concentration in the beadpack and *in-situ* visualisation cell 106
5.2.2 Surface deposition as a function of SR 107
5.2.3 Assessment of surface deposition kinetics from the *in-situ* visualisation cell technique 109
5.2.4 Comparing surface deposition in the beadpack and the *in-situ* visualisation cell 110
5.2.5 Bulk precipitation in static jar versus surface deposition in beadpack 112
5.3 Effect of surface roughness, area-to-volume ratio, and flowrate on the kinetics of $CaCO_3$ deposition study. 114
5.3.1 Effect of surface roughness on the kinetics of $CaCO_3$ deposition. 114
5.3.2 The effect of A/V on the kinetics of $CaCO_3$ deposition 121
Chapter 6 - Discussion 132
6.1 Introduction 132
6.2 Bead pack technique 133
6.2.1 Introduction 133
6.2.2 Area-to-volume ratio 133
6.2.3 Kinetics of scale deposition at low SR 134
6.2.4 Constant composition environment 134
6.2.5 Investigation of different experimental parameters:Temperature, flowrate, porosity, surface roughness and surface energy 135
6.2.6 Bead pack capability to better quantify the induction time for low SR 135
6.3 Comparing the induction time for bulk precipitation to surface deposition 138
6.3.1 Effect of surface roughness on induction time 142
6.4 Kinetics of $CaCO_3$ precipitation in the bulk at low SR 143
6.4.1 Effect of SR on the kinetics of bulk precipitation at low SR 143

6.4.2 Effect of temperature on the kinetics of bulk precipitation at low SR. 145

6.5 Kinetics of $CaCO_3$ surface deposition at low SR 146

6.5.1 Growth-rate of $CaCO_3$ on the surface as a function of area-to-volume ratio (A/V).....152

6.5.2 Effect of surface roughness on the kinetics of $CaCO_3$ deposition on the surface 153

6.5.3 The growth-rate of $CaCO_3$ on the surface as a function of flowrate. 155

6.5.4 Comparing the effect of A/V to the effect of flowrate on the kinetics of $CaCO_3$ deposition on the surface. 159

6.6 Mechanisms of $CaCO_3$ precipitation on the surface at low SR.....161

6.7 Comparing the kinetics of $CaCO_3$ precipitation in the bulk to the surface at low SR.....166

6.7.1 Synergy between the effect of saturation ratio (SR) and effect of flowrate on the kinetics of $CaCO_3$ deposition at low SR 168

Chapter 7 – Conclusion and Recommendations for Future work.....170

7.1 Conclusion 170

7.1.1 Factors influencing $CaCO_3$ formation in the bulk solution and on the surface at low SR 170

7.1.2 The development of a new technique for studying the kinetics of scale deposition at low SR 171

7.1.3 Comparing the kinetics of bulk precipitation to surface deposition at low SR. 172

7.1.4 The sensitivity of the beadpack to different parameters such as surface roughness, area-to-volume ratio, and flowrate.....173

7.2 Summary of Novelty 174

7.3 Relevance of the research to academia and industry 175

7.4 Recommendations for future work 177

7.4.1 Matching $\boldsymbol{V\,T\,A}$ in the *in-situ* visualisation cell and the beadpack to field conditions.....177

7.4.2 The development of a reliable model for predicting the kinetics of $CaCO_3$ deposition on the surface at low SR. 178

7.4.3 Improving the beadpack design.....179

7.4.4 Inhibition studies 180

7.4.5 Effect of coatings and use of glass for surface deposition tests180

References.....181

Appendix.....195

Procedures for processing the images from the *in-situ* visualisation cell with the MATLAB algorithm developed in this study. 202

List of Figures

Figure 1. 1- Historical and future projections of the primary sources of energy consumed in the world[4]. 1

Figure 1. 2 – Historical and future projections for the use of Petroleum and other liquids in the transportation, industrial, residential and commercial sectors of the world[4]. 2

Figure 1. 3 - An anticline oil and gas reservoir[9]. 3

Figure 1. 4 - A summary of the three oil recovery processes[12]. 3

Figure 1. 5 - The cross section of a pipe (a) with scale deposited compared with a pipe (b) without scale[19]. 5

Figure 2. 1– Illustrating the stages necessary for crystal growth and deposition of $CaCO_3$ to occur from a supersaturated solution[40]. 13

Figure 2. 2 - Calcium carbonate induction time vs the supersaturation for solutions containing magnesium to calcium ions concentrations ratios of a) 0 to 2 and b) 0 to 5[49]. 15

Figure 2. 3 – Free energy diagram for nucleation and critical radius[54].....17

Figure 2. 4 - Calcium carbonate polymorphs as a function of temperature[74]22

Figure 2. 5 - Schematic of the rig used for calcium carbonate scale experiment[36]. 23

Figure 2. 6 - The effect of SR on bulk precipitation kinetics determined by carrying out turbidity measurements, the result shows an increase in bulk precipitation as SR increased at 80^{o}C [44]. 26

Figure 2. 7 – Rate of covering of the working electrode [47].....27

Figure 2. 8 - Induction time versus aMg^{2+}/aCa^{2+} at 80^{o}C [50]. 28

Figure 2. 9 – Total precipitation of calcium carbonate as a function of pH at different circulation times on a non-magnetised (NM) sample and a magnetised sample (M) [88].....30

Figure 2. 10 – Dependence of the coverage of glass slides by calcium carbonate concentration (supersaturation) of the aqueous phase with respect to the reacting ions [67]. 34

Figure 2. 11 – Contact angle measured as a function of the supersaturation with respect to calcium carbonate concentration of the solution in which the glass slides were exposed [67].....34

Figure 2. 12 - Dependence of the contact angle measured on calcium carbonate covered glass slides as a function of the temperature of the supersaturated solution [67]. 35

Figure 2. 13 – Fouling rate per unit area versus time for samples with different roughness [68]. 35

Figure 2. 14 - Crystals size with time for SR 40 using the microfluidics technique [69]. 36

Figure 2. 15 - Crystals size with time for SR 61.7 using the microfluidics technique [69]. 37

Figure 2. 16 - Showing the effect of increasing the flowrate and SR on the growth-rate of $CaCO_3$ for (a) silanised surface and (b) non-silanised surface [72]. 38

Figure 2. 17 – Nucleation rate, J, at various ∅_area for three different substrates[105]. 39

Figure 2. 18 – SEM images of calcium carbonate crystals on hard surface at 25^{o}C (a,b) and 55^{o}C (c,d) at pH 10 for 1hr [73].....40

Figure 2. 19 – Showing the effect of surface energy on the amount of $CaCO_3$ deposited on different substrates at 50^{o}C and 90^{o}C, where (A) PTFE, (B) Pre-treated UNS S31603, (C) DLC and (D) UNS S31603[114].....43

Figure 2. 20 - Variation in the rate of covering of the working electrode in the electrochemical cell [81].....44

Figure 2. 21 – Comparison of growth rate constants [83]. 46

Figure 2. 22 - Schematic diagram for the once through flow visualisation rig [43]. 46

Figure 2. 23 – (a) number of crystals (b) average crystal size for $CaCO_3$ at T = 25^{o}C for 4 hours and flowrate of 20ml/min [43]. 47

Figure 2. 24 - Surface growth rate as a function of SR [43]. 47

Figure 3. 1 - Water bath for bulk precipitation test at 50^{o}C. 52

Figure 3. 2 - Experimental setup for 90^{o}C bulk precipitation test.....52

Figure 3. 3 - A calcium combination ion selective electrode. 53

Figure 3. 4 - Once through visualisation rig for surface and bulk scaling experiments [92]. 54

Figure 3. 5 - Fluid flow on sample surface[97].....55

Figure 3. 6 - A summary of the procedures taken to assess the number, average size and surface coverage of crystals on the image from the *in-situ* visualisation cell tests using the new MATLAB algorithm.....57

Figure 3. 7 - Histogram plot showing the greyscale of the image from the *in-situ* visualisation cell. This is useful for converting the image from the flow cell into a binary image for quantifying the crystals in the image. 58

Figure 3. 8 - *In-situ* visualisation cell images of the crystals formed on the stainless-steel sample at from 5 - 240minutes with SR 10 brine at 50^{o}C. 60

Figure 3. 9 – *In-situ* visualisation cell images of the crystals formed on the stainless-steel sample at 5 - 240minutes for the repeat SR 10 test at 50^{o}C. 60

Figure 3. 10 - Showing the repeatability results for (a) Number of crystals with time (b) Average size of crystals and (c) Surface coverage of crystals at SR 10, 50^{o}C with the *in-situ* visualisation cell.....61

Figure 3. 11 - Image of short beadpack of 54mm height in the oven. 64

Figure 3. 12 - Image of the longer bead pack of 150mm height in the oven.64

Figure 3. 13 - Pressure drop (Pa) versus flowrate (ml/min) graph for the stainless steel beadpack for different A/V.....67

Figure 3. 14 - Shear stress (Pa) versus flowrate (ml/min) graph for the beadpack for different area-to-volume ratio, A/V. 68

Figure 3. 15 - Residence time (s) versus flowrate (ml/min) graph for the steel beadpack for different area-to-volume ratio, A/V.....69

Figure 3. 16 - Carl Zeiss EVO MA15 Scanning Electron Microscope.....71

Figure 4. 1- Average Ca^{2+} ion concentration vs time graph for SR 10, 5 and 3 at 50^{o}C from measured results.....73

Figure 4. 2 - Average Ca^{2+} ion concentration vs time graph for SR 10, 5 and 3 at 90^{o}C from measured results.....73

Figure 4. 3-Average Ca^{2+} ion concentration vs time graph for SR 10 at 90^{o}C and 50^{o}C from bulk precipitation test. 74

Figure 4. 4 – Average Ca^{2+} ion concentration vs time graph for SR 5 at 90^{o}C and 50^{o}C from bulk precipitation test. 74

Figure 4. 5 – Average Ca^{2+} ion concentration vs time graph for SR 3 at 90^{o}C and 50^{o}C from bulk precipitation test. 75

Figure 4. 6 – *In-situ* visualisation cell images for the crystals formed on the stainless-steel sample after 5, 60,120 and 240 minutes for SR (a) 10, (b) SR 5 and (c) SR 3 at 50^{o}C. 76

Figure 4. 7– Comparing the number of crystals deposited on the surface with time at 50^{o}C and SR 3,5,10.....77

Figure 4. 8 – Comparing the average size of crystals formed on the surface with time at 50^{o}C and SR 3,5,10. 78

Figure 4. 9 – Comparing the surface coverage of crystals deposited on the surface with time at 50^{o}C and SR 3,5,10. 79

Figure 4. 10 – SEM images of the $CaCO_3$ crystals formed on the stainless-steel sample for (a) SR 10, (b) SR 5 and (c) SR 3 at 50^{o}C after the 4-hour duration of the test. 80

Figure 4. 11 – SEM images of the crystals formed on the stainless-steel sample for SR 3 at 50^{o}C. 81

Figure 4. 12 - EDX analysis results for the crystal at spectrum 157, for the test conducted at 50^{o}C and SR 3, which suggests the presence of small traces of $CaCO_3$ deposited on the surface of the stainless-steel sample.....81

Figure 4. 13 – *In-situ* visualisation cell images for the crystals formed on the stainless-steel sample after 5, 60, 120 and 240 minutes for SR (a) 8, (b) SR 4 and (c) SR 2 at 84^{o}C. 82

Figure 4. 14 – Comparing the number of crystals deposited on the surface with time at 79^{o}C and SR 2, 4, 8.....84

Figure 4. 15 – Comparing the average size of crystals formed on the surface with time at 79^{o}C and SR 2, 4, and 8. 85

Figure 4. 16 – Comparing the surface coverage of crystals deposited on the surface with time at 79^{o}C and SR 2, 4 and 8. 86

Figure 4. 17 – SEM images of the $CaCO_3$ crystals formed on the stainless-steel sample at (a) SR 8 and (b) SR 4 (C) SR 2 and 79^{o}C after the 4hour duration of the test. 87

Figure 4. 18 – SEM image with spectrum number from the EDX analysis of the crystals formed on the stainless-steel sample at SR 2 and 79^{o}C. 87

Figure 4. 19 - EDX analysis results of the crystal at spectrum 57 in electron image 11 for the test conducted at 79^{o}C and SR 2, which suggests that the crystal on the stainless-steel sample is NaCl. 88

Figure 4. 20 - EDX analysis results of the crystal at spectrum 58 in electron image 11 for the test conducted at 79^{o}C and SR 2, which suggests that the crystal on the stainless-steel sample is NaCl. 88

Figure 4. 21 - EDX analysis results of the crystal at spectrum 62 in electron image 11 for the test conducted at 79^{o}C and SR 2, which suggest the formation of $CaCO_3$ on the stainless-steel sample. 89

Figure 4. 22 - Images of $CaCO_3$ scale deposition for brine with SR 10 at 5, 60, 120 and 240minutes time intervals and flowrate of (a) 20ml/min and (b) 30ml/min at 50^{o}C. 90

Figure 4. 23 – Comparing the number of crystals deposited on the surface with time at 50^{o}C, SR 10 and flowrate of 20 and 30ml/min. 91

Figure 4. 24 – Comparing the average size of crystals formed on the surface with time at 50^{o}C, SR 10 and flowrate of 20 and 30ml/min. 92

Figure 4. 25 – Comparing the surface coverage of crystals deposited on the surface with time at 50^{o}C, SR 10 and flowrate of 20 and flowrate of 30ml/min. 93

Figure 4. 26 - SEM images of the $CaCO_3$ crystals deposited on the stainless-steel surface for brine with SR 10 after 4hours and flowrate of (a) 20ml/min and (b) 30ml/min at 50^{o}C. 94

Figure 4. 27 – *In-situ* visualisation cell images of $CaCO_3$ scale deposition for brine with SR 5 at 5, 60, 120 and 240 minutes time intervals and flowrate of (a) 20ml/min and (b) 30ml/min at 50^{o}C. 95

Figure 4. 28 – Comparing the number of crystals deposited on the surface with time at 50^{o}C, SR 5 for 20 and flowrate of 30ml/min. 96

Figure 4. 29 – Comparing the average size of crystals deposited on the surface with time for 50^{o}C, SR 5 at 20 and flowrate of 30ml/min. 97

Figure 4. 30 – Comparing the surface coverage of crystals formed on the surface with time and their growth-rates at 50^{o}C, SR 5 and flowrate of 20 and 30ml/min. 97

Figure 4. 31 - SEM images of the $CaCO_3$ crystals deposited on the stainless-steel surface for brine with SR 5 after 4hours and flowrate of (a) 20ml/min and (b) 30ml/min at 50^{o}C. 98

Figure 4. 32 – *In-situ* visualisation cell images of $CaCO_3$ deposition for brine with SR 3 at 5, 60, 120 and 240minutes time intervals and flowrate of (a) 20ml/min and (b) 30ml/min at 50^{o}C. 99

Figure 4. 33 – Comparing the number of crystals deposited on the surface with time for 50^{o}C, SR 3 at flowrate of 20 and 30ml/min. 100

Figure 4. 34 – Comparing the average size of crystals formed on the surface with time for 50^{o}C, SR 3 at flowrate of 20 and 30ml/min. 101

Figure 4. 35 – Comparing the surface coverage of crystals deposited on the surface with time for 50^{o}C, SR 3 at flowrate 20 and 30ml/min.....102

Figure 4. 36 - SEM images of the $CaCO_3$ crystals deposited on the stainless-steel surface for brine with SR 3 after 4hours and flowrate of (a) 20ml/min and (b) 30ml/min at 50^{o}C. 103

Figure 4. 37 – EDX analysis results for the crystal at spectrum 7 for the test at 50^{o}C, SR 3 and flowrate of 30ml/min showing evidence for the presence of $CaCO_3$ crystals. 103

Figure 5. 1 – Calcium ion concentration versus time graph for the stainless-steel beadpack (effluent) at SR 10, flowrate of 20ml/hr and 50^{o}C. 109

Figure 5. 2 – Calcium ion concentration versus time graph for the stainless-steel beadpack (effluent) at SR 5, flowrate of 20ml/hr and 50^{o}C.....109

Figure 5. 3 – Calcium ion concentration versus time graph for the stainless-steel beadpack (effluent) at SR 3, flowrate of 20ml/hr and 50^{o}C.....110

Figure 5. 4 – Number of crystals deposited with time at 50^{o}C, SR 3 and 30ml/min. 111

Figure 5. 5 – The graph of the average size of crystals with time at 50^{o}C, SR 3 and 30ml/min. 111

Figure 5. 6 – Comparing the calcium ion concentration versus time graph for the stainless-steel beadpack and static jar test at SR 10,50^{o}C and flowrate of 20ml/hr. 114

Figure 5. 7 – Comparing the calcium ion concentration versus time graph for the stainless-steel beadpack and static jar test at SR 5,50^{o}C and flowrate of 20ml/hr. 114

Figure 5. 8 – Comparing the calcium ion concentration versus time graph for the stainless-steel beadpack and static jar test at SR 3,50^{o}C and flowrate of 20ml/hr. 114

Figure 5. 9- SEM image of (a) smooth stainless-steel bead, (b) Etched stainless-steel bead and (c) PTFE bead before the beadpack test. 116

Figure 5. 10 – Comparing the Ca^{2+} ion concentration vs time graph for the PTFE bead, smooth stainless - steel and etched stainless-steel bead at SR 10, 50^{o}C and 20ml/hr. 119

Figure 5. 11- SEM image of (a) smooth stainless-steel bead (b) PTFE bead and (c) Etched stainless steel bead at SR 10, 50^{o}C and 20ml/hr at 500X magnification after the bead pack experiment. 121

Figure 5. 12 – EDX analysis results of the crystal at spectrum 6, from the 3mm diameter etched stainless-steel bead pack test at 50^{o}C and SR 10, which suggests the presence of $CaCO_3$ on the surface. 121

Figure 5. 13 - Beadpack with (a) 3mm diameter stainless steel beads, (b) 6mm diameter stainless steel beads and (c) 9mm diameter stainless steel beads. 122

Figure 5. 14 - A representation of the hypothesis for the effect of A/V(m^{-1}) on the kinetics of $CaCO_3$ deposition study.....123

Figure 5. 15 - A representation of the hypothesis for the effect of flowrate (from 20ml/hr to 60ml/hr) on the kinetics of $CaCO_3$ deposition study.....124

Figure 5. 16 - Comparing the Ca^{2+} ion concentration vs time graph for the beadpack test with an A/V ratio of 2371.1m^{-1} and flowrate of 20ml/hr to the results obtained at an A/V of 1085.2m^{-1} and flowrate of 60ml/hr at SR 10 and 50^{o}C. ..126

Figure 5. 17 - Comparing the Ca^{2+} ion concentration vs time graph for the beadpack test on effect of flowrate (20ml/hr and 60ml/hr) on the kinetics of $CaCO_3$ deposition at similar A/V (852.5m^{-1} and 1085.2m^{-1}), SR 10 and 50^{o}C.128

Figure 5. 18 - Comparing the Ca^{2+} ion concentration vs time graph for the beadpack test on the effect of A/V (852.5m^{-1} and 455.5m^{-1}) on the kinetics of $CaCO_3$ deposition at a constant flowrate of 20ml/hr, SR 10 and 50^{o}C. 130

Figure 6. 1 - Comparing the induction time from the static jar test and the beadpack test at SR 10 and 50^{o}C. An induction time of 10minutes was observed for both the static jar test and beadpack test, illustrated by point A. 138

Figure 6. 2 - Comparing the induction time from the static jar test and the beadpack test at SR 5 and 50^{o}C. An induction time of 30minutes was observed for the static jar test illustrated by point B, and a shorter induction time of 20 minutes for the beadpack test, as shown by point C. 139

Figure 6. 3 - Comparing the induction time from the static jar test and the beadpack test at SR 3 and 50^{o}C. An induction time of 20 minutes was observed for the beadpack test, as shown by point D, whilst there was no evidence for $CaCO_3$ precipitation from the static jar test for the 240minutes duration of the experiment. 139

Figure 6. 4 – Average Ca^{2+} ion concentration vs time graph for SR 10, and 5 at 50^{o}C from bulk precipitation test. 144

Figure 6. 5 - Average Ca^{2+} ion concentration vs time graph for SR 10, 5 and 3 at 90^{o}C from bulk precipitation test. 144

Figure 6. 6 – Growth-rate vs SR for bulk precipitation at two different temperatures. 145

Figure 6. 7 - Comparing the average size of crystals formed on the surface with time and their growth-rates SR 10, 5, and 3 at 50^{o}C, section A corresponds to a period of both nucleation and growth of $CaCO_3$, section B relates to a period of only crystal growth and section C shows a period of stabilisation in the growth of the $CaCO_3$ on the surface. 147

Figure 6. 8 - Comparing the average size of crystals formed on the surface with time and their growth-rates for SR 8, 4 and 2 at 79^{o}C, section A corresponds to a period of both nucleation and growth of $CaCO_3$, section B relates to a period of only crystal growth and section C shows a period of stabilisation in the growth of the $CaCO_3$ on the surface. 148

Figure 6. 9 - The *in-situ* visualisation cell results for the effect of SR on the growth-rate of $CaCO_3$ at 50^{o}C. 149

Figure 6. 10 - The *in-situ* visualisation cell results for the effect of SR on the growth-rate of $CaCO_3$ at 79^{o}C. 149

Figure 6. 11 - The beadpack results for the effect of SR on the growth-rate of $CaCO_3$ at 50^{o}C. 150

Figure 6. 12 - Comparing the effect of flowrate of on the growth-rate of $CaCO_3$ with time at (i) SR 10, (ii) SR 5 and (iii) SR 3. section A corresponds to a period of both nucleation and growth of $CaCO_3$, section B relates to a period of only crystal growth and section C shows a period of stabilisation in the growth of the $CaCO_3$ on the surface. 156

Figure 6. 13 - Effect of flowrate on the surface coverage of $CaCO_3$ at 50^{o}C, showing an increase in surface coverage as flowrate increased. 157

Figure 6. 14 - Comparing the effect of increasing flowrate (Q) to increasing area-to-volume ratio A/V on the growth-rate (ppm/min) of $CaCO_3$ at SR 10 and 50^{o}C. 160

Figure 6. 15 - Comparing the effect of increasing flowrate (Q) to increasing area-to-volume ratio A/V on the deposition rate (ppm/m^2/min) of $CaCO_3$ at SR 10 and 50^{o}C. 161

Figure 6. 16 – A representation of the steps involved in the deposition $CaCO_3$ on the surface [182]. 162

Figure 6. 17 - Progressive nucleation is represented by (a) - where new crystals continues to deposit on the surface throughout the crystallisation process, whilst (b) corresponds to instantaneous nucleation, where all the crystals nucleate at the same time before crystal growth takes place. 163

Figure 6. 18 – Extended surface coverage graph versus t^2 for (a) SR 10, (b) SR 5 and (c) SR 3 at 50^{o}C. 164

Figure 6. 19 – Effect of SR 10, 5 and 3 on (a) number of crystals deposited on the surface with time and (b) average size of crystals formed on the surface with time at 50^{o}C. 165

Figure 6. 20 - Comparing the growth-rate (ppm/min) of $CaCO_3$ in the bulk solution from the static jar test to the surface from the beadpack test at SR 10, 5 and 3 at 50^{o}C. 167

Figure 6. 21- Synergy between effect of SR and effect of flowrate on the surface coverage of $CaCO_3$ at SR 10, 5 and 3 at 50^{o}C. 169

Figure 7. 1 - $CaCO_3$ growth-rate data for low SR plotted to determine the mass transfer constant K_d, from the slope of the graph and surface reaction constant K_r from the intercept. 179

List of Tables

Table 1. 1 - Interpretation of $CaCO_3$ scale prediction results [26].....6

Table 2. 1 - Common oilfield scales[66].....20

Table 2. 2 - Causes of scale formation 20

Table 2. 3 - Growth rate (gr/hr) of calcium carbonate under the influence of malic acid at different concentrations [36].....24

Table 2. 4 – The surface energy of the substrates determined from the contact angles. 43

Table 3. 1 - Brine composition (g/L) for SR 3, 5 and 10 at 50^{o}C.....50

Table 3. 2 - Brine composition (g/L) for SR 3, 5 and 10 at 90^{o}C.....50

Table 3. 3 - Final water chemistry composition and the final pH for bulk precipitation test at 50^{o}C and 90^{o}C after 4 hours. 51

Table 3. 4 - Hydrodynamics parameters for surface deposition test at 50^{o}C and 90^{o}C. 56

Table 3. 5 - Stainless steel composition used for the study. 56

Table 3. 6 - Comparing the MATLAB algorithm developed in this study to the algorithm developed in previous study[97] with regards to quantifying the number, average size and surface coverage of crystals deposited on the surface. 59

Table 3. 7 - Composition of 3mm diameter stainless steel for beadpack test.65

Table 3. 8 – Beadpack parameters for the experiments with 3mm diameter beads at 20ml/hr. 65

Table 5. 1 - Comparing the experimental conditions for the beadpack test to the *in-situ* visualisation cell tests at SR 3 and 50^{o}C. 111

Table 5. 2 – Surface characterisation of the PTFE, smooth and rough stainless-steel materials used for the beadpack test. 116

Table 5. 3 – Experimental variables for the effect of flowrate on $CaCO_3$ deposition study with the beadpack.....123

Table 5. 4 - Experimental parameters for the beadpack test investigating the effect of A/V (2371.1m^{-1} and 1085m^{-1}) and flowrate (20ml/hr and 60ml/hr) on the kinetics of $CaCO_3$ deposition at SR 10, 50^{o}C. 124

Table 5. 5 - Experimental parameters for the beadpack test studying the effect of flowrate (20ml/hr and 60ml/hr) at similar A/V (852.5m^{-1} and 1085.2m^{-1}) on the kinetics of $CaCO_3$ deposition at SR 10, 50^{o}C.....126

Table 5. 6 - Experimental parameters for the beadpack on the effect of A/V (852.5m^{-1} and 455.5m^{-1}) on the kinetics of $CaCO_3$ deposition at SR 10, 50^{o}C and flowrate of 20ml/hr. 128

Table 6. 1– Comparing the induction time for bulk precipitation (from the static jar tests) and surface deposition using the beadpack with A/V of 2371m^{-1} and the *in-situ* visualisation with A/V of 28m^{-1}. 136

Table 6. 2 - Variation between the induction time bulk precipitation (static jar test) and surface deposition (beadpack test) for SR 10, 5 and 3 at 50^{o}C.....142

Table 6. 3 - The effect of surface roughness on the induction time for $CaCO_3$ deposition. 143

Table 6. 4 - Growth-rate of calcium carbonate as a function of SR from the *in-situ* visualisation cell tests. 148

Table 6. 5 - Growth-rate of calcium carbonate as a function of SR from the beadpack test at 50^{o}C. 150

Table 6. 6 - The effect of A/V on the kinetics of $CaCO_3$ deposition at SR 10 and 50^{o}C 152

Table 6. 7 - The effect of surface roughness on the kinetics of $CaCO_3$ deposition at SR 10, 50^{o}C 154

Table 6. 8 - Effect of flowrate (20 and 30ml/min) on the growth-rate of $CaCO_3$ at SR 10, 5 and 3 at 50^{o}C.....156

Table 6. 9 - Effect of flowrate on the kinetics of $CaCO_3$ deposition results using the beadpack at SR 10 and 50^{o}C.....158

Table 6. 10 - Comparing the results for the effect of increasing flowrate to increasing A/V on the kinetics of $CaCO_3$ deposition. 159

Table 6. 11 - Comparing the growth-rate of $CaCO_3$ in the bulk solution from the static jar test to the surface from the beadpack test at SR 10, 5 and 3 at 50^{o}C166

Table 7. 1 - Experimental conditions for matching VT/A in the beadpack and the *in-situ* visualisation cell.....177

Nomenclature

Terms	Definition	Units
ΔP	Pressure drop	Pa
L	Height of the bed	m
μ	Fluid viscosity	Pa.s
ε	Void space of the bed	
μ_o	Fluid superficial velocity	m/s
d_p	Particle diameter	m
ρ	Density of the fluid	kg/m^3
τ_W	Shear stress	Pa
d_h	Hydraulic mean diameter for the packed bed	m
T	Residence time	secs
C_{ao}	Initial calcium ion concentration	ppm
C_a	Calcium ion concentration in the outlet at equilibrium point	ppm
r_a	Growth rate	ppm/minutes
K_{sp}	Solubility product	
γ_i	Activity coefficient	
r_c	radius of critical nuclei	cm
J	nucleation rate	$cm^{-3}\ s^{-1}$
ΔG_{cr}	Free energy change for the critical cluster size formation	J mole $^{-1}$
k	Boltzmann constant	J/K
T	absolute temperature	K
γ	Free surface energy	$mJ.m^{-2}$
V_m	Molecular volume	$cm^3\ mole^{-1}$
f(θ)	Correction factor	
K_a	Activity based solubility product constant	
t_{ind}	Induction time	S
t_s	Scaling time	S
t_n	Time for system to reach steady state	S
t_g	Time for nuclei to reach a detectable size	S
K_{sp}	Solubility product constant	
θ	Contact angle	Degs
K_d	Mass transfer coefficient	m/s
K_r	Surface reaction coefficient	mol/l/s
V	Flow velocity	m/min
Q	Volumetric flow rate	ml/mins
R_e	Reynolds number	

ρ	Density	Kg/m^3
t_{ind}	Induction time	S
tr	Relaxation time	S
tn	Period of nucleation	S
N_A	Avogadro number	$6.023.1023\ mol^{-1}$
R	Gas constant	$8.31\ J.mol^{-1}\ .K^{-1}$
ΔG	Overall excess free energy	$kJ.mol^{-1}$
γ_S	Solid surface free energy	$N.m^{-1}$
γ_{SL}	Solid/liquid interfacial free energy	$N.m^{-1}$
γL	Liquid surface tension	$N.m^{-1}$
$S_{(t)}$	Surface Coverage	%
$S_{ext(t)}$	Extended surface coverage	%

Abbreviations	Definition
SI	Saturation Index
SR	Saturation ratio
RCE	Rotating Cylinder Electrode
PVS	Polyvinyl sulfonate
SEM	Scanning electron microscopy
ICP	Inductively Coupled Plasma - Atomic Emission Spectroscopy
XRD	X-Ray Diffraction
EDX	Energy Dispersive X-ray analysis system
FW	Formation water
SW	Sea water

Chapter 1- Introduction

The demand for energy in the new global economy continues to increase greatly. This is due to a surge in energy consumption as the world transitions from the pandemic, because of COVID-19, increase in population and the war in Europe [1, 2]. This has led to shortages in supply and increase in energy prices, demonstrating the need for continued developments of alternative sources of energy from renewables such as hydroelectricity, wind, and solar power to meet the ever growing demand for energy [3].

Nonetheless, to support the increasing demand, petroleum and other liquids from the oil and gas industry will remain a significant source of energy especially for developing Asian countries [4]. This is indicated by a report from the United States Energy Information Administration (EIA) presented in Figure 1.1, which shows that petroleum and other liquids are still the primary source of energy. However, the use of renewable sources of energy is dramatically increasing to almost the same level as petroleum.

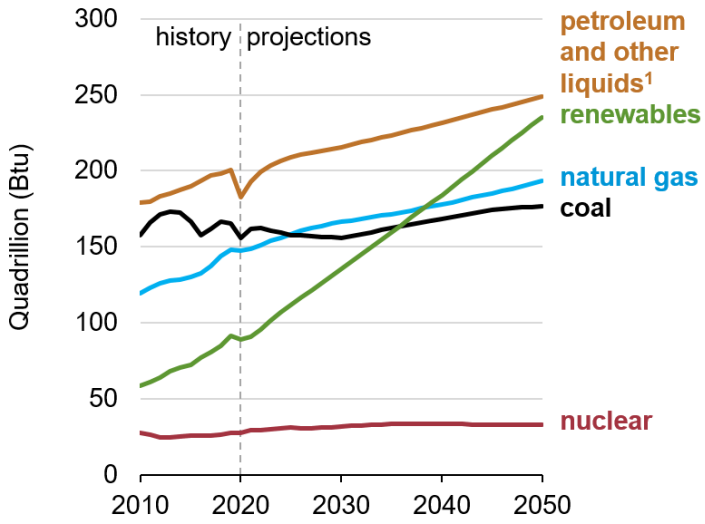

Figure 1. 1- Historical and future projections of the primary sources of energy consumed in the world[4].

The data in Figure 1.2 also illustrates that after the decline in the use of petroleum and other liquids in 2020 due to the pandemic, its consumption is projected to increase for the next 30 years across the transportation and industrial sectors across the world [4].

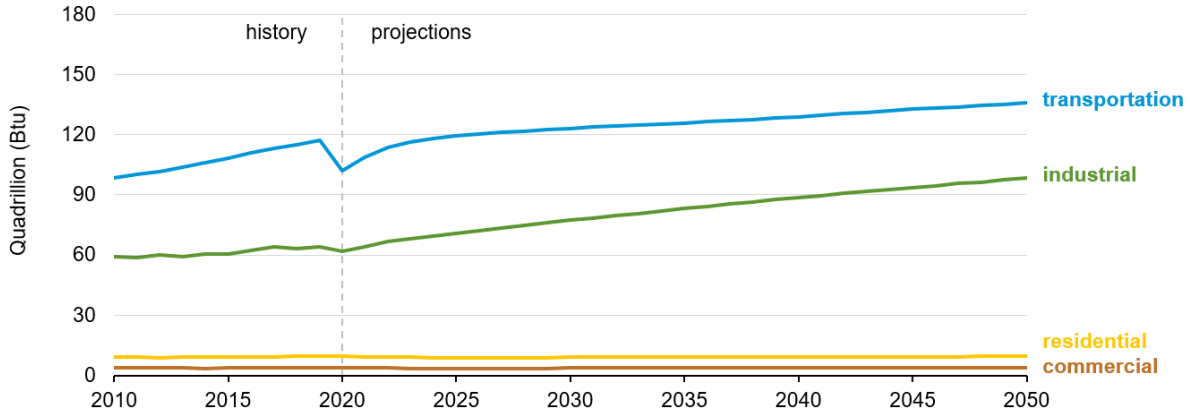

Figure 1. 2 – Historical and future projections for the use of Petroleum and other liquids in the transportation, industrial, residential and commercial sectors of the world[4].

However, there are some challenges that cause flow assurance issues and impact the safe extraction and production of oil and gas in the industry. These include the formation of waxes, asphaltenes, hydrates, corrosion, bio fouling, sand erosion and the deposition of mineral scale [5]. The purpose of this study is to understand the mechanisms and kinetics of mineral scale deposition on surfaces and in the bulk solution. In the next section, an explanation of how oil and gas is formed and produced is presented.

1.1 Oil and gas formation and production

Conventional oil and gas are fossil fuels, which are usually deposited from the remains of plants, algae and bacteria. After a geological period of about 100-200 million years, these organic fossils are decomposed together with the minerals present in the rocks. Under high temperature and pressure they are transformed into oil and gas, which serve as raw materials which can be converted into fuels and other essential products used in our daily lives [6].

Naturally, the oil, gas and water in the rocks tend to migrate from beneath the earth where the pressure is high to the surface where the pressure is lower. The tectonic movement of the rocks also assists the transportation oil and gas through porous rocks such as sandstone, limestone, and dolomite. They eventually settle on a layer of impermeable rock such as salt, shale, chalk, or mudrock [7]. These fossil fuels continue to accumulate in underground pockets called reservoirs, which can be several thousand meters below the surface of the earth [8].

The oil, gas and water typically form a three-level model in the reservoir. Due to the varying densities of the three substances, the gas lies above the oil, and the

water lies beneath the oil (as oil is denser than gas and water is denser than oil) [6], this is illustrated in Figure 1.3.

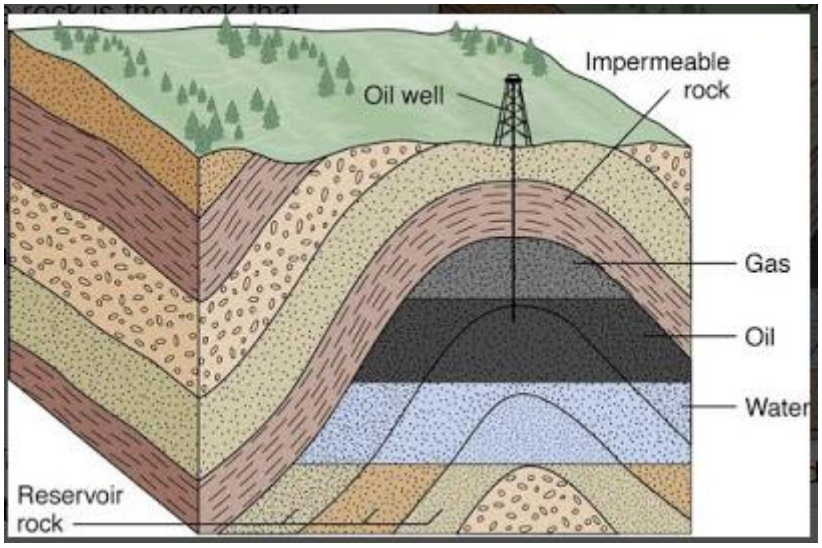

Figure 1. 3 - An anticline oil and gas reservoir[9].

The process of extracting the trapped oil and gas from a reservoir usually requires long term planning and expensive drilling infrastructures to ensure that the reservoir usage is optimised [6]. Typically, there are three distinct phases involved in the extraction of oil and gas from a reservoir, the primary, secondary and tertiary or enhanced oil recovery processes [10-12]. These three processes are summarised in Figure 1.4.

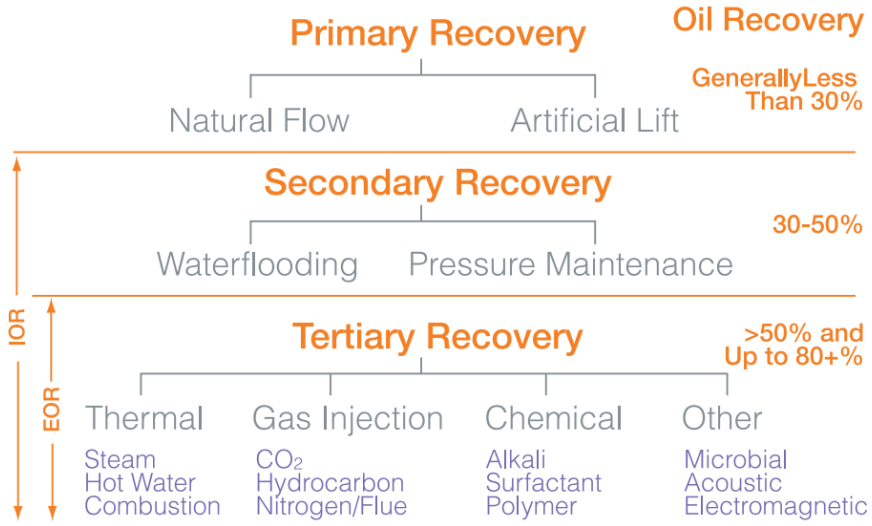

Figure 1. 4 - A summary of the three oil recovery processes[12].

- Primary oil recovery - In this process, the natural pressure of the reservoir is utilised to produce the oil and gas. This phase can also be combined with the use of artificial lift such as pumps to support the recovery of oil due to

the low driving force from the natural pressure in the reservoir. The recovery of oil during the process is generally less than 30% of the oil in place [11].

- Secondary oil recovery – This process helps to extract some of the remaining oil trapped in the reservoir after the primary recovery process. It involves the injection of water or gas into the reservoir to encourage the flow of the oil and gas to the surface [13, 14]. The techniques commonly adapted in this process include water flooding and pressure maintenance. In this process between 30 and 50% of the oil in place is generally recovered [12].

- Tertiary oil recovery –This process helps to produce the oil and gas which could not be recovered during the secondary recovery process, and this remaining oil in the reservoir is regarded as crude oil. In this phase, procedures such as thermal recovery, gas injection, chemical injection or microbial recovery are employed to reduce the viscosity of the oil in the reservoir and ease the extraction of the oil and gas. This process is carried out only when oil and gas can be produced profitably because it requires the use of very expensive improved oil recovery technologies [12].

Although these recovery techniques play a vital role in the production of oil and gas in the industry, there are some issues associated with all these recovery techniques in extracting oil and gas. One these is the formation of inorganic scale. The next section introduces and explains the economic implication of mineral scale formation in the oil and gas industry [15].

1.1.1 Mineral scale formation and its economic implications

Mineral scale formation is the precipitation of solid inorganic salts from aqueous solutions. It is a major problem that causes restrictions and interferes with safe hydrocarbon and carbon capture utilisation and storage operations (CCUS). It leads to blockages in pipes, increase in maintenance cost, and deferred production [16-18]**.** Generally, inorganic scale formation occurs as a result of sudden changes in temperature, pressure or pH. However, the mixing of incompatible substances during drilling, completion operations or after injection water breakthrough can also bring about the precipitation of scale. Scale deposition is typically encountered in subsurface, subsea or processing facilities such as pipes, safety and choke valves, separation equipment and filling vessels [19-21]. An image comparing the cross

section of a pipe with scale deposited and without the presence of scale is presented in Figure 1. 5.

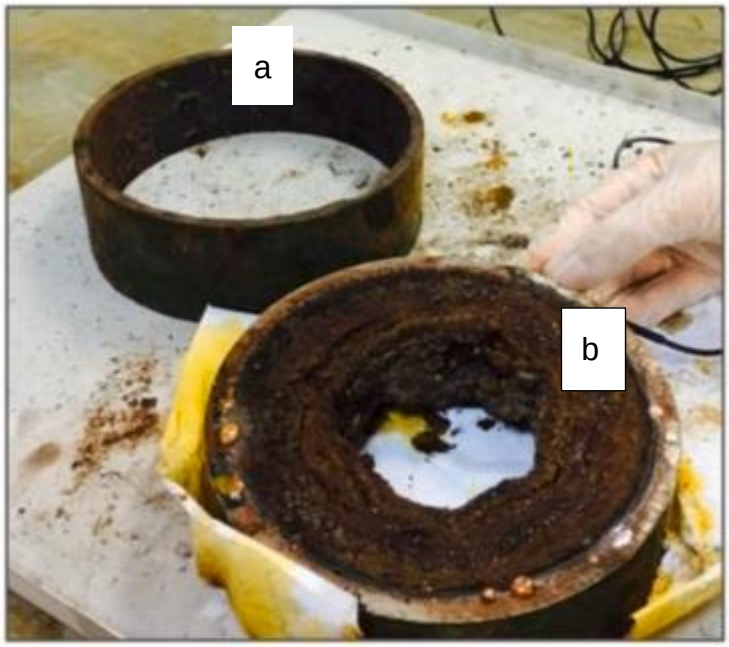

Figure 1. 5 - The cross section of a pipe (a) without scale deposited compared with a pipe (b) with scale[19].

There are several types of inorganic scale experienced in the oil and gas industry, including sulphates (calcium sulphate and barium sulphate), carbonates (calcite, vaterite and aragonite), and sulphide scales. Nonetheless, the most prevalent types of scale in oilfield operations are calcium carbonate and barium sulphate scales [22]. This study is focused on understanding the mechanisms and kinetics of $CaCO_3$ precipitation in the bulk solution and its deposition on surfaces at low SR, because it causes in blockages in pipelines and safety valves, leading to deferred production. In contrast, the $CaCO_3$ crystals formed in the bulk solution can be transported and whilst they may collect in strainers their impact on operations is generally limited.

The economic and financial implications of scale deposition in the oil and gas industry are enormous, especially in relation to the cost associated with treatments and prevention of scale deposition in subsea environments. For instance, A study by Zhang et al[23], revealed that $CaCO_3$ scale deposition issues in a low SR brine, led to an unplanned shutdown of a well for 8month and cost almost $63milion to clean and treat the well using scale squeeze treatments before continuing production. However, this cost drastically increases in deep-water environments[24]. This illustrates the financial implications of $CaCO_3$ deposition issues in the oil and gas industry and the importance of developing a reliable scale prediction tool which would provide better clarity on the likelihood for scale

deposition to occur and can reduce the cost associated with conservatism in the design of facilities to manage the scale threat.

1.2 Research background

The significant financial implications of scale formation illustrate the need for a reliable tool for predicting the tendency for scale to form. This would support operators in the oil and gas industry to better identify whether scale inhibition treatments are required to maximise productivity and it would also help in the optimal design of facilities to manage the threat [24].

There are several commercially available scale prediction software packages used to estimate scale threat in the oil and gas industry, such as Multiscale, OLI studio, ScaleChem, ScaleSoftPitzer and ScaleSim. The limitation of these prediction tools is that they are solubility models based on thermodynamic principles. These software packages are beneficial in assessing the likelihood for scale to form in the bulk solution and estimating the mass of scale. However, they do not account for the rate of scale deposition on the surface with time (i.e. the kinetics of surface deposition) [23, 25].

Therefore, when considering the role of surface deposition kinetics, many operators in the oil and gas industry predict scale threat based on the degree of saturation ratio (SR) and it is a measure of supersaturation which is the driving force for scale formation. A representation of one of the guidelines used to predict the tendency for scale formation to occur is presented in Table 1. 1.

Table 1. 1 - Interpretation of $CaCO_3$ scale prediction results [26]

SR	Interpretation
< 1	Under saturated - No scale expected
> 1 - 3	Slightly supersaturated. Likelihood for scale formation is marginal
3 - 10	Scale is likely, but not severe
10 - 100	Scale is almost certain to occur

This guideline presents a large region of uncertainty at low SR (i.e. above SR 1 and below SR 10). Unfortunately, this area of uncertainty has huge financial implications, as underestimating the likelihood for scale deposition to take place at low SR could lead to serious safety issues, unplanned shutdowns and deferred production. However, overestimating the likelihood for scale deposition to occur could cause unwarranted deployment of expensive scale inhibition facilities. This

highlights the need for the development of a reliable model for predicting the kinetics of scale deposition especially at low SR [23].

A substantial amount of data from a suitable technique is required for the development of a reliable kinetic model for predicting the kinetics of scale deposition at low SR. The drawback of the body of work available in literature on $CaCO_3$ formation is that, whilst most studies has been focused on investigating the mechanisms and kinetics of $CaCO_3$ formation at higher SR (i.e. above SR 10), insufficient research has been directed towards understanding the kinetics of scale formation at lower SR (i.e. below SR 10), this is suspected to be due to a lack of a suitable technique with a high surface area which would support the generation of a substantial amount of deposition at low SR conditions within a reasonable time-frame in the laboratory[25].

In addition, the limitations of the experimental techniques commonly used for studying $CaCO_3$ formation in the laboratory (such as the static jar, *in-situ* visualisation cell and the dynamic tube blocking rig), is that it is either a closed system where SR reduces with time [27], making it difficult to assess the effect of a constant SR on scale formation, or there is a lack of a high area-to-volume ratio (A/V) in the system, which poses a challenge in generating an appreciable amount of deposition needed to effectively quantify the kinetics of $CaCO_3$ deposition within an acceptable time-frame in the laboratory. This demonstrates the need for the development of an appropriate technique with a high A/V which would be necessary for assessing the kinetics of $CaCO_3$ surface deposition within an acceptable time frame at low SR. Another limitation of previous research is that, although a considerable amount of work has been carried out on understanding the kinetics of bulk precipitation, much less is known about the kinetics of surface deposition [28-32].

Furthermore, a growing body of literature has also suggested that there is a distinction between the mechanisms and kinetics of $CaCO_3$ precipitation in the bulk solution in comparison to its deposition on the surface [33-35]. For instance, Setta et al [34] examined the formation of $CaCO_3$ with a rotating disk electrode (RCE), conducting the tests at SR 100, SR 32 and SR 13. The kinetics of $CaCO_3$ precipitation in the bulk solution was investigated by monitoring the turbidity and tracking the reduction in the calcium ion solution with time in the bulk due to the precipitation of $CaCO_3$ in bulk phase. The kinetics of $CaCO_3$ deposition on the surface was assessed by measuring the mass gain on the surface and carrying out SEM analysis of the crystals deposited there. The findings from Setta's research showed that $CaCO_3$ crystals grew noticeably larger on the surface compared to the bulk solution and whilst calcite polymorph of $CaCO_3$ was observed on the surface, vaterite crystals were reported to precipitate in the bulk solution at

comparable experimental conditions. These results demonstrate that the kinetics of $CaCO_3$ precipitation in the bulk is different to its deposition on the surface. Nonetheless, an understanding of the extent to which the presence of surface impacts the kinetics of $CaCO_3$ formation in comparison to only bulk precipitation is still lacking.

Extensive research has also shown that any increase in temperature, SR, flowrate and surface roughness will promote the kinetics of $CaCO_3$ formation [36, 37]. However, there is opportunity for further work to understand the role of area-to-volume ratio, A/V on the kinetics of $CaCO_3$ deposition, enhancing the understanding of the role of surface on $CaCO_3$ deposition. One of the aims of this research is to develop a new technique with a high A/V to provide a better insight into the mechanisms and kinetics of $CaCO_3$ deposition at low SR. The main objectives of this study are described in the next section.

1.3 Research aims and objectives.

The main aim of this project is to assess and develop appropriate methodologies to determine kinetics in low SR (SR 2 – 10) systems.

The intention is to bridge the gap from purely thermodynamic prediction which gives information on the ***potential for scale*** to form in a solution, to ***kinetic predictions***, which will help to predict the rates at which scale will deposit on surfaces in variable conditions such as low SR, mid-range temperature (up to 90^oC) and different hydrodynamic conditions. The key objectives of this research are summarised below.

- To quantify the kinetics of bulk precipitation at low SR using static jar tests.

- To understand the factors that impact the kinetics of scale deposition at low SR using the *in-situ* visualisation cell.

- To develop a new system and technique (a once-through ‘bead-pack’ setup) to study the kinetics of scale deposition in low SR solutions.

- To investigate the sensitivity of the newly developed bead-pack setup to different parameters such as surface roughness, area-to-volume ratio and flowrate.

- To understand the extent to which the presence of surface impacts the kinetics of scale formation in comparison to only bulk precipitation at low SR.

  To create a framework for the development of a reliable kinetic model for predicting scale deposition at low SR, by generating reproducible data on the kinetics of $CaCO_3$ deposition at low SR with the bead-pack setup.

1.4 Thesis Outline

A brief summary of the 9 chapters in this thesis is presented as follows:

Chapter 1 – This chapter introduces the context of this study, an overview of scale formation in the oil and gas industry and its economic implications. The aim and objectives of this study are also stated in this section.

Chapter 2 – This chapter begins by laying out the fundamentals of the scaling process; a review of the existing literature on the formation of scale in the bulk solution and on the surface are also presented.

Chapter 3 – This chapter describes the techniques used for the bulk precipitation and surface deposition experiments. The details of the beadpack design, procedures for analysing the data from the surface deposition tests performed, and description of the beadpack and *in-situ* visualisation cell and the apparatus used for the bulk precipitation tests. The brine composition and samples used are also presented.

Chapter 4 – In this chapter, the results from the study of all the factors affecting the precipitation of calcium carbonate in the bulk solution and its deposition on the surface at low SR are presented.

Chapter 5 – This chapter concentrates on the explanation of the surface deposition results at low SR from the beadpack test, with a comparison of the kinetics of calcium carbonate precipitation in the bulk solution to its deposition on the surface, as well as an evaluation of the distinction between the bead-pack design and the *in-situ* visualisation cell.

The results from the assessment of the sensitivity of the beadpack setup to different experimental parameters such as area-to-volume ratio, surface roughness and flowrate are also presented.

Chapter 6 – In this chapter, a detailed interpretation of the analysed results from Chapters 4 and 5 is provided.

Chapter 7 – In this chapter, the main findings from the research and recommendations for future work in relation to this study are provided.

Chapter 2 - Literature review

This literature review is presented in three main parts to link to the three main aspects of this study. Firstly, an overview of the literature and supporting theory on scale formation in general is presented. Following that, the literature review then presents the current state of the art in the understanding of bulk and surface scaling. This PhD project will understand the relationship between these two processes and will develop an understanding of the factors that affects the kinetics of bulk and surface scaling.

2.1 Introduction to scale formation

Scale formation is a major issue experienced across many industries. A supersaturated solution containing soluble ions promotes the formation of scale. The driving force for scale formation includes supersaturation, nucleation and sufficient contact time [38].

Scale deposition in the oil and gas industry results in blocking of the internal infrastructure. This leads to depletion in the equipment's lifetime and affects the efficiency of the components such as subsurface control valves (SSCV), electrical submersible pumps (ESPs) and hydraulic actuators. There are also economic consequences of scale formation. It can result in reduced oil productivity as well as high maintenance costs [39].

Surface deposition of scale can be separated into two different mechanisms: "a deposition process" which includes heterogeneous nucleation and growth due to roughness and an "adhesion process" which is termed as the adhesion of seed crystals which have been precipitated in the bulk solution and accumulates on the surface [39].

2.1.1 Process of scale formation

The formation of inorganic scale usually takes place as a result of supersaturation of the solution, induction, nucleation and growth of the crystals as illustrated in Figure 2. 1[40]. These processes and previous work which considers each phenomenon are described in this section.

2.1.1.1 Supersaturation

Scale forms when the salts which are denoted as scales exceeds their solubility. This is why the driving force for crystallisation is known to be supersaturation. A supersaturated solution is an unstable solution that contains more of a solute in a solution than it can hold at a particular temperature. It can be prepared by cooling of an unsaturated solution and by isothermal evaporation of a solvent or by the mixing of two or more incompatible streams such as mixing of sulfate rich injection water with barium rich formation waters as part of a water flood programme [41].

The kinetics of scale formation is dependent on the level of supersaturation of the aqueous solution. Low solubility leads to a supersaturated solution, resulting in precipitation of scale. What is important about the scale is that the tendency is well understood but the rate is not.

Supersaturation has to occur before nucleation, crystal growth and polymorphism. Therefore, a good understanding of supersaturation is important in developing an accurate model to predict the kinetics of scale formation.

The tendency for scale to form is a measure of its saturation ratio (SR) which is the product of the concentration of dissolved ions divided by the scale solubility product [42]

$$\mathrm{SR} = \frac{\mathrm{IAP}}{\mathrm{K_{SP}}} \tag{1.10}$$

where IAP is denoted as the product of ion activity and K_{sp} is the solubility product.

In the case of $CaCO_3$ or any other scales, SR is important in determining the induction time, nucleation, growth, crystal morphology and rate of scale formation. To determine the kinetics of scaling, it is important to understand the rate at which the Ca^{2+} in the solution is reducing and from this it can be assumed that the scale formation is progressing. In many studies this is done by monitoring the Ca^{2+} with AAS (atomic absorption spectroscopy) tests and determining the corresponding SR for each Ca^{2+} ion at different intervals [43]. The SR can be calculated as a function of the pH of the solution and the activity coefficient, which is obtained with the Davis equation [44].

$$\mathrm{SR} = \frac{[\mathrm{Ca^{2+}}][\ \mathrm{CO_3^{2-}}]}{\mathrm{K_{SP[CaCO_3]}}} \tag{1.11}$$

Scaling tendency can also be defined in terms of SI, which is the logarithm of SR is given as [45]:

$$\mathrm{SI} = \log_{10} \mathrm{SR} \tag{1.12}$$

Both SR and SI provide information about the tendency for scale to form. This means they only consider the thermodynamics of the scaling system. In the oil and gas industry, SR varies for different brines for different oil fields due to its dependence on temperature, pressure and ionic strength.

Once a solution is supersaturated, nucleation and crystal growth can proceed, the diagram indicating these stages is shown in Figure 2. 1. Prior to nucleation, an induction process has to occur, discussed in the following section.

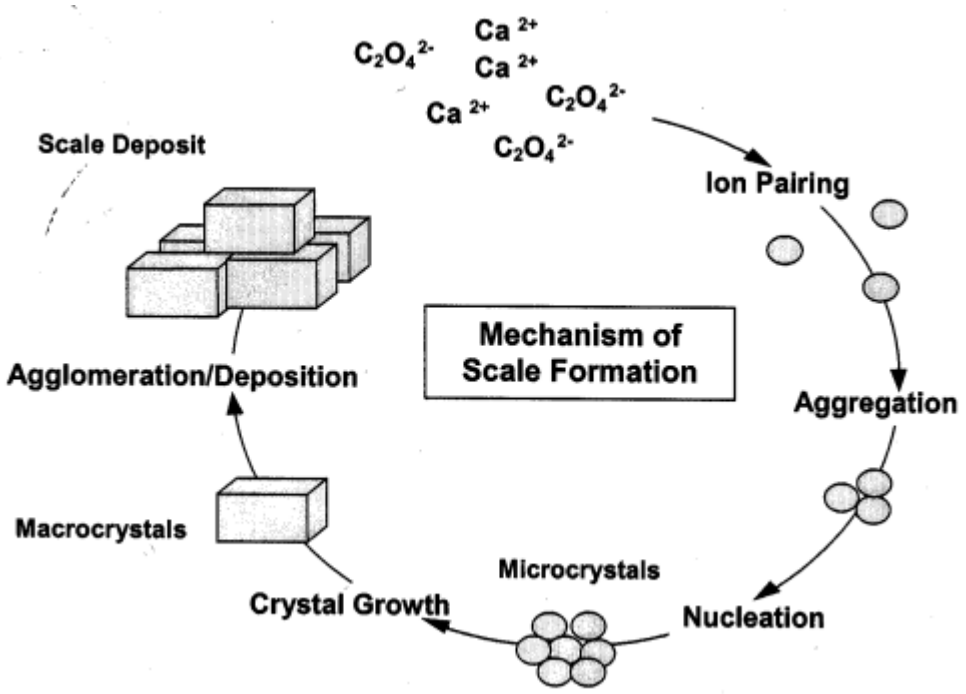

Figure 2. 1– Illustrating the stages necessary for crystal growth and deposition of $CaCO_3$ to occur from a supersaturated solution[40].

2.1.1.2 Induction time for inorganic scale

Induction times are defined in many different ways. Often it is defined as “the time necessary to initiate nucleation of crystals from a supersaturated solution” [46].

The equation for induction time from the classical nucleation theory is presented in equation (1.13) [46];

$$\ln t_{(ind)} = \frac{B}{T^3\ (\triangle G/RT)^2} - \ln A \qquad (1.13)$$

$$\ln t_{(ind)} = \frac{B}{T^3\ (\log SR)^2} - \ln A \qquad (1.14)$$

The free energy barrier, $\triangle G^O$ for the formation of the critical nuclei is proportional to (ln SR) $^{-1}$, where SR is the saturation ratio. The Gibb's free energy, $\triangle G$ of the supersaturation solution is equal to (–RTln S) where R = gas constant, T= temperature, A is an empirical constant (dimensionless) and B is a geometric factor of $16\pi/3$ (for spherical nucleus). Hence, the modified equation for induction time is shown in equation (1.14) and B is determined by using equation (1.15):

$$B = \frac{\gamma^3 V_m^2\ N_A^2\ f(\theta)}{(1.3R)^3} \qquad (1.15)$$

Where, $f(\theta)$ is a correction factor according to the type of nucleation taking place, V_m is the molecular volume (6.132 x 10^{-23} cm^3) for calcite, T is the absolute temperature (Kelvin), R the gas constant (8.3146 J/mol.k), y is the surface energy (mJ/m^2) and N_A is Avogadro's number (6.022 x 10^{-23}/mol) [46].

The theoretical equation for induction time (in equation 1.13) was developed by assuming homogenous nucleation. It has been reported that estimating the likelihood for homogenous nucleation to occur is almost impossible because most solutions are usually not free of foreign particles and most surfaces are not perfectly smooth. In addition, the induction time equation does not consider the effect of surface or flowrate. These factors have a significant effect on the induction time [46]. It is therefore necessary to study the effect of surface, flowrate, brine chemistry and surface area on the induction time of calcium carbonate.

It is also important to note that the time taken to initiate crystal formation depends on the methods used to detect the crystals. Induction times have been measured by many techniques from turbidity to optical techniques. For example, a photo calorimeter can be used to measure the intensity of the light through a solution in order to have an indication of the induction time [47]. In addition, the time it takes for the first crystal to appear on a surface is determined as the induction time using the once-through flow visualisation rig [48].

Figure 2. 2, showed that at high supersaturation the induction time was shorter and at low supersaturation a longer induction time for $CaCO_3$ nucleation in the solution was observed.

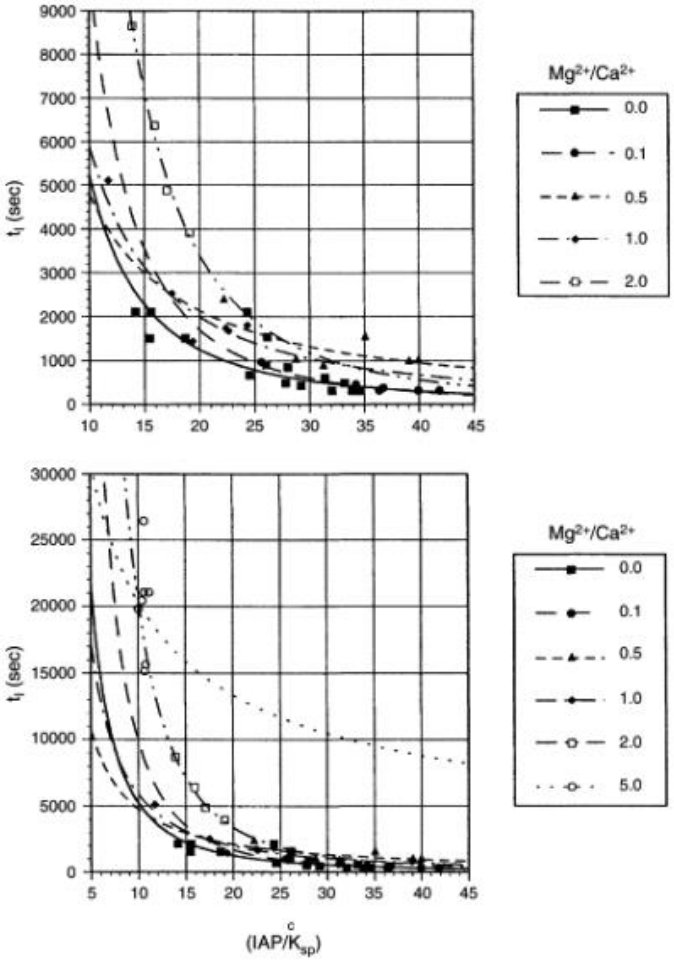

Figure 2. 2 - Calcium carbonate induction time vs the supersaturation for solutions containing magnesium to calcium ions concentrations ratios of a) 0 to 2 and b) 0 to 5[49].

The presence of magnesium was observed to reduce the growth rate of calcite by adsorbing onto the nucleation site and inhibiting the growth of calcite. The expression for this inhibition process is presented in equation 1.16 [49].

$$\frac{k_O}{(k_O - k)} = 1 + k_d \left(k_a T_{Mg^{2+}} \right)^{-1} \qquad (1.16)$$

Where, k_a and k_d denote the rate constants for adsorption and desorption of the magnesium ions on the growth sites, K_O and K are the crystallisation growth rate constants without and with the presence magnesium ion respectively and $T_{Mg^{2+}}$ is the total magnesium ion concentration present in the system [49].

The above correlation was expected; what is difficult to achieve currently is a prediction of the induction time for a range of different solutions and conditions.

This is especially true when low saturation ratio solutions are concerned. At SR below 10 it was observed that calcium carbonate could not precipitate without the presence of a growth surface [49]. It is important to recognise that the induction time for low SR solutions is very important. It could be the case that the induction time is so long that it is very unlikely that the formation of crystals will occur. Currently for low SR solutions (SR 2 – 10) there is no technique reported in the literature which can be used effectively examine the kinetics of $CaCO_3$ deposition in a constant flow environment within a reasonable time-frame in the laboratory.

2.1.1.3 Nucleation of inorganic scale

Nucleation is the process that precedes crystallisation, involving the formation of a stable nuclei from a supersaturated solution due to solvent removal or decrease in the temperature of the solution or a melt [50].

Classical Nucleation Theory (CNT) proposes that thermodynamically, a high energy barrier has to be overcome for homogenous nucleation to occur. This is due to the large surface area-to-volume ratio of the nuclei precipitated from the supersaturated solution [51].

a) Homogenous nucleation

This occurs due to ion pairing by electrostatic interaction until a critical size is attained in a highly supersaturation solution, without the influence of any impurities or foreign particles. The crystal grows until it attains the critical size; at this point it is large enough to promote further growth [52].

The free energy equation describing the process of homogenous nucleation is represented by the classical nucleation theory in equation 1.17:

$$\Delta G = \Delta G_S + \Delta G_V = 4\pi r^2\gamma + \frac{4}{3}\pi r^3 \Delta G_V \qquad (1.17)$$

where ΔG is the overall excess free energy associated with formation of the crystalline body, r is radius of the solute (sphere), ΔG_S is the surface excess free energy (a positive quantity proportional to r^2), ΔG_V is the volume of excess free energy particle of solute (a negative quantity proportional to r^3) and γ is the interfacial tension [53].

The term $4\pi r^2\gamma$ represents the surface contribution, which is positive and proportional to r^2, and the term $\frac{4}{3}\pi r^3 \Delta G_V$ represents the volume contribution, which

is negative and proportional to r^3. Crystals which are smaller than the critical size r_c are unstable and will dissolve whilst any larger than r_c are stable and will grow [53].

Figure 2. 3 shows the free energy diagram for nucleation and critical radius. The difference between the interfacial energy and the volume free energy is the critical radius; as the interfacial energy increases the size of the nucleus reduces and can lead to dissolution of the nucleus, whilst if the volume free energy increases this will lead to an increase in the size of the nucleus.

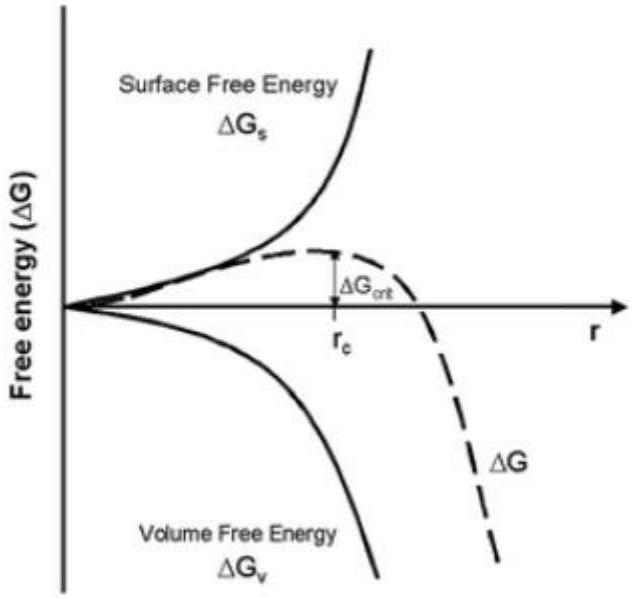

Figure 2. 3 **– Free energy diagram for nucleation and critical radius[54]**.

Nucleation occurs when ΔG reaches a maximum value or critical free energy. The critical free energy relates to the critical radius (r_c), the minimum size for a stable nucleus [55].

b) Heterogeneous nucleation

Zhao et al [56] showed that heterogeneous nucleation was the major cause of $CaCO_3$ formation on metal surfaces. The analysis of the scaling elements obtained from the surface showed that metals such as copper, nickel, and iron were present on the surface. It was also observed that these elements acted as active sites which enhanced the process of heterogeneous nucleation[56].

A study by Sohniel and Mullin [57, 58] provided evidence for the rate of calcium carbonate formation when the nucleation mechanism changed from homogenous to heterogeneous. At low supersaturation heterogeneous nucleation was dominant and homogenous nucleation was dominant at high supersaturation [59]. The CNT was also adapted for the effect of an active site on the rate of nucleation. This

significantly reduced the energy required to initiate the nucleation process. An expression for the free energy during heterogeneous nucleation (ΔG_{Het}) is presented as [60];

$$\Delta G_{Het} = V_s \Delta G_V + A_{LS} \gamma_{LS} - A_{SM} (\gamma_{LM} + \gamma_{SM}) \quad (1.18)$$

Where V_s (m^3) is the volume of the solid spherical cap, ΔG_V is the volume free energy of the solid spherical cap (J/m^3), A_{LS} and A_{SM} (m^3) are the surface areas of the interfaces between the liquid and the solid and between the solid and the mould respectively. γ_{LS} , γ_{LM} and γ_{SM}(J/m^2) are the interfacial energy between the liquid and the solid, liquid and the mould and between the solid and the mould respectively [60].

c) Secondary nucleation

Secondary nucleation differs from homogenous and heterogeneous nucleation processes in that it occurs in the presence of an existing crystal of the nucleating compound [55]. An expression for secondary nucleation as a function suspension density is proposed by the power law [61]. This is shown in equation (1.19).

$$B_{Tot} = k M_T^a N^b \Delta C^m \quad (1.19)$$

Where k is the nucleation rate constant in (µm/s), M_T is the suspension density (g/l), N is the mixing speed (rev/min), ΔC is the concentration driving force (g/l) and a, b and m are constants. The limitation of this equation is that it does not consider the effect of surface on the rate of secondary nucleation [61]. In addition, an industrial crystalliser can be used to demonstrate secondary nucleation. This is due to the collision of crystal molecules in the crystalliser or by contact between the crystals and the walls of the container or the agitation system [62]

The rate of secondary nucleation can be denoted by [62];

$$\frac{1}{v} \frac{dn_2}{dt} = k_{V_2} (C - C^*)^{V_2} \quad (1.20)$$

k_{V_2}Increases with the mass concentration of crystals in the slurry and with the agitation of the system and k_{V_2} decreases as the velocity increases, at low temperature. Where V is the velocity of the system (m/s), k is the growth rate constant (µm/s), C is the mass concentration of crystals (mg/l) at time (t) and C* is the initial mass concentration of the crystals (mg/l). The limitation of this model is

that it does not provide insight into the effect of surface on the rate of secondary nucleation [62].

2.1.1.4 Crystal growth of inorganic scale

Crystal growth occurs after nucleation. It involves the diffusion of molecules towards the surface of a growing nucleus. The rate of diffusion can be affected by temperature, impurities and the saturation ratio [63]. The relationship between growth rate of a crystal and supersaturation can be represented by equation (1.21)[64].

$$G = k_p(S - 1)^n \tag{1.21}$$

where G is the overall growth rate (mmol m^{-2} h^{-1} kg^{-1}), k_p is the precipitation rate constant which depends on temperature and surface area of the crystal, S is the saturation ratio and N is the order of reaction, which is 1 for diffusion-controlled reaction and 2 for surface linear integration mechanisms [64]. The expression for growth rate in equation (1.21) does not account for the effect of flowrate on the precipitation rate.

Furthermore, Reddy et al[65] studied the kinetics of calcium carbonate precipitation in the presence of seed crystals. The tests were conducted by measuring the change in pH with time. The pH range of the solution was between 8.4 - 8.8. They observed that the rate of calcium ion removal from the solution followed a first order reaction rate with respect to the calcium and bicarbonate ions [44]. The kinetic model proposed for the rate of change of calcium ion concentration with time is

$$-\frac{d[Ca]}{dt} = k\,[\,CaCO_3(S)]([Ca^{2+}\,]\,[CO_3^{2-}\,]- K_{sp}\,/f^2d) \tag{1.22}$$

where k is the crystal growth constant ($l.mol^{-1}$ min^{-1})/(mgl^{-1}), [Ca] is the molar calcium concentration (mol/L), [CO_3^{2-}] is the molar carbonate concentration (mol/L) , $CaCO_3$(s) is the crystal mass at any time t (mg/L), K_{sp} is solubility product for $CaCO_3$ (mol^2l^2), f^2d is the activity factor for divalent ions[44].The limitation of this model is that it does not account for the effect of surface on the kinetics of calcium carbonate precipitation.

There are different types of scales experienced in the oil and gas industry, as shown in Table 2.1 [66].

Table 2. 1 - Common oilfield scales[66]

Mineral	Formula
Anhydrite	$CaSO_4$
Aragonite	$CaCO_3$
Barite	$BaSO_4$
Calcite	$CaCO_3$
Celestine	$SrSO_4$
Galena	PbS
Gypsum	$CaSO_4$
Mackinawite	FeS
Pyrite	FeS_2

These different types of scales are formed due to several factors, which are summarised in Table 2.2 [66].

Table 2. 2 - Causes of scale formation

Causes of scale formation	**Chemical Name**	**Mineral name**
Loss of dissolved gases	Calcium carbonate	Calcite, aragonite, vaterite
Solution of gases	Ferric, hydroxide, Ferrous sulfide	Goethite, Amorphous iron sulfide
Commingling of water	Barium sulfate, strontium sulphate, calcium sulphate, calcium carbonate	Barite, Celestine, calcite
Heating without evaporation	Calcium carbonate, calcium sulfate, mixed iron oxide	Calcite, aragonite, gypsum, anhydrite, magnetite
Cooling of water	Barium and strontium sulfate	Barite

This project is concentrated on the study of $CaCO_3$ and will not address other scales. The results and developed methodologies are however relevant to other types of scale because the framework for the study could be easily adapted for the study of other scales. Scale formation can occur both in the bulk solution and on the surface. These phenomena are explained in the next section.

2.2 Scale formation in the bulk solution

The precipitation of calcium carbonate scale in the bulk solution is a very common occurrence in the oil and gas, water transport and power generation industries.

This is caused by the formation of sparingly soluble inorganic salts from aqueous solution [67].

It is important to understand the kinetics of crystallisation of calcium carbonate in the bulk solution to determine if the crystallisation process on the surface is influenced by $CaCO_3$ deposition in the bulk solution or if the scale formation process is exclusively controlled by $CaCO_3$ deposition on the surface [68].

The current scale prediction tools are mostly based on thermodynamic principles which assumes the reaction reaches thermodynamic equilibrium which in practice may not happen with some scales. In addition, the thermodynamic models do not provide any information on the rate at which scale precipitation will occur [69].

Previous studies on bulk precipitation have shown that amongst other factors, saturation ratio and temperature play a major role to the rate of $CaCO_3$ formation in the bulk [70]. Others have addressed the effect of inhibitors on the rate of calcium carbonate formation [71]. Some of the factors causing scale formation in the bulk solution are explained in the next section.

2.2.1 Factors affecting scale formation in the bulk solution

Scale formation in the bulk can be affected by various factors which are described below.

2.2.1.1 Temperature

The solubility of calcium carbonate reduces as temperature increases. This is unusual in comparison to other chemical compounds such as sodium chloride [45]. The scaling potential of calcium carbonate also increases with an increase in pH because the solution becomes less acidic due to the concentration of the bicarbonate ions [72].

Figure 2. 4 shows the effect of temperature on the polymorph of $CaCO_3$ precipitated. The results show that calcite is the most stable phase at low temperature and the least stable phase is vaterite. The effect of temperature on scaling in oil and gas production was also studied by Dyer et al [73]. It was reported that the scaling tendency of carbonate brines increased with the increase in temperature, while sulphate scale precipitation reduced as temperature increased.

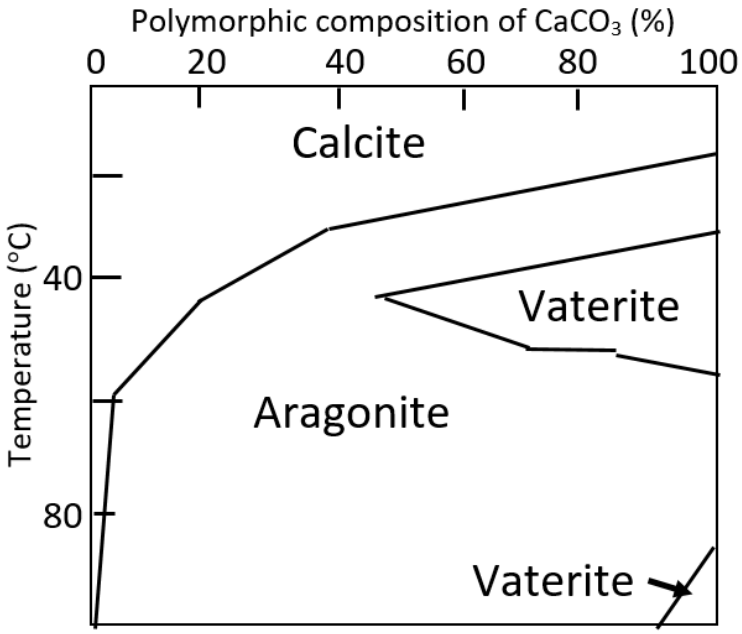

Figure 2. 4 - Calcium carbonate polymorphs as a function of temperature[74]

Wided et al. [75] also conducted a study on the effect of temperature on the kinetics of calcium carbonate. The methodology used to carry out the study was atomic absorption spectroscopy, X-ray diffraction and scanning electron microscopy. At constant temperature and brine composition, the presence of magnesium ion in the solution increased the induction time for calcium carbonate precipitation and led to a reduction in the growth-rate of calcium carbonate formation. However, at higher temperature the growth rate of calcium carbonate increased in the presence of magnesium ions. The results showed that an increase in temperature alters the effect of magnesium ion on the precipitation of calcium carbonate and temperature plays a major role in increasing the kinetics of calcium carbonate formation due to the inverse solubility relationship between temperature and calcium carbonate precipitation. The polymorphs of the crystals formed were analysed and aragonite crystals were observed at high temperature in the magnesium solution. The limitation of this study is that there is a gap in understanding the effect of temperature on the induction time of low SR solutions between (2–10).

2.2.1.2 Flow velocity and hydrodynamic conditions

Flowrate plays an important role on the kinetics of scale formation in the bulk solution. An increase in flowrate has been reported to increase the rate of scale formation in pipes, this can be attributed to a more effective mixing of the brine which promotes the deposition of scale. The effect of flowrate on the morphology

of calcium carbonate also shows that at supersaturation ratios greater than 7, the formation of elongated (columnar) and calcite crystals was favoured [76].

The effect of flowrate on salts such as calcium sulphate has been previously modelled by computational fluid dynamics. The tests were carried out at constant temperature in order to examine the effect of flowrate at laminar and turbulent flow conditions. It was reported that reducing the flowrate resulted in an increase in the residence time. The formation of sparingly soluble salts increased in the region where the residence time was longer [77]. Flowrate has a major impact on the kinetics of scale formation and there is inadequate research on the effect of velocity on the of fouling rate of calcium carbonate in the bulk solution [77].

The flow regime used in the study was laminar and the flowrates used were 30, 40 and 50ml/min. A schematic diagram of the rig used is shown in Figure 2. 5 . It comprises of two stainless steel vessels (1 and 2) which contained the calcium carbonate brines, the pumps used are represented by 3 and 4, and the test pipe where growth of the scale occurred is shown in 5.

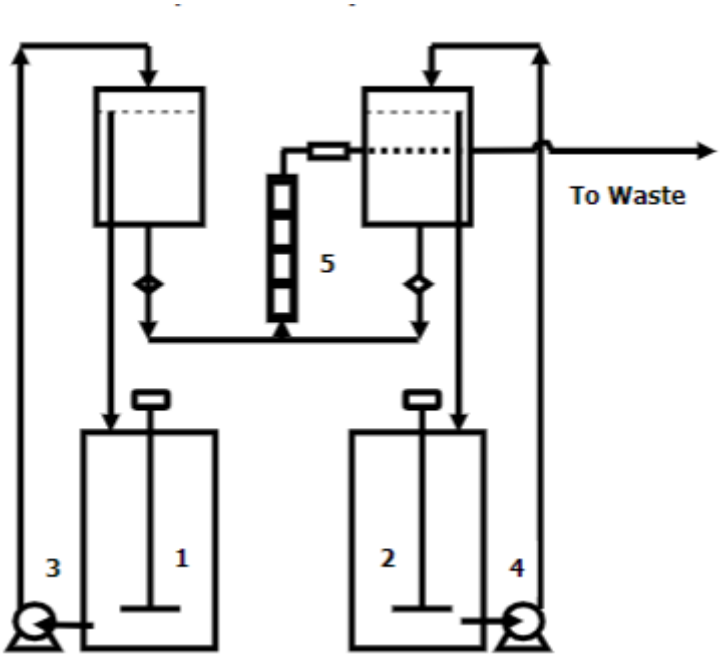

Figure 2. 5 **- Schematic of the rig used for calcium carbonate scale experiment[36].**

The effect of flowrate and malic acid concentration on the growth rate of $CaCO_3$ scale was studied. Conductivity measurement was adopted to monitor the process of scale formation in this test. This was carried out by detecting the conductivity of the solution in the outlet of the system. In addition, the growth rate of the crystal was determined by measuring the weight of the scale mass deposited on the surface of the coupons per hour. The result shows that as the flowrate increased

the growth rate of $CaCO_3$ increased, also as the concentration of malic acid increased the flowrate generally decreased. This is presented in Table 2.3 [36].

Table 2. 3 - Growth rate (gr/hr) of calcium carbonate under the influence of malic acid at different concentrations [36].

Malic acid concentration (ppm)	30ml/min	40ml/min	50ml/min
0	0.038	0.041	0.046
3	0.022	0.032	0.040
5	0.016	0.019	0.032

Flowrate also increases the efficiency of inhibitors on heat transfer surfaces, and in the absence of an inhibitor, the potential for scale to form increases. Hence, at high velocity, more inhibitor molecules are absorbed onto the growing $CaCO_3$ surface [78].

2.2.1.3 Effect of SR on bulk precipitation

Saturation ratio is widely known to be the driving force for scale formation as mentioned earlier in Section 2.1. Tao et al [79] studied the effect of different SRs (SR 18 - solution A, SR 4 – solution B and SR 1.1 – Solution C) on the early stages of $CaCO_3$ scale precipitation in the bulk solution under static conditions; by using ICP (Inductively Coupled Plasma) to measure the calcium ion concentration in the solution over a period of 24 hours at 20^{o}C. The SR of the solution was calculated by using ScaleSoft-Pitzer^{TM} software from Rice University.

The findings from the ICP analysis provided evidence for the formation of $CaCO_3$ in the bulk solution at SR 18 and SR 4. However, at SR 1.1 there is no evidence for bulk precipitation in the solution after 12 hours. Additionally, the induction time for bulk precipitation was observed to be less than 1 hour for SR 18 and SR 4, this suggests that the time for scale formation is shorter at a higher SR compared to a lower SR. Furthermore, for SR 18 after 8 hours, the kinetics of scale formation in the bulk solution began to reduce steadily, after rapidly increasing initially. This was attributed to the reduction in the SR with time in solution as the experiment was carried out under static conditions.

Sanni et al [80], also investigated the kinetics of $CaCO_3$ precipitation in the bulk solution for SR 10, 15, 25, 45 and 60 at 25^{o}C and a flowrate of 20ml/min by measuring the turbidity of the solution. The experiment was carried out with the *in-situ* visualisation flow cell[48]. The SR of the solution was determined using

Multiscale software. In contrast to the findings from Tao et al research, after the 4 hour duration of the test, a turbidity value of zero was detected for all the SR studied, which indicates that there was no precipitation of $CaCO_3$ in the bulk solution regardless of the SR. These results illustrate that the different techniques used for assessing the kinetics of $CaCO_3$ formation in the bulk solution proposed a different induction time and demonstrate the need for a reliable technique for quantifying scale formation especially at low SR conditions.

Moreso, Mavredaki et al [81], also examined the effect of SR on the kinetics of $CaCO_3$ in the bulk solution by using a turbidity meter. The range of SR investigated was from SR 1.5 – SR 55, the SR of the brine was determined with the Multiscale software. The experiment was conducted in a jacketed vessel at 80^oC.

In agreement with the study from Tao et al. [35] induction time reduced as SR increased, and a measurable induction time of 64 minutes was observed for SR 1.5, which can be attributed to the increased temperature used in this experiment. This suggests that a higher temperature can be useful for quantifying scale formation at very low SR.

Furthermore, the graph of turbidity versus time in Figure 2. 6 for SR 4.8 – SR 54.8, shows that initially there was a notable increase in the turbidity of the solution with time, this increase is more evident above SR 6. Afterwards, the turbidity progressed slowly until stabilisation was achieved.

The rapid increase observed initially is attributed to the nucleation of $CaCO_3$ crystals from the bulk solution. Subsequently, the region where the turbidity reduced slowly corresponds to the onset of the crystal growth stage and finally stabilisation of the turbidity value is attained which indicates that the solution has attained equilibrium and no further precipitation of crystals from the solution can occur.

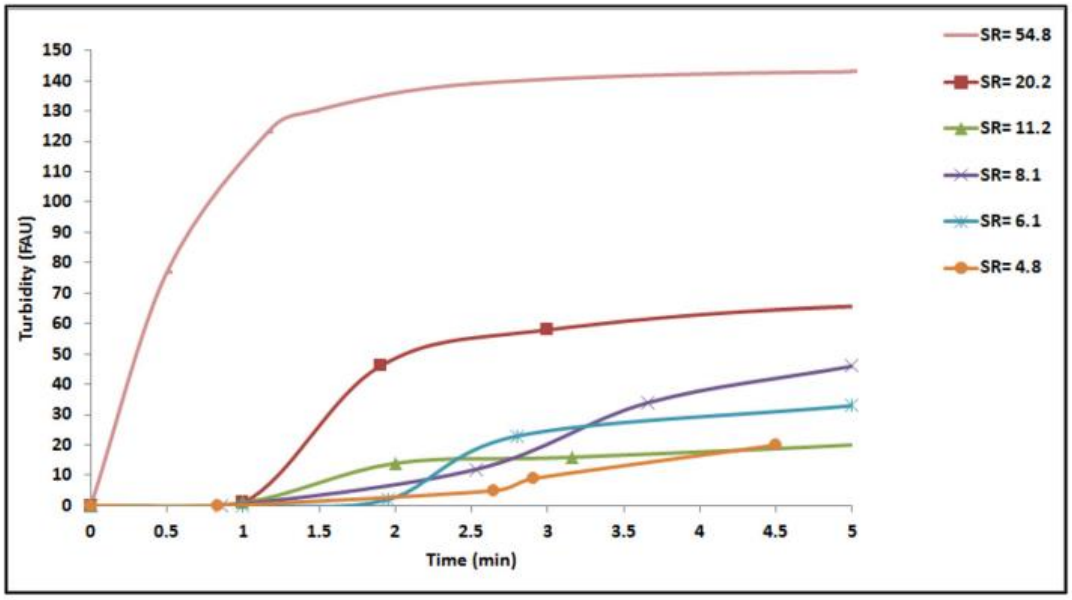

Figure 2. 6 - The effect of SR on bulk precipitation kinetics determined by carrying out turbidity measurements, the result shows an increase in bulk precipitation as SR increased at 80°C [44].

It is also important to consider how the SR of the solution was determined and the underlying thermodynamic principles of the scale prediction tools adopted for calculating the SR of the solution, because the ionic composition of a solution could vary for the same SR depending on the software used to calculate the SR of the solution.

2.2.1.4 Solution chemistry

This is also known as water composition, which affects the precipitation kinetics of calcium carbonate from a solution [82]. For example, the effect of zinc ions on the rate of nucleation and crystal growth of calcium carbonate was studied in the water of a town called Hamma, which is noted for its high scaling tendency. The tests were carried at 0.05, 0.1 and 10mg/L concentrations of zinc. The results showed that the presence of zinc ions resulted in a decrease in rate of crystallisation of calcium carbonate. In addition, it was observed that zinc ions also changed the morphology of the crystals in the solution. This study confirms the inhibition characteristics of zinc in the crystallisation of calcium carbonate [83].

The methodology adopted to monitor the scaling process was electro-crystallisation. The experimental set-up consisted of an electrochemical cell and a video set-up. The electrochemical cell was made of an electrode of stainless steel, a PMMA plate which worked as the counter electrode and silver wire acting as

silver chloride electrode. The video setup was used to monitor the rate of scale coverage on the surface [83].

In Figure 2. 7, the surface coverage of the electrode in the water with the high scaling tendency was compared to the surface coverage of the electrode when zinc ions were added. The result showed that when 0.01mg/L of zinc ions was added, the difference in the surface coverage of the electrode compared to the reference water was small. However, a larger difference in the surface coverage was observed when a high concentration of zinc (10mg/L) was added to the reference water. This indicates that high concentrations of zinc ions in a solution lead to a faster reduction in the nucleation rate of calcium carbonate compared to the presence of lower concentrations of zinc [83].

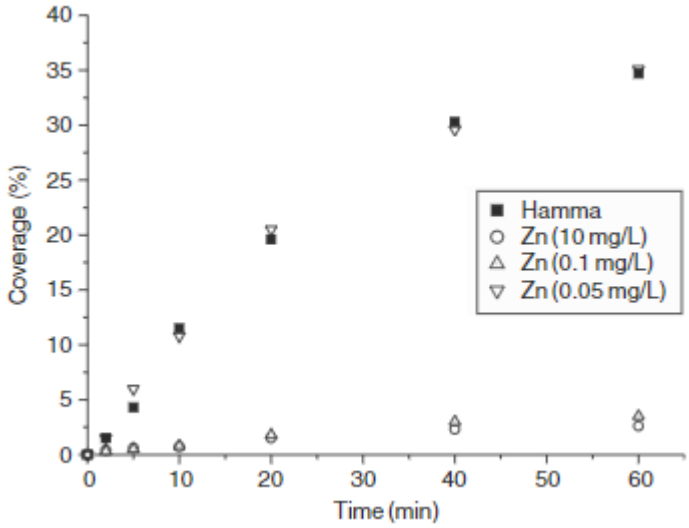

Figure 2. 7 – Rate of covering of the working electrode [47]

2.2.1.5 Effects of impurities

The effect of impurities on the precipitation of calcium carbonate in the bulk solution is of major interest to the oil and gas industry. A significant amount of research has been undertaken to understand this phenomenon. However, there is still a gap in predicting the best method of obtaining a product with desired characteristics [29].

Mullin and Sohnel [29] reviewed the effect of specified impurities on the kinetics of calcium carbonate precipitation. The impurities selected have been commonly experienced in the oil and gas industries. The impurities studied included Mn^{2+}, Br^{-}, Cl, F and NO_3. The effect of these impurities on the induction time of calcium carbonate was observed. The results indicate that only Mn^{2+} ions have a noticeable effect on the formation of calcium carbonate by increasing the induction time at low

supersaturation. In addition, at low supersaturation there was an increase in the induction time as the Mn^{2+} ions concentration increased [29]. On the other hand, Br^-, Cl, F and NO_3 did not have a detectable effect on the induction time at low SR. This study provides insight into the effect of impurities on induction time at low SR (SR 5-7), but it provides no information on the effect of surface on the induction time of $CaCO_3$.

Furthermore, the presence of magnesium ions in the formation water was found to increase the induction time of $CaCO_3$ [84] This is illustrated in Figure 2. 8, showing that as the concentration of magnesium increased the induction time also increased. In addition, the effect of magnesium on the polymorph of calcium carbonate scale formed showed that it incorporates into the calcite growth site and increases the solubility of impure calcite, which results in aragonite being kinetically favoured to precipitate [85].

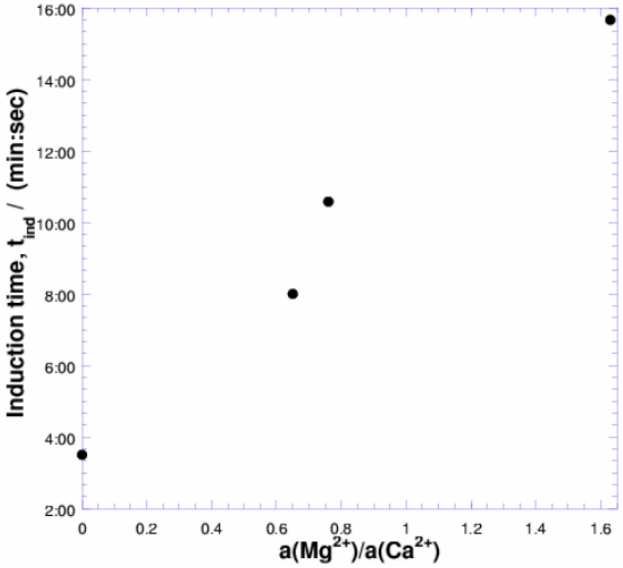

Figure 2. 8 - Induction time versus aMg^{2+}/aCa^{2+} at 80^{o}C [50].

Bulk precipitation of $CaCO_3$ can be studied in the laboratory by monitoring the calcium ion concentration, turbidity measurement [28, 65] and pH measurements [30] in supersaturated systems. These methodologies are explained in this section.

2.2.2 Experimental studies of the bulk scaling phenomenon

In this section, commonly used experimental methodologies for determining the rate of scale formation in the bulk solution are explained.

2.2.2.1 The effect of pH

pH has a significant impact on kinetics of scale formation. When calcium carbonate precipitates, the pH of the solution decreases due to reduction in the carbonate ions concentration in the solution. The ionic interaction between the calcium and bicarbonate species in the solution can be monitored by measuring the pH at different time intervals [86]. A pH meter can be used for pH measurements [87].

Saksono et al [88] studied the effect of pH on the precipitation of calcium carbonate under the influence of magnetic field. The results showed that at high SR (pH 8.5) there was a fast rate of nucleation of calcium carbonate, because an increase in the pH of a solution supports an increase in the concentration of hydroxide ions (OH^-) in the solution which reacts with the calcium ions present in the solution to form ($Ca(OH)_2$). This leads to an increase in the calcium ion concentration in the solution which reacts with the carbonate ions (CO_3^{2-}) to form calcium carbonate. However, at a low SR (pH 6.4), the rate of formation of calcium carbonate is reduced as a low pH does not encourage the release of hydroxide ions from the solution, thereby reducing the tendency for nucleation of calcium carbonate crystals to take place [88].

Figure 2. 9, compares the total precipitation of $CaCO_3$ (%) at different pH under a magnetic field. The results shows that more $CaCO_3$ precipitated from the solution when magnetic treatment was applied in comparison to the absence of a magnetic field (i.e. non –magnetic treatment) at all the pH (i.e. pH 6.4 – 8.5) values investigated. A plausible reason for this is because magnetisation increases the tendency of the scaling ions in the solution to react together which support the precipitation of $CaCO_3$, in contrast to the absence of magnetic treatment[88].

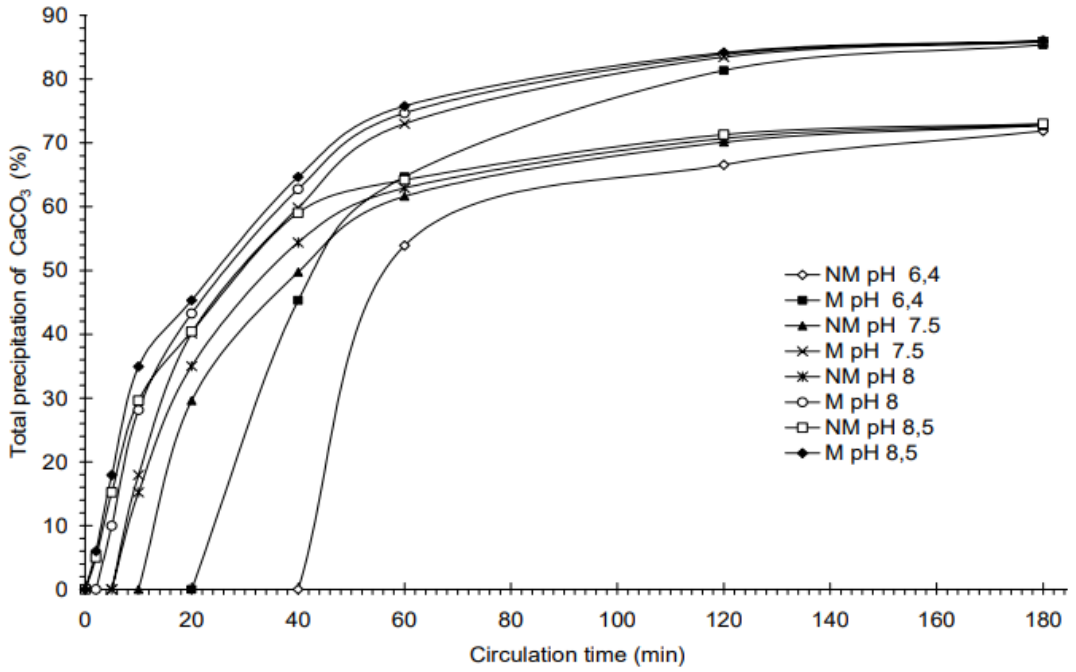

Figure 2. 9 – Total precipitation of calcium carbonate as a function of pH at different circulation times on a non-magnetised (NM) sample and a magnetised sample (M) [88].

The measurement of the pH of a solution has shown to be beneficial for assessing the kinetics of $CaCO_3$ precipitation in the bulk solution[89]. Nonetheless, the limitation of this technique is that the accuracy of the pH measurements can be influenced by changes in temperature, pressure, and concentration of ions the solution, therefore, all these factors needs to be carefully considered before using this technique [90].

2.2.2.2 Measurement of calcium ion concentration

Monitoring the changes in calcium ion concentration, which can be done by Atomic Absorption Spectroscopy (AAS) [91], can be used to study the precipitation process of $CaCO_3$ in the bulk solution. As $CaCO_3$ precipitates, the calcium ion concentration in the solution decreases [44].

In a study by Sanni et al [92], static jar test was used to determine the minimum inhibitor concentration (MIC) for calcium carbonate brines, setting a benchmark inhibition efficiency of 90%. The experiment was conducted by measuring the change in calcium ion concentration with time, assuming that as the calcium ion concentration in the bulk solution decreases, calcium carbonate is being produced. From the study at SR 126, the MIC was observed to be 1ppm while the MIC was higher than 8ppm at SR 631. These results suggest that an increase in SR requires

a corresponding increase in MIC in order to effectively inhibit the formation of scale in the bulk solution [92].

Seegar et al [93] also determined the calcium ion concentration of solutions with low levels of crude oil by using AAS. It was reported that the AAS technique was effective in predicting the calcium ion concentration in the solution, it was quick and easy and it also reduced the tendency for contamination of the solution [93].

The rate of formation of calcium carbonate can be followed by measuring the calcium ion concentration and the degree of precipitation (α) is defined as [65]:

$$\alpha = \frac{([Ca^{2+}]_0 - [Ca^{2+}]_t)}{[Ca^{2+}]_0} \quad (1.23)$$

Where $[Ca^{2+}]_0$ is the calcium concentration at time 0 and $[Ca^{2+}]_t$ is the calcium concentration at time, t [94]. This methodology has shown to be useful for effectively assessing the kinetics of $CaCO_3$ precipitation in the bulk solution. However, the limitations of the method is that the mandatory sample preparation procedure which includes preparation of the standard solutions, sample dilution and extraction can be time consuming, also the presence of interferences in the solution lead to inaccuracies in the measurements of the ions in the solution[93].

2.2.2.3 Turbidity measurements

This technique measures the intensity of light passing through a solution. The light transmitted through a solution corresponds to the concentration of particles suspended in the solution. This method is also easy and low cost, and can be used to determine the rate of nucleation and growth of crystals [95].

Turbidity measurement provides insight into the solubility of some chemical compounds and their average size. In addition, the polymorphic transformation of crystals can be studied using turbidity measurements [95]. Other studies have used turbidity measurement to determine the induction of time of bulk solutions. The time it takes for the turbidity to change from 0 to 1 gives an indication of the induction time of the solution [96].

The once through flow cell which is used to quantify the kinetics of inorganic salts, uses a turbidity probe to measure the induction of the bulk solution. The rate of scale formation in the bulk solution can also be monitored using this technique as well[68]. For instance, In a previous study conducted the *in-situ* visualisation cell,

the kinetics of $CaCO_3$ precipitation in the bulk solution was examined by performing turbidity measurements, the results showed evidence for $CaCO_3$ precipitation in the bulk solution at SR 60 and 40^oC as the turbidity of the solution increased from 0 to 28 FTU (Formazine Turbidity Unit) at the onset of the experiment [97].

However, there was no evidence of $CaCO_3$ precipitation in bulk solution at SR 10, SR 15, SR 25 and SR 45 at 40^oC, as the turbidity value at these SRs remained at zero for the entire 4hour duration of the experiment[97]. This indicates that turbidity measurements is useful for quantifying the kinetics of $CaCO_3$ precipitation at high SR(above SR 60) at low temperature, but it is not suitable for tracking the kinetics of $CaCO_3$ precipitation in the bulk at low SR and low temperature. Therefore, in this study turbidity measurements not performed with the *in-situ* visualisation cell because this study is focused on understanding kinetics of $CaCO_3$ formation at low SR and low to mid-range temperatures.

Instead, Atomic Absorption Spectroscopy (AAS) technique was used in this study to determine the kinetics of $CaCO_3$ precipitation in the bulk solution, by measuring the change in the calcium ion concentration ($\Delta\ Ca$) in the solution with time. This methodology was selected because earlier observations in literature has shown that tracking the ($\Delta\ Ca$) in the solution with time, which can be carried out with ICP (Inductively Coupled Plasma) or AAS is effective for obtaining quantifiable data on the kinetics of $CaCO_3$ precipitation in the bulk solution at low SR (i.e. SR 18, SR 11 and SR 1.1)[35].

2.3 Scale formation on solid surfaces

Studies on the surface scaling phenomenon have received a lot less attention compared with bulk scaling mechanisms. However, scaling problems are usually a result of scale deposition on tubular or equipment surfaces[71]. This contributes to corrosion and flow restrictions in oil and gas pipelines which reduces productivity.

It is important to be able to predict the kinetics of scale formation on solid surfaces in order to manage better the issues relating to scale formation. Currently, there is no kinetic model for predicting the rate of scale formation on surfaces. There is extensive research on the thermodynamics of scale formation which provides information on the amount and type of scale expected to form, but it does not account for the rate of scale deposition on surfaces[68].

Previous studies have provided insight into the effect of inhibitors, temperature and brine composition on the rate of scale deposition[48], but there is inadequate understanding on the interplay between bulk precipitation and surface deposition. Some common causes of scale formation on solid surfaces are discussed in the next section.

2.3.1 Factors affecting scale formation on surfaces

2.3.1.1 Surface roughness and wettability

Roughness is defined as an estimate of the finely spaced micro-irregularities on a surface texture. The three parameters used to describe the texture of a surface includes roughness, waviness and form [98].

Wettability is the measure to which a solid can remain in contact with a liquid. The intermolecular interaction of the adhesive type (liquid to surface) and cohesive type (liquid to liquid) determines the wettability of a surface [99].

Contact angles can be used to measure wettability. A surface with contact angle less than 90^oC is considered hydrophilic, while contact angle values greater than 90^oC are generally hydrophobic [99].

Orkoula et al. studied the wettability of calcium carbonate deposited on glass slides. The effect of supersaturation and temperatures on the contact angles of the glass slides was observed [100]. The results show that the surface coverage and mass of calcium carbonate on the glass slides increased as the supersaturation (SR) increased, due to the faster rate of scale deposition on the surfaces at high SR. This is presented in Figure 2. 10 [100]. The contact angles also reduced as supersaturation increased, as shown in Figure 2. 11, due to an increase in the mass and surface coverage of scale deposited on the glass at high SR.

The effect of temperature on contact angle was also observed and is shown in Figure 2. 12. The results indicate that as temperature increased, the mass and surface coverage of the scale deposited on the surface also increased which led to a reduction in the contact angle. This confirms that the more hydrophilic a surface becomes, its contact angle reduces because the wettability of the surface improved with increase in temperature [99]. In addition, as temperature increased the level of supersaturation also increased, which caused more deposition of calcium carbonate on the surface and resulted in a decrease in the contact angle [100]. There is a gap on the effect of low SR on contact angles.

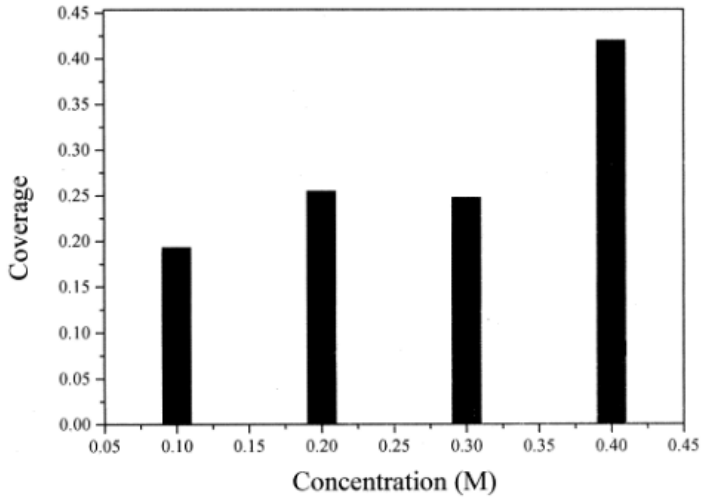

Figure 2. 10 – Dependence of the coverage of glass slides by calcium carbonate concentration (supersaturation) of the aqueous phase with respect to the reacting ions [67].

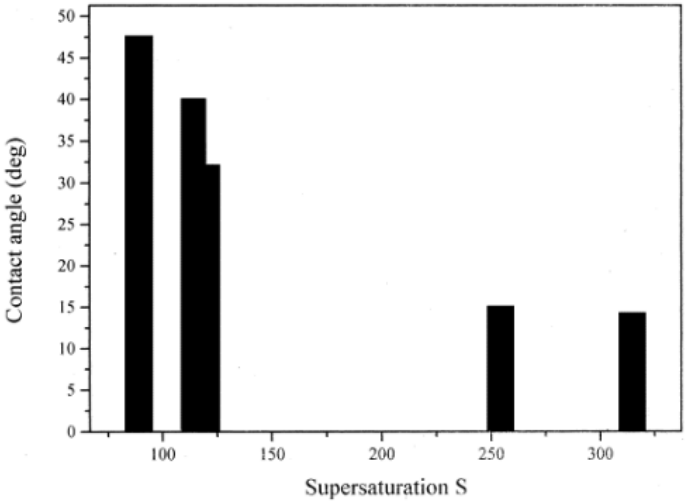

Figure 2. 11 – Contact angle measured as a function of the supersaturation with respect to calcium carbonate concentration of the solution in which the glass slides were exposed [67].

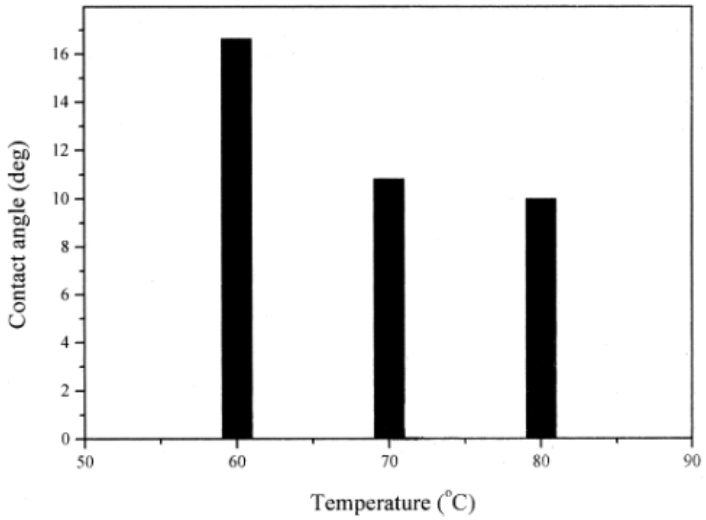

Figure 2. 12 - Dependence of the contact angle measured on calcium carbonate covered glass slides as a function of the temperature of the supersaturated solution [67].

In a study on the effect of surface roughness on the adhesion of $CaCO_3$ on stainless steel surfaces, the analysis of the results identified that the correlation between the roughness of a sample and the ability for scale to adhere to its surface is more complex than previously reported in literature. However, it was mentioned that the corrosion resistance capabilities of the sample is a better indicator for estimating the likelihood for scale deposition to take place on the surface. The surface roughness for samples No.1, No.2, No.3, No.4, No.5 and No.6 was 0.25, 0.18, 0.16, 0.11, 0.06, 0.02 µm respectively. The results also showed that the surface with the least surface roughness cannot improve antifouling property of stainless steel [101], this is shown in Figure 2. 13.

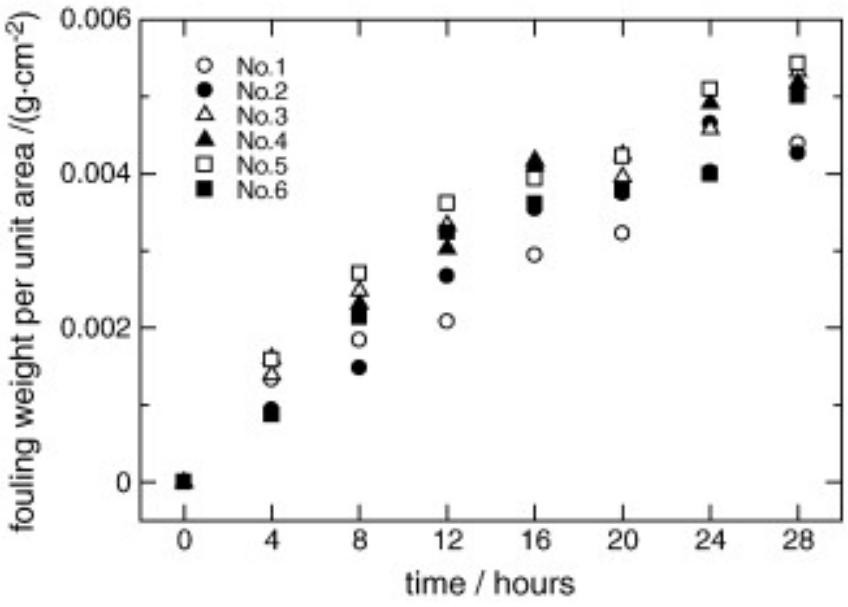

Figure 2. 13 – Fouling rate per unit area versus time for samples with different roughness [68].

2.3.1.2 Effect of SR on surface deposition

SR is well known to be a key factor in controlling the mechanisms and kinetics of scale deposition in the oil and gas industry.

Tzachristas et al [102] used a microfluidic reactor to study the relationship between SR and the rate of $CaCO_3$ deposition on the surface of a microchannel. The experiment was conducted for both SR 40 and SR 61.7 at 25^{o}C, and the image of the crystals formed with time were captured and analysed to assess the particle size distribution with time.

The outcome of the test demonstrated that as expected the induction time reduced as SR increased, which is in accordance with the classical nucleation theory [58]. In addition, at SR 40 there was evidence for progressive nucleation, denoted by the exponential growth observed at the initial stage of the crystal growth with time Figure 2. 14. This implies that both nucleation and crystal growth occurred simultaneously until there were no more nucleation sites available for scale formation to take place, which is illustrated by the region in the curve where growth of crystals starts to plateau.

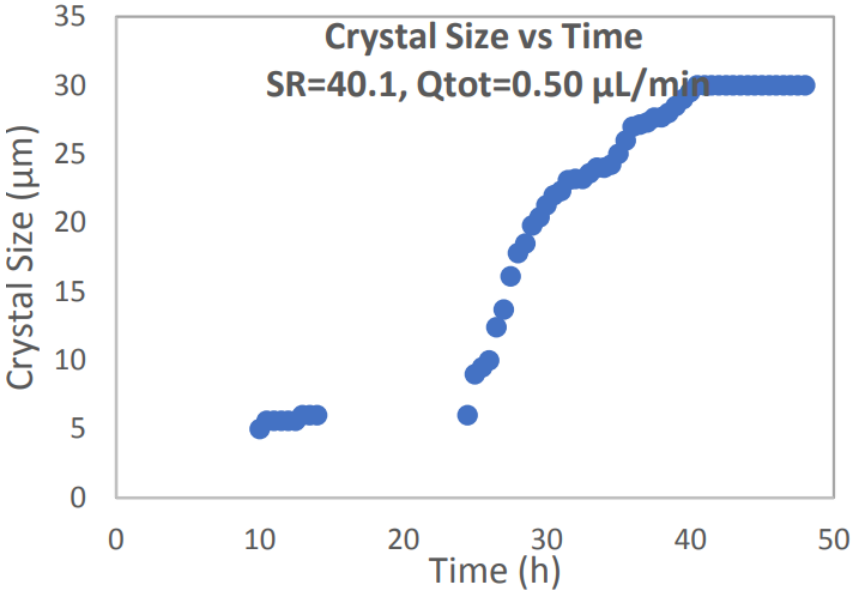

Figure 2. 14 - Crystals size with time for SR 40 using the microfluidics technique [69].

However, at SR 61.7 the crystals nucleated rapidly initially, which is illustrated by the linear relationship observed between the growth of the crystals with time (Figure 2. 15). This is attributed to instantaneous nucleation (where all the nuclei precipitate on the surface prior to the onset of the crystal growth process) of scale experienced at a higher SR. Space resolved Raman spectroscopy was used to identify the morphology of the crystals precipitated on the surface and there was evidence of calcite, vaterite and aragonite polymorphs of $CaCO_3$, but aragonite was more prominent.

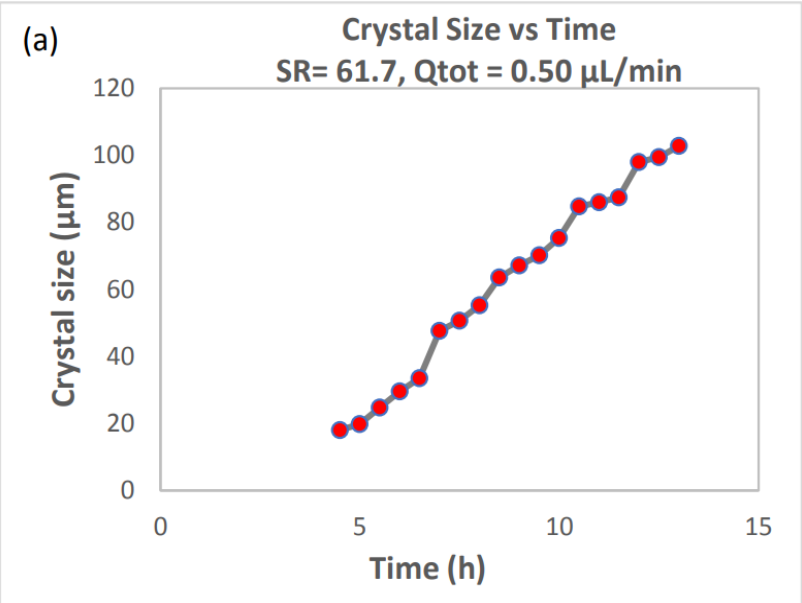

Figure 2. 15 **- Crystals size with time for SR 61.7 using the microfluidics technique [69].**

Similarly, Sanni et al [80] also investigated the effect of SR on the kinetics of $CaCO_3$ scale deposition using the *in-situ* visualisation cell, for SR 10 – SR 90 at 25^{o}C. The results from the study showed that as expected; the number of crystals nucleated on the surface and the surface coverage of $CaCO_3$ on the stainless steel material increased as SR increased. This indicates that the degree of nucleation on the surface increased as SR increased.

Moreso, it was also observed that above SR 60, instantaneous nucleation was dominant, whilst at low SR (below SR 10, SR 15 and SR 25) there was evidence for progressive nucleation and the nucleation process was identified to be exclusively controlled by heterogeneous nucleation [59], which is in agreement with previous work in literature [35, 59, 80, 103]. However, at higher SR the crystallisation process was influenced by both homogenous nucleation of $CaCO_3$ in the bulk solution as well as heterogeneous nucleation on the surface [80].

In line with the previous studies, Raheem et al studied the role of SR on the kinetics of surface deposition on both silainised and non-silanised surfaces using the tube blocking rig and proposed an inverse relationship between induction time and SR on surface deposition. The growth-rate of $CaCO_3$ was also observed to increase as SR increased at a constant flowrate (Figure 2. 16), this is attributed to the increase in the ionic composition of the solution as SR increased[104]

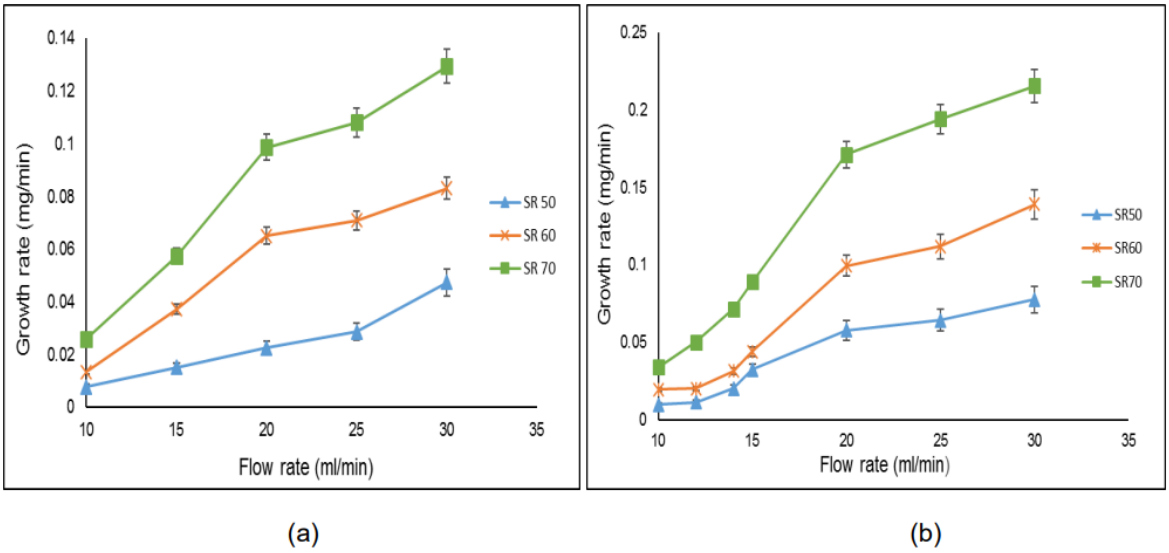

Figure 2. 16 **- Showing the effect of increasing the flowrate and SR on the growth-rate of $CaCO_3$ for (a) silanised surface and (b) non-silanised surface [72].**

The limitation of these research is that it does not provide any insight into mechanisms and kinetics of scale deposition at low SR (below SR 10) and it also does not quantify the difference between the kinetics of bulk precipitation and surface deposition.

2.3.1.3 Surface nature

The effect of substrate nature on the nucleation of colloid crystals was investigated by Guo et al. [105]. The first substrate was an uncoated cover glass, the second was a Pt-coated cover glass and the third was an Au-coated covered glass. The attractive force between the colloidal particle (polystyrene) and the substrate was determined by using atomic force microscopy. It was observed that at constant saturation ratio, nucleation rate was fastest on the uncoated cover glass, followed by the Au-coated glass. The Pt-coated cover glass showed the slowest rate of nucleation. It was proposed that the uncoated cover glass scaled the fastest due to its small interfacial energy change, whilst Pt-coated cover glass scaled slowest due to its large interfacial energy [105].

In addition, the adhesive force which exists between the particles on the uncoated cover glass was the weak Van der Waals forces which resulted in faster rate of nucleation. In the Pt-coated cover glass, a stronger interactive force existed between the particles, which explains the slower rate of nucleation and the large interfacial energy [105].

Figure 2. 17 shows the graph of nucleation rate (J) against area fraction $\emptyset_{area}$ which represents the surface area concentration of the 3 different glasses. The results indicate that the uncoated glass showed the fastest rate of nucleation, followed by the Au-coated glass and the Pt-coated glass, which showed the slowest nucleation rate. This study explains the effect of surface nature on the rate of nucleation. However, it does not explain the effect of surface area on nucleation rate [105].

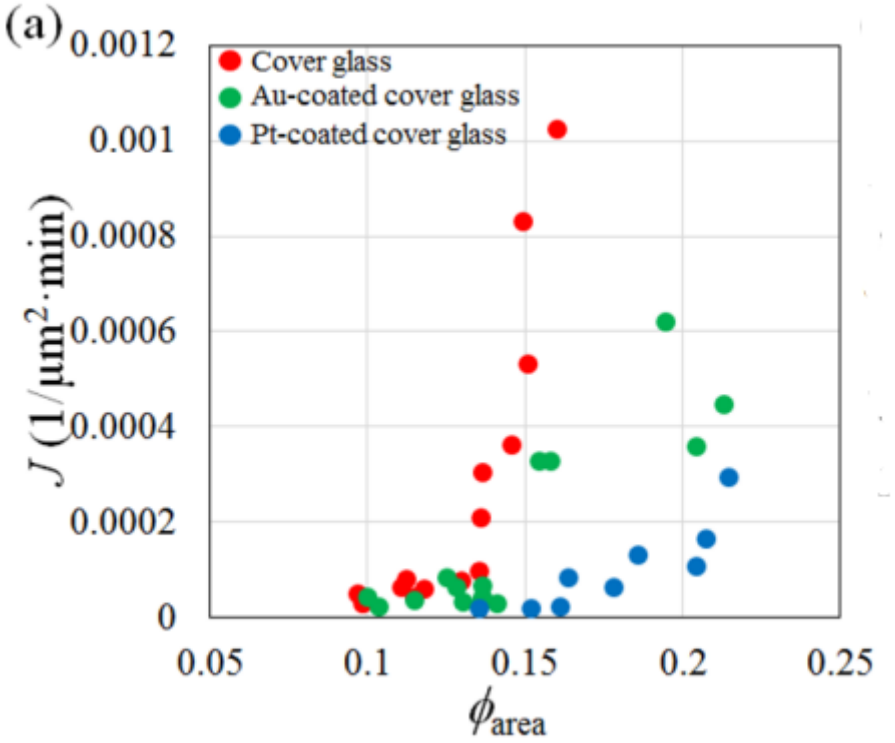

Figure 2. 17 – Nucleation rate, J, at various ∅_area for three different substrates[105].

The nucleation and crystal growth of calcium carbonate on hard surfaces at different temperatures was examined by Wang et al [106]. This study was carried out using scanning electron microscopy and X-ray diffraction (XRD). The morphology of the crystals formed on hard surfaces was observed at different temperatures. The analysis showed that only calcite crystals formed at 25^{o}C whilst aragonite and calcite crystal were formed at 55^{o}C. This study confirmed the effect of temperature on the precipitation of calcium carbonate on the surface. This study also showed that calcite crystals are more likely to form on hard surfaces compared to the other types of crystals [106]. This is shown in Figure 2. 18.

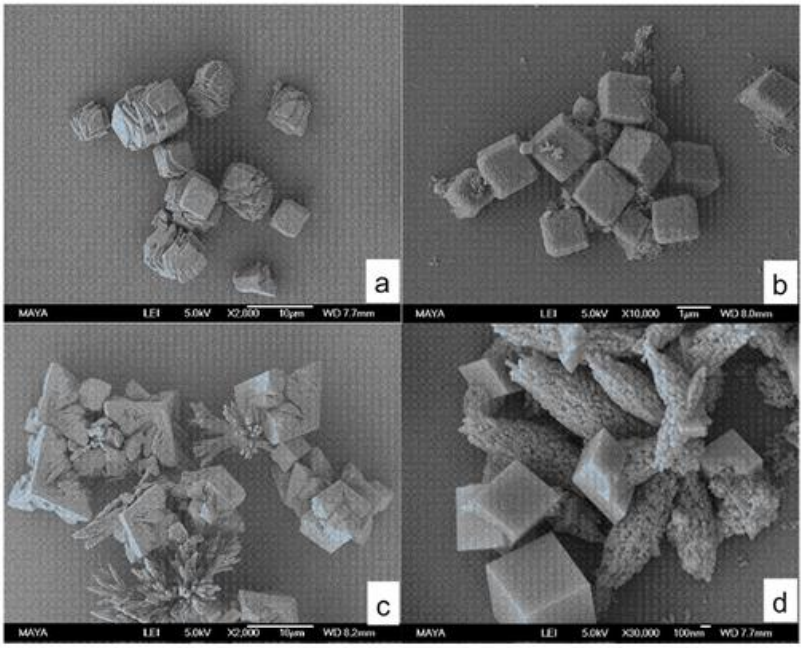

Figure 2. 18 – SEM images of calcium carbonate crystals on hard surface at 25°C (a,b) and 55°C (c,d) at pH 10 for 1hr [73].

2.3.2 Laboratory studies of surface scaling phenomenon

Surface crystallisation has been studied with techniques such as electro-crystallisation and by quantifying the nucleation and growth process in real time [107, 108]. Some experimental methods of studying the kinetics of scale deposition are explained in this section.

2.3.2.1 Electrochemical methods

Calcium carbonate scale can be generated by applying a cathodic potential, a process referred to as electrodeposition. This methodology enables a better control of the scale deposition processes especially with regards to the amount of scale formed and their polymorphic phases. This technique also has the potential to increase the rate of scale deposition in a systematic way [109].

The electrochemical principle works by applying a negative potential in order to induce oxygen reduction reaction. Therefore, excess hydroxide ions are formed. The pH increases in area surrounding the surface, allowing crystallisation of calcium carbonate on metal surfaces [110].

$$O_2 + 2H_2O + 4e^- \rightarrow 4OH^- \quad (1.24)$$

Addition of negative electrodes to water molecules results in hydrogen-evolution and production of more hydroxide ions, which increases the surface pH.

$$H_2O + 2e^- \rightarrow 2OH^- + H_2 \uparrow \quad (1.25)$$

Calcium carbonate is formed on the metallic surfaces due to the presence of OH ions near the surface of the metallic structures, which reduces the pH of the surface.

$$HCO_3^- + OH^- \leftrightarrow H_2O + CO_3^{2-} \quad (1.26)$$

$$Ca^{2+} + CO_3^{2-} \leftrightarrow CaCO_3 \downarrow \quad (1.27)$$

The electrochemical technique is useful for understanding the kinetics of $CaCO_3$ deposition on the surface because it accelerates the process of $CaCO_3$ precipitation on the surface for an extended duration of time without a drop in bulk precipitation. The electrochemical technique has also being refined by using the quartz crystal microbalance (QCM) to determine the mass of $CaCO_3$ deposited on the surface and chronoelectrogravimmetry (CEG) was also adopted to estimate the induction time for $CaCO_3$ precipitation on the surface [108]. The relationship between the local SR and the precipitation rate of $CaCO_3$ can be evaluated from the increase in mass of $CaCO_3$ deposited on the surface with time [107]. The limitation of this technique is that it is only effective for understanding the initial stages of the crystallisation process and the QCM technique is expensive to setup.

2.3.2.2 Rotating disc/cylinder electrode (RDE/RCE)

This methodology measures the diffusion of oxygen on a surface at variable experimental conditions such as flowrate and temperature. The kinetics of calcium carbonate formation and its extent of coverage on scaled electrodes can be studied using this technique [111, 112].

The cell set-up consists of a working electrode, a reference electrode, and a counter electrode to enable flow of the current [111].The precipitation and deposition of calcium carbonate formation in the bulk and on the surface can be studied using this set-up [113].

In a study by Chen et al [35] , the formation of $CaCO_3$ on the surface was investigated with the rotating disk electrode (RDE), by measuring the surface coverage of $CaCO_3$ on the stainless-steel sample using electrochemical

measurements at 1, 4, 8, 12, 16 and 24hours time frames. Whilst, inductively coupled plasma (ICP) was used to follow the kinetics of $CaCO_3$ formation in the bulk solution at the same intervals. The experiment was conducted at SR 18, SR 4, and SR 1.1, and 20^oC.

The findings from this study demonstrated that as expected, the kinetics of $CaCO_3$ formation both in the bulk solution and on the surface increased as SR increased. It was also observed that the induction time for bulk precipitation was longer than for surface deposition, as for instance, at SR 1.1, the induction time for bulk precipitation was longer than 12hours, whilst the surface induction time at the same condition was less than 1hour. The result from this research indicates that $CaCO_3$ has more tendency to deposit on the surface than to precipitate in the bulk solution especially at very low SR. In addition, the data from this research also revealed that the average area of $CaCO_3$ crystals deposited on the surface was larger than the crystals formed in the bulk solution, implying that the presence of a surface promotes crystals growth over bulk precipitation. The drawback of this research is that the test was conducted in a static system where the SR reduces with time, therefore, understanding the effect of $CaCO_3$ formation at constant SR would be difficult with using technique.

In another study by Wang et al. [114] the effect of substrate nature on the formation of $CaCO_3$ was assessed using the RDE technique. Gravimetric analysis was used to determine the amount of $CaCO_3$ deposited on the surface of the different substrates. The substrates that were investigated was stainless steel UNS S31603, pre-treated UNS S31603, DLC coating and PTFE coating, the experiment was conducted at 50^oC and 90^oC.

The surface energy of all 4 substrates was estimated from their contact angles with ultra-pure water, the results are presented in Table 2. 4. The findings from this study showed that at both 50^oC and 90^oC, as the surface energy of the substrates increased, the amount of scale deposited on the surface also increased as shown in Figure 2. 19, suggesting that an increase in surface energy results in an increase in the amount of scale deposited on the surface.

Table 2. 4 – The surface energy of the substrates determined from the contact angles.

Substrates	Contact angle (°C)	Surface energy(mN/m)
PTFE	105	22
DLC	81.4	33
Pre-treated UNS S31603	63.5	34
UNS -S31603	83.5	45

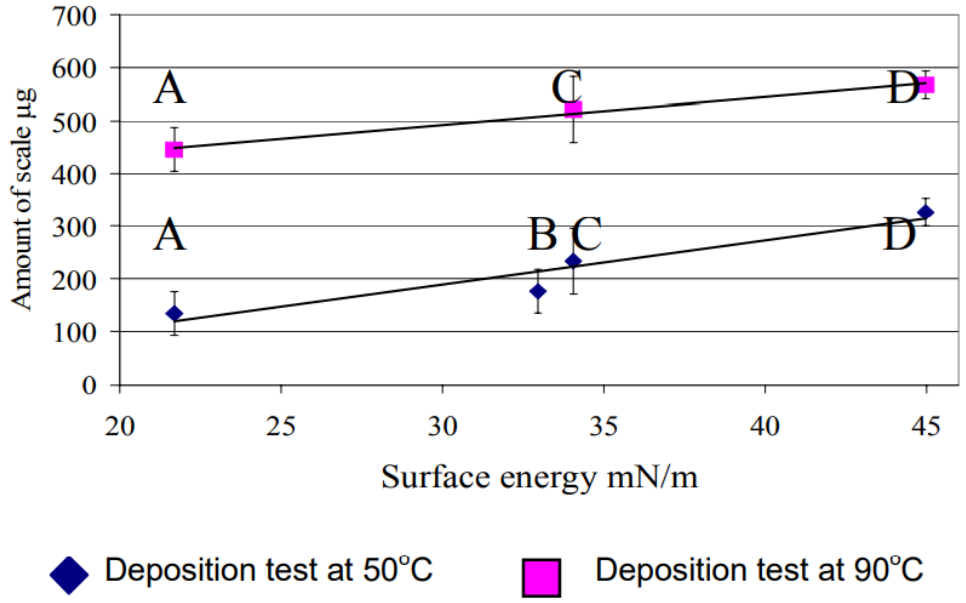

Figure 2. 19 – Showing the effect of surface energy on the amount of $CaCO_3$ deposited on different substrates at 50°C and 90°C, where (A) PTFE, (B) Pre-treated UNS S31603, (C) DLC and (D) UNS S31603[114].

2.3.2.3 *In-situ* electrochemical cell

An *in-situ* electrochemical cell was developed by Euvrard et al [115] to visualise the crystallisation of calcium carbonate in real time. It contains a working reference electrode, and a window coated with tin oxide is the counter electrode. This cell can be used to provide information on the number of crystals, mean size of crystals and the surface coverage of crystals on a metallic electrode [115].

A study of the crystallisation of calcium carbonate in a synthetic water with different degrees of hardness and (10°F, 30°F and 50°F) temperatures was carried out with the cell. It was observed that the number of crystals formed in the solution at 10°F

was the least, followed by the number of crystals formed in the solution at 30°F, while the solution at 50°F had the highest number of crystals. Furthermore, the surface coverage of the electrode also increased as the temperature increased, as shown in Figure 2. 20[115].

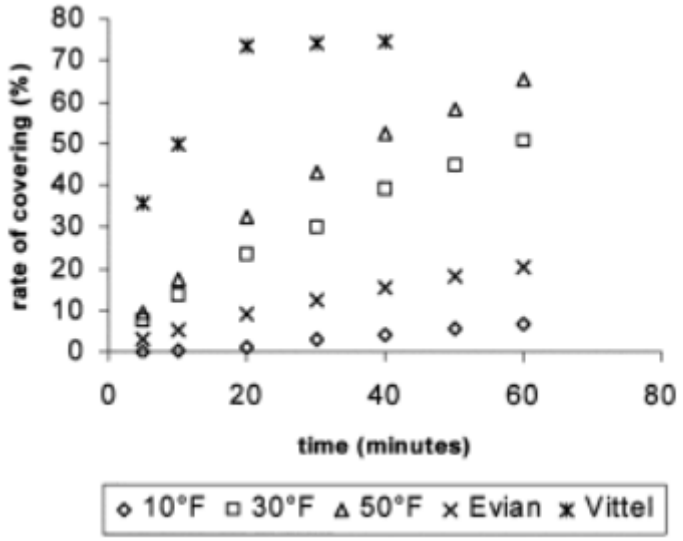

Figure 2. 20 - Variation in the rate of covering of the working electrode in the electrochemical cell [81].

This setup can also be used to study the effect of scale inhibitors on the nucleation and growth of scale. The mechanisms of crystallisation based on the type of inhibitor used was also studied. The results showed that PPCA performed better in preventing the growth of scale compared to PMA [116]. However, the limitation of this method is that, it is not suitable for quantifying the kinetics of $CaCO_3$ deposition at very low SR (i.e. below SR 10) due to the absence of a high surface area in the cell which would support the generation of a substantial amount of deposition at low SR within a reasonable time frame in the laboratory.

2.3.2.4 Microfluidics

Microfluidics is a relatively new method of quantifying nucleation and growth of crystals on surfaces. Previously, batch methods and AFM has been used. This technique is unique in its ability to control diffusion, flow dynamics, water- oil interface, and liquid gas interface [117].

Most microfluidic research on $CaCO_3$ has been centred around the preliminary stages of calcium carbonate crystal formation, types of polymorphs precipitated and others on the effect wettability and coatings on scale formation [117].

This technique provides a more precise information on the polymorphs of crystals which are considered to be thermodynamically unstable in the presence of other crystals. The growth rate of the crystals can also be accurately calculated using this methodology [117].

Using this technique, the growth rate of calcite was determined from the image of the crystals formed on the surface. The change in the size of the crystal was quantified in relation to its initial size. The linear fit of the position data with time was used to calculate the growth rate. The value for the growth rate of calcite obtained using microfluidics was 3160nm/h and 20nm/h from atomic force microscopy (AFM) [117]; this is shown in Figure 2. 21. This highlights a major discrepancy between the two methodologies and raises some questions regarding the accuracy of these techniques. It was proposed that one of the reasons for the difference in the growth rate between the AFM and microfluidics technique could be because the calcite crystals were untouched with human hands and were not exposed to the external environment whilst using the microfluidics technique. However, AFM tests were carried out on flat surfaces which could contain impurities[117]. This result shows that the kinetics of calcium carbonate deposition still requires a lot of work especially in developing a reliable model for predicting scale deposition mechanisms.

Figure 2. 21 also compares values for growth rate constant obtained using different methodologies. It shows that the growth rate constant from microfluidics experiments was 5 times larger than the values predicted from Reddy's prediction and 160 times larger than the rate constant from Teng et al. studies [117]**.**

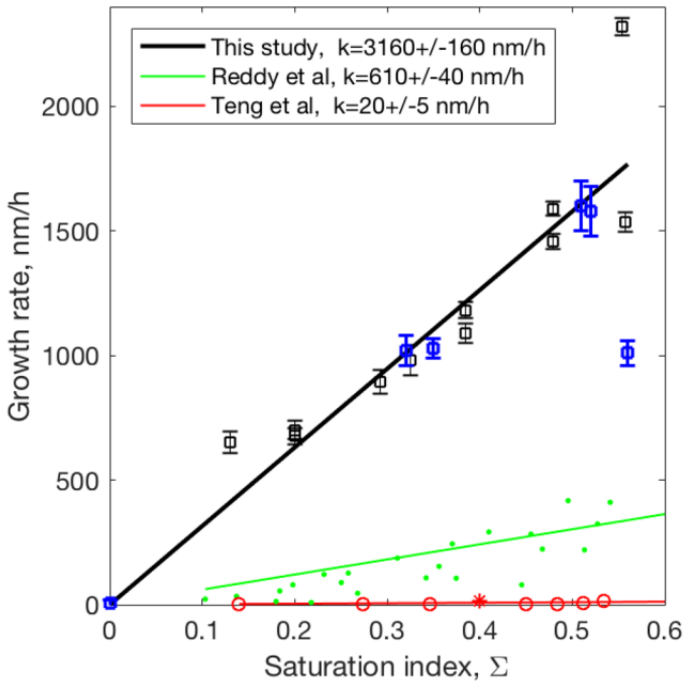

Figure 2. 21 – Comparison of growth rate constants [83].

2.3.2.5 Once-through flow visualisation rig

This rig is designed to study the kinetics of scale nucleation and growth on surfaces in real time. The flow rig also allows a constant flow of brine which will help to maintain the saturation ratio of the solution. The schematic diagram for the once through flow visualisation rig is shown in Figure 2. 22[48].

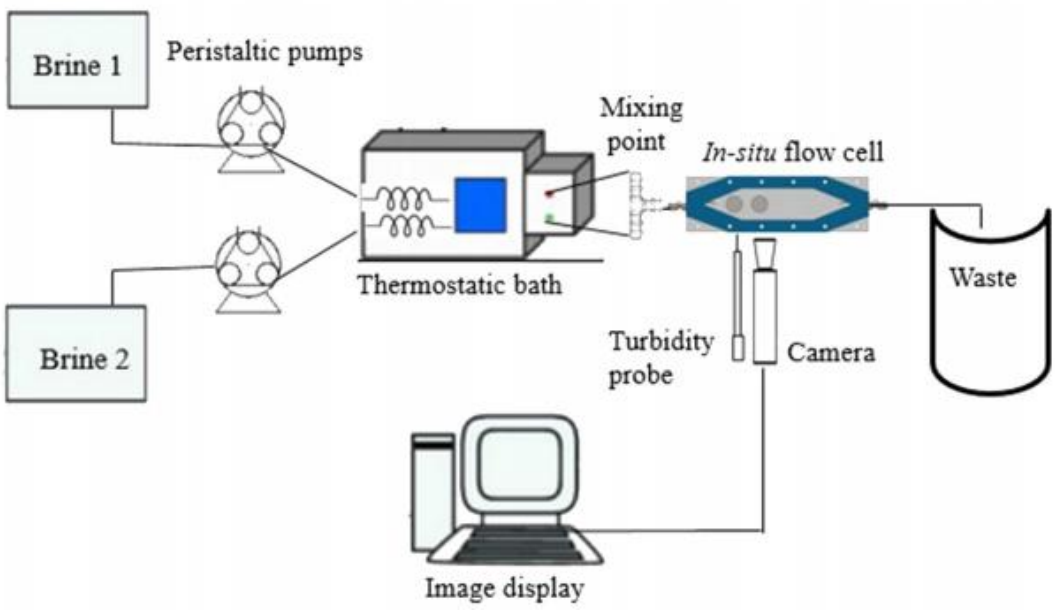

Figure 2. 22 - Schematic diagram for the once through flow visualisation rig [43].

The rate at which calcium carbonate precipitates on a surface can be studied using this cell. In addition, variable factors such as temperatures, saturation ratio and flow rates with their effects on scale formation can also be studied. Sanni et al[48] investigated the effect of SR on the kinetics of calcium carbonate scale formation on a surface using the once-through flow rig. The flow cell was able to provide information on the number and average size of the crystals formed at SR values above 10 as shown in Figure 2. 23. The study showed that the number of active sites required to initiate nucleation of crystals on a surface corresponds to the SR[48].

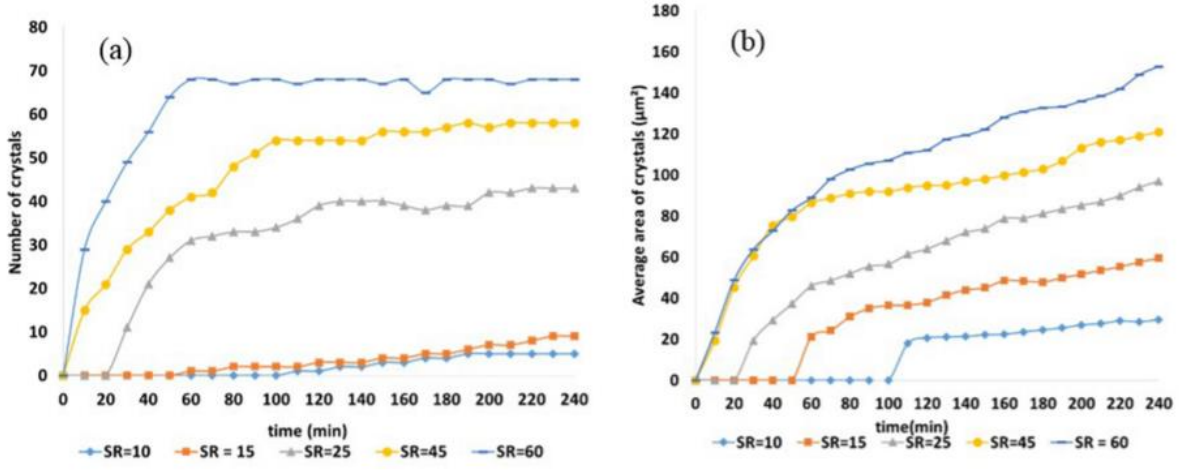

Figure 2. 23 – (a) number of crystals (b) average crystal size for $CaCO_3$ at T = 25°C for 4 hours and flowrate of 20ml/min [43].

Furthermore, the growth rate from the average area of crystals against time was plotted against SR in order to model the relationship that exist between them. An exponential relationship was observed as shown in Figure 2. 24[48].

.

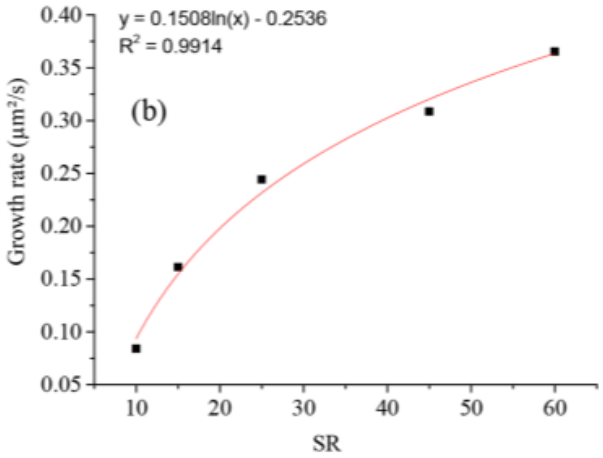

Figure 2. 24 - Surface growth rate as a function of SR [43].

In addition, the study was able to clearly show that surface crystallisation can proceed without any crystals being formed in the bulk solutions especially at the lower values of SR. However, the effect of surfaces on the kinetics of precipitation as well as surface area to volume ratio was not studied. The study was also unable to provide insight into the effect of low SR (2-10) on the mechanism and growth rate of calcium carbonate on the surface.

The *in-situ* visualisation cell has demonstrated the capability to effectively visualise the nucleation and growth of $CaCO_3$ crystals in real time in a constant composition environment. This technique is also very useful for assessing the early stages of $CaCO_3$ nucleation and growth, but it is not effective for quantifying the later stages of $CaCO_3$ growth, because the crystal growth can only be observed in 2D.

2.4 Limitations and gaps in literature

The limitation in the understanding of $CaCO_3$ scale formation is that there is no kinetic model. Thermodynamics models exist and can be used to predict scale precipitation in the bulk solution, but they do not indicate how fast scale will occur. Also, there is normally no mention of the kinetics of scale deposition on surfaces at low SR[118]. As a result, the oil and gas industry and other process industries have no tools to enable them to assess the rates of fouling as a function of flowrate, surface area and SR for calcium carbonate.

In the bulk scale studies discussed in the literature review, the effect of SR (10 - 45) on the induction time was shown [119]. At low SR, the induction time is longer compared to high SR generally, also the tendency for scale to form at SR values below 10 was reported to be unlikely without the presence of a growth surface as the solution is considered to be in a metastable state [49].

Li Lei [117] studied the effect of low SR on the growth rate of $CaCO_3$. The results showed that compared to the microfluidics technique; the growth rate constant of calcite was 5 times larger than the predictions from the batch methods, while using atomic force microscopy (AFM) the growth rate constant was 160 times larger than the value obtained from the microfluidics technique [117]. This suggests that there are still questions regarding the accuracy of the current methodologies used to study the kinetics of scale formation on surfaces. It also shows the need for reliable techniques which can be used accurately to predict the kinetics of scale deposition on surfaces.

The limitation of the studies on the effect of SR on precipitation of $CaCO_3$ is that it provides no insight into the effect of SR values between (2 – 10) on the rate of scale formation and how the presence of a surface influences the kinetics of the reactions. Furthermore, there is a gap in the understanding of the effect of area-to-volume ratio (A/V) on the kinetics of $CaCO_3$ deposition and there is no knowledge of any potential connection between the kinetics of scale deposition and bulk precipitation at low SR.

The limitation of the classical nucleation theory [120] in equation (1.14) is this: it is based on thermodynamic principles which give information on the potential for $CaCO_3$ to form in the bulk solution but do not indicate the rate at which $CaCO_3$ will form in the bulk and on the surface. Kinetic information is useful because it provides a more accurate estimate of the amount of scale expected to form in a given time. This will be useful for oil and gas companies to discern the amount of scale expected to form in their pipelines and will provide a better guide into whether scale inhibitors are required to combat scale formation issues and to design optimal facilities to manage the scale threat. A better understanding of the kinetics of scale formation can result in reduced cost of scale inhibition processes such as squeeze treatment and maintenance costs.

Furthermore, the classical nucleation theory does not account for the effect of flowrate, surface area, and brine composition on induction time. This study aims to develop an appropriate methodology for quantifying the kinetics of $CaCO_3$ deposition at low SR. This can serve as the building block for the development of a reliable kinetic model for scale deposition which accounts for the effect of bulk precipitation, surface, flowrate, surface area and temperature on the rate of $CaCO_3$ deposition in low SR conditions.

Chapter 3 - Experimental Methodology

3.1 Brine Composition

The brine solutions are prepared by mixing two different salt solutions in the ratio 1:1. Simplified salt solutions were used to create slightly different cation brines containing calcium, and anion brines containing bicarbonate, using the methodology provided in the appendix. The ion composition for each brine was adjusted to reach three different calcite SR values (SR 3, 5 and 10) at 50^{o}C and 90^{o}C – these are provided in Table 3. 1 and Table 3. 2.

Table 3. 1 - Brine composition (g/L) for SR 3, 5 and 10 at 50^{o}C.

	SR 3		SR 5		SR 10	
	Cation Brine	Anion Brine	Cation Brine	Anion Brine	Cation Brine	Anion Brine
NaCl	44.35	42.17	43.8	41.52	43.8	41.16
$NaHCO_3$	0.00	0.85	0.00	1.08	0.00	1.37
$CaCl.2H_2O$	0.92	0.00	1.20	0.00	1.84	0.00

Table 3. 2 - Brine composition (g/L) for SR 3, 5 and 10 at 90^{o}C.

	SR 3		SR 5		SR 10	
	Cation Brine	Anion Brine	Cation Brine	Anion Brine	Cation Brine	Anion Brine
NaCl	44.59	41.91	44.59	41.91	44.59	41.91
$NaHCO_3$	0.00	0.35	0.00	0.45	0.00	0.65
$CaCl.2H_2O$	0.70	0.00	0.80	0.00	1.20	0.00

The final water chemistry composition including the calcium ion concentration, bicarbonate ion concentration and the final pH of the solution from the bulk precipitation test at 50^{o}C and 90^{o}C after the 4 hours duration of the test are also presented in Table 3. 3. The bulk precipitation experiments were conducted at 50^{o}C and 90^{o}C temperature to develop an understanding of the kinetics of $CaCO_3$ precipitation at low and mid-range temperature environments.

Table 3. 3 - Final water chemistry composition and the final pH for bulk precipitation test at 50°C and 90°C after 4 hours.

	50°C			90°C		
	SR 3	SR 5	SR 10	SR 3	SR 5	SR 10
Ca^{2+} (g/l)	0.1330	0.1240	0.1690	0.0680	0.0690	0.1020
HCO_3^- (g/l)	0.2980	0.3390	0.3410	0.0002	0.0079	0.0379
Final pH	8.32	8.08	7.72	8.29	8.08	8.18

3.2 Bulk precipitation method

Bulk precipitation tests were conducted to understand the kinetics of $CaCO_3$ precipitation in the bulk solution and to determine the induction time and growth-rate of $CaCO_3$ in the bulk solution. This information is useful for assessing whether the scale deposited on the surface from the *in-situ* visualisation cell and the beadpack test is influenced by homogenous nucleation in the bulk solution or if the deposition process is exclusively controlled by heterogeneous nucleation on the surface.

Two different experimental setups were utilised for bulk precipitation tests, depending upon the temperature. The 50°C test was performed in 250ml duran borosilicate glass bottles, which are temperature rated up to 130°C and pressure of 22psi. The experiments were carried out in a water bath (Figure 3. 1) to maintain the temperature of the solution. The setup at 90°C test consisted of a hot plate, to increase the temperature of the solution, a DN 100 beaker which could withstand temperatures up to 200°C, a condenser connected to a coolant circulating cold water at 7°C to prevent evaporation of the solution and a thermocouple for monitoring the temperature of the solution (Figure 3. 2).

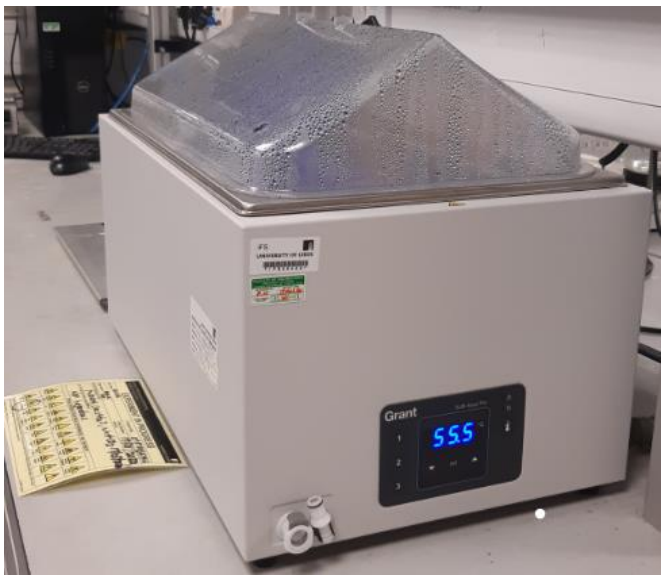

Figure 3. 1 - Water bath for bulk precipitation test at 50ºC.

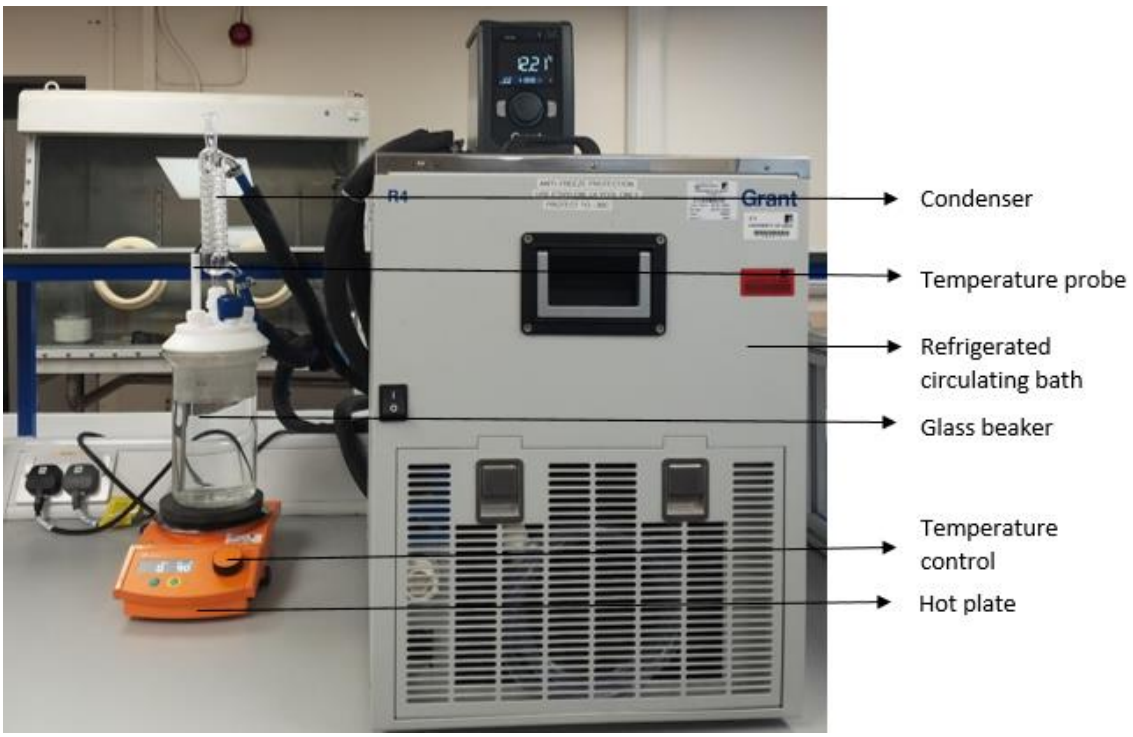

Figure 3. 2 - Experimental setup for 90ºC bulk precipitation test.

Brine composition obtained for the different temperatures and SR were prepared and poured into 250ml duran bottles for the 50ºC test and 1 litre beaker for the 90ºC test. At different time intervals (every 5 minutes for the first 30 minutes and then every 30 minutes until the end of the 4-hour duration of the test) 1 ml of the solution was extracted and initially filtered through a 0.1µm syringe filter to remove any $CaCO_3$ crystals precipitated in the bulk solution. Afterwards, the solution was immediately added to 9 ml of quenching solution (prepared from 5.71 g of KCl and 1 ml of PVS (Poly vinyl sulfonate) in 1 litre of deionized water) to prevent further

precipitation of $CaCO_3$. A mono calcium ion selective electrode from Sentek was used to determine the calcium ion concentration in the solution with time.

3.2.1 Calcium combination ion selective electrode

A calcium combination ion selective electrode (ISE) from Sentek (shown in Figure 3. 3) was used to determine the calcium ion concentration in the solution with time for the bulk precipitation test at 50^{o}C and 90^{o}C. The electrode used is a low maintenance solid state calcium sensor that does not require filling; it was used with a pH meter from Orion which had a millivolt mode.

The addition of 2ml of 4MKCl (ISAB) Ionic Strength Adjustment Buffers solution to 50ml of each sample or standards is recommended before using the calcium ion electrode to ensure that all the ions in the solution have an equal chance of contacting the electrode. Standard solutions of varying calcium ion concentrations which are similar to the calcium ion concentrations expected during the experimental tests were prepared by a straightforward dilution method and direct calibration was used for the measurements.

The electrode can be used in solution with a temperature range of 5 – 50^{o}C and a pH range of 3.5 – 11 with a reproducibility of 2%.

Figure 3. 3 - A calcium combination ion selective electrode.

3.3 Surface deposition study

Surface deposition tests were carried out to determine the mechanisms and kinetics of scale deposition in terms of the nucleation and growth of $CaCO_3$ crystals at temperatures of 50^{o}C and 90^{o}C with a flowrate of 10ml/min, 20ml/min and 30ml/min. The results from this test will help to build on the understanding of the kinetics of scale deposition in low SR (SR 10 - 2) solutions.

3.4 Set-up for surface deposition test

The *in-situ* visualisation rig for surface deposition and bulk precipitation test is shown in Figure 3. 4.

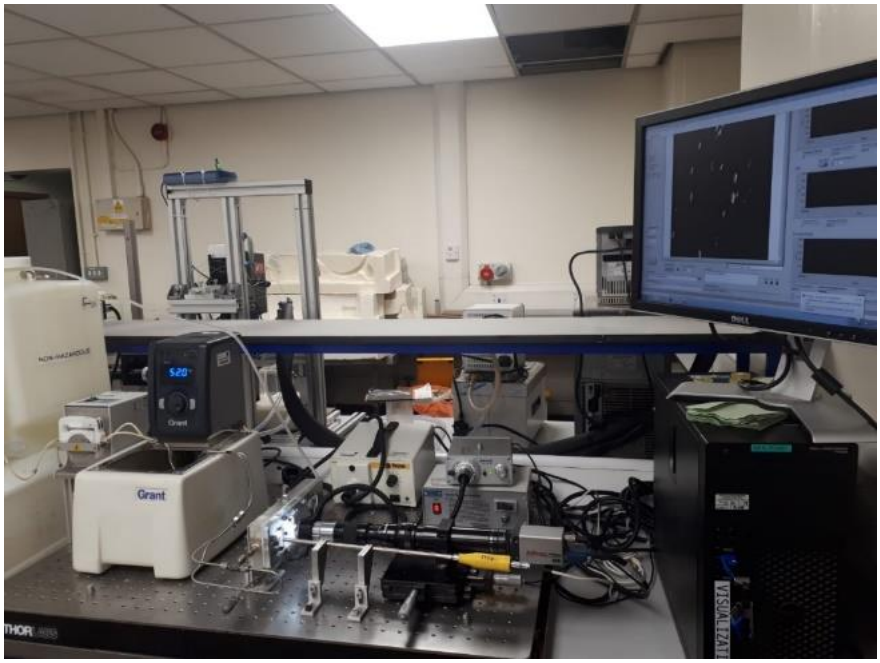

Figure 3. 4 - Once through visualisation rig for surface and bulk scaling experiments [92].

3.5 Methodology for *in-situ* visualisation tests

The methodology for the in-situ visualisation cell test is subdivided into 2 sections. These includes the experimental and computational procedure. The experimental procedure involves the steps taken to perform the visualisation cell test and sample preparation, whilst the computational part involves the protocol for image processing with the newly developed MATLAB algorithm to quantify the crystals deposited on the stainless steel sample. Further details on the two different aspects is provided in the next section.

3.5.1 Experimental procedure for surface deposition test

A peristaltic pump was used to pass the anion and cation brines in different tubes from the containers into the thermostatic bath, where the brine was heated up to the required temperature. Afterwards, the two brines flowed separately into the T-Junction, where the brines were mixed before flowing into the cell. A thermocouple was used to determine the temperature of the fluid at the mixing point to ensure that the experimental test was running at the required temperature [92]. The once through flow cell was designed to ensure a constant saturation ratio. Therefore, it is important that the brine used was enough for the entire duration of the test and the waste brine was collected at the outlet of the cell [92]. The cell was designed to incorporate turbidity measurement and image capture of the metal surface very close to the point of mixing the brine [48].

3.5.1.1 Surface preparation

The samples used for the surface deposition tests were made of stainless-steel material with a diameter of 1cm. The sample was polished until a surface roughness of 0.01µm was attained, which was achieved by using a silicon carbide p-800 and 1200 followed by 3µm and 0.25µm diamond paste for polishing. Afterwards, a removable plug was used to insert the sample into the once through flow rig[97]. An illustration of the flow path is presented in Figure 3. 5.

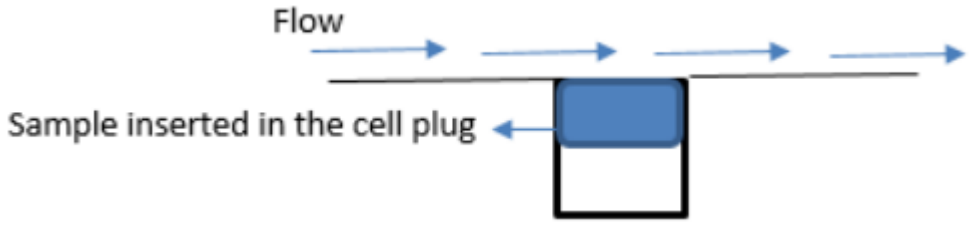

Figure 3. 5 - Fluid flow on sample surface[97].

3.5.1.2 Fluid dynamics in the *in-situ* visualisation flow cell

The flow velocity across the cell was modelled by Sanni et al. [97] using computational fluid dynamics. The hydrodynamic characteristics of the flow cell suggested a laminar flow regime for the surface deposition tests at 50^{o}C and 90^{o}C. The *in-situ* visualisation cell was developed to study the mechanisms and kinetics of scale deposition on surfaces under laminar flow conditions to avoid the effect of

shearing during the process of scale formation. The experimental tests were carried out at a flowrate of 10ml/min, 20ml/min and 30ml/min, the Reynolds number for each flowrate is presented in Table 3. 4, and the elemental composition of the stainless-steel material used for the experiments is shown in Table 3. 5.

Table 3. 4 - Hydrodynamics parameters for surface deposition test at 50ºC and 90ºC.

Flowrate (ml/min)	Flowrate (m^3/s)	Reynolds number		Regime
		50ºC	90ºC	
10	1.67 $x10^{-7}$	7.9	13.8	
20	3.34 x 10^{-7}	15.7	27.3	
30	5.00 x 10^{-7}	23.7	41.3	LAMINAR

Table 3. 5 - Stainless steel composition used for the study.

Element	Composition %
C	0.03
Mn	2
Si	1
Cr	16.0 - 18.0
Ni	10 - 14.0
P	0.045
Si	0.03
Mo	2.0 - 3.0
Ni	0.1

3.5.2 Computational protocol for Image capture and processing

The rate of nucleation and growth of the $CaCO_3$ crystals precipitated on the surface of the stainless-steel samples from the *in-situ* visualisation cell tests was assessed by analysing the images captured from the state-of-the art digital monochrome camera at 5-minute intervals. The image processing technique which was established by Eroini [121], and modified by Sanni et al[122] was not suitable for quantifying images with few crystals formed at the low saturation ratio because of the interference of the background noises. A new MATLAB algorithm was developed that considers the appropriate thresholds for detecting few and smaller crystals formed at low saturation ratio.

The series of steps performed to quantify the number of crystals, average size of crystals and surface coverage of the crystals on each image is summarised in Figure 3. 6.

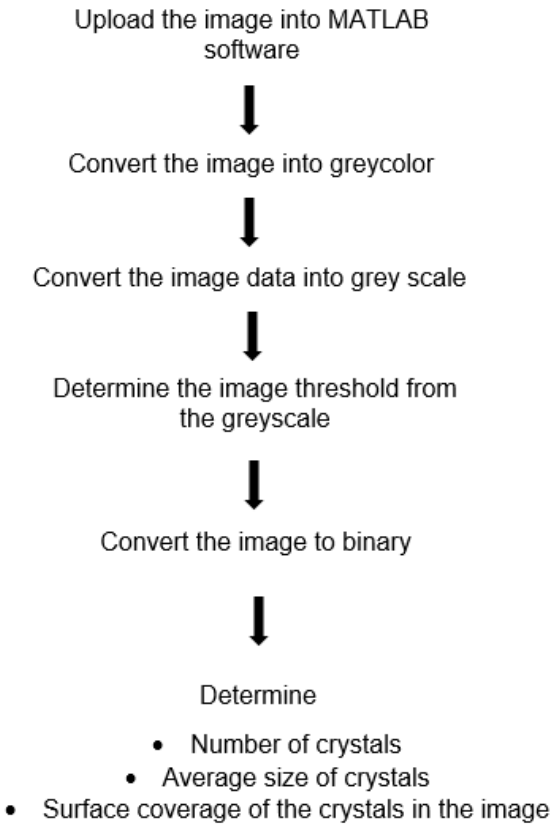

Figure 3. 6 - A summary of the procedures taken to assess the number, average size and surface coverage of crystals on the image from the *in-situ* visualisation cell tests using the new MATLAB algorithm.

The steps involve analysing the histogram profile of each image to improve the contrast of the image, and to better quantify the crystals formed on each image. This MATLAB code and a step by step guide of how the images were processed to quantify the kinetics of scale on each image is presented in the appendix. The algorithms developed was used to process the *in-situ* visualisation images, and determine the number of the crystals, average size of crystals, and the surface coverage of the crystals.

The results obtained from processing the images using the MATLAB algorithms are presented in the results section. In the next section, the distinctions between the newly developed MATLAB algorithm and the previously used algorithm for image processing in literature are explained.

3.5.2.1 Comparing the MATLAB algorithm used in this study to the algorithm developed in literature.

This section details the distinction between the MATLAB algorithm developed in this study and the algorithm used in the previous study by Sanni et al[97]. A new algorithm was developed this study to better quantify the kinetics of $CaCO_3$

deposition at low SR (below SR 10) in relation to assessing the number, average size and surface coverage of the crystals deposited on the surface.

The MATLAB algorithm developed in the previous study [97] was beneficial for quantifying the kinetics of $CaCO_3$ surface deposition at higher SR (i.e. above SR 10). However, it was not suitable for quantifying the kinetics of $CaCO_3$ deposition at low SR i.e. (below SR 10). One of the main distinctions between the algorithm developed in this study and the algorithm from the previous work in literature is the 'imhist(g);' feature in the newly developed algorithm, which converts the image from the *in-situ* visualisation cell into a binary image, by initially, converting the image data into a grey scale from 0 – 255 on an histogram, this is illustrated in Figure 3. 7.

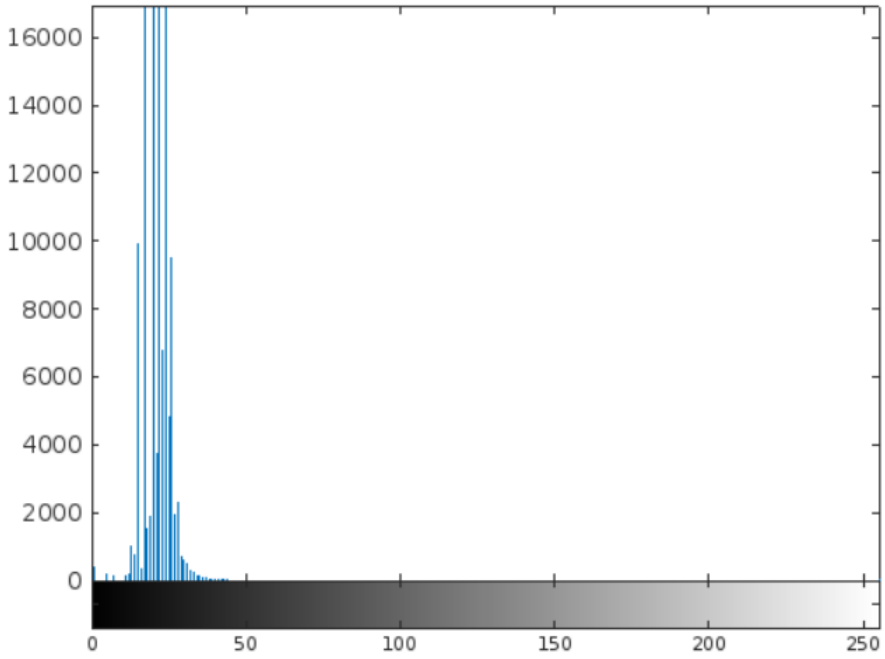

Figure 3. 7 - Histogram plot showing the greyscale of the image from the *in-situ* visualisation cell. This is useful for converting the image from the flow cell into a binary image for quantifying the crystals in the image.

Afterwards, the image is converted into a binary image, with the all crystals in in black and the background in white. This is achieved by selecting a threshold setting, for instance, for Figure 3. 7, a threshold setting of g<50 was used because the histogram profile shows that the black section of the image is in the region below 50 on the scale. This value can vary depending on the image as different threshold applies to different images.

In contrast, the procedure established by Sanni et al did not create a histogram plot of the image data to determine the threshold setting rather, the 'sobel', 'canny', 'roberts' and 'prewit' algorithm was used for the threshold setting and the 'basic' command was used to assess the area of crystals on the surface. However, this

method is not effective for detecting the tiny crystals present in the image. Further details on the differences between the algorithms developed in this study and the algorithm used Sanni et al's work with regards to quantifying the number, average size and surface coverage of the crystals are presented in Table 3. 6.

Table 3. 6 - Comparing the MATLAB algorithm developed in this study to the algorithm developed in previous study[97] with regards to quantifying the number, average size and surface coverage of crystals deposited on the surface.

Variable	MATLAB algorithm used in this study	MATLAB algorithm developed in previous study
Numbers of crystals	[L,num]= bwlabel(binaryimage);	cc = bwconncomp (e5, 8); cc.NumObjects
Average size of crystals	area = regionprops(binaryimage,"Area"); %% areaValues = zeros(1,n); for i = 1:n areaValues(1,i) = area(i).Area; end meanArea = mean(areaValues); where, n represents the number of crystals on the image, determined using the algorithm for counting the crystals.	area = regionprops (cc, 'basic'); area.Area; sizex=zeros(length(area),1); i=1:length(area); sizex(i) = area(i).Area; 217 mn=mean(sizex);
surface coverage of the crystals	nWhite = nnz (binaryimage); nBlack = numel (binaryimage) - nWhite; srfc = nWhite/nBlack;	nWhite = nnz (e5); nBlack = numel (e5) - nWhite; srfc = nBlack/nWhite;

3.5.3 Reproducibility for the *in-situ* visualisation cell

Initial scale deposition tests were conducted to determine the reproducibility of the *in-situ* visualisation cell in studying the precipitation of scale on surface. This test was carried out by using the high-quality digital camera in the setup to capture the images of the scale deposited on the surface of the stainless-steel material. The images were taken every 5 minutes and analysed to provide a better insight into the mechanism and kinetics of the nucleation and growth of the crystals formed.

The experiment was conducted at SR 10, 50^{o}C, flowrate of 20ml/minutes and the test ran for 4hours. The images illustrate that identical number of crystals was formed on the surface for first test, presented in Figure 3. 8 and the result for the repeat test is shown in Figure 3. 9, indicates that the *in-situ* visualisation cell is a

repeatable technique understanding the mechanisms and kinetics of scale formation at this condition.

SR 10 - Test 1 *in-situ* visualisation cell images

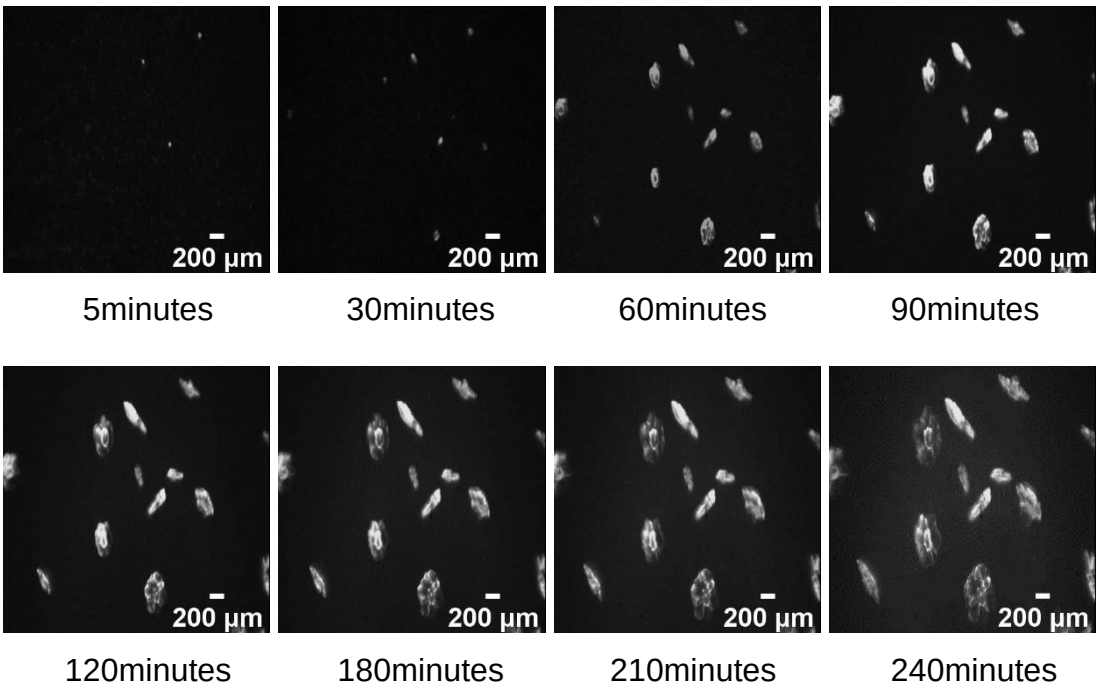

Figure 3. 8 - *In-situ* visualisation cell images of the crystals formed on the stainless-steel sample at from 5 - 240minutes with SR 10 brine at 50°C.

SR 10 - Test 2 *in-situ* visualisation cell images

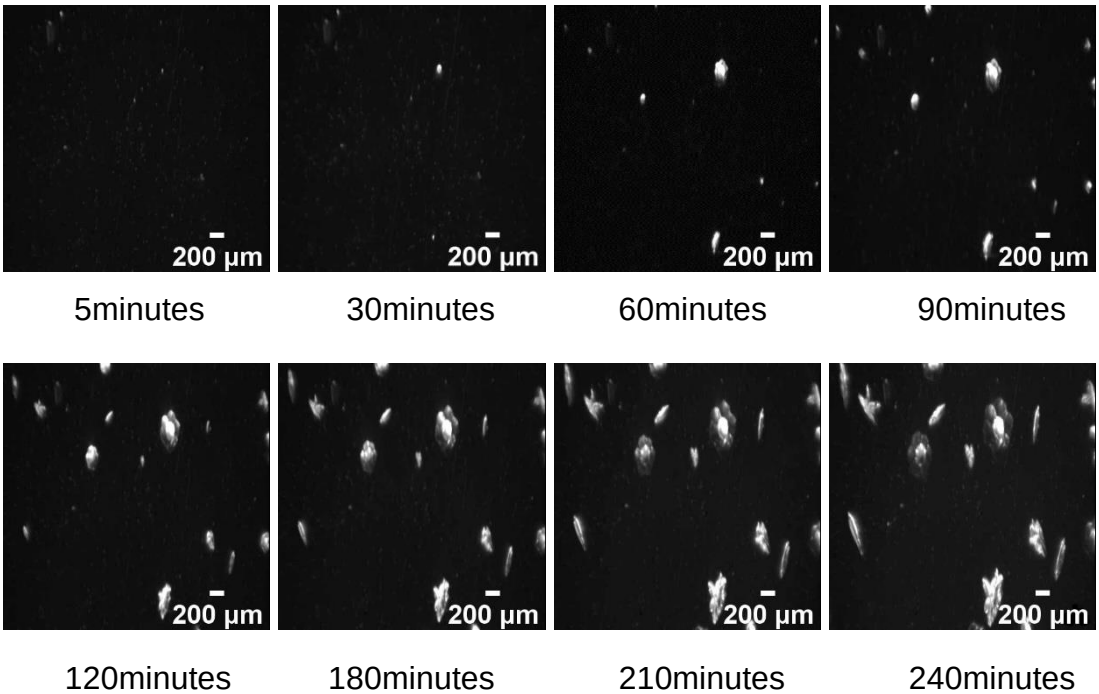

Figure 3. 9 – *In-situ* visualisation cell images of the crystals formed on the stainless-steel sample at 5 - 240minutes for the repeat SR 10 test at 50°C.

Furthermore, the results obtained for the number of crystals formed on the surface with time also demonstrates the repeatability of this technique as the number of crystals deposited on the surface at equilibrium point was 16 for first test and 14 crystals was observed on the surface at equilibrium point for the repeat test. In addition, a similar trend was also observed for the average size of the crystals and the surface coverage of the crystals with time also illustrates the repeatability of this technique as shown in Figure 3. 10.

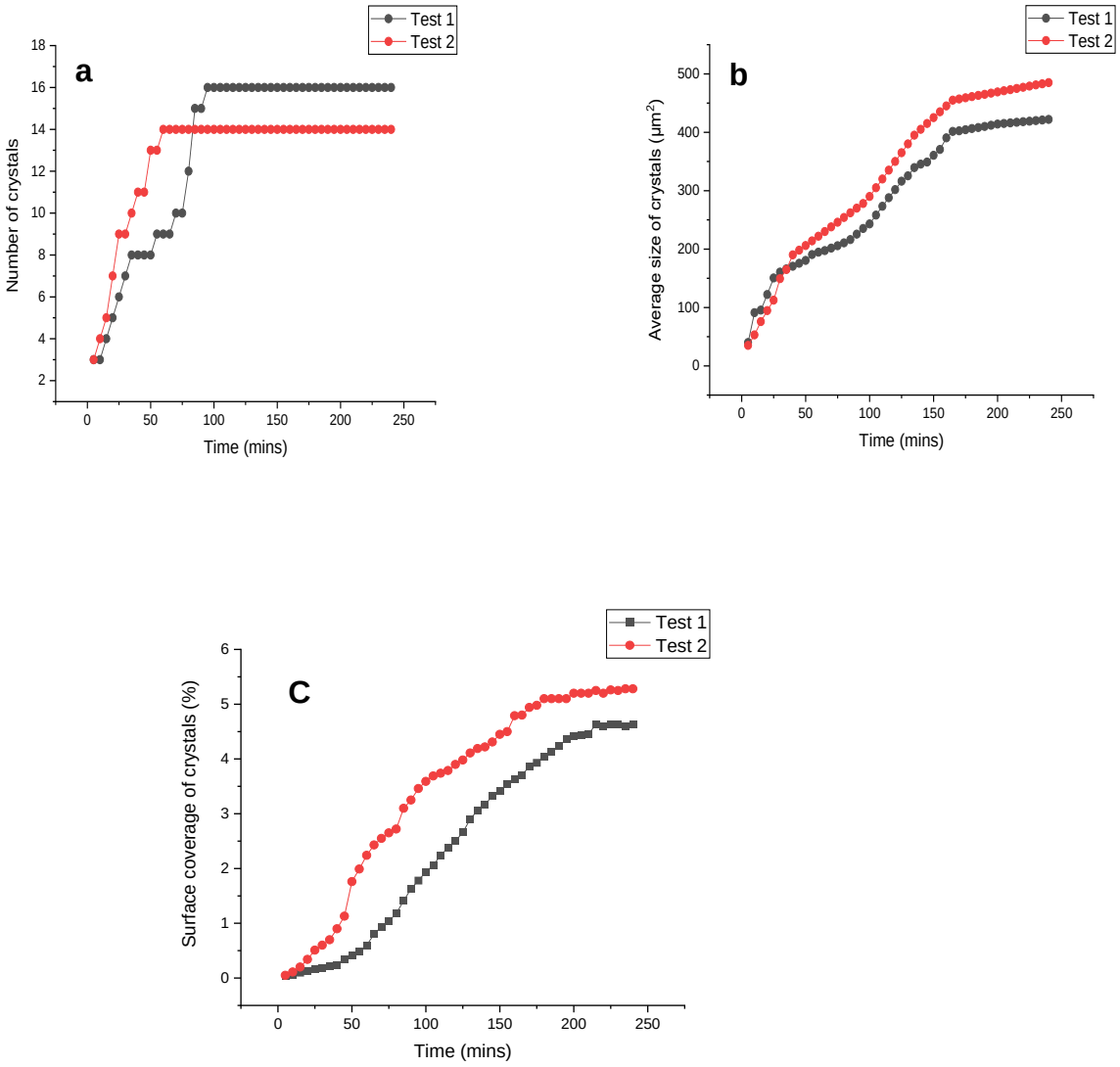

Figure 3. 10 - Showing the repeatability results for (a) Number of crystals with time (b) Average size of crystals and (c) Surface coverage of crystals at SR 10, 50°C with the *in-situ* visualisation cell.

3.6 Bead pack method

3.6.1 Introduction

The beadpack is one of the key novelties of this work, this methodology has been adopted from the sand pack technique, which has a wide range of applications in the oil and gas industry. This includes investigating the adsorption and desorption of chemical species such as inhibitors in a porous media [123], and the examination of the extent to which precipitation of scale in a porous medium affects permeability reduction mechanisms [124]. However, the sand pack technique has not been used as a means of accurately assessing the kinetics of $CaCO_3$ deposition on the surface. The sand pack technique is been translated into the beadpack with a constant SR environment to determine whether it can provide reliable data on the kinetics of $CaCO_3$ surface deposition.

3.6.1.1 Translation of the sand pack methodology to $CaCO_3$ surface deposition kinetics in low SR systems.

In contrast to the sand pack experiments, typically conducted with sand materials such as silica, the pack is filled with stainless steel beads for the surface deposition tests with the beadpack. In addition, the configuration of the beadpack is in terms of a once through flow cell with a high surface area, which expected to support the generation of a substantial amount of deposition on the surface at low SR due to heterogeneous nucleation.

Theoretically, the deposition of $CaCO_3$ on the surface, should result in a reduction in the Ca^{2+} ion concentration through the cell, the change in Ca^{2+} concentration in the beadpack with time can be measured with Atomic Absorption Spectroscopy (AAS) and data from this analysis can provide insights into the kinetics of $CaCO_3$ deposition.

The newly developed beadpack technique could help to address the limitations of common techniques such as the capillary rig and the *in-situ* visualisation cell where there has been difficulty in effectively quantifying the kinetics of $CaCO_3$ surface deposition at low SR within a reasonable time frame in the laboratory.

The next section describes the AAS techniques and how it can be used to measure the concentration of calcium ion in solution.

3.6.1.2 Development of the bespoke beadpack setup

A polycarbonate material was used for the column due to its ability to maintain rigidity up to 140^{o}C and its transparency for clear viewing of the pack. The beadpack experiments were conducted in a bed with two different heights. The height of the shorter bed was 54mm and 150mm height for the longer bead, both bed had an internal diameter of 20mm, which is shown in Figure 3. 11 and Figure 3. 12 respectfully. The diameter of the beads used for the experiments were 3mm, 6mm and 9mm diameter beads, PTFE and stainless-steel beads was used in this study.

The brine used for the beadpack test consisting of the cation brine and anion brine, pumped through two separate tubes with an R404 step pump, this was mixed at a T-junction before flowing through the packed column. The experiments were conducted in an oven to maintain a constant temperature for the entire 4-hour duration of the test. Afterwards 1ml of the effluent were collected at the outlet at different time intervals, filtered with a 0.1µm syringe filter and added to 9ml of quenching solution to prevent further precipitation of $CaCO_3$. AAS was then used to determine the calcium ion concentration of the effluent solution.

The change in the calcium ion concentration as a function of time obtained from the beadpack test was compared to the static jar test results to distinguish how the presence (heterogeneous nucleation) of a surface impacts the growth-rate of $CaCO_3$ in comparison to the bulk precipitation (homogenous nucleation). The sensitivity of the beadpack methodology to different experimental parameters such as surface roughness, flowrate and area-volume-ratio was also assessed to have a deeper insight into the capabilities of the newly developed techniques in quantifying the kinetics of $CaCO_3$ deposition at low SR.

The chemical composition of the 3mm stainless steel bead used for the beadpack test is presented in Table 3. 7. and the parameters for the beadpack characterisation is shown in Table 3. 8. The equations used to calculate the parameters are provided in the appendix.

Figure 3. 11 - Image of short beadpack of 54mm height in the oven.

Figure 3. 12 - Image of the longer bead pack of 150mm height in the oven.

3.6.1.3 Sample preparation for beadpack test

The stainless-steel beads which were used for the beadpack test were etched with 0.1M of HCl to increase the number of nucleation sites on the surface which would

increase the chances of $CaCO_3$ deposition on the surface. The procedure for etching the stainless-steel sample is discussed in this section.

3.6.1.4 Procedure for etching the stainless-steel beads

- HCl solution with a concentration of 0.1M and pH of 0.92 was prepared.
- The smooth stainless-steel beads were placed in the prepared 0.1M HCl solution for 1hr at room temperature
- Afterwards, the beads were removed from the 0.1M of HCl solution, rinsed with distilled water and dried.
- SEM analysis was used to visualise the etched surface of the stainless-steel material.

Table 3. 7 - Composition of 3mm diameter stainless steel for beadpack test.

Elements	**Composition weight (%)**
Carbon C	0.08
Chromium Cr	16 – 18
Nickel Ni	10 – 14
Molybdenum Mo	2 – 3
Manganese Mn	2
Phosphor P	0.045
Sulphur S	0.03
Silicon Si	1

Table 3. 8 – Beadpack parameters for the experiments with 3mm diameter beads at 20ml/hr.

Parameter	**Value**
Diameter of pack	2.0×10^{-2}m
Particle diameter	3.0×10^{-3}m
Density of the brine	1041kg/m^3
Height of beads in the bed	5.4×10^{-2}m
Void fraction of bed	0.46
Volume of void	$7.8 \times 10^{-6}m^3$
Volume of bed	$1.7 \times 10^{-5}m^3$
Number of beads	651
Volume of beads	$9.2 \times 10^{-6}m^3$

Residence time	1404secs
Surface area of beads	$1.8 \times 10^{-2} m^2$
Surface area to volume ratio	$2371.1 m^{-1}$
Shear rate	$3.2 \times 10^{-4} (1/s)$
The fluid superficial velocity	$1.1 \times 10^{-4} m/s$
Pressure drop	$5.0 \times 10^{-2} Pa$
Viscosity of solution	$5.8 \times 10^{-4} Pa.s$

3.6.2 Characterisation for the beadpack parameters

The beadpack was characterised to have an insight into the pressure drop, shear rate and residence time in the beadpack. These are valuable information which is necessary before carrying out an experiment test in a porous medium.

3.6.2.1 Pressure drop calculation.

The Ergun's equation (Equation 1.6) was used to determine the pressure drop in the beadpack because it provides an approximate representation of the pressure drop in a packed column [125]. An understanding of the pressure drop is beneficial for having a better insight into the flow properties of the beadpack and its potential resistance to flow.

The pressure drop in the beadpack was observed to be low (0.12 – 1.6pa) for the range of flowrate (20ml – 60ml/hr) used, which indicates that a low amount of energy is required to maintain the flow of brine in the beadpack.

Furthermore, Figure 3. 13 illustrates that generally as the flowrate increases, this results in an increase in the pressure drop of the beadpack. This can be attributed to the increase in the rate of scale deposition on the surface of the beads as the flowrate increases, because no shearing is expected in the pack and the force of attraction between the crystals and the surface is stronger than the shearing rate of the fluid due to the laminar flow regime in the pack. It was also observed that there was a general increase in the trend of the pressure drop versus flowrate as the area-to-volume ratio (A/V) in the pack increased. The A/V in the pack is a measure of the extent to which the surface area of beads in the pack varies with respect to the pore volume in the pack. The surface area of the beads in the pack was varied by changing the diameter of beads. The sizes of beads used for the surface deposition test with the beadpack includes 3mm, 6mm and 9mm diameter beads.

The increase in pressure drop as A/V ratio increased is suspected to be due to the increase in the rate of scale deposition as the A/V increased.

$$\frac{\Delta p}{L} = \frac{150\mu\,(1-\varepsilon)^2\,\mu_o}{\varepsilon^2\,d_p^2} + \frac{1.75\,(1-\varepsilon)\,\rho\,\mu_0^2}{\varepsilon^3\,d_p} \qquad (1.6)$$

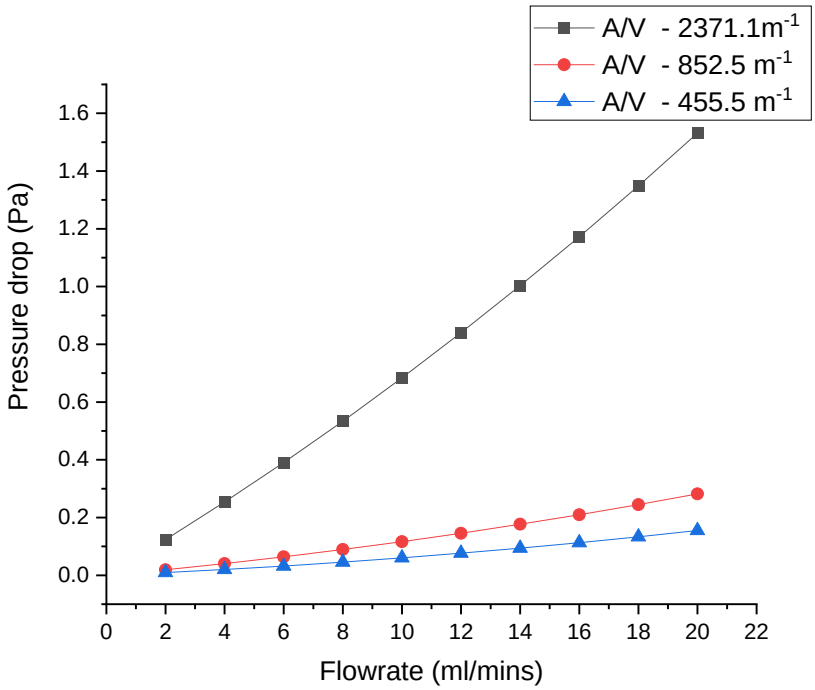

Figure 3. 13 - Pressure drop (Pa) versus flowrate (ml/min) graph for the stainless steel beadpack for different A/V.

3.6.2.2 Shear stress determination for the beadpack

The shear stress is a measure of the tangential force per unit area of the fluid flowing on the surface of the tube transporting the brine [126]. The stress rate in the beadpack was determined as a function of the pressure drop in the pack, its hydraulic diameter and the length of the pack using Equation 1.7 [127]

A linear relationship was established between the shear stress and the flowrate for the three different A/V as shown in Figure 3. 14. This demonstrates that as the flowrate increases, the shear stress also increased proportionally, also the flow regime in the beadpack is laminar and the shear rate is also low, which suggests that no shearing of scale is expected at the liquid-solid interface. In line with the data from the pressure drop versus flowrate results at different area-to volume ratio (A/V), it was also observed that as the A/V ratio increased, the shear rate also increased in the pack for the different flowrates investigated.

$$\text{Shear stress } (\tau w) = \frac{d_h}{4}\left(\frac{-\Delta p}{L}\right) \tag{1.7}$$

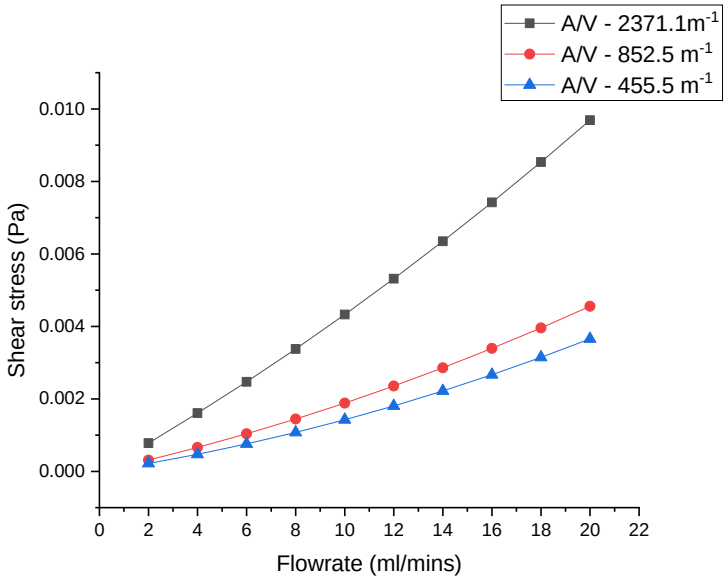

Figure 3. 14 - Shear stress (Pa) versus flowrate (ml/min) graph for the beadpack for different area-to-volume ratio, A/V.

3.6.2.3 Residence time calculation for beadpack

The residence time is the duration of time that the brine spends in the system boundary. It can be useful for understanding the mechanisms controlling scale deposition in a packed column by determining whether the homogenous nucleation of scale in the bulk solution influences the process of scale formation in the beadpack or if the precipitation of scale is solely due to heterogeneous nucleation on the surface.

The residence time was calculated as a function of the voidage of the pack, its volume and the flowrate as presented in equation 1.8. As expected, the residence time reduced as the flowrate increased in the pack, also a very similar trend in the graph of the residence time versus flowrate was observed for all 3 A/V investigated as shown in Figure 3. 15.

$$\text{Residence time} = \frac{\text{Voidage x Pack volume}}{\text{Flowrate}} \tag{1.8}$$

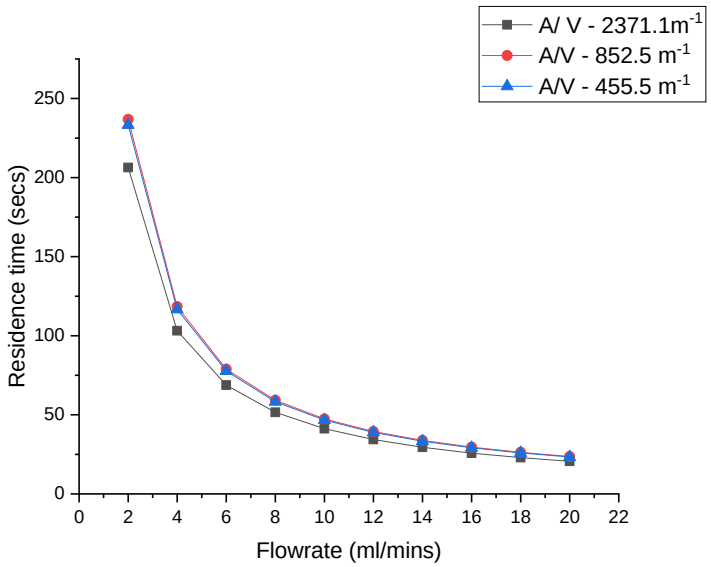

Figure 3. 15 - Residence time (s) versus flowrate (ml/min) graph for the steel beadpack for different area-to-volume ratio, A/V.

3.7 Post experimental analysis

The post experimental analysis explains the procedures that were carried out to characterise the samples from the bulk precipitation test conducted with the static jar setup and the surface deposition test conducted with the beadpack and the *in-situ* visualisation cell.

These includes the atomic absorption spectroscopy(AAS) technique which was used to monitor the calcium ion concentration in the solution from the static jar test and the beadpack test to have an insight into the kinetics of calcium carbonate formation at these conditions. Scanning electron microscopy (SEM) and energy dispersive x-ray spectroscopy, EDX was also used to investigate the morphology and elemental composition of the crystals deposited on the surface. A description of these two techniques is provided in the next section.

3.7.1 Atomic Absorption Spectroscopy (AAS) technique

AAS is a commonly used analytical technique for detecting and measuring the concentration of several trace metals, such as calcium, lead, aluminum, zinc, nickel, chromium, copper, and mercury at the parts per million levels of concentration. This methodology works based on the principle that a specified metal atom in a solution would strongly absorb a characteristic wavelength of light that corresponds to the emission of a spectral line of that particular metal[128, 129]. In this study, the AAS technique was used to determine the concentration of

calcium ions in solutions to track the kinetics of $CaCO_3$ precipitation in the bulk solution from the static jar test and on the surface from the beadpack test.

To achieve this, the solution containing the calcium ion concentration was first passed into the atomizer of the AAS equipment to transform the solution into a spray of tiny droplets. This helps to enhance the interaction between the solution and the light source from the hollow cathode lamp containing calcium ions. Afterwards, a monochromator was used to focus the light from the lamp on the atomized solution. As the light is transmitted through the atomized solution, the calcium ions present in the solution would absorb the light at a specified wavelength[129].

The intensity of light absorbed by the calcium ion concentration typically corresponds to the concentration of calcium ions present in the solution. Thereafter, this transmitted light is absorbed by a detector that produces a signal that is compared to a calibration curve created by analysing solutions of known calcium ion concentration. The calibration curve is used to determine the calcium ion concentration of the unknown solution[128].

The AAS technique is beneficial for accurately measuring the concentration of trace metals in complex mixtures and can also be used for analysing a wide range of samples, including solid, liquid, and gaseous samples. However, the sample preparation procedure requires precise measurements and can be time-consuming[93].

3.7.2 SEM and EDX spectroscopy

SEM (scanning electron microscopy) was used to determine the morphology of the crystals deposited on the surfaces and in the bulk solution after the experimental test, whilst EDX (energy dispersive x-ray spectroscopy) was used to provide an insight into the elemental composition of the crystals formed on the surfaces.

Prior to carrying out the SEM and EDX analysis, the samples were coated with carbon due to its transparent nature to create a conductive film of metal on the sample, which would improve the quality of the images obtained from the SEM analysis by avoiding charging of the samples. Afterwards, the carbon coated samples were placed into the Carl Zeiss EVO MA15 device for a high spatial resolution analysis of the sample. The images of the samples were taken at different magnifications ranging from 50 – 1500. Figure 3. 16 shows the image of the Carl Zeiss EVO MA15 microscope.

EDX analysis was carried out alongside the SEM to obtain information on the elemental composition of the samples. This involves qualitative microanalysis of

the samples to identify the elements present in a sample from their distinctive X-ray peaks. These X-ray peaks are generated as a focused beam of electrons in the SEM penetrates through the samples. Thereafter, the EDX detector identifies the X-rays and represents the signal in the form of a graph of intensity against energy. The energy corresponds to a characteristic element, which helps to determine the elements present in the sample.

Figure 3. 16 - Carl Zeiss EVO MA15 Scanning Electron Microscope.

Chapter 4 - Factors influencing $CaCO_3$ formation in the bulk solution and on steel surfaces at low SR

This chapter presents the results from the study of the factors that influences the kinetics of $CaCO_3$ precipitation in the bulk solution and on stainless steel surfaces at low SR conditions. The role of temperature, SR and flowrate on the kinetics of $CaCO_3$ formation was examined. The *in-situ* visualisation cell was used to assess the kinetics of $CaCO_3$ deposition on the surface whilst the static jar method was used to study the kinetics of $CaCO_3$ precipitation in the bulk solution.

4.1 Kinetics of $CaCO_3$ formation in the bulk:

In this section, the results obtained from the study of the effect of SR and temperature on the kinetics of $CaCO_3$ precipitation in the bulk solution using the static jar setup are presented. An understanding of the kinetics of $CaCO_3$ precipitation in the bulk solution is important for assessing the induction time and the growth-rate of $CaCO_3$ in the bulk solution. This information is useful for the once-through surface deposition tests conducted with the beadpack and the *in-situ* visualisation cell to determine whether the deposition of $CaCO_3$ on the surface is being influenced by the precipitation of $CaCO_3$ in the bulk solution or if the deposition process is exclusively controlled by heterogeneous nucleation on the surface.

4.1.1 Effect of SR on bulk precipitation kinetics

Extensive research has been undertaken to understand the thermodynamics of bulk precipitation. However, the effect of SR and temperature on the kinetics of bulk precipitation especially in low SR solutions is an area that still requires research attention. An improved understanding of the kinetics of bulk precipitation is required to relate this to experiments considering surface deposition in constant composition environments to determine whether homogeneous nucleation and growth is likely to occur in conjunction with heterogeneous nucleation and growth on stainless-steel surfaces.

Previous research on the effect of SR on the kinetics of $CaCO_3$ precipitation in the bulk solution, performed with a turbidity meter showed no evidence for the precipitation of $CaCO_3$ in the bulk at low SR (i.e. SR 10, SR 15, SR 25 and SR 45)[119]. The findings from the study demonstrated that heterogeneous nucleation on the surface can take place without the influence of homogenous nucleation in

the bulk solution, in the work it was reported that the mechanism controlling the formation of $CaCO_3$ at low SR is surface crystallisation [119]. In this study, the AAS (Atomic absorption spectroscopy) technique is used to determine the effect of SR on the induction time as well as the mechanisms and kinetics of $CaCO_3$ formation in the bulk solution at low SR (below SR 10).

Static jar tests were performed to investigate the kinetics of bulk precipitation in solutions of SR 10, 5 and 3 at 50°C and 90°C. The results at both 50°C and 90°C are shown in Figure 4. 1 and Figure 4. 2 respectively, indicating that the rate of scale formation increased as the SR was increased, which is to be expected due to the higher concentration of scaling ions in the solution as SR increased.

The induction time for the bulk precipitation test relates to the time it takes for the first measurable drop in the calcium ion concentration of the bulk solution to be observed. The results for the 50°C test show an induction time of 10 minutes for SR 10 and 25 minutes for SR 5. However, for SR 3, there was no change in calcium ion concentration for the whole 240 minutes duration of the test. The bulk precipitation tests at SR 3 were conducted for 240 minutes to compare the results obtained from the tests to the results observed at SR 10 and SR 5 at the same temperature (50°C), as a quantifiable amount of precipitation was achieved within a duration 240minutes at SR 10 and SR 5. The data suggests that there is no precipitation of $CaCO_3$ crystals in the bulk at SR 3 within the associated timeframe. A similar trend was observed for SR 10 and SR 5 results at 90°C, where the induction time increased as SR reduced. The only exception was SR 5 and SR 3 at 90°C, where an indistinguishable induction time of ~25 minutes was observed for both (Figure 4. 2).

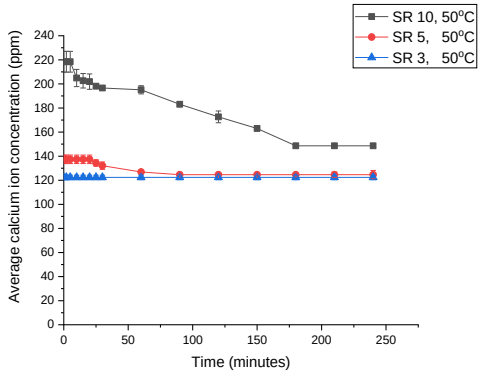

Figure 4. 1- Average Ca^{2+} ion concentration vs time graph for SR 10, 5 and 3 at 50°C from measured results.

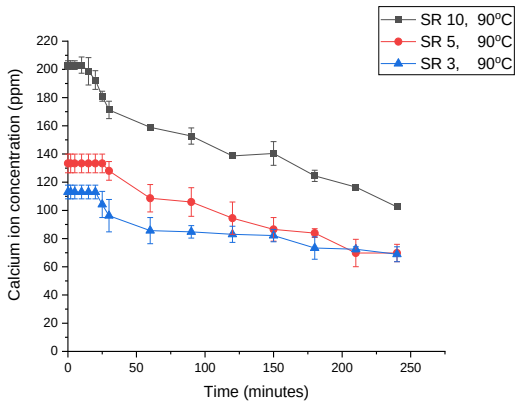

Figure 4. 2 - Average Ca^{2+} ion concentration vs time graph for SR 10, 5 and 3 at 90°C from measured results.

4.1.2 Effect of temperature on bulk precipitation kinetics

An increase in temperature accelerates the fouling process due to the inverse solubility relationship of calcite scale with temperature. However, little attention has been given to assess the implications of increased temperature on the kinetics of scale precipitation in the bulk solution in low SR brines.

The data presented in this section consist of the same temperature/SR combinations as the results shown earlier for bulk precipitation experiments. However, the information is represented differently to highlight the role of increasing the temperature from 50°C to 90°C at the same SR. The results for the effect of increasing temperature on the induction time show no appreciable difference in induction time as temperature increased in both SR 10 and 5 solution (Figure 4. 3 and Figure 4. 4). It is only at SR 3 that a significant, notable difference in induction time was noted due to the increase in temperature. At 90°C the induction time was 25 minutes. However, at 50°C there was no formation of $CaCO_3$ in the solution within the 4 hours duration of the test (Figure 4. 5).

The pronounced effect of increased temperature was evident for all three SRs (SR 10, 5 and 3) after the induction period, for example, at SR 10 and 50°C, there was no further change in the calcium ion concentration after 120 minutes, whilst at 90°C the calcium ion concentration continued to decrease steadily for the entire 240 minutes duration of the test. A similar trend was observed for SR 5 and SR 3. This demonstrates the impact of higher temperature in accelerating the formation of $CaCO_3$ in low SR solutions.

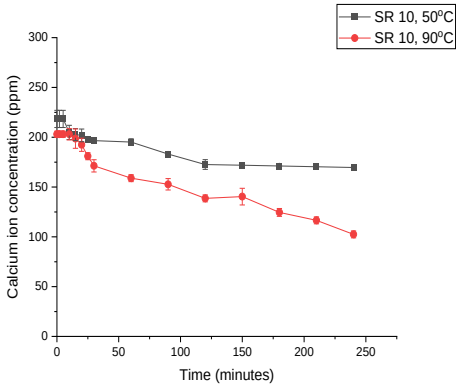

Figure 4. 3 - Average Ca^{2+} ion concentration vs time graph for SR 10 at 90°C and 50°C from bulk precipitation test.

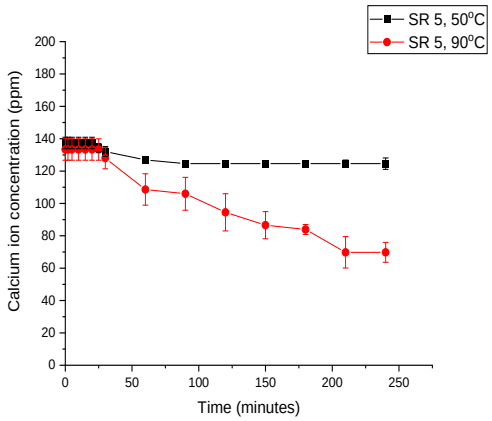

Figure 4. 4 – Average Ca^{2+} ion concentration vs time graph for SR 5 at 90°C and 50°C from bulk precipitation test.

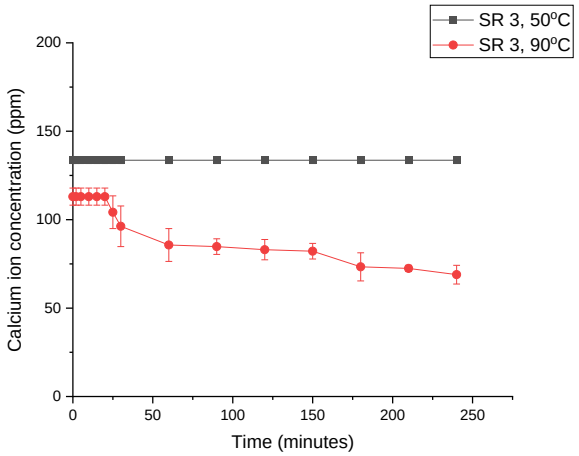

Figure 4. 5 – Average Ca^{2+} ion concentration vs time graph for SR 3 at 90°C and 50°C from bulk precipitation test.

4.2 Factors influencing $CaCO_3$ deposition on the surface

4.2.1 Introduction

In this section, the results obtained for the effect of SR and flowrate on the mechanisms and kinetics of scale deposition on the surface are discussed.

The images from the *in-situ* visualisation cell experiements were processed using the MATLAB programme developed in this study, this is detailed in the method section section 3.5.2. The images were analysed to obtain information such as the number of crystals, average size and surface coverage of crystals deposited on the surface of the stainless steel material with time to quantify the kinetics of $CaCO_3$ deposition at low SR.

In the next section the results from the study of the effect of SR on the kinetics of $CaCO_3$ deposition on the surface at 50°C is presented.

4.2.2 Effect of SR on the surface deposition $CaCO_3$ at 50°C

The *in-situ* visualisation cell images of the crystals deposited on the surface of the stainless steel sample during the test for effect of SR (10, 5 and 3) on the kinetics of surface deposition at 50°C and 20ml/min, was captured at every 5 minutes interval, the images of the crystals at 5, 60, 120 and 240 minutes are presented in Figure 4. 6. The images clearly showed that the kinetics of scale deposition increased as SR increased. Furthermore, the images were processed to have an

insight into the number of crystals formed, average size of the crystals and the surface coverage of the crystals.

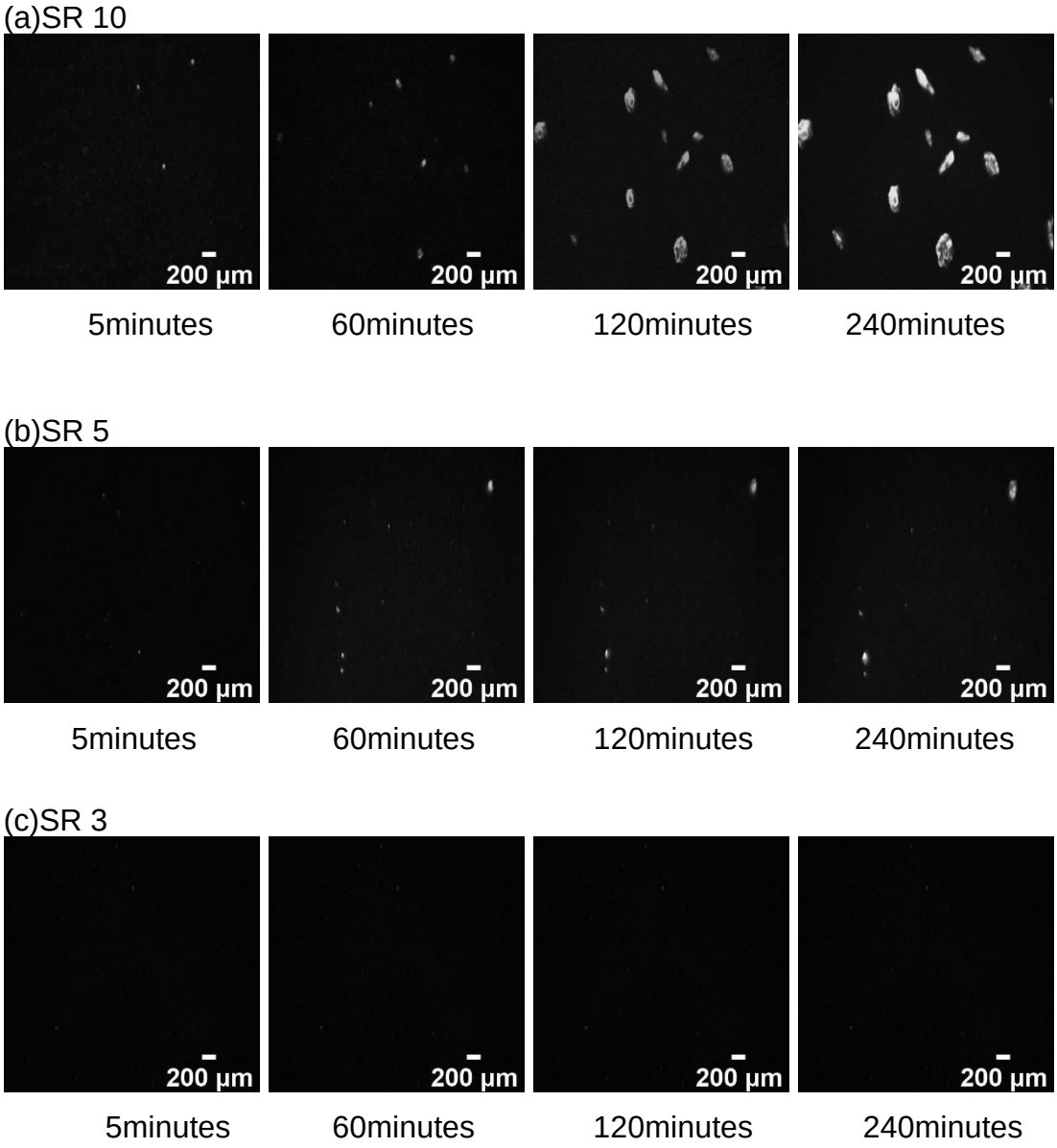

Figure 4. 6 – *In-situ* visualisation cell images for the crystals formed on the stainless-steel sample after 5, 60,120 and 240 minutes for SR (a) 10, (b) SR 5 and (c) SR 3 at 50^{o}C.

4.2.2.1 Effect of SR on number of crystals at 50^{o}C

Figure 4. 7 shows the number of crystals formed on the surface as a function of time for SR 10, 5 and 3 at 50^{o}C. The results demonstrate that generally, the number of crystals deposited increased as SR increased. This finding is consistent with that of Sanni et al[97], who investiagted the effect of SR (i.e SR 10, 15, 25, 45 and 60) on the number of crystals deposited on the surface at 40^{o}C, the study also reported that as SR increased, the number of crystals also increased. However,

this study provides insight into the kinetics of $CaCO_3$ deposition on the surface at lower SR (i.e below SR 10).

There was no induction time observed for all 3 SRs investigated. In addtion, at SR 10 within the first 30 minutes of the experiment, 6 crystals nucleated on the surface and this number increased to 16 after 60 minutes before stabilisation was attained.

At SR 5, there were 6 crystals observed on the surface for the first 40 minutes of the experiment, which increased to 8 crystals shortly after. Thereafter, there was no further increase in the number of crystals precipitated on the surface until the end of the experiment. At SR 3, only 3 crystals was observed to be deposited on the surface within the view of the camera from the start of test to the end of the experiment, which ran for 4 hours.

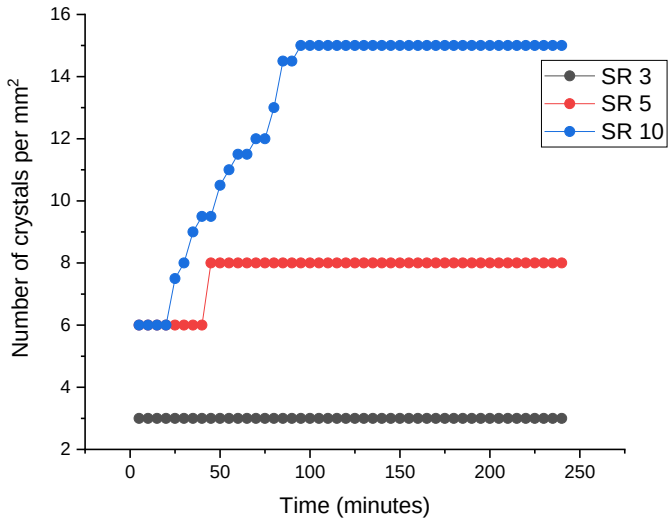

Figure 4. 7 – Comparing the number of crystals deposited on the surface with time at 50°C and SR 3,5,10.

4.2.2.2 Effect of SR on the average size of crystals at 50°C

Figure 4. 8, shows the plot for the average size of crystals formed on the surface for SR 10, 5 and 3 at 50°C after a duration of 4 hours. Generally, it was observed that the average size of the crystals increased as the SR increased. This result is in line with the previous work also conducted with the *in-situ* visualisation cell at higher SR (above SR 10)[97].

This is expected due to the higher concentration of scaling ions in the brine, which supports the growth of crystals on the surface. At SR 10, a sharp linear increase in the size of the crystals was observed for the first 180 minutes, but after this the

rate at which the crystals grew reduced steadly, until the end of the test. This suggests that the growth of the crystals is approaching equillibrium point.

At SR 5, the rate at which the size of the crystals increased with time was slower compared to the trend at SR 10, which is expected due to the lower concentration of scaling ions at this condition. A linear increase in the size of the crystals with time was also observed which is similar to the results obtained at SR 10. However at SR 5, the steady linear increase in the size of the crystals continued from the start of the experiment until its termination after 240 minutes.

Moreso, it was also observed that the average size of crystals generally increased with time at SR 10 and SR 5, this can be attributed to the constant flow of fresh brine (rich in scaling ions, Ca^{2+} and CO_3^{2-}) in the *in-situ* visualisation cell, which encouraged the continous growth of the crystals for the entire duration of the experiement.

In constrast to the result obtained at SR 10 and SR 5, at SR 3 there was no increase in the size of the crystals formed on the surface for the entire 240 minutes duration of the test, indicating that there was no crystal growth at this condition. This is attributed to the very low concentration of scaling ions, in the brine, which was insufficient for the crystal growth process at SR 3.

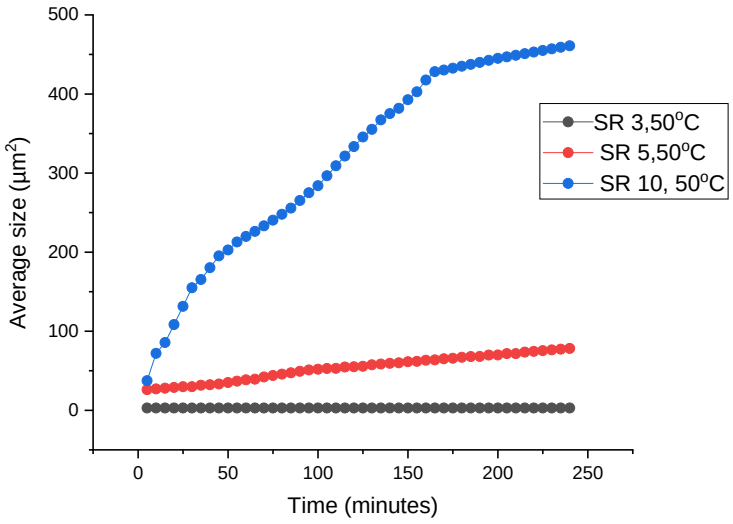

Figure 4. 8 – Comparing the average size of crystals formed on the surface with time at 50°C and SR 3,5,10.

4.2.2.3 Effect of SR on the surface coverage of crystals at 50°C

The results for the surface coverage of the crystals with time for SR 10, 5 and 3 at 50°C are presented in Figure 4. 9**.** These show that generally the surface coverage

increased as SR increased due to the higher number and larger size of crystals precipitated on the surface as SR increased. This result is also in agreement with previous research on the kinetics of $CaCO_3$ surface deposition, which found that at higher SR (i.e. above SR 10), surface coverage of crystals also increased as SR increased [119] .

At SR 10, the surface coverage of the crystals increased noticeably, following a linear trend for the first 180 minutes of the experiment. Afterwards, the growth in surface coverage started to reduce slowly with time, which suggests that growth of the crystals is approaching stabilisation.

At SR 5, a less pronounced increase in the surface coverage of the crystals with time was observed, which can be attributed to the lower ionic composition at this condition in comparison with the SR 10. The surface coverage of the crystals increased slowly from the start of the experiment until the end of the test, which lasted for 240 minutes.

However, at SR 3, there was no change in the surface coverage of the crystals for the whole 240 minutes duration of the test, suggesting that there was no growth of crystals on the surface at this condition.

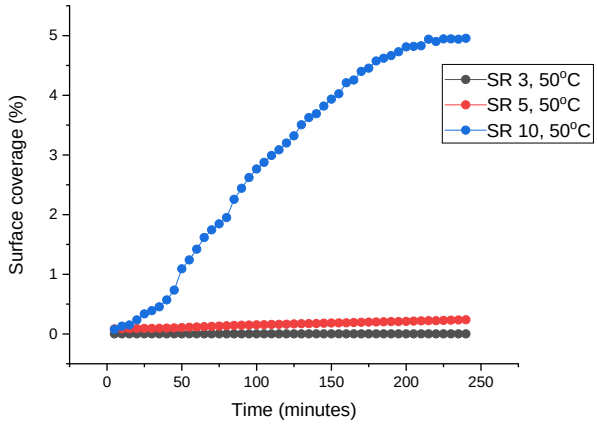

Figure 4. 9 – Comparing the surface coverage of crystals deposited on the surface with time at 50°C and SR 3,5,10.

4.2.2.4 SEM images for SR 10, 5 and 3 at 50°C

The SEM images of the crystals deposited on the surface of the stainless-steel samples after 4 hours for SR 10, 5 and 3 at 50°C are presented in Figure 4. 10. At SR10, the SEM images provided evidence for predominantly deformed calcite polymorphs of $CaCO_3$; this is assumed due to the morphology of the crystals. However, vaterite polymorphs were also observed at this condition.

At SR 5, mainly cubic shaped calcite crystals were observed. However, it was observed that the least number of crystals was deposited at SR 3, which is expected as it is the lowest SR investigated in this experiment, also the crystals formed at this condition did not appear to have a defined structure or grow into a substantial size. This findings match those of Kitamura et al[130] whose research found that stable calcite polymorph of $CaCO_3$ precipitated in the bulk solution at low SR whilst vaterite crystals was predominantly formed at high SR.

The number of crystals observed on the SEM images is generally higher than the crystal count from the *in-situ* visualisation cell images because the SEM images captures a broader area of the stainless steel sample compared to the *in-situ* visualisation cell images. Nonetheless, in line with the results obtained for the number of crystals deposited on the surface with time from the *in-situ* visualisation cell (Figure 4.7), the SEM images shows that the number of crystals deposited increased as the SR increased i.e. 25 crystals observed at SR 10, 11 at SR 5 and only 3 formed crystals at SR 3.

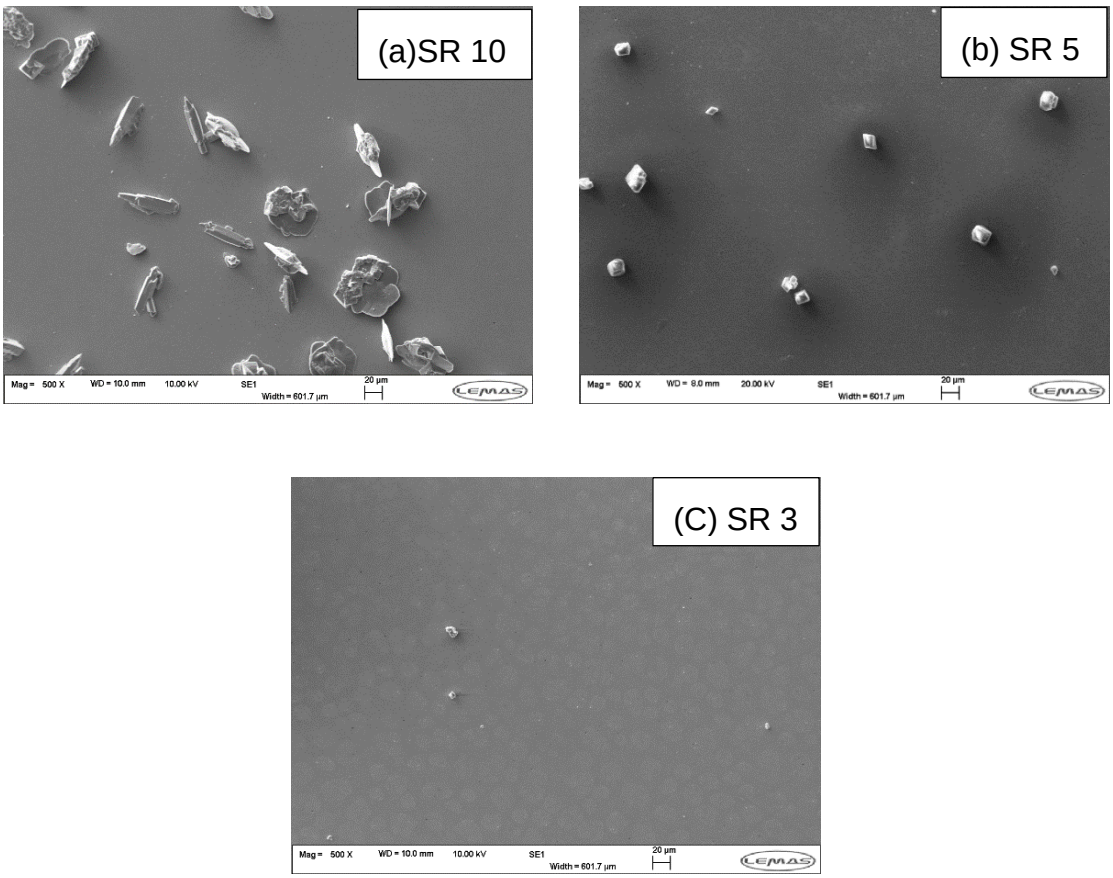

Figure 4. 10 – SEM images of the $CaCO_3$ crystals formed on the stainless-steel sample for (a) SR 10, (b) SR 5 and (c) SR 3 at 50ºC after the 4-hour duration of the test.

In addition, EDX analysis was also carried out on the crystals formed at SR 3 to determine the elemental composition of the crystals and to verify if the crystals

formed were $CaCO_3$ crystals, the SEM image with the spectrum numbers from the EDX analysis are shown in Figure 4. 11 and the EDX result for the elemental composition of the crystal is presented in Figure 4. 12 provides little evidence for the formation of $CaCO_3$ scale.

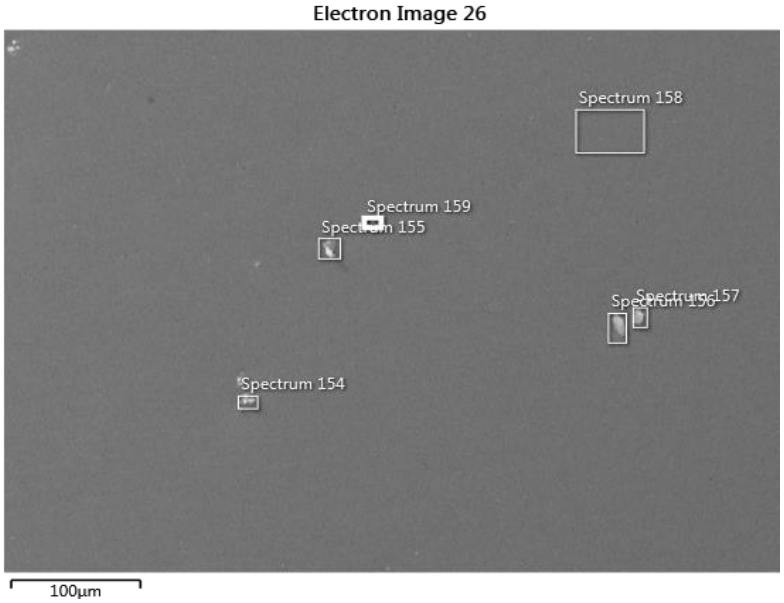

Figure 4. 11 – SEM images of the crystals formed on the stainless-steel sample for SR 3 at 50°C.

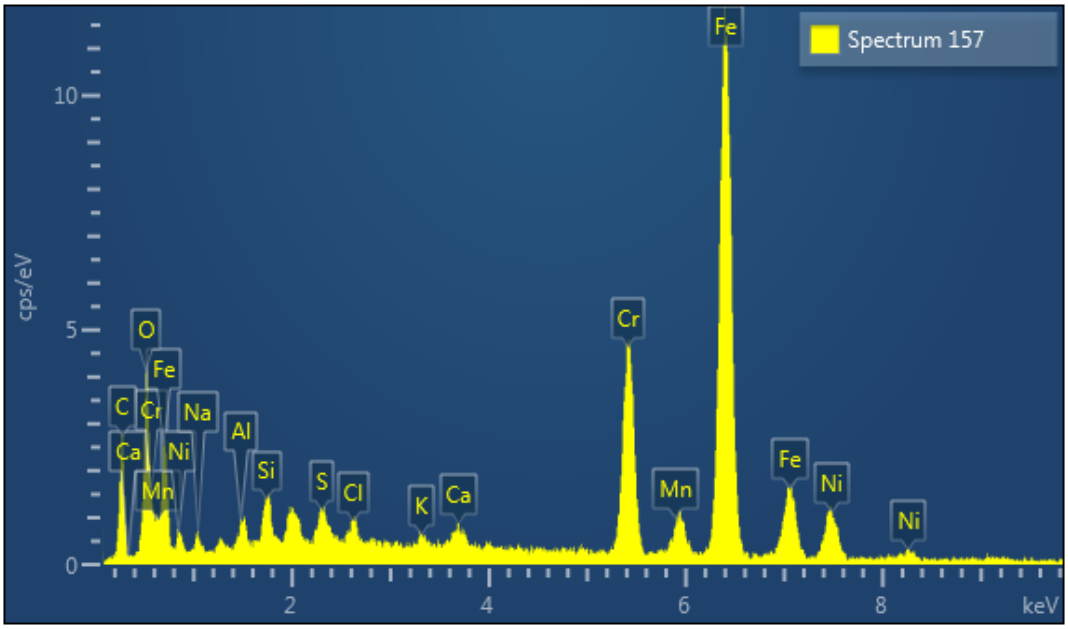

Figure 4. 12 - EDX analysis results for the crystal at spectrum 157, for the test conducted at 50°C and SR 3, which suggests the presence of small traces of $CaCO_3$ deposited on the surface of the stainless-steel sample.

4.2.3 Effect of SR on the quantification of $CaCO_3$ growth on the surface at 79°C

The effect of SR 8, SR 4 and SR 2 at 79°C on the number of crystals, Figure 4. 13**,** average size of crystals, Figure 4. 14 and surface coverage of crystals, Figure 4. 15 was examined. The results generally illustrates that as the SR increased, there was an increase in nucleation which relates to the number of crystals. There was also evidence for increase in the growth of crystals as the SR increased from the average size of crystals results. In addition, the surface coverage results which accounts for both the nucleation and growth of crystals also demonstrates an increase in the overall kinetics of $CaCO_3$ deposition on the surface as SR increased.

This results are in accordance with earlier observations by Eleftheria et al[81] whose study on the kinetics of $CaCO_3$ deposition performed with the capillary rig at SR 5 , SR 6, SR 8, and and SR 11 at 80°C also revealed that the kinetics of $CaCO_3$ deposition increased as SR increased. It was also reported in the study that the induction time for $CaCO_3$ deposition to take place on the surface at SR 5 was 92 hours. The very long induction time observed at this SR indicates that the capillary rig is not suitable for assesing the kinetics of $CaCO_3$ deposition at low SR 5 (i.e below SR 5) because it takes a long time to obtain reasonable data on the kinetics in the laboratory.

Nonetheless, the increase in the kinetics of $CaCO_3$ deposition as SR increased is expected due to the higher ionic composition present at the higher SR. However, the number of crystals nucleated on the surface at SR 4 was very similar to the number of crystals at SR 2.

In addition, at SR 8, the number of crystals precipitated increased rapidly from the onset of the experiment until 75 minutes, during which 42 crystals were observed to be deposited on the surface. Afterwards, there was no further increase in the number of crystals until the end of the experiment which lasted for 240 minutes, indicating the end of the nucleation process.

At SR 4, considerably fewer crystals were observed to be deposited on the surface when compared to SR 8 at the same temperature. A maximum of 10 crystals were counted on the surface from the start of the test until about 30 minutes. Thereafter, there was no further increase in the number of crystals until the termination of the experiment.

The kinetics of the nucleation of crystals at SR 2 was observed to be comparable to the results obtained at SR 4, which is unexpected, as the brine composition is higher at SR 4. The similar rate of nucleation at SR 4 and SR 2 can be attributed

to the low concentration of scaling ions (Ca^{2+} and CO_3^{2-}) in the brine at these conditions and the lack of a high area-to-volume ratio in the *in-situ* visualisation cell which did not favor the nucleation of a considerable about $CaCO_3$ crystals on the surface these condition. The presence of a high area-to-volume ratio in the cell is suspected to be beneficial for effectively assessing the differences in the kinetics of $CaCO_3$ deposition at these two low SR conditions.

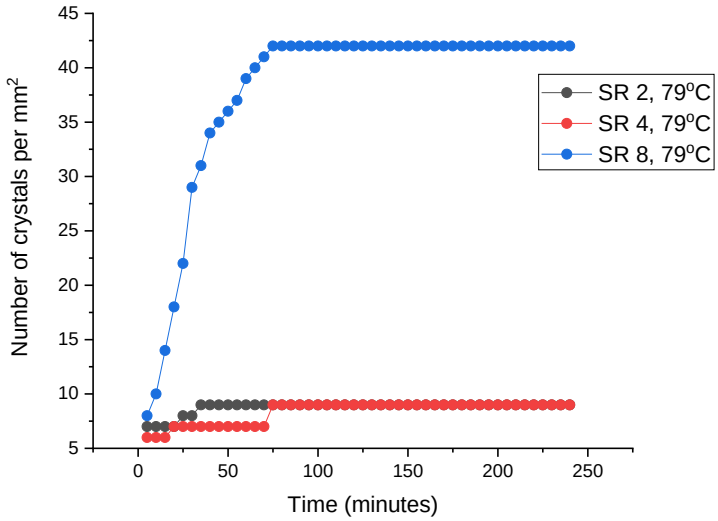

Figure 4. 13 – Comparing the number of crystals deposited on the surface with time at 79°C and SR 2, 4, 8.

In line with the previous data obtained for the effect of SR on the average size of crystals with time at 50°C, the kinetics of crystal growth on the surface increased as SR increased. Previous research on scale deposition has been focused on understanding the mechanisms and kinetics of scale deposition at higher SR (above SR 10) [102, 119, 131]. However, this study provides insight into the kinetics of scale deposition at a lower SR (below SR 10).

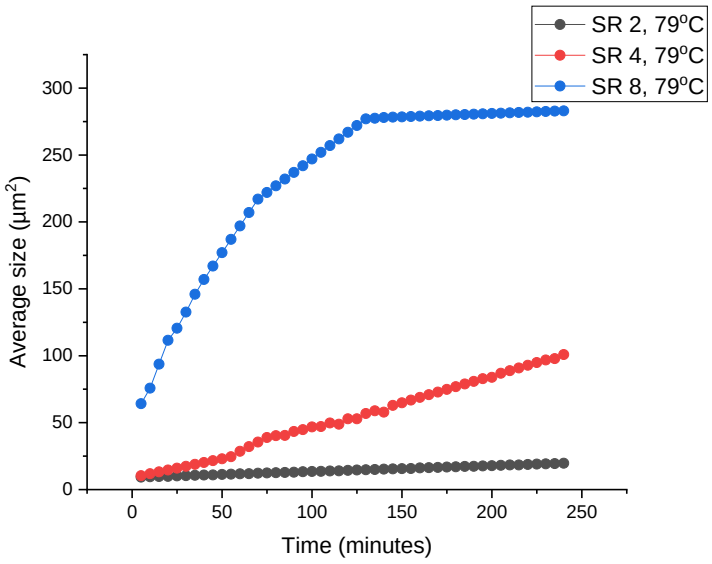

Figure 4. 14 – Comparing the average size of crystals formed on the surface with time at 79°C and SR 2, 4, and 8.

Figure 4. 16 shows the graph of the surface coverage of the crystals with time for SR 8, 4 and 2 at 79°C. The result illustrates that generally, the surface coverage increased as SR increased. This results in line with the *in-situ* visualisation cell images presented in Figure 4. 16, the data is also in accordance with the findings from previous research reported in literature [97].

Nonetheless, as observed earlier from the results for the average size of crystals deposited on the surface with time, shown in Figure 4.15, the surface coverage at SR 4 and SR 2 were observed to be comparable. This can be attributed to the low concentration of scaling ions in the solution at these two low SR conditions, as well as the lack of a high area-to-volume ratio in the *in-situ* visualisation cell which did not encourage the deposition of a substantial amount of $CaCO_3$ scale on the surface.

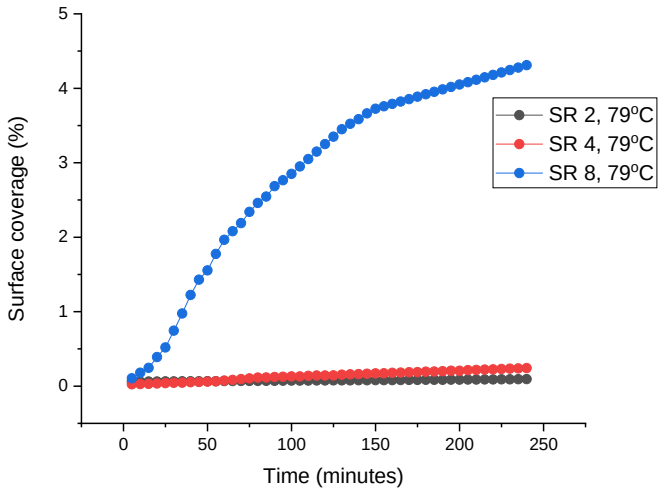

Figure 4. 15 – Comparing the surface coverage of crystals deposited on the surface with time at 79°C and SR 2, 4 and 8.

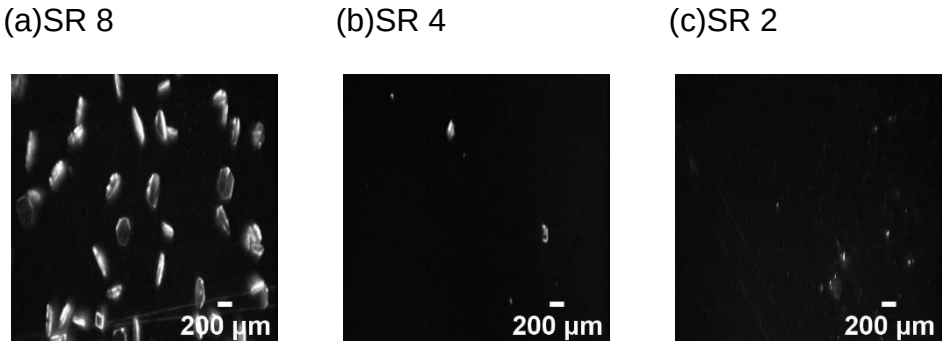

Figure 4. 16 – *In-situ* visualisation cell images for the crystals formed on the stainless-steel sample after 240 minutes for SR 8, SR 4 and SR 2 at 79°C.

4.2.3.1 SEM images for the crystals formed at 79°C and SR 8, SR 4 and SR 2

The SEM image of the crystals deposited on the surface of the stainless-steel material after 4hours at SR 8, SR 4 and SR 2 at 79°C and flowrate of 20ml/min is shown in Figure 4. 17. The morphology of the crystals deposited at SR 8 and SR 4 appeared to mainly have a cubic shape, indicating that the crystals deposited are calcite polymorph of $CaCO_3$ scale. However, there was also evidence of elongated calcite crystals at both SR. This observation is consistent with those of Hu et al[132], whose study found that above 60°C, calcite polymorph of $CaCO_3$ was more likely to precipitate in the bulk solution.

Meanwhile at SR 2, the crystals observed on the surface did not have a defined shape, EDX analysis was carried on the crystals to determine their elemental

composition, this is presented in Figure 4. 18, the EDX results suggest that the crystals observed was mostly NaCl as shown in Figure 4. 19 and Figure 4. 20. Nonetheless, there was little evidence for the deposition of $CaCO_3$ at SR 2 as the EDX analysis of the crystal at spectrum 62 as shown in Figure 4. 21 indicates that $CaCO_3$ was present on the surface. Overall, the SEM images of the $CaCO_3$ crystals deposited at the different SR's investigated illustrates that the number of $CaCO_3$ crystals deposited on the surface increased as SR increased.

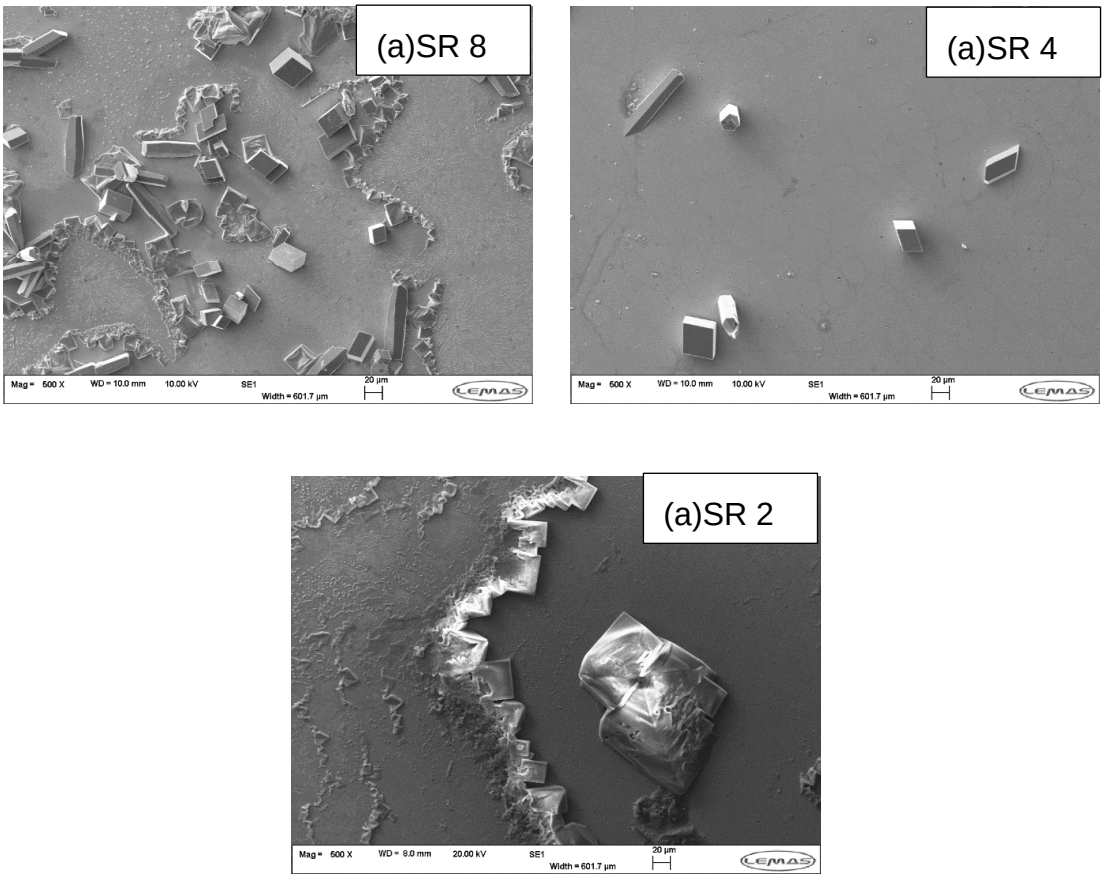

Figure 4. 17 – SEM images of the $CaCO_3$ crystals formed on the stainless-steel sample at (a) SR 8 and (b) SR 4 (C) SR 2 and 79^oC after the 4hour duration of the test.

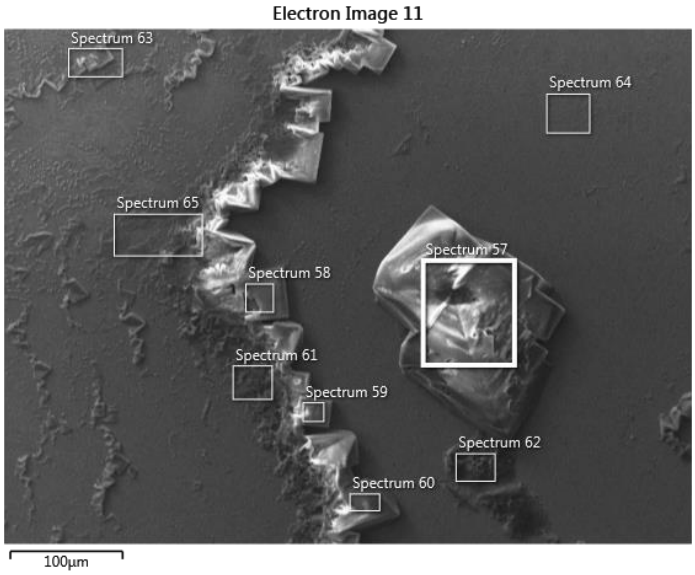

Figure 4. 18 – SEM image with spectrum number from the EDX analysis of the crystals formed on the stainless-steel sample at SR 2 and 79ºC.

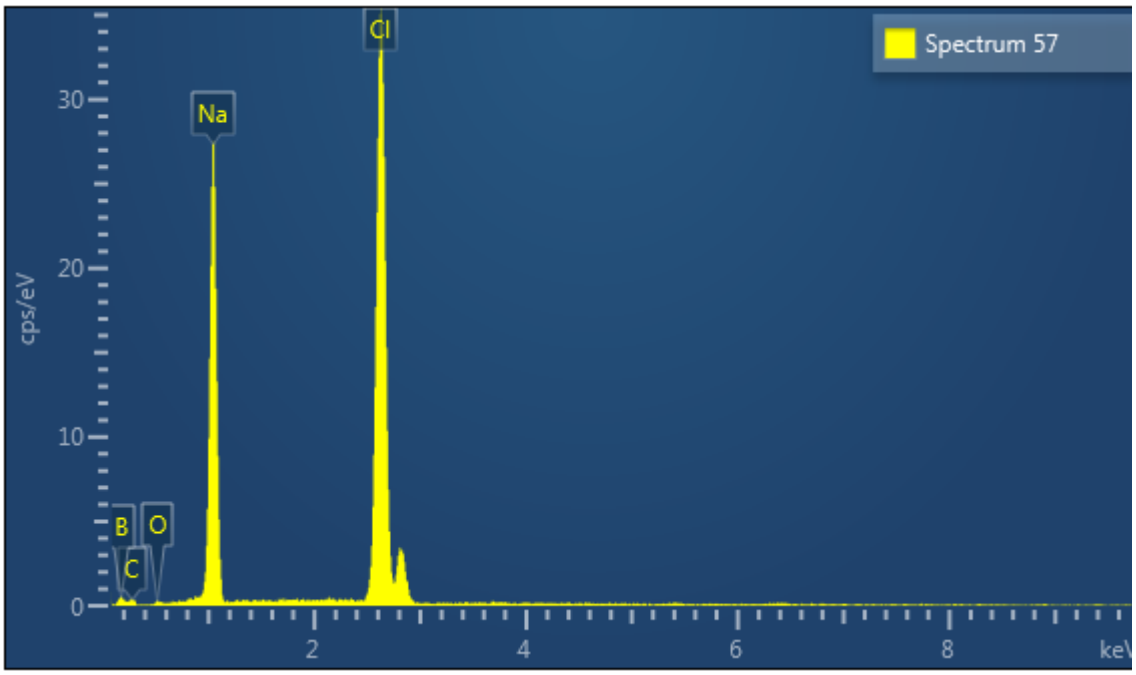

Figure 4. 19 - EDX analysis results of the crystal at spectrum 57 in electron image 11 for the test conducted at 79ºC and SR 2, which suggests that the crystal on the stainless-steel sample is NaCl.

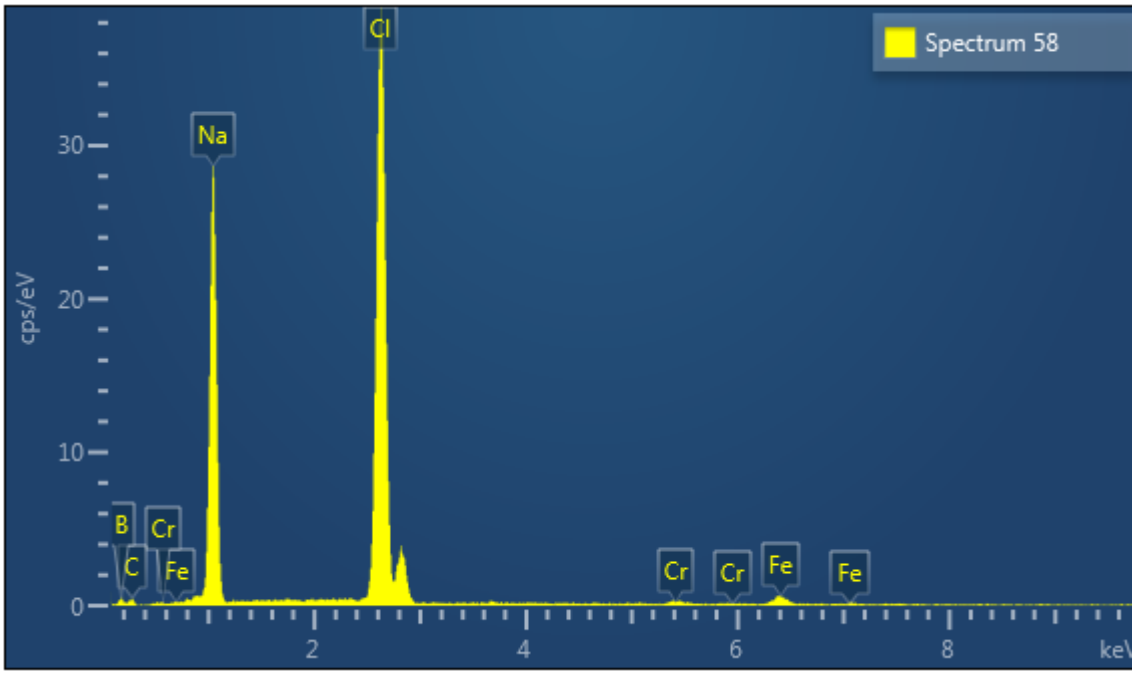

Figure 4. 20 - EDX analysis results of the crystal at spectrum 58 in electron image 11 for the test conducted at 79ºC and SR 2, which suggests that the crystal on the stainless-steel sample is NaCl.

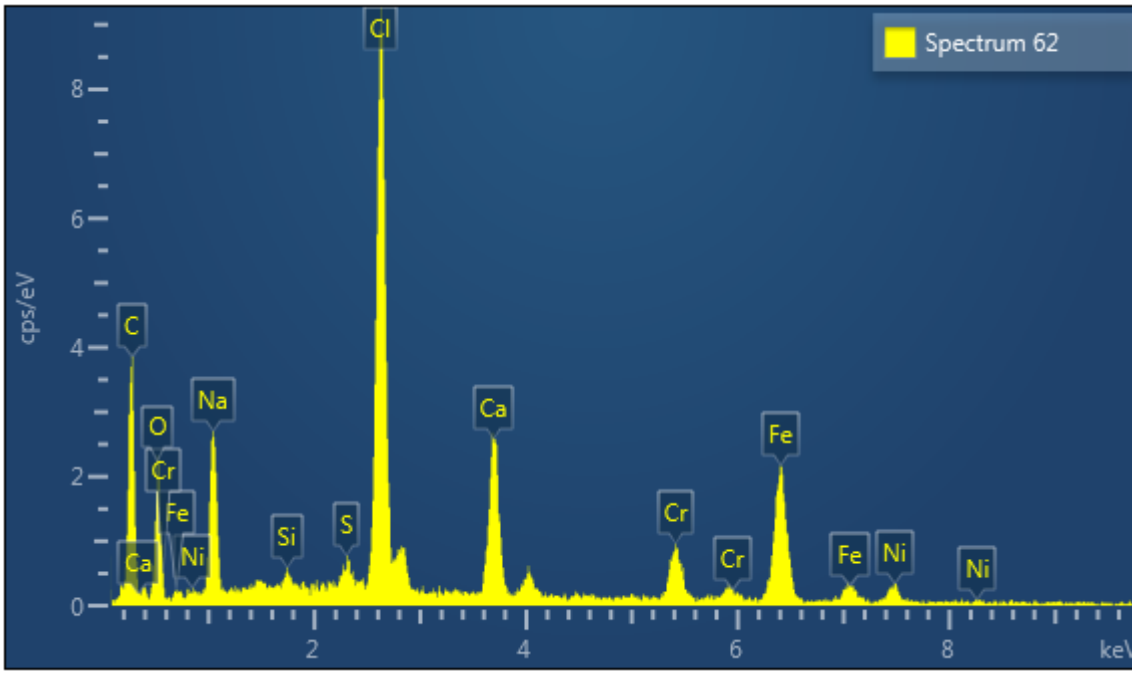

Figure 4. 21 - EDX analysis results of the crystal at spectrum 62 in electron image 11 for the test conducted at 79ºC and SR 2, which suggest the formation of $CaCO_3$ on the stainless-steel sample.

4.2.4 Effect of flowrate on surface deposition of $CaCO_3$ at 50°C

The effect of flowrate (20 and 30 ml/min) on the kinetics of surface deposition for SR 10, 5 and 3 at 50°C were investigated and the results are presented in this section.

The *in-situ* visualisation cell images showing the crystals deposited on the surface of the stainless-steel bead at 5, 60, 120 and 240 minutes at a flowrate of 20ml/min and 30ml/min at SR 10 and 50°C is presented in Figure 4. 22.

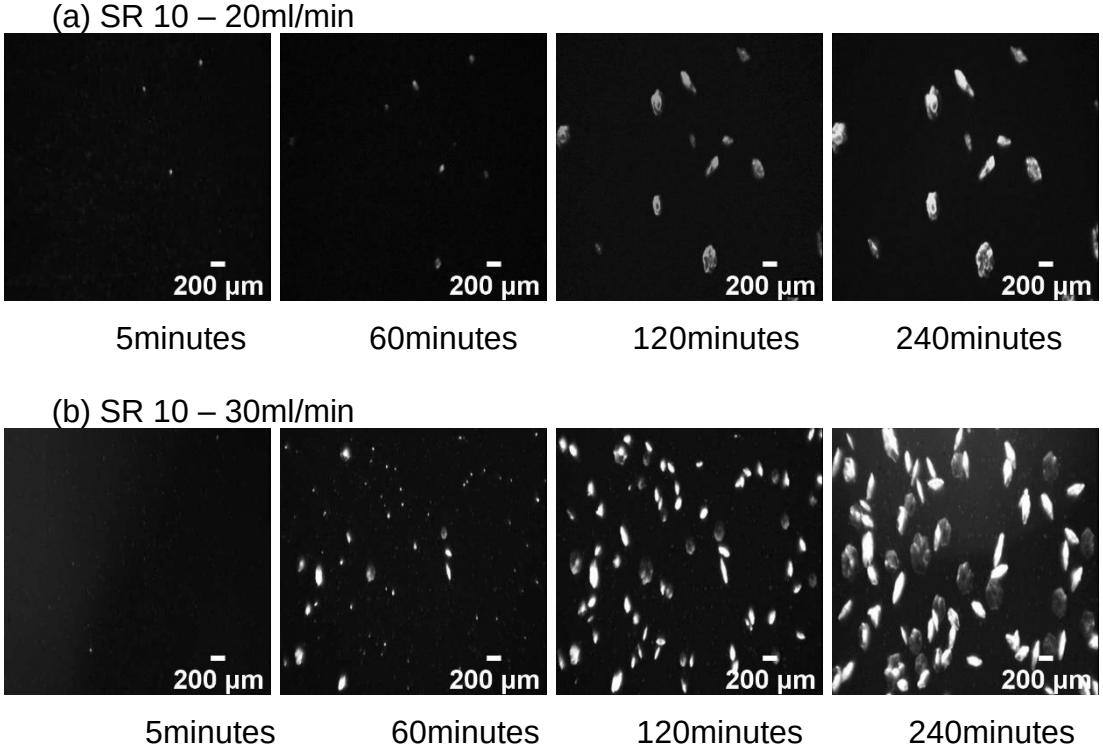

Figure 4. 22 - Images of $CaCO_3$ scale deposition for brine with SR 10 at 5, 60, 120 and 240minutes time intervals and flowrate of (a) 20ml/min and (b) 30ml/min at 50°C.

4.2.4.1 Effect of flowrate on number of crystals at SR 10

Figure 4. 23 shows the trend for the effect of increasing the flowrate from 20ml/min to 30ml/min at SR 10 on the number of crystals deposited on the surface with time, the experiment was conducted at 50°C.

It was observed that the increase in flowrate resulted in a significant increase in the number of crystals precipitated on the surface with time. These results was also reported by Sanni et al[122], who investigated the effect of increasing the flowrate from 10ml/min to 40ml/min on the number of crystals deposited on the surface at SR 45, the results showed a pronounced increased in the number of crystals deposited on the surface due to the increase in flowrate. The gap in the

study is that it does not provide any insight into the kinetics of $CaCO_3$ deposition at low SR (below SR 10). However, this study helps to understand the kinetics of $CaCO_3$ deposition at low SR.

At SR 10, a total of 15 crystals was deposited during the test at 20ml/min, whilst 55 crystals were deposited on the surface at 30ml/min, illustrating the impact of increasing the flowrate on the number of crystals formed on the surface.

Furthermore, at 20ml/min, the number of crystals formed on the surface steadily increased from the start of the test until about 100 minutes. Afterwards, there was no further increase in the number of crystals deposited on the surface, suggesting that equilibrium point has been attained. However, at 30ml/min, the number of crystals precipitated on the surface increased rapidly from the onset of the experiment till 25 minutes, and subsequently there was no further increase in the number of crystals until the termination of the experiment which ran for 240 minutes. This suggests that an increase in flowrate results in a reduction of the time it takes for equilibrium point to be attained due to the increase in the kinetics of scale deposition as the flowrate increased [122, 133]. This might be explained by the fact that an increase in flowrate encourages a better mixing of the brine which increases the likelihood for nucleation to take place on the surface, thereby, causing a faster rate of $CaCO_3$ deposition on the surface.

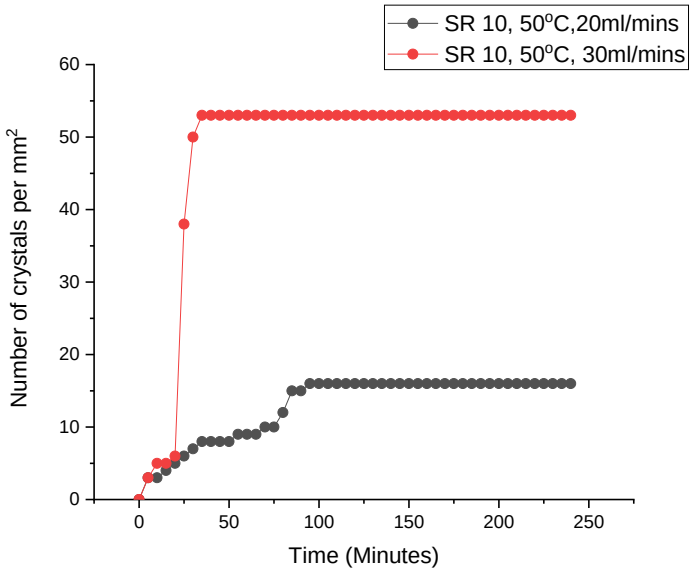

Figure 4. 23 – Comparing the number of crystals deposited on the surface with time at 50°C, SR 10 and flowrate of 20 and 30ml/min.

4.2.4.2 Effect of flowrate on average size of crystals at SR 10

The graph showing the results for the effect of increased flowrate from 20ml/min to 30ml/min on the average size of crystals deposited on the surface with time at SR 10 and 50^{o}C is presented in Figure 4. 24.

The findings from this test demonstrates that an increase in flowrate led to a slight reduction in the average size of the crystals formed on the surface with time. An average area of 500µm^2 was attained at 20ml/min and a lower average area of 350µm^2 was attained at the higher flowrate of 30ml/min. This can be attributed to the significantly higher number of crystals which formed at 30ml/min, where 55 crystals formed on the surface in comparison to the 20ml/min, where only 15 crystals were observed. It is suspected that the crystals grew larger at 20ml/min in comparison to 30ml/min due to the notably lower amount of nucleation on the surface at the lower flowrate (20ml/min) in contrast to the higher flowrate (30ml/min). This result is in agreement with the findings from literature which suggests an inverse relationship between nucleation rate and crystal growth [63]. At 20ml/min, the average size of crystals increased continuously at a linear rate from the start of the experiment until 150 minutes. Afterwards, the growth rate of the size of crystals started to reduce slowly, indicating that equilibrium point was approaching. Whilst at 30ml/min, initially the average size of crystals also increased steadily for the first 20 minutes duration of the test. Afterwards, the average size of the crystals started to reduce gradually, this is due to the nucleation of new crystals on the surface which caused a reduction in the overall size of the crystals. Thereafter, the average size of crystals continued to increase steadily at a linear rate until the termination of the experiment, suggesting that there was no further nucleation of crystals, and the crystal growth process was dominat at this stage.

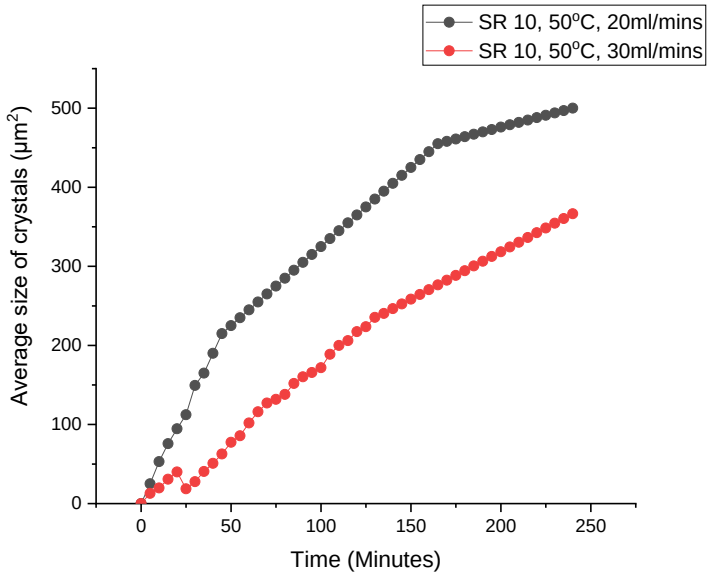

Figure 4. 24 – Comparing the average size of crystals formed on the surface with time at 50°C, SR 10 and flowrate of 20 and 30ml/min.

4.2.4.3 Effect of flowrate on surface coverage of crystals at SR 10

The graph showing the effect of increasing the flowrate from 20-30ml/min on the surface coverage of the crystals with time at SR 10 is presented in Figure 4. 25.

The results illustrate that generally as the flowrate increased, the surface coverage of the crystals also increased, this finding in agreement with previous work published in literature [122]. At 30ml/min, the surface coverage of the crystals increased rapidly at a linear rate from the commencement of the test till the termination of the experiment which lasted for 240minutes. A linear increase in the surface coverage of the crystals with time was also reported in earlier studies conducted the *in-situ* visualisation cell at SR 15, 25 and 45 at flowrates of 10, 20 and 40ml/min[97].

Similarly, at 20ml/min, the surface coverage of the crystals also initially increased linearly with time. However, the surface coverage at 20ml/min was evidently lower in comparison to the results obtained at 30ml/min. This is attributed to significantly higher number of crystals which deposited on the surface at 30ml/min even though the crystals grew slightly bigger at 20ml/minutes compared to 30ml/min, illustrating the role of increased flowrate in increasing the percentage of the stainless-steel surface covered by crystals.

In addition, for the 20ml/min test after 150 minutes, the surface coverage of the crystals started to reduce slowly until the termination of the experiment, suggesting that equilibrium point was approaching but in contrast, at 30ml/min the surface

coverage of the crystals continued to increase linearly with time until the end of the experiment.

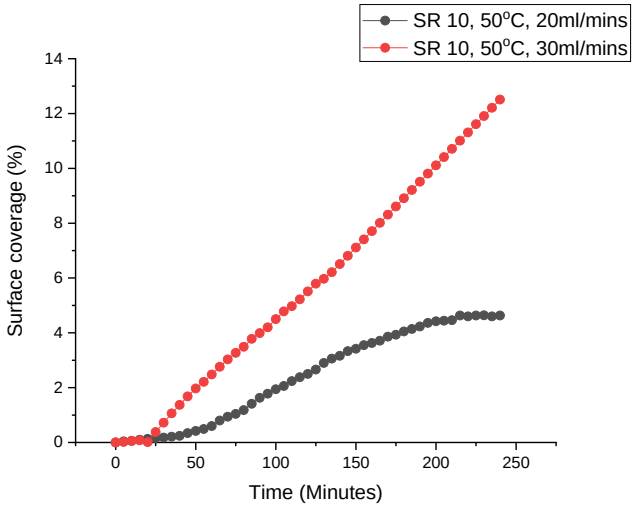

Figure 4. 25 – Comparing the surface coverage of crystals deposited on the surface with time at 50°C, SR 10 and flowrate of 20 and flowrate of 30ml/min.

4.2.4.4 SEM images for the crystals formed on the surface at 20ml/min and 30ml/min at SR 10

The SEM image of the $CaCO_3$ crystals deposited on the surface of the stainless steel sample after 4 hours, at SR 10, 50°C and flowrate of 20ml/min and 30ml/min are shown in Figure 4. 26.

The SEM images show that the number of crystals were notably higher at 30ml/min compared to 20ml/min, which is in line with the results obtained from the image processing software. Furthermore, at 20ml/min, the crystals appeared to have mostly a deformed cubic shape suggesting the presence of calcite polymorphs of $CaCO_3$ scale; there was also some evidence for leaflike vaterite polymorphs. At 30ml/min, predominantly leaf-like vaterite crystals were observed on the surface. This indicates that flowrate plays a role in the morphology of scale deposited on the surface at SR 10 and 50°C. This finding is in agreement with previous research in the literature [110, 130]. For instance, Yong[110] study revealed that, the formation of vaterite crystals was favoured at a high flowrate, this was attributed to the faster kinetics at the higher flowrate which reduced the tendency for vaterite to transform into calcite. However, at a lower flowrate only calcite polymorph was observed.

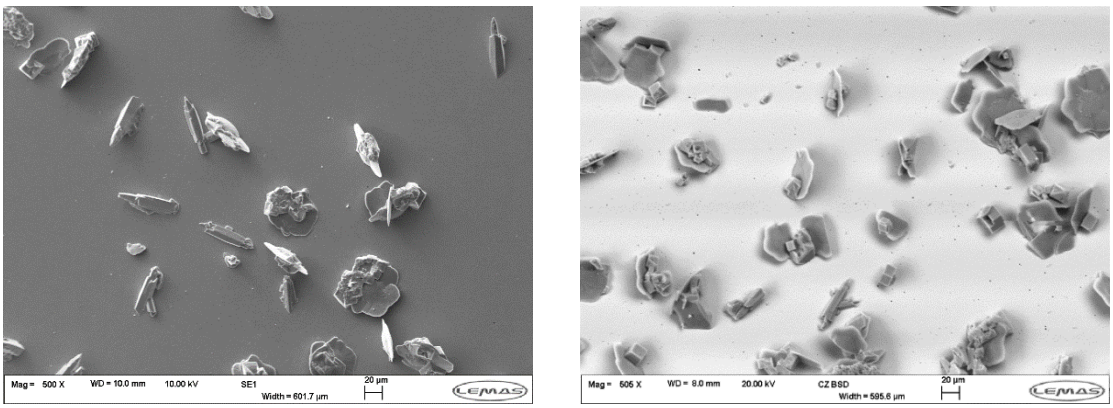

(a)SR 10 – 20ml/min (b)SR 10 – 30ml/min

Figure 4. 26 - SEM images of the $CaCO_3$ crystals deposited on the stainless-steel surface for brine with SR 10 after 4hours and flowrate of (a) 20ml/min and (b) 30ml/min at 50°C.

4.2.4.5 Effect of flowrate at SR 5

In – situ visualisation cell Images showing effect of flowrate on surface deposition at SR 5 is presented in Figure 4. 27.

(a)SR 5 – 20ml/minutes

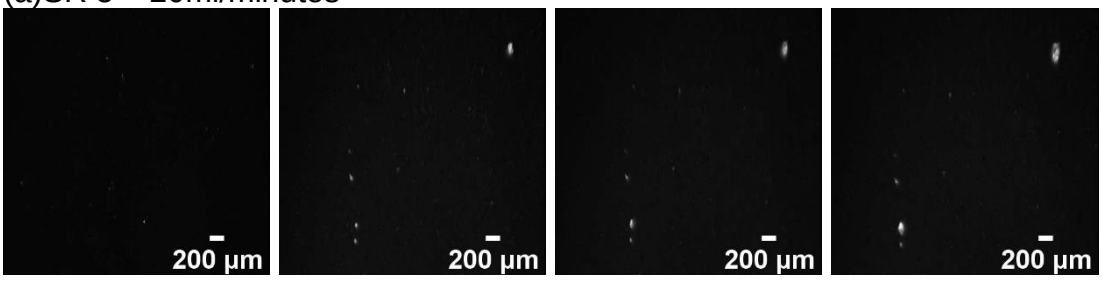

5minutes 60minutes 120minutes 240minutes

(b)SR 5 – 30ml/minutes

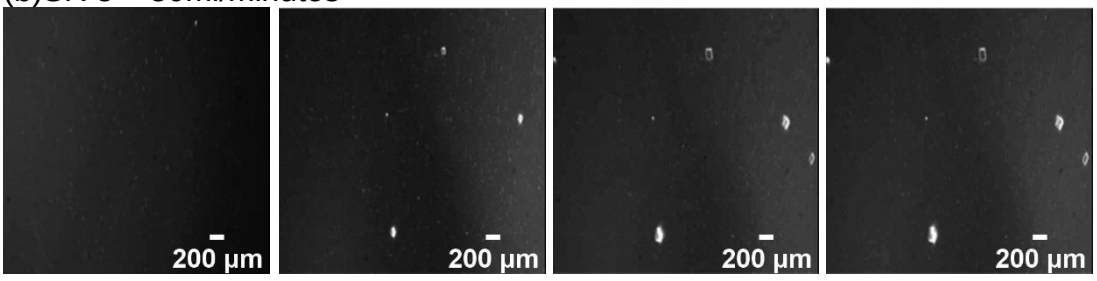

5minutes 60minutes 120minutes 240minutes

Figure 4. 27 – *In-situ* visualisation cell images of $CaCO_3$ scale deposition for brine with SR 5 at 5, 60, 120 and 240 minutes time intervals and flowrate of (a) 20ml/min and (b) 30ml/min at 50°C.

4.2.4.6 Effect of flowrate on number of crystals at SR 5

The plot for the effect of increasing the flowrate from 20ml/min to 30ml/min on the number of crystals deposited on the surface with time at SR 5 and 50^{o}C is presented in Figure 4. 28.

The data demonstrates that generally, an increase in flowrate resulted in a notable increase in the number of crystals deposited on the surface with time, which is in line with the results obtained at SR 10. Furthermore, at 20ml/min, the number of crystals increased from zero to two crystals after 10 minutes, and a total of 4 crystals was observed on the surface after 30 minutes. Subsequently, there was no further increase in the number of crystals until the end of the experiment which lasted for 240 minutes, indicating that equilibrium point was attained for the nucleation process after 30 minutes.

However, at 30ml/min, the number of crystals increased at a faster rate compared to the results at 20ml/min. The number of crystals increased from zero to six crystals within the first 10 minutes of the test and a total of 8 crystals precipitated on the surface after 45 minutes. Thereafter, there was no further increase in the number of crystals deposited on the surface until the termination of the experiment which also lasted for 240 minutes.

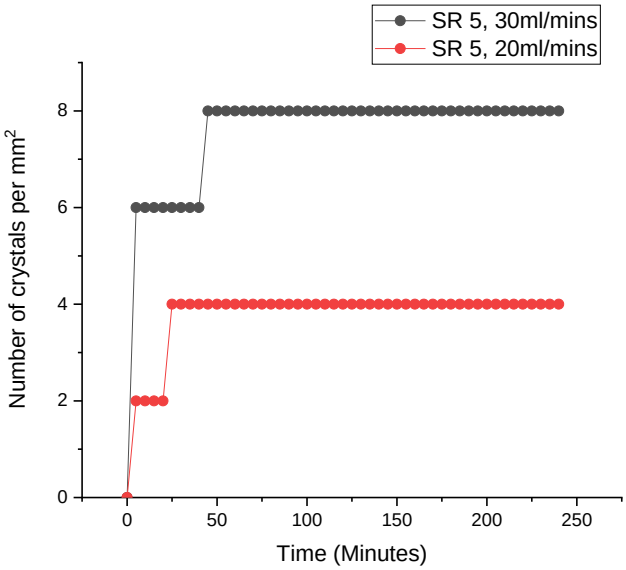

Figure 4. 28 – Comparing the number of crystals deposited on the surface with time at 50^{o}C, SR 5 for 20 and flowrate of 30ml/min.

4.2.4.7 Effect of flowrate on average area of crystals at SR 5

The graph for the average size of crystals formed on the surface with time as the flowrate increased from 20ml/min to 30ml/min at SR 5 and 50^{o}C is shown in Figure 4. 29.

The results demonstrates that, contrary to the results obtained at SR 10, as the flowrate increased the average size of the crystals also increased at SR 5. The crystals grew to an average area of 80µm^2 at 20ml/min, whilst at the higher flowrate of 30ml/min, the average area of crystals was 160µm^2, indicating that the size of crystals increased by a factor of two due to the increase in flowrate. In addition, at 30ml/min it was observed that the average size of the crystals increased rapidly for the initial 60 minutes duration of the test. Afterwards, the average size of the crystals continued to increase steadily at a linear rate until the termination of the experiment which ran for 240 minutes. However, at 20ml/min, the trend for the average size of the crystal with time was observed to progress more slowly in comparison to 30ml/min. Nonetheless, the average crystal size also increased linearly from the start of the experiment until the end.

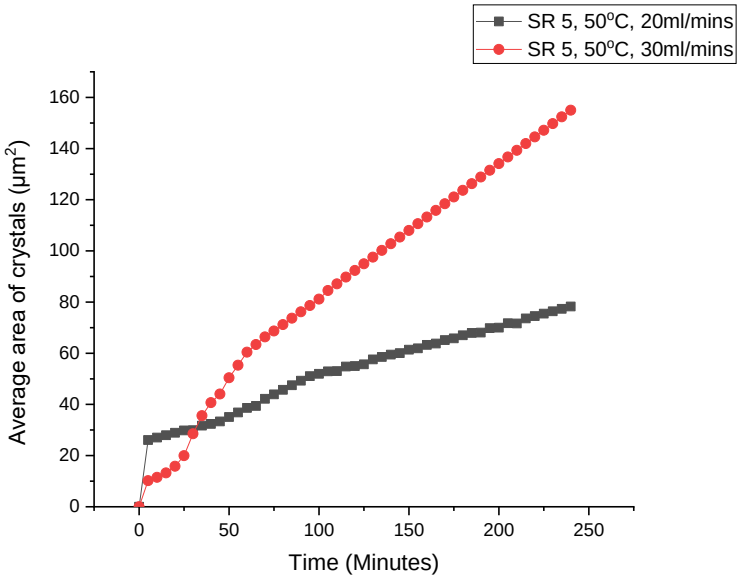

Figure 4. 29 – Comparing the average size of crystals deposited on the surface with time for 50°C, SR 5 at 20 and flowrate of 30ml/min.

4.2.4.8 Effect of flowrate on surface coverage of crystals at SR 5

Figure 4. 30, shows the results for the effect of increasing the flowrate from 20ml/min to 30ml/min on the surface coverage of crystals at SR 5 and 50°C.

The data showed a similar trend for the results obtained at 20ml/min compared to the results at 30ml/min. However, the surface coverage was notably higher at the higher flowrate compared to the lower flowrate, demonstrating the role of increased flowrate in increasing the surface coverage of crystal at the same SR and temperature.

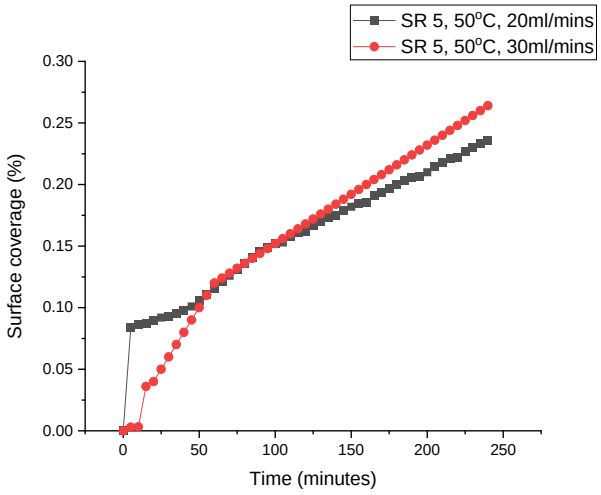

Figure 4. 30 – Comparing the surface coverage of crystals formed on the surface with time and their growth-rates at 50°C, SR 5 and flowrate of 20 and 30ml/min.

4.2.4.9 SEM images for the crystals formed on the surface at 20ml/min and 30ml/min at SR 5

Figure 4. 31 shows the SEM image of the $CaCO_3$ crystals deposited on the surface of the stainless-steel material after 4 hours at SR 5, 50°C and flowrate (a) 20ml/min and (b) 30ml/min. The SEM images confirms that the number of crystals formed at 30ml/min was clearly higher compared to the number of crystals deposited on the surface at 20ml/min.

In addition, at 20ml/min, the crystals appeared to have a cubic shape, indicating that calcite polymorph of $CaCO_3$ scale was formed at this condition, whilst at 30ml/min there appears to calcite crystals formed on the surface, there was also some evidence for leaf-like vaterite polymorph of $CaCO_3$, which is in line with the findings from the surface deposition test at SR 10.

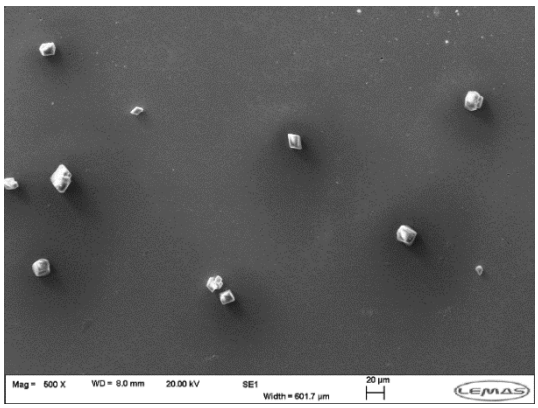

(a) SR 5 – 20ml/min

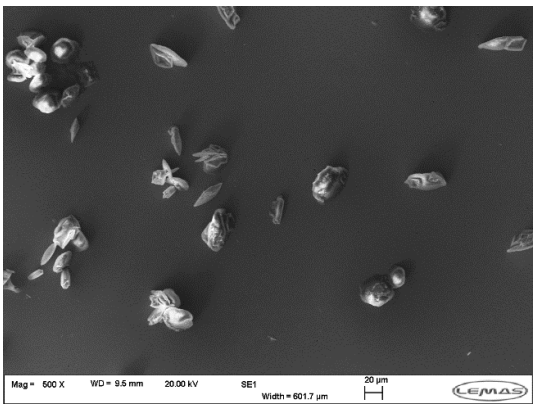

(b)SR 5 – 30ml/min

Figure 4. 31 - SEM images of the $CaCO_3$ crystals deposited on the stainless-steel surface for brine with SR 5 after 4hours and flowrate of (a) 20ml/min and (b) 30ml/min at 50°C.

4.2.4.10 Effect of flowrate at SR 3

In-situ visualisation cell Images showing effect of flowrate (20ml/min and 30ml/min) on surface deposition at SR 3, Figure 4. 32.

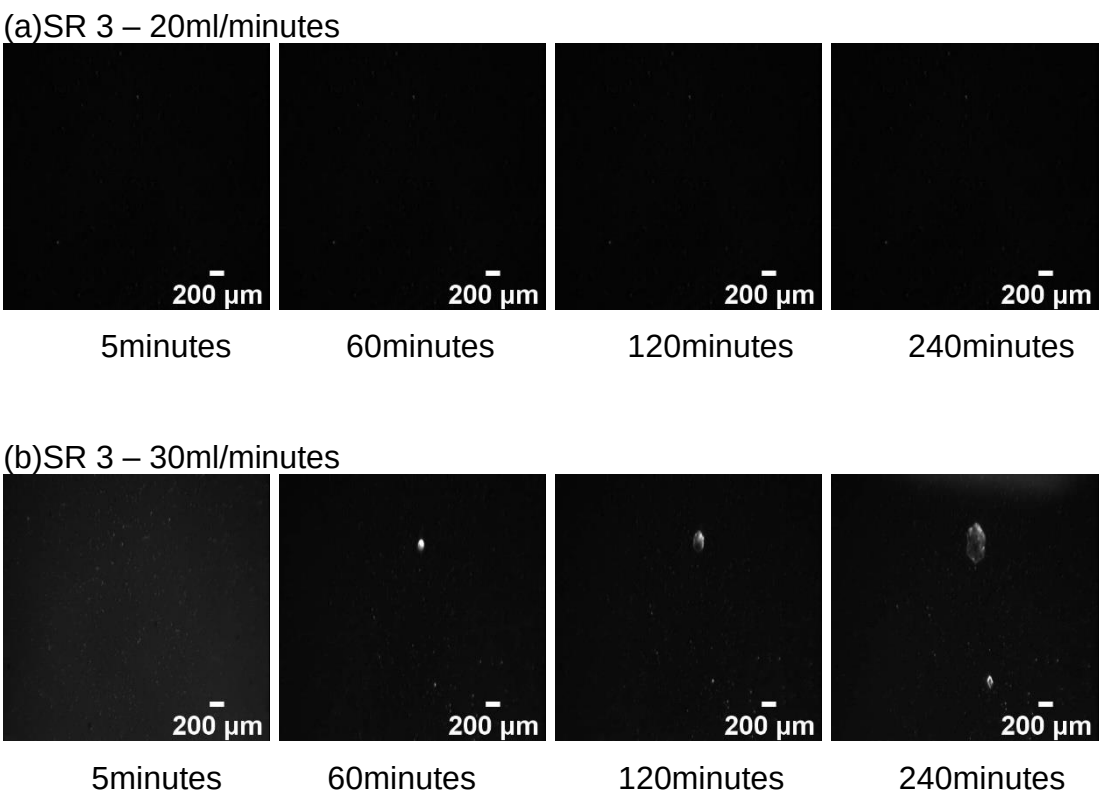

Figure 4. 32 – *In-situ* visualisation cell images of $CaCO_3$ deposition for brine with SR 3 at 5, 60, 120 and 240minutes time intervals and flowrate of (a) 20ml/min and (b) 30ml/min at 50°C.

4.2.4.11 Effect of flowrate on number of crystals at SR 3

The plot illustrating the effect of increasing the flowrate from 20ml/min to 30ml/min on the number of crystals deposited on the surface with time at SR 3 and 50°C is presented in Figure 4. 33.

In contrast to the data obtained from SR 10 and SR 5 test on the effect of flowrate on the number of crystals formed on the surface, at SR 3 the same number of crystals precipitated at 20ml/min and 30ml/min, showing that, In contrast to previous trend observed at SR 10 and SR 5 at 50°C, an increase in flowrate does not cause an increase in the number of crystals deposited at SR 3 and 50°C. This result might be explained by the fact that there is a lack of sufficient area-to-volume ratio A/V in the *in-situ* visualisation cell which did not support the nucleation of a substantial amount of deposition at SR 3 even when the flowrate was increased from 20ml/min to 30ml/min.

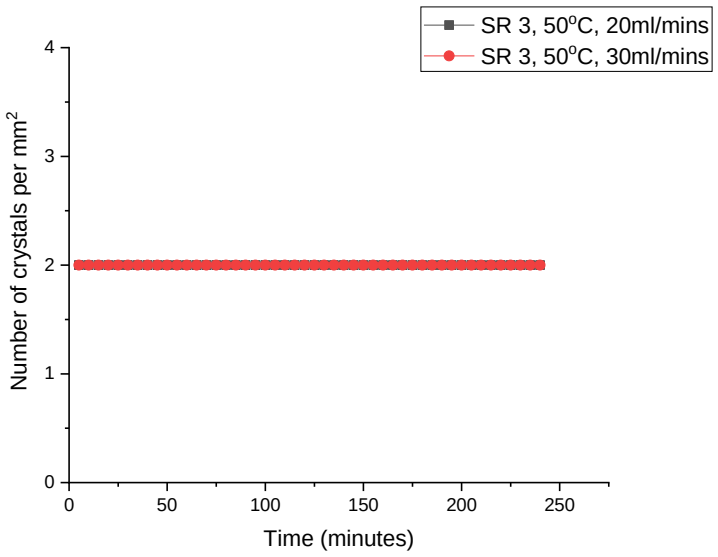

Figure 4. 33 – Comparing the number of crystals deposited on the surface with time for 50°C, SR 3 at flowrate of 20 and 30ml/min.

4.2.4.12 Effect of flowrate on average size of crystals at SR 3

The graph showing the effect of increasing the flowrate from 20ml/min to 30ml/min on the average size of crystals formed on the surface with time at SR 3 and 50°C is presented in Figure 4. 34. The data show a dramatic increase in the average size of the crystal formed on the surface at 30ml/min in comparison to 20ml/min, in line with the results from the experiment conducted at SR 5 and contrary to the results obtained at SR 10.

At 20ml/min, there was no change in the average size of the crystals formed for the entire 240 minutes duration of the test, implying that crystal growth did not take place at this condition. However, at 30ml/min the average size of the crystals increased quickly from the onset of the experiment until the termination of the test which ran for 240 minutes. This highlights the significant role of increasing the flowrate in increasing the average of crystal at SR 3.

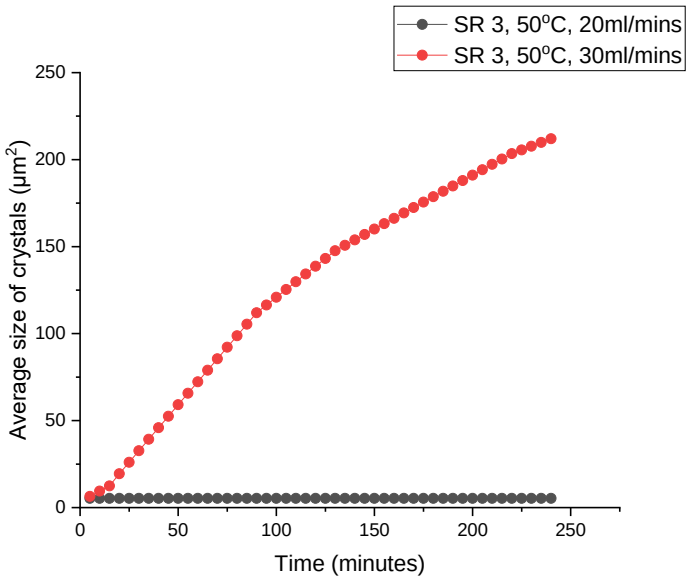

Figure 4. 34 – Comparing the average size of crystals formed on the surface with time for 50°C, SR 3 at flowrate of 20 and 30ml/min.

4.2.4.13 Effect of flowrate on surface coverage of crystals at SR 3

The graph of the surface coverage of the crystals with time as a function of increased flowrate, from 20ml/min to 30ml/min at SR 3 and 50°C is shown in Figure 4. 35.

In line with the results obtained for the average size of crystal deposited on the surface with time due to increased flowrate at SR 3, the data showed a remarkable difference in the surface coverage at 20ml/min compared to 30ml/min. At 20ml/min, there was no increase in the surface coverage with time for the entire duration of the test, whilst at 30ml/min the surface coverage of the crystals initially increased rapidly for the first 100 minutes of the test. Afterwards, the surface coverage continued to increase steadily with time at a linear rate until the termination of the test after 240 minutes. This result demonstrates the impact of increased flowrate in causing a noteworthy increase the surface coverage of crystals at SR 3.

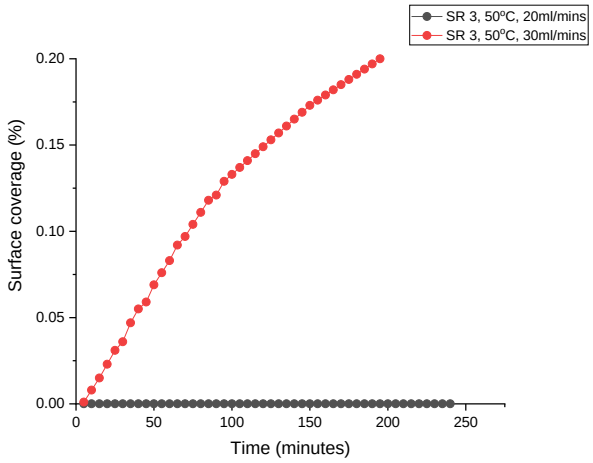

Figure 4. 35 – Comparing the surface coverage of crystals deposited on the surface with time for 50°C, SR 3 at flowrate 20 and 30ml/min.

4.2.4.14 SEM images for the crystals formed on the surface at 20ml/min and 30ml/min at SR 3

The SEM image of the $CaCO_3$ crystals deposited on the surface of the stainless steel material after 4 hours at SR 3, 50°C and flowrate 20ml/min and 30ml/min is presented in Figure 4. 36. The SEM image shows that the same number of crystals were deposited on the surface at 20ml/min and 30ml/min after the 4 hour duration of the test, but the crystals grew larger at 30ml/min in comparison to 20ml/min which is in line with the results obtained for the number and average size of crystals formed on the surface using the images analysis software.

In addition, at 30ml/min the crystals deposited on the surface had a cubic shape which suggests that calcite polymorphs are formed at this condition. The EDX analysis of the crystals in Figure 4. 37, also indicates that the crystals formed are $CaCO_3$. The evidence for the presence of calcite crystals at SR 3 and 30ml/minutes is in contrast with the findings at SR 5 and SR 10 where mainly vaterite crystals were observed. This demonstrates that the SR plays a role in polymorph of crystals formed on the surface at the same flowrate and temperature, in accordance with earlier observations in literature [110, 130, 134]

However, at 20ml/min the crystals formed did not have a defined shape. Hence, it is difficult to identify the polymorph of the crystals formed at this condition, also because the crystal formed did not grow, but the EDX analysis of the crystals suggested that the crystal formed is $CaCO_3$.

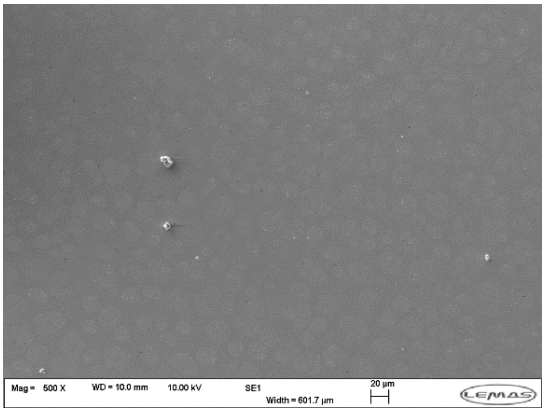

(a)SR 3 – 20ml/min

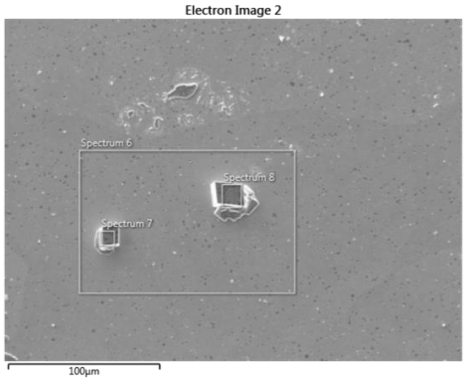

(b)SR 3 – 30ml/min

Figure 4. 36 - SEM images of the $CaCO_3$ crystals deposited on the stainless-steel surface for brine with SR 3 after 4hours and flowrate of (a) 20ml/min and (b) 30ml/min at 50°C.

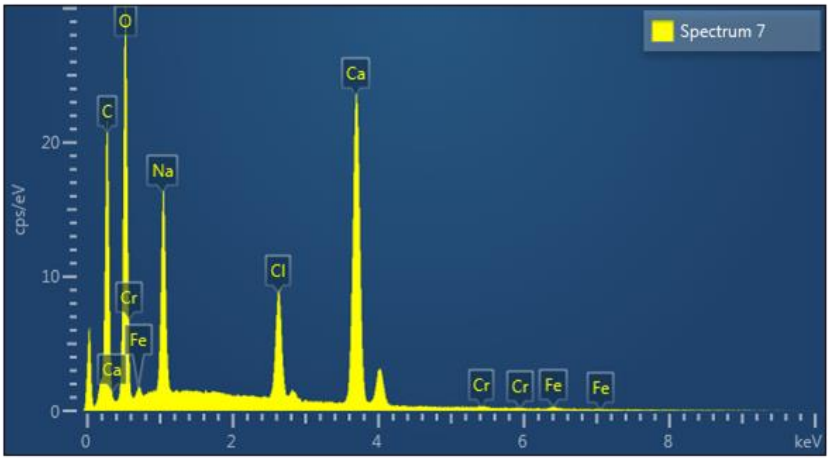

Figure 4. 37 – EDX analysis results for the crystal at spectrum 7 for the test at 50°C, SR 3 and flowrate of 30ml/min showing evidence for the presence of $CaCO_3$ crystals.

Summary

In this chapter, the role of some key parameters such as SR, temperature, and flowrate on the kinetics of $CaCO_3$ formation in the bulk solution and on the surface was examined. The bulk precipitation tests was conducted with the static jar setup and the surface deposition tests was performed with the *in-situ* visualisation cell.

The major findings from the study are summarised as follows;

The findings from the bulk precipitation study using the bulk jar scaling test highlight the role of increasing the SR and temperature (from 50^{o}C to 90^{o}C) in increasing the kinetics of bulk precipitation in low SR solutions.

The results from the surface deposition tests also revealed that the kinetics of $CaCO_3$ deposition increased as SR increased at low SR (SR 2 – SR 10), this was demonstrated by the increase in the surface coverage of the crystals with time as the SR increased for tests performed at both 50^{o}C and 79^{o}C.

The SEM images of the crystals deposited on the surface from the *in-situ* visualisation cell experiments with the low SR brines at 50^{o}C and 79^{o}C showed evidence for predominantly cubic shaped calcite polymorph of $CaCO_3$ scale.

The findings from the study of the effect of flowrate on the kinetics of surface deposition at low SR showed that when the flowrate was increased from 20ml/min to 30ml/min there was an increase in the number, average size and surface coverage of crystals deposited with time, indicating that an increase in flowrate increases the kinetics of $CaCO_3$ deposition at low SR.

At SR 3, only 2 crystals nucleated on the surface at both 20 and 30ml/min, at 50^{o}C for the entire 4hour duration of the experiment. This low amount of deposition is challenging to extrapolate for a long period of time, making it difficult to effectively assess the mechanisms of scale deposition kinetics at this condition.

These results highlight the effect of SR and temperature on the kinetics of $CaCO_3$ precipitation in the bulk solution and on the surface, the data also showed that an increase in flowrate increases the kinetics of $CaCO_3$ deposition on the surface at low SR. Moreso, the findings from the *in-situ* visualisation and the static jar test at SR 3 and 50^{o}C demonstrates that these techniques are not suitable for generating

an appreciable amount of deposition which would be necessary to effectively assess the mechanisms of $CaCO_3$ formation at this condition.

A new technique was developed due to the limitations of the static jar and *in-situ* visualisation cell in quantifying the kinetics of $CaCO_3$ formation at low SR, with particular interest in SR 3. The presence of a high area-to-volume ratio in the new system is assumed to be able to facilitate the deposition of a quantifiable amount of scale at very low SR. The results obtained from this new technique are presented in the next chapter.

Chapter 5 - Comparing the kinetics of bulk precipitation to surface deposition at low SR

5.1 Introduction

In the previous chapter, the data obtained from the study of the kinetics of $CaCO_3$ bulk precipitation with the static jar setup and the kinetics of $CaCO_3$ surface deposition with the *in-situ* visualisation cell at low SR were presented. The results from the static jar tests provided insight into the induction time and equilibrium point of $CaCO_3$ precipitation in the bulk solution at SR 10 and SR 5 at 50^oC. However, at SR 3, there was no evidence for $CaCO_3$ precipitation in the bulk for the entire 4 hour duration of the experiment.

Furthermore, the results from the *in-situ* visualisation cell experiments was also beneficial for assessing the kinetics of $CaCO_3$ nucleation and growth on the surface at SR 10 and SR 5 at 50^oC. However, at SR 3 and 50^oC, there was a limited amount of deposition on the surface and the $CaCO_3$ crystals formed on the surface did not grow for the whole 4 hour duration of the experiment. This is attributed to the low area-to-volume ratio in the flow cell which did not support the deposition of a considerable amount of scale on the surface at very low SR conditions. The results indicates that both the static jar setup and the *in-situ* visualisation cell are not suitable for effectively quantifying the kinetics of $CaCO_3$ formation at very low SR (i.e. SR 3).

Therefore, to better asses the kinetics of $CaCO_3$ deposition at very low SR, a new setup was required, this led to the development of the beadpack design. It is suspected that the availability of a large area-to-volume ratio (A/V) in the beadpack would support in the generation of a substantial amount of deposition within a reasonable time frame in the laboratory. This would be necessary for providing a richer insight into the mechanisms and kinetics of $CaCO_3$ deposition at low SR (i.e. below SR 5) and can serve as the framework for the development of a reliable kinetic model for predicting the likelihood for scale deposition to occur at low SR.

This chapter introduces the development and testing of the beadpack setup, the results obtained from the study of the kinetics of $CaCO_3$ surface deposition with the beadpack at low SR are described. The surface deposition results from the beadpack experiments were also compared to the bulk precipitation results from the static jar tests to understand the extent to which the presence of a surface impacts the kinetics of $CaCO_3$ formation in comparison to only bulk precipitation. In addition, the surface deposition results from both the beadpack and the *in-situ* visualisation cell were compared to have an insight into the unique strength of each

technique in assessing the kinetics of $CaCO_3$ deposition at low SR. To begin with, in the next section an introduction into the beadpack design is presented.

5.2 Bead pack method

The beadpack design has been adopted from the sand pack technique, which has a wide range of applications in the oil and gas industry. This includes investigating the adsorption and desorption of chemical species such as inhibitors in a porous media [123], and the examination as to the extent to which precipitation of scale in a porous medium affects permeability reduction mechanisms [124].

The objective of the beadpack design is to provide a constant composition environment with a sufficient area to provide a measurable degree of precipitation under exposure to low SR environments. It is expected that the presence of high surface area in the beadpack would significantly increase the degree of surface deposition to promote a measurable drop in the scaling ion concentration within the solution.

5.2.1 Theoretical calculation for change in calcium ion concentration in the beadpack and *in-situ* visualisation cell

Theoretical calculations were performed to determine whether there would be measurable difference between the inlet (C_{ao}) and outlet (C_a) calcium ion concentrations with time in the beadpack and in the *in-situ* visualisation cell as a result of the deposition of $CaCO_3$ on the surface. The calculation was carried out based on the experimental results from the *in-situ* visualisation cell at SR 10, 50^oC and flowrate of 10ml/min.

The aim of the calculation is to understand whether tracking the change in the calcium ion concentration with time using AAS technique is suitable for investigating the mechanisms and kinetics of $CaCO_3$ deposition with the beadpack and the *in-situ* visualisation cell at low SR. The full details of the calculations are provided in the appendix.

The findings from the calculation estimated a change of 0.0000267ppm after 4 hours in the *in-situ* visualisation cell and change of 0.0076ppm in the beadpack, suggesting that a small ΔCa is expected in using the two different techniques. Nonetheless, a notably larger ΔCa with time was observed in the beadpack in comparison to the *in-situ* visualisation cell, which implies that there is more potential for obtaining a measurable change in ΔCa in the beadpack in comparison to the *in-situ* visualisation cell. Therefore, AAS was used to follow the kinetics of

$CaCO_3$ formation in the beadpack and an image processing software was used to determine the mechanisms and kinetics of $CaCO_3$ formation in the *in-situ* visualisation cell, by assessing the number, average size and surface coverage of crystals deposited on the surface with time.

5.2.2 Surface deposition as a function of SR

The SR values investigated in this study are SR 10, 5 and 3 at 50^oC at a beadpack flow rate of 20ml/hr. The induction time for bulk precipitation was determined with static jar tests before carrying out the beadpack experiment to understand the factors controlling the nucleation and growth processes. The results of the bulk precipitation from the static jar show an induction time of 10 minutes for SR 10, and 30 minutes for SR 5. However, there was no precipitation of $CaCO_3$ crystals in the bulk solution for SR 3, after a period of 240 minutes. Given the 23 minutes residence time in the beadpack, homogenous nucleation in the bulk solution at SR 10 is expected in the beadpack test because it has been observed in the static tests, and any scaling at SR 5 and 3 in the beadpack test must be due to heterogeneous nucleation because the static tests confirm that homogenous scaling does not occur in that time frame.

Furthermore, the results from the beadpack test also showed an induction time of 10 minutes for SR 10 (Figure 5. 1) which is the same as the induction time from the static jar test. However, at SR 5 there was a lower induction time of 20 minutes observed in the beadpack (Figure 5. 2) compared to 30 minutes in the static jar test also at SR 5. However, at SR 3, the induction time for beadpack was also 20 minutes (Figure 5. 3), but there was no precipitation of $CaCO_3$ at the same condition in the static jar test. This difference in induction time at lower SR is likely attributable to the presence of the high surface area and the constant composition in the beadpack, which caused a significant reduction in the induction time for $CaCO_3$ formation in comparison to a closed system with only bulk precipitation in the static jar test. This result is in agreement with a study by Chen et al. [35] who reported a lower induction for the surface deposition of $CaCO_3$ in comparison to its precipitation in the bulk at low SR, a plausible explanation for this is that heterogeneous nucleation is favoured over homogenous nucleation at low SR because it requires less energy for nucleation to take place on the surface in contrast to the bulk at this condition [97].

Overall, the results imply that the presence of a surface initiates a reduction in induction time in the two experiments where no homogeneous nucleation was expected (SR 3 and 5). Following from the induction period in the beadpack at SR 10, there was a sharp drop in the calcium ion concentration of 65 ppm. Afterwards,

the calcium ion concentration reduced slowly with time until after 120 minutes and subsequently there was no further change in the calcium ion concentration with time, suggesting that equilibrium point had been attained. The initial drop in the calcium ion concentration with time is assumed to be due to the nucleation of $CaCO_3$ crystals on the surface, whilst the region where there was no change in the calcium ion concentration with time is suspected to signify the termination of the nucleation process and to mark the onset of the crystal growth process [81].

However, a smaller change in calcium ion concentration of 17 ppm was observed for SR 5 and 11 ppm for SR 3. This is likely attributed to the fact that only heterogeneous nucleation and growth occurs on the surface of the beads in both SR 5 and 3, in addition to the fact that the kinetics of growth are lower with lower SR values. Many studies in literature also agree that heterogeneous nucleation controls the scaling process in low SR solutions. For example Amor et al[135] investigated the effect of low temperature, low SR and substrate nature on the nucleation of $CaCO_3$ in a cylindrical cell, and the results illustrated that precipitation is exclusively heterogeneous at low supersaturation.

Previously, the kinetics of scale formation on surfaces in low SR have been challenging to correctly quantify with techniques such as static jar tests or dynamic tube blocking tests due to the absence of a high surface area to promote the scaling process and the reduction of SR with time in these designs [48]. However, the beadpack has the potential to be useful in enhancing the knowledge of the kinetics of the scaling process in a system with a high surface area and constant SR.

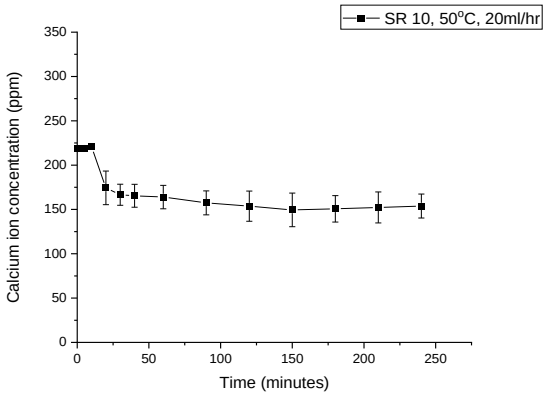

Figure 5. 1 – Calcium ion concentration versus time graph for the stainless-steel beadpack (effluent) at SR 10, flowrate of 20ml/hr and 50°C.

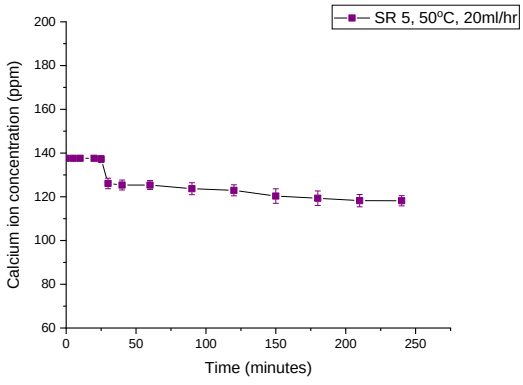

Figure 5. 2 – Calcium ion concentration versus time graph for the stainless-steel beadpack (effluent) at SR 5, flowrate of 20ml/hr and 50°C.

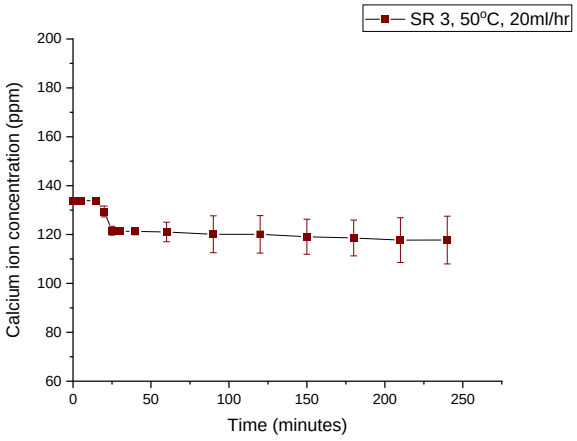

Figure 5. 3 – Calcium ion concentration versus time graph for the stainless-steel beadpack (effluent) at SR 3, flowrate of 20ml/hr and 50°C.

5.2.3 Assessment of surface deposition kinetics from the *in-situ* visualisation cell technique

The *in-situ* visualisation cell experiment was conducted at SR 3, 50°C and 30ml/min. The experiment ran for 4 hours. The plot for the number of crystals deposited on the surface with time, presented in Figure 5. 4 shows that 2 crystals precipitated on the surface after 5 minutes which is the time the first image was taken with the *in-situ* visualisation cell camera. Afterwards, there was no increase in the number of crystals deposited on the surface for the remaining 4-hour duration of the test.

Furthermore, the graph of the average size of crystals with time presented in Figure 5. 5, illustrates that the average size of the $CaCO_3$ crystals increased rapidly at a linear rate from the start of the test until 90 minutes. Thereafter, the rate of increase in the average size of the crystals reduced slightly. Nonetheless, the average size of crystals continued to increase steadily until the termination of the experiment.

It is interesting that only 2 $CaCO_3$ crystals deposited on the surface even at a flowrate of 30ml/min at SR 3. This suggests that the *in-situ* visualisation cell is not able to generate an appreciable amount of deposition which would be useful for effectively quantifying $CaCO_3$ deposition at SR 3. The low number of crystals formed on surface can be attributed to the low area-to volume-ratio (A/V) in the flow cell.

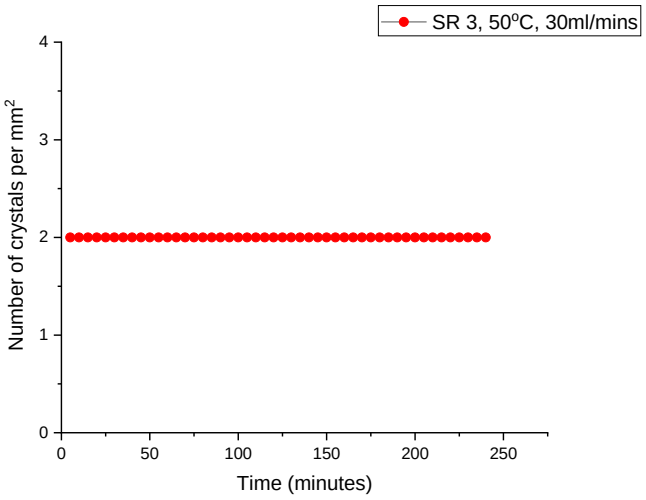

Figure 5. 4 – Number of crystals deposited with time at 50°C, SR 3 and 30ml/min.

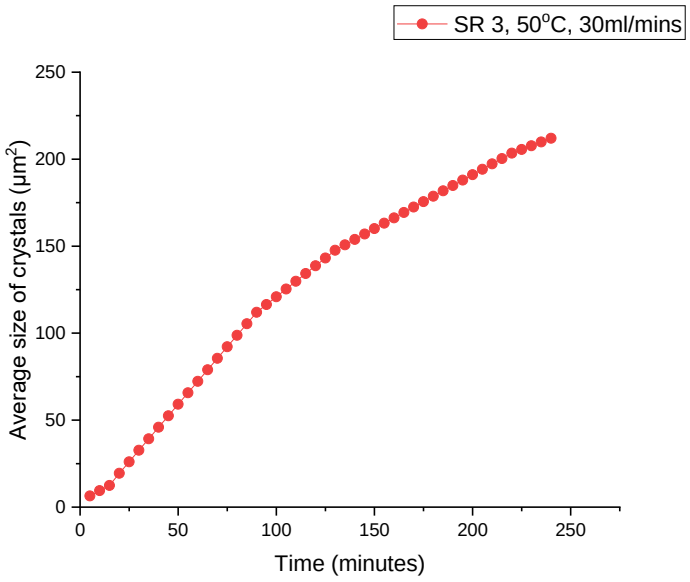

Figure 5. 5 – The graph of the average size of crystals with time at 50°C, SR 3 and 30ml/min.

5.2.4 Comparing surface deposition in the beadpack and the *in-situ* visualisation cell

The beadpack and the *in-situ* visualisation cell were designed primarily to understand the mechanisms and kinetics of $CaCO_3$ deposition on surfaces. One of the unique features of the beadpack is the presence of a high surface area in the pack, which is expected to improve the quantifying of scale deposition at low SR, whilst the *in-situ* visualisation cell is useful for visualising surface nucleation

and growth of scale in real time which helps to determine whether the mechanism controlling the deposition process is progressive or instantaneous nucleation of $CaCO_3$.

These two techniques, though different, are complementary, as they are beneficial for providing unique insights into the crystallisation of $CaCO_3$ on surfaces. The kinetics of $CaCO_3$ deposition at low SR was compared using these two different techniques to better understand their specific strengths and to comment on where the two techniques fit in the crystallisation process.

To better understand the flow characteristics in the beadpack and the *in-situ* visualisation cell, preliminary calculations were carried out to determine the residence time, Reynolds number, and shear-rate using the two different sets of equipment. The results from the calculations as well as the information on the experimental conditions for the tests are shown in Table 5. 1. The details of the equations used for the calculations are presented in the appendix.

Table 5. 1 - Comparing the experimental conditions for the beadpack test to the *in-situ* visualisation cell tests at SR 3 and 50ºC.

Parameters	**Beadpack**	***In-situ* visualisation cell**
Flowrate	20ml/hr	30ml/min
Residence time	1404 sec	2 sec
Reynolds number	2	24
Shear stress	3.2×10^{-4} (Pa)	3.1(Pa)
Area to volume ratio (A/V)	$2371.1 m^{-1}$	$28 m^{-1}$

The data from the calculation illustrates that although the experiments in both the beadpack and *in-situ* visualisation cell were conducted under laminar flow regimes as their Reynolds number is less than 3500, and there is also no shearing expected in the two different setups because the wall shear stress estimated to cause a removal of scale from the surface is 82.5pa[97] and the shear stress in the two different techniques is lower than this value. Nonetheless, the A/V in the two techniques are notable different, which has an impact on the kinetics of $CaCO_3$ deposition.

The main advantage of the *in-situ* visualisation cell lies in its ability to decouple nucleation and growth and assess surface coverage of $CaCO_3$ at low SR, but it cannot provide reliable kinetic data at low SR as the precipitation is very limited – so it provides a good qualitative analysis, but unreliable quantitative data.

However, the beadpack is more suitable for quantifying the kinetics of $CaCO_3$ deposition at very low SR such as SR 3, which could not be effectively measured with the *in-situ* visualisation cell, this is due to the presence of a high A/V ratio in

the pack which supported the generation of a considerable amount deposition within an acceptable time frame in the laboratory.

The beadpack and *in-situ* visualisation cell offer distinct and useful information on the mechanisms and kinetics of $CaCO_3$ deposition at different SR and flowrate at the nucleation and growth stage of the crystallisation process.

5.2.5 Bulk precipitation in static jar versus surface deposition in beadpack

In this study the static jar methodology was adopted to understand the kinetics of bulk precipitation, and the beadpack was used to assess if the presence of a high surface area can enable sufficient deposition to obtain measurable data on the kinetics of scale deposition in low SR solutions. The growth-rate of $CaCO_3$ determined from the static jar test was compared to the growth-rate in the beadpack to improve the understanding of the extent to which the presence of stainless-steel surface in the beadpack impacts the rate of scale formation. The growth-rate of $CaCO_3$ in the beadpack was determined as a function of the difference between the initial and final near steady-state calcium ion concentration of the effluent after the 4-hour duration of the test and the residence time in the beadpack. The equation used for this calculation is in the appendix, whilst the growth-rate from the static jar test was assessed by applying a linear fit to the calcium ion concentration results with time after the induction period and prior to equilibrium point as shown earlier in the bulk precipitation results section.

At SR 10, the growth rate of $CaCO_3$ was 2.7ppm/minute in the beadpack and 0.27 ppm/minute from the static jar test **(**Figure 5. 6). The significant increase in the growth rate in the beadpack can be attributed to the high surface area provided.

At SR 5, the growth rate of $CaCO_3$ was 0.73 ppm/minute from the beadpack test and 0.15 ppm/minute from the static jar test (Figure 5. 7). Again, this demonstrates the influence of the presence of high surface area on scaling. However, the scaling process at this condition is attributed to only heterogeneous nucleation on the surface because the induction time for bulk precipitation is longer than the residence time in the pack.

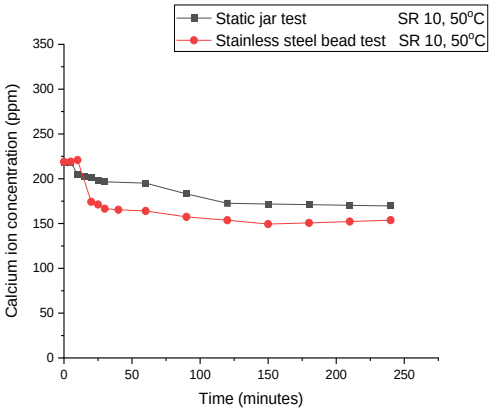

Figure 5. 6 – Comparing the calcium ion concentration versus time graph for the stainless-steel beadpack and static jar test at SR 10,50°C and flowrate of 20ml/hr.

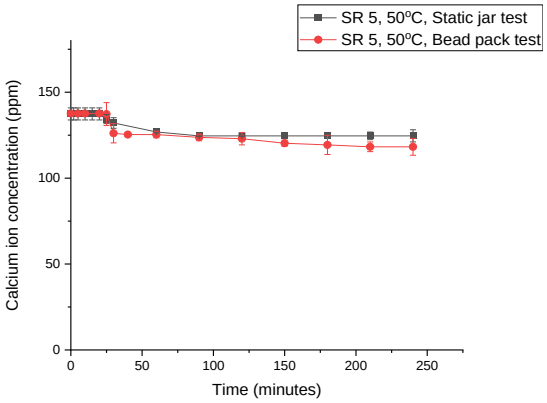

Figure 5. 7 – Comparing the calcium ion concentration versus time graph for the stainless-steel beadpack and static jar test at SR 5,50°C and flowrate of 20ml/hr.

In line with the previous data, at SR 3 the growth rate in the beadpack was 0.47 ppm/minute but there was no growth of crystals observed from the static test at this condition as there no change in the calcium ion concentration. This is shown in Figure 5. 8.

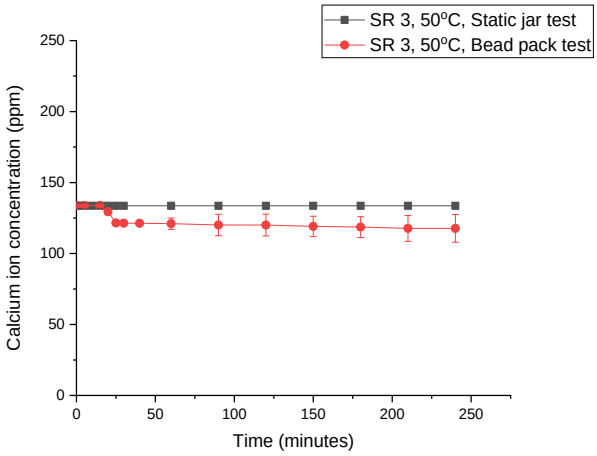

Figure 5. 8 – Comparing the calcium ion concentration versus time graph for the stainless-steel beadpack and static jar test at SR 3,50°C and flowrate of 20ml/hr.

Overall, the results from this study have shown the extent to which the heterogeneous nucleation on the surface impacts the growth-rate of $CaCO_3$ in comparison to only homogenous nucleation in the bulk solution. This study is paving the way for further research on the effect of area-to-volume-ratio and surface energy on the kinetics of scale deposition in low SR to validate the results over a wider range of conditions including different flowrates and retention times.

5.3 Effect of surface roughness, area-to-volume ratio, and flowrate on the kinetics of $CaCO_3$ deposition study.

The results from the previous section has shown that the newly developed bead pack design is suitable for effectively quantifying the kinetics of $CaCO_3$ surface deposition at very low SR. In this chapter, the beadpack design is probed further to understand its sensitivity to different experimental parameters such as surface roughness, area-to-volume ratio (A/V) and flowrate.

5.3.1 Effect of surface roughness on the kinetics of $CaCO_3$ deposition.

The effect of surface roughness on the kinetics of $CaCO_3$ deposition was investigated with the beadpack to determine whether it is the surface roughness of the material i.e. smooth versus etched stainless steel material, that promotes the generation of an appreciable amount of deposition within a reasonable time-frame in the laboratory at low SR, or if a quantifiable amount of deposition can be achieved at low SR solely due to the presence of a high A/V regardless of the type of material (i.e. PTFE or stainless steel material) used for the surface deposition test. A better insight into the effect of surface roughness on the kinetics of $CaCO_3$ deposition would be useful for the development of a reliable kinetic model for predicting scale deposition at low SR.

The beadpack experiment was conducted by following the kinetics of $CaCO_3$ deposition on PTFE beads, smooth stainless-steel beads, and etched stainless-steel beads at different time intervals. The SEM image of the PTFE bead, smooth and etched stainless steel bead samples before the beadpack test is shown in Figure 5. 9. The details on how the stainless-steel sample was etched is discussed in the method section.

(a) SEM image of the smooth stainless-steel bead

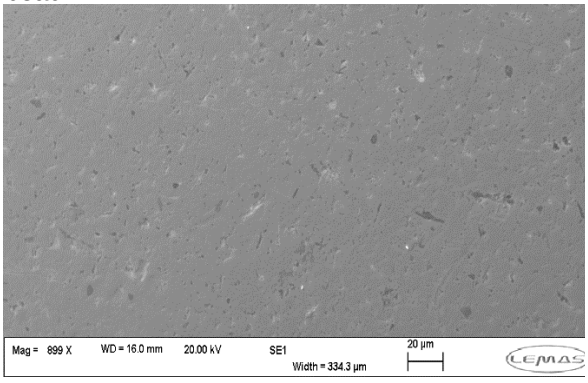

(b) SEM image of the etched stainless-steel bead

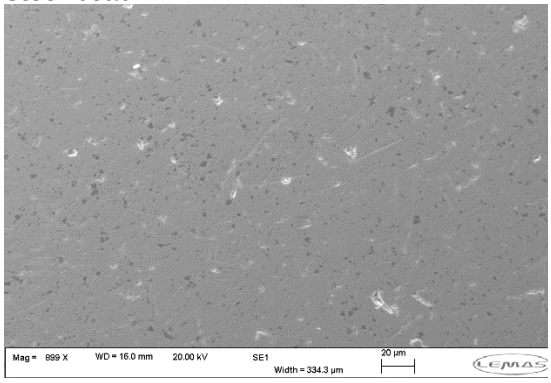

(c) SEM image of the PTFE bead

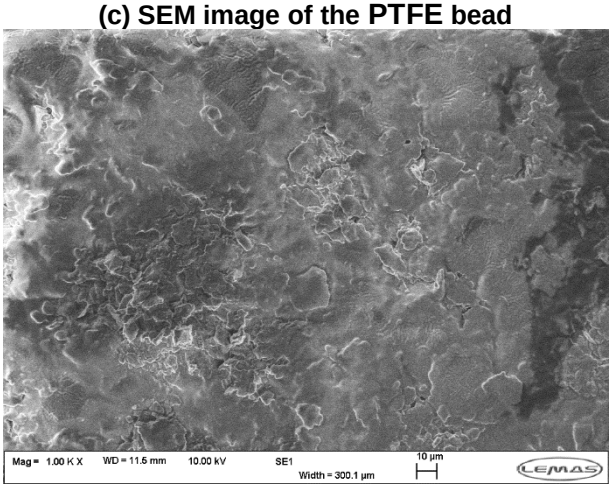

Figure 5. 9- SEM image of (a) smooth stainless-steel bead, (b) Etched stainless-steel bead and (c) PTFE bead before the beadpack test.

The surface roughness of the smooth and etched stainless steel bead sample was measured using the Talysurf, the roughness profile for the smooth and etched steel beads is presented in the appendix, whilst the surface roughness of the PTFE material was obtained from literature [114].

The results from the assesment of the surface roughness of the materials showed that the PTFE material had the highest surface roughness value,460nm, followed by the etched stainless steel material with a surface roughness of 57nm. The smooth stainless-steel material had the lowest surface roughness value of 41nm. These information are summaried in Table 6.1.

The surface energy of the 3 different materials was also determined with equation 1.1

$$Cos\ \theta = \frac{\gamma}{\gamma_i} \qquad 1.1$$

Where θ, and γ_i represents the contact angle and the surface energy of the testing drop respectively, the surface energy of the distilled water which was used for the measurement is 72.8 mJ.m^{-2} [136]

The values obtained for the surface roughness and surface energy of the different materials as well as information on their contact angles (the contact angle was determined with a contact angle goniometer), surface roughness and the area-volume ratio (A/V) in the bead in the pack are also provided in Table 5. 2.

Table 5. 2 – Surface characterisation of the PTFE, smooth and rough stainless-steel materials used for the beadpack test.

Materials	Contact angle (°C)	Area-volume ratio (m^{-1})	Surface roughness(nm)	Surface energy ($mJ.m^{-2}$)
PTFE	108.1	2371	460	-22.6
Smooth stainless steel	63.13	2371	41.32	32.9
Etched stainless steel	81.2	2371	57	11.4

The data obtained from the contact angle measurements of the materials indicates that the stainless-steel materials (i.e. both the smooth and etched stainless steel) are hydrophilic and can support the deposition of scale as their contact angle is less than 90 degrees, and the PTFE material is hydrophobic and would not support the deposition of scale as its contact angle is greater than 90 degrees [137].

In addition, the surface energy calculation also showed that the PTFE material had the lowest surface energy followed by the etched stainless-steel sample, the smooth-stainless steel sample had the highest surface energy. This order of increase in surface energy is in slight contrast to what is expected, whilst it is expected the PTFE material would have the least surface energy amongst the three different materials investigated as it is the only polymer of all 3 samples. Polymers are known to have a low surface energy in comparison to stainless steel materials, as demonstrated in research conducted by Wang et al [114]; this is what was observed in this study as well.

It was also expected that the etched stainless-steel material would have a higher surface energy compared to the smooth stainless-steel material, because the etched sample had a higher value of surface roughness. However, the smooth stainless-steel bead had a higher surface energy of $32.9mJ.m^{-2}$, whilst the etched stainless-steel bead had a lower surface energy of $11.4mJ.m^{-2}$. This can be attributed to the etching process, which is assumed to have increased the number of nucleation sites available on the etched stainless sample, as shown in the SEM image of sample in Figure 6.1; this could have contributed to the reduction of its surface energy in comparison to the smooth stainless-steel sample.

5.3.1.1 Experimental results for the study of the effect of surface roughness on the kinetics of $CaCO_3$ deposition.

The scale deposition tests were conducted with PTFE beads with a surface roughness of 460nm, smooth stainless steel beads with surface roughness of 41nm and etched stainless steel beads with a surface roughness of 57nm. All the beads used for the experiment had a diameter of 3mm and an A/V ratio of 2371m^{-1}, and the experiment was conducted at SR 10, 50^oC and 20ml/hr. The experiment ran for a duration of 4 hours.

The effect of surface energy on the kinetics of $CaCO_3$ deposition was also examined by comparing the kinetics of $CaCO_3$ deposition on PTFE beads, which has a low surface energy to smooth and etched stainless steel beads with a higher surface energy [114].

The calcium ion concentration versus time results obtained from the beadpack tests are presented in Figure 5. 10. The results showed that there was no change in the calcium ion concentration with time data for the experiment conducted with the PTFE beads and the smooth stainless-steel beads for the entire 4 hours duration of the experiment. In contrast to these results, there was a sharp drop in the calcium ion concentration with time after 20 minutes in the experiment conducted with the etched stainless-steel beads. After this initial drop, the calcium ion concentration continued to reduce slowly with time until stabilisation was attained after 120 minutes. Thereafter, there was no further reduction in the calcium ion concentration until the end of the test which ran for 240 minutes. In addition, a change of 65ppm was observed between the initial calcium ion concentration (C_{ao}) and equilibrium calcium ion concentration (C_a) for the etched stainless steel bead test.

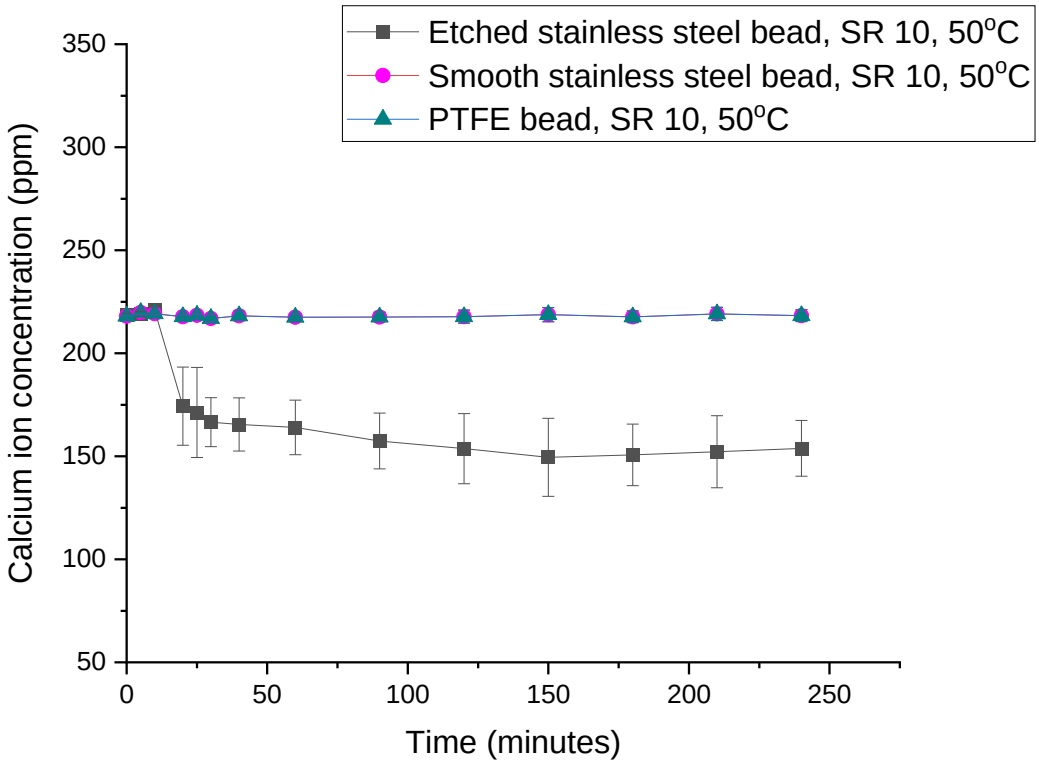

Figure 5. 10 – Comparing the Ca^{2+} ion concentration vs time graph for the PTFE bead, smooth stainless - steel and etched stainless-steel bead at SR 10, 50ºC and 20ml/hr.

The data illustrates that there was no change in the calcium ion concentration versus time results for the test conducted with the PTFE bead, implying that there was no deposition of $CaCO_3$ on the surface of the PTFE material, which had the least surface energy and the highest surface roughness. This result suggests that the low surface energy counteracts the high surface roughness, this can be attributed to the hydrophobic nature of the PTFE material as it does not favour the nucleation of scaling ions to the surface for $CaCO_3$ deposition to take place [114]. However, there was also no change in the calcium ion concentration with time for the test conducted with the smooth stainless-steel bead, which can be attributed to lower surface roughness of the material, making it difficult for $CaCO_3$ to nucleate on the surface of the smooth stainless-steel material. Nonetheless, a significant change in the calcium ion concentration with time was observed in the experiment performed with the etched stainless-steel beads which had a higher surface roughness compared to the smooth stainless-steel bead. This result is in line with the findings from literature which reported that for stainless steel materials, a higher surface roughness enhances the process of $CaCO_3$ deposition on the surface [138].

The findings from the tests indicate that, although a very low surface energy does not favour the deposition of $CaCO_3$ on the surface, the deposition of $CaCO_3$ is not

influenced exclusively by the presence of a high surface energy or a high area-to-volume ratio, but rather it is the combined effect of a high area-to-volume ratio, high surface energy as well as the surface roughness of the sample that promotes the kinetics of $CaCO_3$ deposition on the surface.

5.3.1.2 Surface characterisation

The SEM image of the surface of the smooth, etched stainless-steel beads and PTFE bead sample after the surface deposition test are shown in Figure 5. 11. In agreement with the calcium ion concentration versus time results, the SEM image shows evidence for the formation of $CaCO_3$ crystals on the surface of the etched stainless-steel bead, where the cubic shaped morphology of the crystals deposited on the surface suggests that mainly calcite polymorph of $CaCO_3$ was formed on the surface. In addition, the findings from the EDX analysis of the crystals deposited on the surface shown in also suggest that $CaCO_3$ was deposited on the surface, Figure 5. 12.

In contrast, the SEM image of the PTFE bead and smooth stainless-steel bead after the surface deposition also presented in Figure 5. 11 demonstrates that there was no formation of $CaCO_3$ on their surfaces. This illustrates that it is not just the presence of a high area-to-volume ratio that causes the deposition of $CaCO_3$ on the surface, as the three different tests were conducted with the same area –to-volume ratio. Instead, it is the addition of the presence of high area-to-volume ratio, high surface energy as well as the surface roughness of the sample that facilitates the deposition of $CaCO_3$ on surfaces. A better insight into the factors that encourages the deposition of $CaCO_3$ at low SR is useful for the development of a reliable kinetic model for predicting scale deposition at low SR [25].

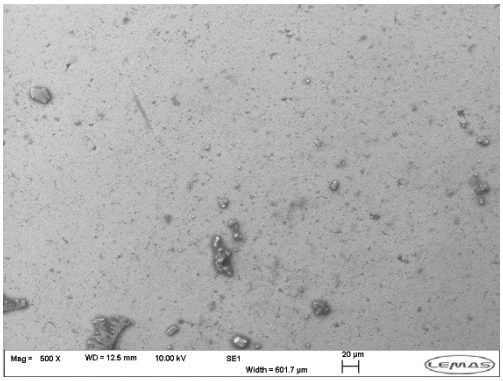

(a) SEM image of the smooth stainless-steel bead after the experiment.

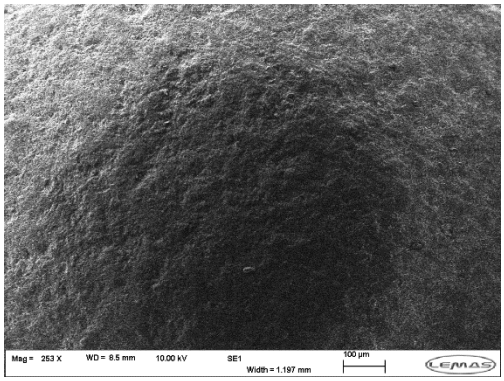

(b) SEM image of the PTFE bead after the experiment.

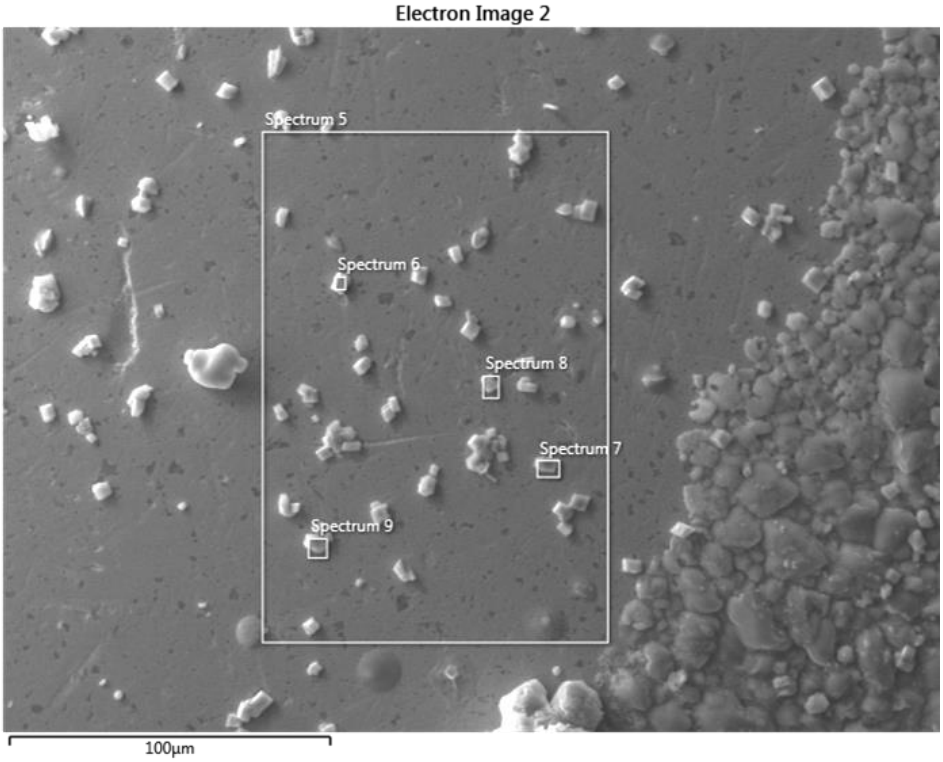

(c) SEM image of the etched stainless-steel bead after the experiment, showing evidence for crystals deposited on the surface.

Figure 5. 11- SEM image of (a) smooth stainless-steel bead (b) PTFE bead and (c) Etched stainless steel bead at SR 10, 50°C and 20ml/hr at 500X magnification after the bead pack experiment.

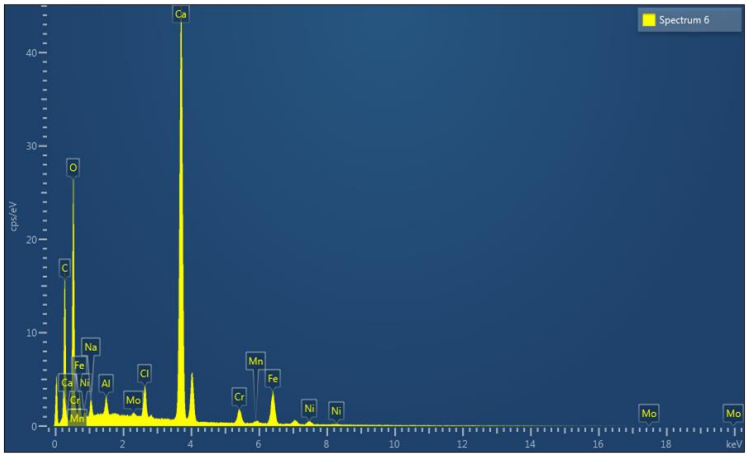

Figure 5. 12 – EDX analysis results of the crystal at spectrum 6, from the 3mm diameter etched stainless-steel bead pack test at 50°C and SR 10, which suggests the presence of $CaCO_3$ on the surface.

As a result of the findings from this section which suggests that it is the surface roughness of the stainless-steel sample that drives the process of $CaCO_3$ deposition, all the bead pack experiments from this time forward were carried out with etched stainless-steel beads.

5.3.2 The effect of A/V on the kinetics of $CaCO_3$ deposition

One of the main objectives of the bead pack design is to assess the effect of area-to-volume ratio (A/V) on the kinetics of $CaCO_3$ deposition, by carrying out bead pack test with different sizes of beads i.e., 3mm, 6mm and 9mm diameter beads. A better insight into the role of A/V would help to build on the knowledge of how the presence of a surface impacts the kinetics of $CaCO_3$ deposition particularly at low SR conditions.

5.3.2.1 Hypothesis for study of effect of A/V ratio on the kinetics of $CaCO_3$ deposition

A general decrease in the effluent calcium ion concentration with respect to time is expected for the beadpack test conducted with all the 3 different sizes of stainless-steel beads (3mm, 6mm and 9mm diameter beads) as shown in Figure 5. 13, because of the deposition of $CaCO_3$ on the surface of the beads with time.

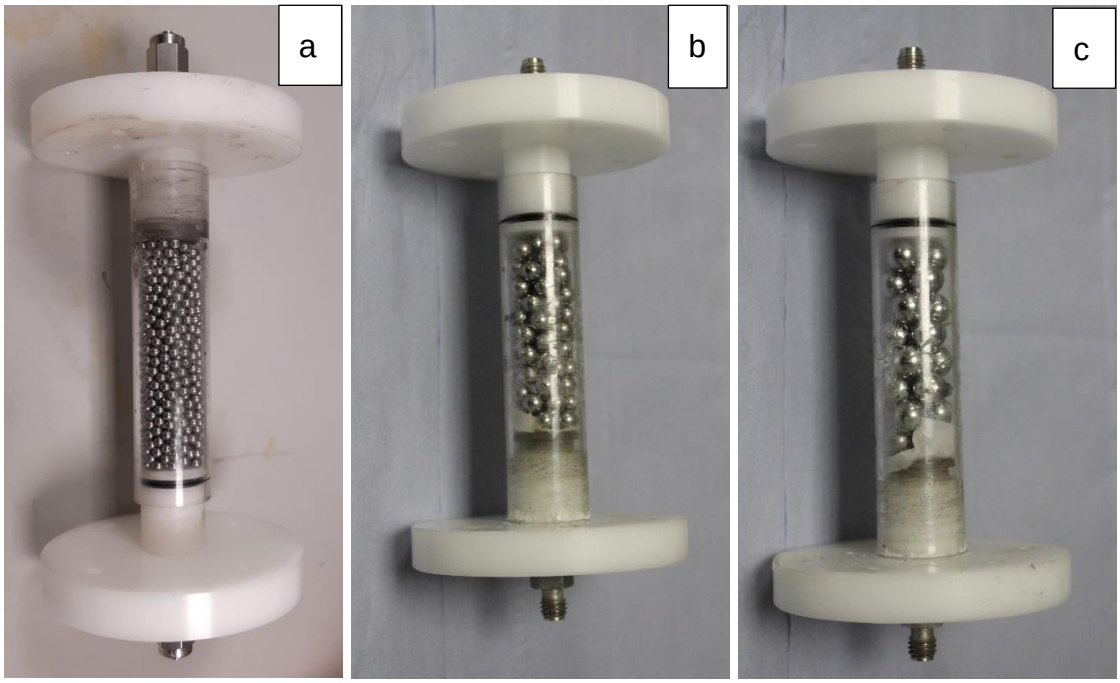

Figure 5. 13 - Beadpack with (a) 3mm diameter stainless steel beads, (b) 6mm diameter stainless steel beads and (c) 9mm diameter stainless steel beads.

However, it is suspected that the solution with the largest beads (9mm), will reach equilibrium at the slowest rate whilst the solution with smallest size of beads (3mm) will attain equilibrium at the fastest rate, as this condition will have the largest area-to-volume ratio. It is also assumed that as the A/V increases, the degree of heterogeneous nucleation of $CaCO_3$ on the surface would also increase, thereby causing a larger reduction in the calcium ion concentration with time and enabling

the solution to attain stabilisation at a faster rate. An illustration of the proposed hypothesis is presented in Figure 5. 14.

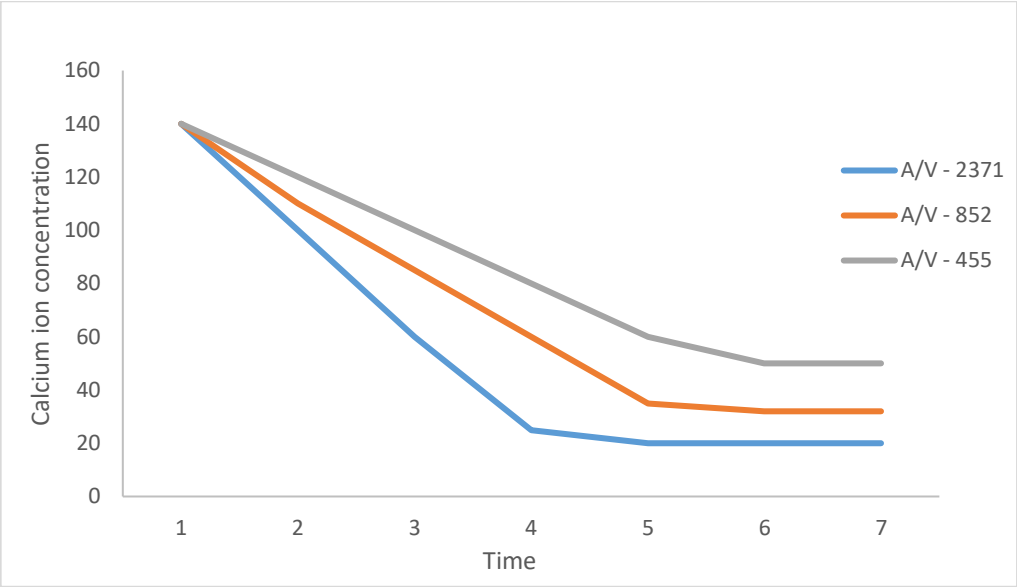

Figure 5. 14 - A representation of the hypothesis for the effect of A/V(m^{-1}) on the kinetics of $CaCO_3$ deposition study.

5.3.2.2 Hypothesis for study of effect of flowrate on the kinetics of $CaCO_3$ deposition

The effect of increasing the flowrate from 20ml/hr to 60ml/hr on the kinetics of $CaCO_3$ deposition was assessed by carrying out beadpack experiments with two different pack lengths to keep the residence time constant as the flowrate was increased. The experiment conducted at the lower flowrate of 20ml/hr was conducted with a pack length of 0.054m whilst the experiment at the higher flowrate of 60ml/hr was performed with a longer pack of 0.148m. An image of the two different packs is presented in Figure 3.11 and 3.12 respectively in the methodology section, Chapter 3.

The details of the experimental parameters such as porosity, residence time, and A/V in the pack for the effect of flowrate study in shown in Table 5. 3.

Table 5. 3 – Experimental variables for the effect of flowrate on $CaCO_3$ deposition study with the beadpack.

Diameter of stainless-steel balls (m)	Number of beads in pack	Volume of void (m^3)	Surface area (m^2)	Area - to - volume ratio (m^{-1})	Porosity	Flowrate (ml/hr)	Residence time (minute)
0.006	214	2.23×10^{-5}	0.0242	1085	0.48	60	23.4
0.006	69	9.15×10^{-6}	0.0078	852.46	0.54	20	27.5

Although, there is a slight variation in the A/V as well as the porosity, this is because it is difficult to keep the A/V constant as the experimental conditions change (i.e. a change in the length of the pack alters the porosity, A/V, and other parameters). Nonetheless, it was ensured that the magnitude of increase in the flowrate was notably higher compared to the A/V to have a better understanding of the effect of flowrate of $CaCO_3$ deposition.

It is expected that an increase in flowrate would increase the kinetics of $CaCO_3$ deposition, which would correspond to a larger drop in the calcium ion concentration with time due to a higher deposition of $CaCO_3$ on the surface. This is because a higher flowrate has been reported to assist the transportation of the scaling ions in the brine to the surface for the formation of $CaCO_3$ to occur. A faster flowrate would also support effective mixing of the brines and increase the amount of scaling ions passing through the beadpack per unit time. Hence, encouraging more crystallisation of $CaCO_3$ on the surface [36, 131]. An illustration of the hypothesis for effect of flowrate is shown in Figure 5. 15.

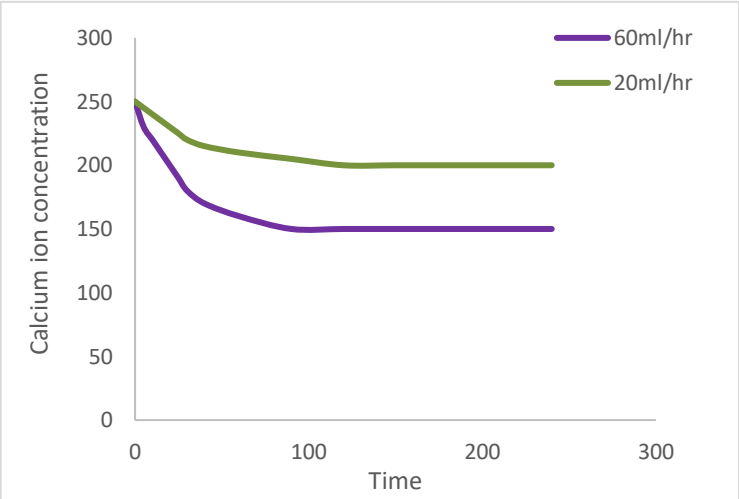

Figure 5. 15 - A representation of the hypothesis for the effect of flowrate (from 20ml/hr to 60ml/hr) on the kinetics of $CaCO_3$ deposition study.

5.3.2.3 Experimental results for the study of effect of area-volume ratio (A/V) and flowrate on the kinetics of $CaCO_3$ deposition

The effect of varying the A/V and the flowrate on the kinetics of $CaCO_3$ deposition was examined with the beadpack at SR 10 and 50^oC, the experiments running for 4 hours. The aim of these is to understand which factor between the A/V and flowrate plays a more dominant role in enhancing the kinetics of scale deposition on surfaces. A better clarity on the factor that contributes more to deposition process at low SR would be beneficial for accurate prediction of the likelihood for scale deposition to take place and support in the design of optimal facilities to manage the threat of $CaCO_3$ deposition at this condition.

In the first experiment, 3mm diameter stainless steel beads were used for the surface deposition test, the A/V in the pack was 2371m^{-1} and the test was conducted at a flowrate of 20ml/hr, whilst in the second experiment, 6mm diameter stainless steel beads were used for the test, and the pack contained a lower A/V of 1085m^{-1}. However, this test was performed at a higher flowrate of 60ml/hr.

The other parameters such as the porosity and residence time in the two different tests were very similar. A summary of the information on the experimental conditions of the two different experiments are provided in Table 5. 4.

Table 5. 4 - Experimental parameters for the beadpack test investigating the effect of A/V (2371.1m^{-1} and 1085m^{-1}) and flowrate (20ml/hr and 60ml/hr) on the kinetics of $CaCO_3$ deposition at SR 10, 50^oC.

Diameter of stainless-steel balls (m)	Number of beads in pack	Volume of void (m^3)	Surface area (m^2)	Area - to - volume ratio (m^{-1})	Porosity	Flowrate (ml/hr)	Residence time (minute)	(C_{ao} - C_a) ppm
0.003	651	7.76 x 10^{-6}	0.0184	2371.1	0.46	20	23.4	65
0.006	214	2.23 x 10^{-5}	0.0242	1085	0.48	60	23.4	61.1

The calcium ion concentration versus time results for the two different systems are presented in Figure 5. 16 and show that for the test conducted at the higher A/V of 2371m^{-1}, there was a notably sharp drop in the calcium ion concentration with time after 10 minutes. This initial sharp drop in the Ca^{2+} observed after the induction time can be attributed to instantaneous nucleation of $CaCO_3$ crystals, where all the $CaCO_3$ crystals nucleate at the same time and the crystal growth process takes place afterwards [139]. The crystal growth stage is indicated by the period of stabilisation in the Ca^{2+} concentration observed after 90 minutes.

However, in the experiment performed at the lower A/V of 1085m^{-1} and the higher flowrate of 60ml/hr, the initial change in the calcium ion concentration with time was observed after a slightly longer period of 30 minutes. Subsequently, the

calcium ion concentration continued to reduce steadily with time. The slower reduction in the Ca^{2+} concentration noticed at the lower A/V contrasts with the sharp drop observed at the higher A/V. This could be attributed to progressive nucleation of $CaCO_3$ crystals, where both the nucleation and growth processes occur simultaneously [140], until stabilisation in the calcium ion concentration was attained after 120 minutes, suggesting that the crystal growth process is dominant at this stage.

These results reveal that the presence of higher A/V led to a reduction in the induction time and equilibrium point for $CaCO_3$ deposition, in comparison to the experiment conducted at a lower A/V and a higher flowrate. In addition, there was evidence for instantaneous nucleation at the higher A/V and progressive nucleation at the lower A/V.

Nonetheless, the difference between the initial and final calcium ion concentration ($\Delta C_{ao} - C_a$) was determined to be 65ppm for the experiment conducted at a higher A/V and 61ppm for the test carried out at a lower A/V and a higher flowrate, which suggests that the overall kinetics of $CaCO_3$ deposition in the two different systems are comparable.

Overall, the findings from this study indicate that both A/V and flowrate play an important role in driving the kinetics of $CaCO_3$ deposition on surfaces. However, from these two experiments it not clear which factor contributes more to the kinetics of surface deposition of $CaCO_3$.

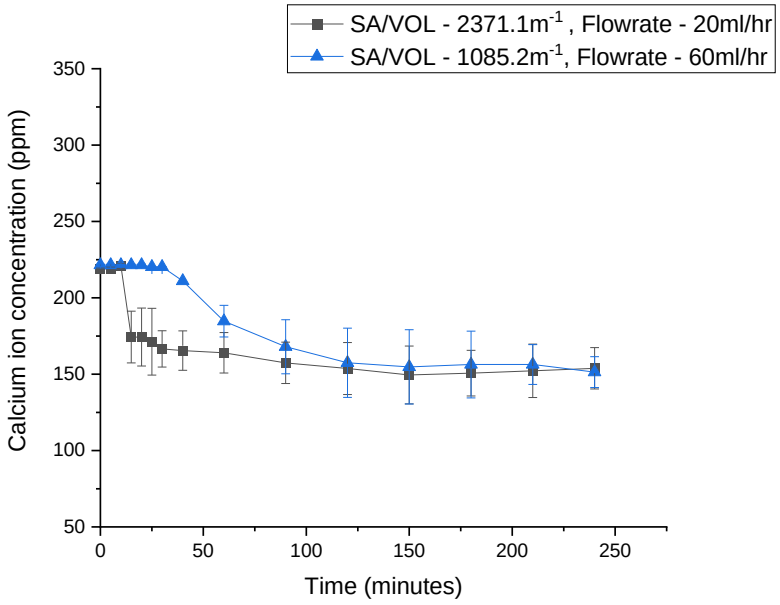

Figure 5. 16 - Comparing the Ca^{2+} ion concentration vs time graph for the beadpack test with an A/V ratio of 2371.1m^{-1} and flowrate of 20ml/hr to the results obtained at an A/V of 1085.2m^{-1} and flowrate of 60ml/hr at SR 10 and 50°C.

5.3.2.4 Experimental results for the study of effect of flowrate on the kinetics of $CaCO_3$ deposition

The effect of increasing the flowrate from 20 to 60 ml/hr on the kinetics of $CaCO_3$ deposition was investigated at SR 10 and 50^oC.The test ran for 4 hours.The first experiment was conducted in the pack with a length of 0.15m, with 6 mm diameter stainless-steel beads being used, while the A/V in the column was 1085.2m^{-1} and the flowrate was 60ml/hr. The second test was carried out in a shorter pack with a length of 0.054m, and 6mm diameter beads were also used for this test. The A/V ratio at this condition is 852.5m^{-1}, which is slightly lower (by a factor of 1.3) than the A/V ratio in the first test. However, a significantly lower flowrate of 20ml/hr was used for this experiment.

A longer pack was used for the surface deposition test at 60ml/hr to have a similar residence to test at 20ml/hr (i.e. a residence time of 27.5minute for the experiment at 60ml/hr and 23.4minute for the experiment at 20ml/hr). Assuming the shorter pack length was used for both 20ml/hr and 60ml/hr experiment, the residence time would have been notably different (i.e. 11.6minute for the experiment at 60ml/hr and 23.4minute for the experiment at 20ml/hr).

It is important to note that it is difficult to vary only one experimental parameter in the beadpack and keep all the other experimental parameters such as porosity and A/V constant. This is because a change in one variable causes a change another variable, for instance, a change in the length of the pack will led to a change in the porosity, residence time and A/V. However, there is an acceptable range for the experimental variables.

The flowrate was the main factor significantly different in the two tests in comparison to the other parameters such as the A/V, porosity, and residence time as shown in Table 5. 5**.** The flowrate was reduced by a factor of three from the first to the second test, to understand the effect of the flowrate on the kinetics of $CaCO_3$ deposition.

Table 5. 5 - Experimental parameters for the beadpack test studying the effect of flowrate (20ml/hr and 60ml/hr) at similar A/V (852.5m^{-1} and 1085.2m^{-1}) on the kinetics of $CaCO_3$ deposition at SR 10, 50^oC.

Diameter of stainless-steel balls (m)	Number of beads in pack	Volume of void (m^3)	Surface area (m^2)	Area - to - volume ratio (m^{-1})	Porosity	Flowrate (ml/hr)	Residence time (minute)	(C_{ao} - C_a) ppm
0.006	214	2.23 x 10^{-5}	0.0242	1085	0.48	60	23.4	61.10
0.006	69	9.15 x 10^{-6}	0.0078	852.46	0.54	20	27.5	42.18

Figure 5. 17 shows a larger change in the calcium ion concentration versus time results at the higher flowrate of 60ml/hr in comparison to the test at the lower flowrate of 20ml/hr. In addition, the difference between the initial calcium ion concentration (C_{ao}) and the equilibrium calcium ion concentration (C_a) at the higher flowrate was estimated to be 61ppm whilst a notably lower change of 42pmm was obtained from the test at the lower flowrate. This demonstrates that increasing the flowrate increases the kinetics of $CaCO_3$ deposition on the surface at SR 10 and 50^{o}C, which is in line with the hypothesis proposed.

However, the initial drop in calcium ion concentration was observed after 30 minutes for both tests and the equilibrium point was observed to be attained at the same time of 120 minutes for the test at 20ml/hr and 60ml/hr, indicating that the flowrate did not affect the induction time and equilibrium point for $CaCO_3$ deposition in this condition. This result is contrary to previous work reported in literature [133]. For instance, Sanni et al[122] study performed with the *in-situ* visualisation cell revealed that at SR 10, the induction time reduced as flowrate increased from 10ml/min to 20ml/min due to more effective mixing of the brine which encouraged a faster nucleation of $CaCO_3$ on the surface. Nonetheless, the larger change in the calcium ion concentration observed with time at the higher flowrate in the beadpack test, indicates a faster kinetics at the higher flowrate which supports several published data in literature [36, 131, 141, 142].

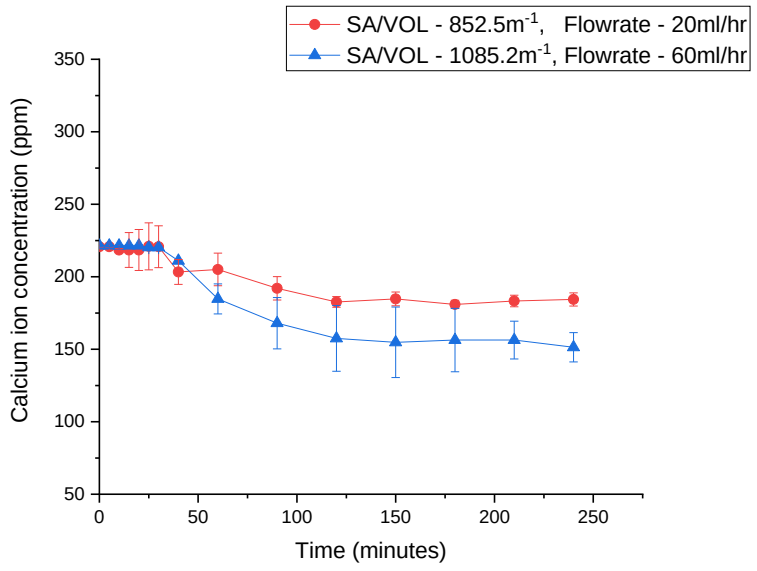

Figure 5. 17 - Comparing the Ca^{2+} ion concentration vs time graph for the beadpack test on effect of flowrate (20ml/hr and 60ml/hr) on the kinetics of $CaCO_3$ deposition at similar A/V (852.5m^{-1} and 1085.2m^{-1}), SR 10 and 50^{o}C.

5.3.2.5 Experimental results for the study of effect of area-to-volume ratio (A/V) on the kinetics of $CaCO_3$ deposition

The effect of A/V on the kinetics of $CaCO_3$ deposition was examined with the beadpack by varying the size of the beads in the pack. In the first experiment, 6mm diameter stainless-steel beads were used for the test and the A/V in the pack was 852.5m^{-1}, whilst in the second experiment, 9mm diameter stainless-steel beads was used and the A/V at this condition was 455.5m^{-1}. The two experiments were conducted at SR 10, 50^oC and flowrate of 20ml/hr. The tests ran for a duration of 4 hours. Furthermore, the porosity and residence time in the pack at the different A/V was also similar as shown in Table 5. 6.

Table 5. 6 - Experimental parameters for the beadpack on the effect of A/V (852.5m^{-1} and 455.5m^{-1}) on the kinetics of $CaCO_3$ deposition at SR 10, 50^oC and flowrate of 20ml/hr.

Diameter of stainless-steel balls (m)	Number of beads in pack	Volume of void (m^3)	Surface area (m^2)	Area - to - volume ratio (m^{-1})	Porosity	Flowrate (ml/hr)	Residence time (minute)	(C_{ao} - C_a) ppm
0.006	69	9.15 x 10^{-6}	0.0078	852.46	0.54	20	27.5	42.2
0.009	18	1.01 x 10^{-5}	0.0046	455.45	0.6	20	30.5	39.9

Figure 5. 18 shows the calcium ion concentration versus time results for study of the effect of A/V on the kinetics of the $CaCO_3$ deposition. The findings illustrate a similar trend in the tests conducted at the higher and lower A/V. The first reduction in the calcium ion concentration versus time graph was observed after 30 minutes for both tests. However, the condition with the higher A/V attained equilibrium point after 120 minutes whilst the solution with the lower A/V reached equilibrium after 150 minutes, suggesting that a higher A/V reduces the time it takes for an equilibrium state to be achieved.

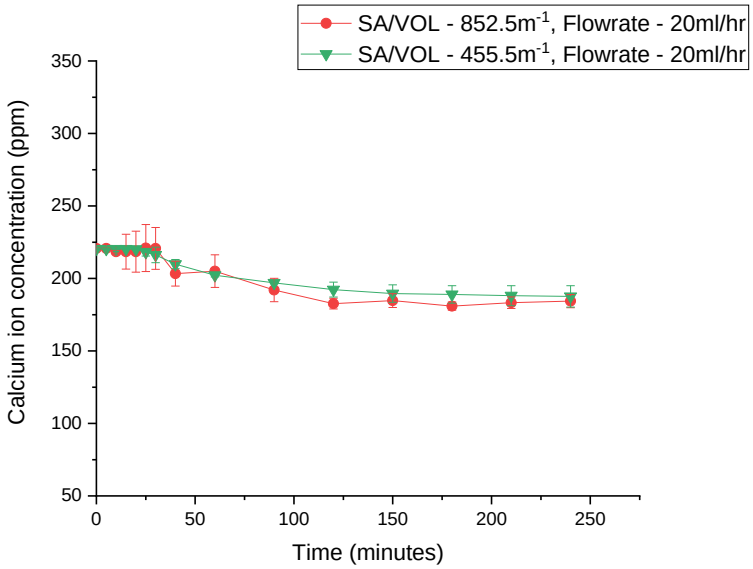

Figure 5. 18 - Comparing the Ca^{2+} ion concentration vs time graph for the beadpack test on the effect of A/V (852.5m^{-1} and 455.5m^{-1}) on the kinetics of $CaCO_3$ deposition at a constant flowrate of 20ml/hr, SR 10 and 50°C.

Furthermore, the change between the initial calcium ion concentration (C_{ao}) and equilibrium calcium ion concentration (C_a) was determined to be 42.2ppm at the higher A/V of 852.5m^{-1} and 39.9ppm at the lower A/V of 455.5m^{-1}, indicating that a higher A/V causes only a slight increase in the kinetic rate of $CaCO_3$ deposition on the surface. This result does not support the hypothesis than an increase in A/V corresponds to a proportional increase in the kinetics of $CaCO_3$ deposition. A possible explanation for this might be because there is a specified amount of scaling ions ((i.e. the Ca^{2+} and CO_3^{2-} ions) passing through the pack at any given time, this implies that there is limit to the amount of deposition that can take place. Therefore, it will get to a point where a further increase in A/V will not lead to an increase in the kinetics of $CaCO_3$ deposition as the maximum amount of deposition has occurred.

Summary

In this chapter, the kinetics of $CaCO_3$ precipitation in the bulk solution was solution was compared to its deposition on the surface at low SR. The distinctions between the *in-situ* visualisation cell and the beadpack setup in relation to their unique strengths and limitations in assessing the kinetics of $CaCO_3$ deposition on the surface at low SR was also explained. Furthermore, the results obtained from the study of the effect of surface roughness, area-to-volume ratio (A/V) and flowrate on the kinetics of $CaCO_3$ deposition at low SR with the beadpack are also presented.

The major findings are summarised as follows:

The results from the beadpack test showed a measurable drop Ca^{2+} concentration across all brine SR and temperature combinations including SR 3, which was difficult to achieve with the static jar and *in-situ* visualisation cell as discussed in Chapter 4, this indicates that the beadpack is more suitable for quantifying the kinetics of $CaCO_3$ deposition at low SR.The beadpack is an effective means of providing reproducible information relating to surface deposition rates in low SR environments within short timeframe experiments.

The induction time for $CaCO_3$ surface deposition is shorter in the beadpack compared to the bulk precipitation induction time from the static jar test for SR 5 and SR 3, and the growth-rate of $CaCO_3$ was 10 times faster at SR 10 in the beadpack compared to the static jar test and 5 times faster for SR 5.

The data reveals that the results obtained from the beadpack differ from the result from the *in-situ* visualisation cell. This is expected as the experiments were conducted at different flowrates, residence times, and area-to-volume ratio (A/V), but the Reynolds number for both tests are in the laminar region, and the shear rate is also low for the two systems, suggesting that no shearing is expected on the surface.

The beadpack can also be used investigate the effect of area-to-volume ratio and surface energy on the kinetics of $CaCO_3$ deposition by changing the sizes and surface energies of the beads in the pack, this type of experiments would be challenging to carry out with the *in-situ* visualisation cell.

The *in-situ* visualisation cell proved to be more beneficial for understanding the early stages of $CaCO_3$ nucleation and growth due to the significantly shorter residence time of 2 seconds in the *in-situ* visualisation cell compared to the beadpack with a residence time of 1404 seconds. The results demonstrate that both the *in-situ* visualisation cell and beadpack techniques are useful for understanding different aspects of the crystallisation process.

The results from the effect of surface roughness on the kinetics of $CaCO_3$ deposition study showed that for the stainless steel materials a slight increase in surface roughness led to a notable change in the Ca^{2+} concentration after an induction period of 20minutes, indicating a marked increase in the kinetics of $CaCO_3$ deposition due to a little increase in surface roughness at low SR. In addition, there was no evidence for $CaCO_3$ deposition on the surface of the PTFE material despite it having the highest value of surface roughness.

The results obtained from the study of the kinetics of $CaCO_3$ deposition at different flowrates and A/V showed that, when the test was conducted at a lower flowrate and high A/V, a short induction time of 10minutes was observed and there was evidence for instantaneous nucleation of $CaCO_3$. In contrast, when the experiment was conducted at a higher flowrate and lower A/V, a longer induction time of 30minutes was observed and there was evidence for progressive nucleation of $CaCO_3$. Nonetheless, the overall kinetics of $CaCO_3$ deposition at the two different conditions were comparable.

The results obtained from the study of the effect of flowrate on the kinetics of $CaCO_3$ deposition at similar A/V revealed that increasing the flowrate from 20 – 60ml/min led to a noticeable increase in the kinetics of $CaCO_3$ deposition.

The data from the effect of A/V on the kinetics of $CaCO_3$ deposition study at low SR showed that an increase in A/V from $852m^{-1}$ to $455.5m^{-1}$ led to only a small increase in the kinetics of $CaCO_3$ deposition at a similar porosity and residence time in the pack.

The findings from this chapter demonstrates into the role of surface roughness, A/V and flowrate on the kinetics of $CaCO_3$ deposition at low SR. In the next chapter, an in-depth discussion of the results presented in the three results chapters (Chapter 4, 5 and 6) is provided.

Chapter 6 - Discussion

6.1 Introduction

The deposition of $CaCO_3$ in pipelines is a major issue experienced in the oil and gas industry, which is caused by the mixing of incompatible brines as well as changes in temperature, pressure, and increased flowrate. This results in the blockage of pipelines and safety valves which can lead to deferred production. To design optimal facilities to manage this threat effectively, a reliable kinetic model is essential. However, the current models used for scale prediction in the oil and gas industry are based on the thermodynamics of bulk precipitation with no consideration for surface deposition kinetics.

Some early research has been directed towards understanding the kinetics of $CaCO_3$ deposition on surfaces, but the drawback of these studies is that they are predominantly conducted at SRs above 10, leaving an area of uncertainty at SRs below 10. Scale deposition at low SR which is caused by heterogeneous nucleation on the surface normally progresses slowly and unnoticeably, but it is of particular interest to the oil and gas industry because of the challenges being faced with scale formation at this condition.

A reliable kinetic model for predicting scale formation at low SR would better identify when treatments are needed to maximise productivity and reduce conservatism in the design barriers to manage scale. This could reduce costs associated with hydrocarbon production and carbon capture utilisation and storage (CCUS) projects.

The development of an accurate scale prediction tool for low SR brines requires a suitable methodology to obtain data on the kinetics of scale deposition at low SR. In this study, the beadpack design was developed to assess the effect of area-to-volume ratio (A/V) on the kinetics of $CaCO_3$ deposition and to provide a better insight into the kinetics of $CaCO_3$ deposition at SR values below 10.

This chapter expands on the interpretation and practical relevance of the results presented in chapters 4, and 5. The contribution of this study to the body of work available in the literature is also discussed. The chapter consists of six sections. The first elaborates on the newly developed beadpack technique and its practical applications. Secondly, the difference between the bulk precipitation and surface deposition induction time is discussed. In the third section, the kinetics of $CaCO_3$ precipitation in the bulk at low SR is discussed. The fourth focuses on $CaCO_3$ deposition on the surface at low SR, detailing the effect of area-to-volume ratio, surface roughness and flowrate on the kinetics. In the fifth section, the kinetics of $CaCO_3$ precipitation in the bulk was compared to the surface at low SR conditions.

Finally, in the sixth section the mechanisms of $CaCO_3$ precipitation in the bulk was compared to the surface at low SR.

6.2 Bead pack technique

6.2.1 Introduction

The beadpack design is a new technique developed to improve the current understanding of the mechanisms and kinetics of $CaCO_3$ deposition on surfaces at low SR.

Some of the common equipment used for studying $CaCO_3$ deposition in the laboratory includes the *in-situ* visualisation cell, the dynamic tube blocking rig, rotating disk electrode (RDE) and the static jar test [25, 131]. The limitation of these techniques is that they are either a closed system where SR reduces with time and the effect of hydrodynamic conditions on $CaCO_3$ deposition cannot be assessed, or there is absence of a high area-to-volume ratio which would be beneficial for generating a quantifiable amount of scale within an acceptable timeframe at low SRs.

A better understanding of $CaCO_3$ deposition kinetics at low SR would be valuable for the development of a reliable scale prediction tool which would be used in the oil and gas industry to determine whether inhibition is required. The next section provides a broader insight into the unique strengths of the beadpack design.

6.2.2 Area-to-volume ratio

The previous studies on the kinetics of $CaCO_3$ deposition has been focused on understanding the effect of factors such as brine composition, temperature, pressure, and flowrate [36, 141, 143, 144]. However, the effect of area-to-volume ratio (A/V) on the kinetics of $CaCO_3$ deposition is an area that requires research attention.

In addition, the current methodologies used to study scale deposition in the laboratory, such as the dynamic tube blocking rig or the *in-situ* visualisation cell, are not suitable for investigating the effect of A/V on kinetics of $CaCO_3$ deposition due to the nature of their design. The beadpack design can be used to assess the effect of A/V ratio on the kinetics of $CaCO_3$ deposition by changing the diameter of the beads in the pack.

An understanding of the effect of A/V can provide insight into the amount of $CaCO_3$ which expected to deposit on a unit area of the surface within a given period of time. This could serve as the building block for the development of an accurate scale prediction tool for providing clarity on the most effective strategy to use to tackle the $CaCO_3$ deposition issues.

6.2.3 Kinetics of scale deposition at low SR

One of the main advantages of the beadpack lies in its ability to quantify effectively $CaCO_3$ deposition at low SR (below SR 10) due to the presence of a high area-to-volume ratio (A/V) in the pack. The drawback of the other techniques used for studying $CaCO_3$ deposition in the laboratory is the lack of a high A/V which is necessary for obtaining measurable data on the kinetics of $CaCO_3$ deposition at low SR within an acceptable timeframe [25].

The formation of $CaCO_3$ at low SR has been reported by many published works to be exclusively controlled by heterogeneous nucleation on the surface [35, 119, 135, 145, 146]. The presence of a high A/V in the pack is expected to increase the amount of $CaCO_3$ deposition, due to heterogeneous nucleation on the surface at low SR, which would help to better quantify the kinetics of $CaCO_3$ deposition at low SR. The mechanisms and kinetics of $CaCO_3$ nucleation and growth can be determined by measuring the effluent calcium ion concentration with time in the outlet of the beadpack using AAS (Atomic Absorption Spectroscopy) technique.

6.2.4 Constant composition environment

The static jar test and RDE test is a closed system [48, 111, 147] in which the SR reduces with time. This causes difficulties in evaluating the mechanisms and kinetics of $CaCO_3$ nucleation and growth as a function of SR.

In contrast to this, the beadpack design is a once-through flow system in which fresh brine continuously passes through the pack without any recirculation of the brine. This enables the surface deposition tests to be conducted in a constant composition environment which is more representative of field conditions [131].

6.2.5 Investigation of different experimental parameters:Temperature, flowrate, porosity, surface roughness and surface energy

The beadpack design allows the assessment of a variety of different factors such as temperature and flowrate on the kinetics of $CaCO_3$ deposition. The effect of surface roughness on $CaCO_3$ deposition can also be examined by changing the roughness of the beads through coating or etching of the material.

In addition, the effect of surface energy can be determined using the beadpack, by using different bead materials such as PTFE, glass or stainless-steel material for the deposition test. The beadpack experiments are conducted in an oven which ensures an isothermal environment for the surface deposition tests and the setup is only suitable for laminar flow tests.

6.2.6 Bead pack capability to better quantify the induction time for low SR

In this study, the beadpack setup and the *in-situ* visualisation cell were used to investigate the effect of SR on the induction time for surface deposition. The induction time is initiated by the reaction between clusters of growth units in a system until the formation of a critical nuclei is achieved, which can be detected in a system by an observable change in the physical property in the system. The induction time has been previously measured by a change in turbidity, conductivity, pH or the time it takes for the differential pressure in a capillary rig to increase from 0 psi [29, 131, 148]. The method of determining the induction time for the beadpack and the *in-situ* visualisation has been described earlier in this chapter.

The $CaCO_3$ precipitation process in the two systems is assumed to be controlled by heterogeneous nucleation on the surface for all the SRs investigated, as the induction time for bulk precipitation (10 mins) is longer than the residence time (2 secs) in the *in-situ* visualisation cell, from the mixing point to the sample in the cell. In the beadpack, although the induction time for bulk precipitation obtained from the static jar test is longer than the residence time in the beadpack (23 mins), the results obtained from the beadpack test conducted with PTFE beads indicate that there is no precipitation of $CaCO_3$ in the bulk solution (Figure 5.2).

This result might be explained by the fact the change in the calcium ion concentration from the static jar test within 23mins (the residence time of the beadpack) was only 17ppm, it is suspected that because the change in Ca^{2+} concentration in the static jar test within the duration of the residence time of the beadpack is minimal, the precipitation of $CaCO_3$ in the bulk solution during the

beadpack experiment was not sufficient to cause a noticeable drop in the calcium ion concentration in the outlet of beadpack.

Instead, the presence of a high A/V in the beadpack is assumed to have induced a substantial amount of deposition on the surface in relation to the bulk. Therefore, the shorter induction time observed during the beadpack test conducted with the etched stainless-steel bead is attributed to heterogeneous nucleation of $CaCO_3$ on the surface. This finding is consistent with that of Sanni et al [80] whose work demonstrated that $CaCO_3$ formation at low SR (SR 10 and SR 25) is controlled surface crystallisation without the influence of pre-precipitated $CaCO_3$ crystals in the bulk solution.

Table 6. 1 summarises the results obtained for the induction time from the beadpack and the *in-situ* visualisation cell at SR 10, 5, and 3 at 50^{o}C. The data shows that different induction times were obtained from the two different techniques at the same SR and temperature. This variation is attributed to the different experimental conditions such as flowrates and A/V in which the tests were performed, which were discussed earlier in Chapter 5.

Table 6. 1 – Comparing the induction time for bulk precipitation (from the static jar tests) and surface deposition using the beadpack with A/V of 2371m^{-1} and the *in-situ* visualisation with A/V of 28m^{-1}.

	Induction time (minutes)		
	Bulk precipitation	Surface deposition	
SR	Static jar	Beadpack (20ml/hr)	In-situ visualisation (20ml/min)
SR 10	10	10	-
SR 5	30	20	-
SR 3	no scale formed	20	-

The data also identified from the beadpack test that as the SR increased from SR 5 to SR 10 the induction time reduced. This appears to be due to the higher ionic composition at the higher SR, which enhances the likelihood for nucleation and growth of $CaCO_3$ to take place. This finding agrees with a great deal of previous work reported in the literature [35, 97, 119, 131]. However, the same induction time was observed for SR 5 and 3, which is attributed to their comparable ionic compositions.

Contrary to the surface deposition results from the beadpack tests, the *in-situ* visualisation cell results presented in Chapter 4 section 4.2 showed no induction time for surface deposition at SR 10, SR 5 and SR 3 at 20ml/min and 30ml/min. This can be attributed to the threshold setting in the image processing software, which was able to detect the deposition of very small crystals on the surface; the

details of the MATLAB algorithm used are presented in the appendix. There was evidence for the deposition of $CaCO_3$ crystals on the surface of the first image captured by the camera in the *in-situ* visualisation cell after 5minutes at all the SR (i.e. SR 10, 5 and 3) investigated.

This result differs from previous work reported in literature, as a much longer induction time of 50 minutes was observed for SR 10 at 40^{o}C [97], this is attributed to the different threshold setting in the image processing software used to analyse the images from the deposition test.

Nonetheless, the beadpack results demonstrate a better capability than the *in-situ* visualisation cell in assessing the kinetics $CaCO_3$ at very low SR (below SR 5). This is demonstrated in the *in-situ* visualisation cell results at SR 3, and 20ml/min which showed no evidence for the growth of crystals Figure 4.13 and at 30ml/min, only 2 crystals were formed for the entire 240 minutes duration of the experiment. However, the beadpack result at SR 3 provided evidence for both nucleation and growth of $CaCO_3$ within a shorter time frame of 150 minutes (Figure 5.4), despite the fact that the beadpack test was conducted at a markedly lower flowrate of 20ml/hr. This result attributed to the substantially higher A/V in the pack, which helps to generate an appreciable amount of deposition compared to the *in-situ* visualisation cell.

In line with the previous findings, Mavredaki [81], also conducted deposition tests with the dynamic flow rig, and reported a very long induction period of 92 hours for the deposition of $CaCO_3$ at SR 5 and 80^{o}C. It was also mentioned that surface deposition tests were not conducted at SR 2.5 and SR 1.5 with the dynamic flow rig, because it would take a considerable amount of time to obtain substantial information on the kinetics of surface deposition at these conditions, suggesting that the dynamic flow rig is not a suitable technique for quantifying the deposition of $CaCO_3$ at low SR within an acceptable timeframe.

Overall, these findings suggest that, in comparison to the current techniques used for studying $CaCO_3$ deposition [81, 119] the beadpack helps to assess the induction time for $CaCO_3$ deposition at low SR within a shorter time frame, due to the presence of high A/V, supporting a faster generation of a measurable amount of deposition.

One implication of having a better understanding of the induction time for $CaCO_3$ deposition at low SR is that it might help in the development of a reliable prediction tool for estimating when and where the scale deposition is likely to start. This would also support the deployment of scale inhibitors to the correct location for effective management of scaling issues [81].

6.3 Comparing the induction time for bulk precipitation to surface deposition

In accordance with literature [46, 55, 57, 149, 150], induction time is described as the time in which the commencement of precipitation can be observed after mixing the brines. In this study, the onset of precipitation in the bulk solution is the time where a drop in the calcium ion concentration was observed during the static jar tests.

The surface deposition tests were performed using the beadpack and the *in-situ* visualisation cell. The induction times in these flowing systems supposes that there is no formation of $CaCO_3$ before the cation brine (rich in calcium ion) and the anion brine (rich in carbonate ions), which are flowing from two different tubes, mixes at the T-junction and flows into the *in-situ* visualisation flow cell or the beadpack.

The surface scaling induction time in the beadpack is the time when a reduction in the calcium ion concentration was observed in the outlet of the beadpack, whilst the time it takes for the first crystal to be observed and quantified using the image analysis software relates to the induction time for the *in-situ* visualisation cell.

The results for the induction time for bulk precipitation from the static jar tests and surface deposition from the beadpack test for SR 10, 5 and 3 and 50°C are presented in Figure 6. 1, Figure 6. 2 and Figure 6. 3 respectively.

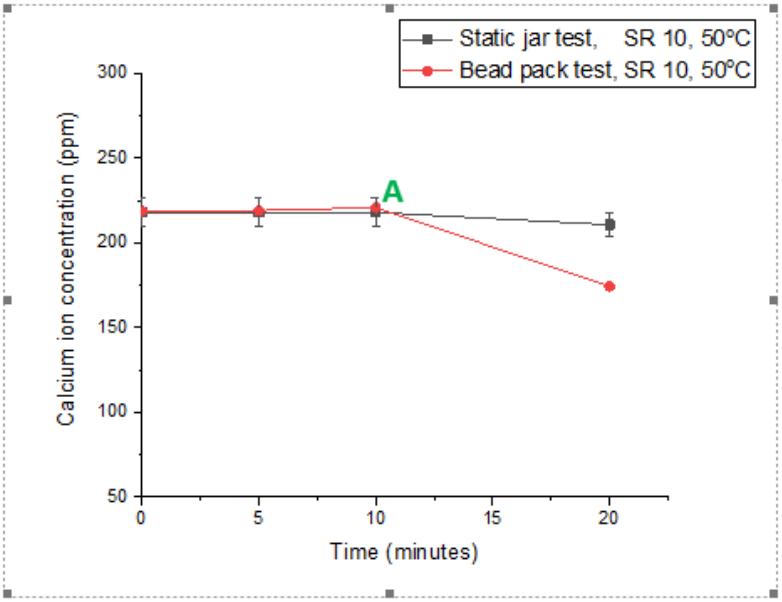

Figure 6. 1 - Comparing the induction time from the static jar test and the beadpack test at SR 10 and 50°C. An induction time of 10minutes was observed for both the static jar test and beadpack test, illustrated by point A.

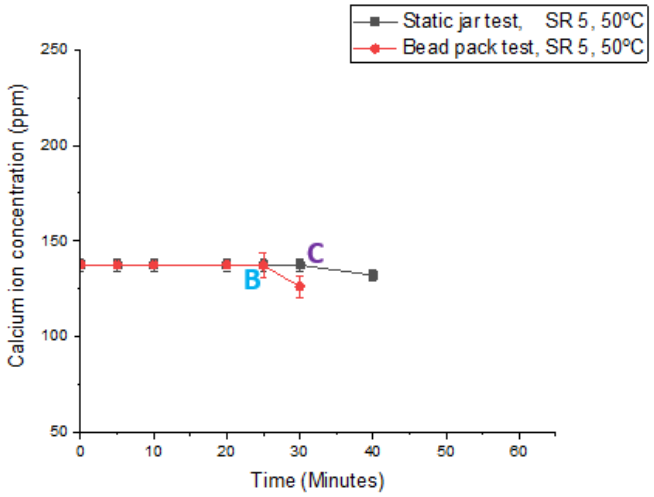

Figure 6. 2 - Comparing the induction time from the static jar test and the beadpack test at SR 5 and 50°C. An induction time of 30minutes was observed for the static jar test illustrated by point B, and a shorter induction time of 20 minutes for the beadpack test, as shown by point C.

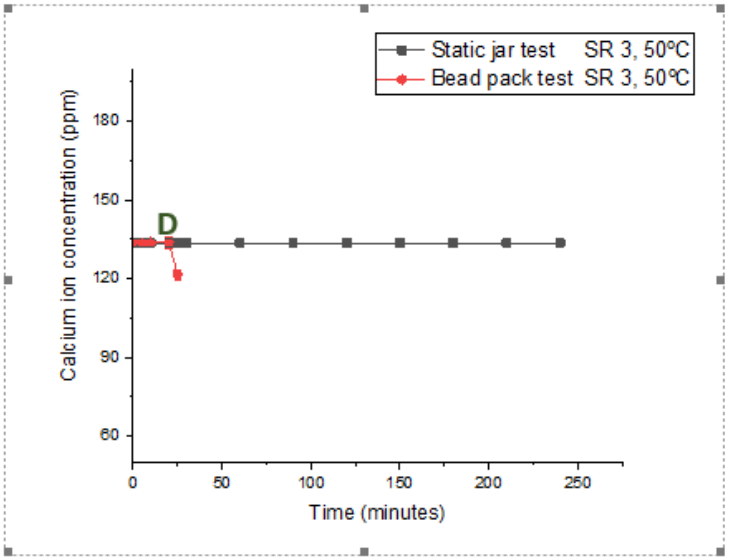

Figure 6. 3 - Comparing the induction time from the static jar test and the beadpack test at SR 3 and 50°C. An induction time of 20 minutes was observed for the beadpack test, as shown by point D, whilst there was no evidence for $CaCO_3$ precipitation from the static jar test for the 240minutes duration of the experiment.

The results from both the bulk precipitation test conducted using static jar and the surface deposition test carried out with the beadpack, demonstrates that as the SR increased the induction time reduced generally (except for the SR 5 and SR 3 results from the beadpack test where their induction time was the same). The inverse relationship between the SR and induction time observed is consistent with a large body of work available in literature [26, 29, 102, 131, 151-156], including the classical nucleation theory. The induction time for precipitation of crystals is expressed by equation 7.10 [55]

$$\log t_{ind} = C + \frac{BT^3}{(SI)^2} \quad 7.10$$

Where C is a constant, SI represents the saturation index (log SR), and B is a function of interfacial tension, γ as presented in equation 7.11.

$$B = \frac{\beta\gamma^3 \ f(\theta)N_A^2 v_m^2}{(1.3R)^3} \quad 7.11$$

Where β is a geometric factor of $16\pi/3$ for the spherical nucleus, f(θ) is a correction factor according to the type of nucleation taking place, V_m is the molecular volume (6.132 x 10^{-23} cm^3) for calcite, T is the absolute temperature (Kelvin), R the gas constant (8.3146 J/mol.k), y is the surface energy (J/m^2) and N_A is Avogadro's number (6.022 x 10^{-23}/mol).

However, the findings from the *in-situ* visualisation cell tests showed no measurable induction time for all three saturation ratios investigated. The different induction times obtained from the beadpack and *in-situ* visualisation is attributed to the different experimental conditions in which the test was conducted as explained in Chapter 5.

The induction time can also vary depending on the sensitivity of the techniques used for the study. For instance a work by Sanni et al [92] showed that the induction time for $CaCO_3$ deposition in the dynamic tube blocking rig was longer in comparison to the *in-situ* visualisation cell at the same SR, flowrate and temperature. This was attributed to the unique method of determining induction time with the different techniques. The span of time it takes for the differential pressure in the capillary rig to deviate from zero is the induction time for the capillary rig, whilst the time it takes for the image analysis software to identify and measure the size of the first crystal deposited on the surface is the induction time for *in-situ* visualisation cell.

It was also observed that the *in-situ* visualisation cell was more suitable for understanding the early stages of $CaCO_3$ deposition, whilst the tube blocking rig was better for understanding the later stages of $CaCO_3$ deposition.

Despite the sensitivity of the different techniques, the induction time for bulk precipitation was still observed to be longer than the induction time for surface deposition on the etched stainless steel beads. The results from the beadpack test conducted with PTFE beads in Figure 5.2 illustrates this, as there was no change in the calcium ion concentration for the entire 4 hours duration of the test, indicating that there was no formation of $CaCO_3$ at this condition. The SEM image of the

PTFE bead after the deposition test also showed no evidence for $CaCO_3$ deposition on the surface (Figure 6.3).

This result is attributed to the low surface energy of the PTFE material, which did not favour the nucleation of $CaCO_3$ on the surface. Nonetheless, it was expected that, if there was precipitation of $CaCO_3$ in the bulk solution, this would have led to a drop in the calcium ion concentration. Therefore, this finding suggests that the induction time for bulk precipitation was longer than the 4 hours' time frame for the experiment. In contrast, there was a noticeable reduction in the calcium ion concentration in the beadpack test conducted with the etched stainless-steel bead after 20 minutes at the same condition, implying that $CaCO_3$ deposition occurred on the surface.

These findings are in line with many published studies [34, 35, 80, 122]. The classical nucleation theory also proposes that heterogeneous nucleation on the surface is kinetically prioritised over homogenous nucleation in the bulk solution at low SR, as there is a greater resistance to nucleation due to the lower concentration of scaling ions (i.e. the Ca^{2+} and CO_3^{2-} ions) in the brine. The formula for nucleation rate J_n is shown in equation 7.12.

$$J_{n=} J_0 \exp\left(-\frac{16\pi v_m^2 \alpha'^3}{3k_B^3 T^3 \sigma^2}\right) \qquad 7.12$$

Where J_0 is a kinetic factor related to the frequency and efficiency of collision, α' is the effective interfacial energy (mJ/m^2), v_m is the molecular volume of the forming phase (cm^3/molecule), k_B is the Boltzmann constant (1.38 x 10^{-23} JK^{-1}), T is the temperature (K), and σ represents supersaturation in the form $\ln(IAP/K_{sp})$. Hence, surface deposition is given precedence because it requires less energy in comparison to bulk precipitation [146]. This is a possible explanation for the shorter induction time observed on the surface of the etched stainless beads in contrast to the bulk at SR 10.

In addition, the high A/V in the pack, as well as the surface roughness of the etched stainless-steel beads, is also assumed to play an important role in reducing the induction time for surface deposition. This is by causing a higher degree of heterogeneous nucleation in comparison to homogenous nucleation. Furthermore, surface roughness has also been reported to contribute to the induction for $CaCO_3$ deposition [157-159]. For instance, Epstein et al [160] found that an increase in surface roughness reduced the induction time for $CaCO_3$ deposition by improving the ability for the scaling ions to nucleate on the surface due to the increased contact area, thereby enhancing the tendency for scale deposition to take place.

Another interesting observation from the results in Table 6. 2, is that the variation between the induction time for bulk precipitation and surface deposition increased

as the SR reduced. For instance, at SR 3, the surface scaling induction time was 20 minutes, whilst there was no evidence for the formation of $CaCO_3$ in the bulk solution for the 4-hour duration of the test at the same SR. In contrast, at SR 10, the same induction time of 10 minutes was observed on the surface and in the bulk solution. This result agrees with previous research in this area [97]. These findings may be explained by the fact that as the SR reduced from SR 10 to SR 3, the driving force for scale deposition to take place on the surface also reduces.

Therefore, the process of heterogeneous nucleation on the surface becomes more favourable and the likelihood for homogenous nucleation in bulk solution taking place is significantly reduced, thereby causing a larger disparity between the induction time for surface deposition and bulk precipitation as SR reduces. The study builds on the current knowledge on the kinetics of surface deposition by providing a richer insight into the distinction between the induction time for bulk precipitation and surface deposition at low SR. This work also expands on the role of A/V on the induction time for $CaCO_3$ deposition at low SR.

Table 6. 2 - Variation between the induction time bulk precipitation (static jar test) and surface deposition (beadpack test) for SR 10, 5 and 3 at 50°C.

SR	Static jar	Beadpack	Variation in induction time (minutes)
SR 10	10	10	0
SR 5	30	20	10
SR 3	no scale formed	20	>220

These results indicate that surface scaling processes occur faster than bulk precipitation in low SR brines and should be considered when developing inhibition systems to manage scale formation issues in these conditions. The data from this section also suggests that the presence of a high A/V also contributes to the reduction of the induction time for surface deposition. Therefore, it should be considered when designing facilities to manage scale deposition issues at low SR.

6.3.1 Effect of surface roughness on induction time

The results presented in Table 6. 3 demonstrate the effect of surface roughness on the induction time for $CaCO_3$ deposition. The data illustrates that, for the stainless-steel beads, the induction time reduced as their surface roughness increased. However, there was no evidence for the formation of $CaCO_3$ on the PTFE beads despite it having the highest value for surface roughness.

Table 6. 3 - The effect of surface roughness on the induction time for $CaCO_3$ deposition.

Material	Type	Roughness (nm)	Induction time (min)
Stainless steel	Etched stainless steel bead	57	10
	Smooth stainless steel bead	41	> 240
PTFE	PTFE bead	460	>240

These findings are in accordance with previous work in literature [138, 159, 161, 162]. Stainless steel materials have been reported to have a notably lower contact angle and a higher surface energy which supports the deposition of scale, in contrast to PTFE materials which have a lower surface energy, higher contact angle and are hydrophobic, and do not favour the deposition of scale [163-166].

It is assumed that increasing the roughness of the stainless steel material led to an increase in the contact area and number of nucleation sites on the surface, thereby improving the ability for $CaCO_3$ to nucleate to its surface. This is a possible explanation for the lower induction time observed as the surface roughness increased [138, 157, 167].

This result demonstrates that surface roughness in isolation is not the decisive factor causing a reduction in the induction time for $CaCO_3$ deposition. Instead, the type of material should also be considered. Regarding the stainless-steel beads, a slight increase in their surface roughness induced a notable reduction in the induction for $CaCO_3$ deposition at low SR, whilst the PTFE bead with the highest value of surface roughness did not provide any evidence for $CaCO_3$ deposition. An understanding of the tendency for $CaCO_3$ to nucleate on different materials is useful for the design of facilities and coatings which could help to reduce $CaCO_3$ deposition issues.

6.4 Kinetics of $CaCO_3$ precipitation in the bulk at low SR

In this section, the results obtained from the study of the effect of SR (SR 10, 5 and 3) and temperature (50^{o}C and 90^{o}C) on the kinetics of $CaCO_3$ precipitation in the bulk solution are discussed.

6.4.1 Effect of SR on the kinetics of bulk precipitation at low SR

The results presented in Chapter 4 section 4.1 show the kinetics of $CaCO_3$ precipitation in the bulk solution at SR 10, 5 and 3 at 50^{o}C and 90^{o}C. The data demonstrates that, generally, as the SR increased there was a higher change in the Ca^{2+} concentration with time, indicating a faster kinetic as SR increased.

The effect of SR on the growth-rate of $CaCO_3$ in the bulk solution was also determined by applying a linear fit after the induction period and prior to any stabilisation in the calcium ion concentration. A linear fit was used because it best represents the relationship between the calcium ion concentration and time. The R^2 values for both 90°C and 50°C tests were greater than 0.91, which suggests a good correlation. The growth-rate (evaluated in ppm/minutes and determined by the gradient of the linear fit) increased as SR increased for both 50°C and 90°C, as illustrated in Figure 6. 4 and Figure 6. 5. The growth-rate corresponds to the time it takes for the crystals that have attained critical size in the bulk solution to grow and simultaneously slow nucleation of new crystals [168]

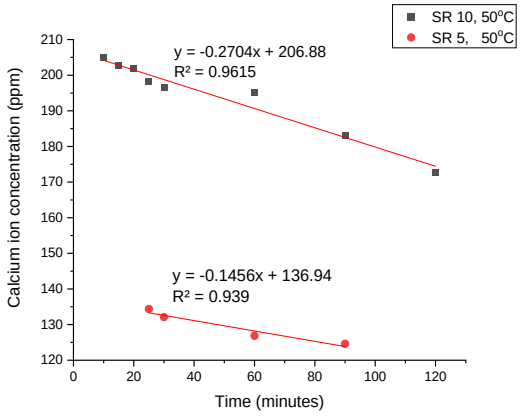

Figure 6. 4 – Average Ca^{2+} ion concentration vs time graph for SR 10, and 5 at 50°C from bulk precipitation test.

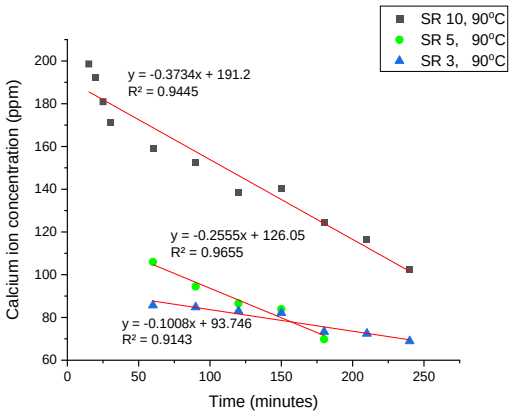

Figure 6. 5 - Average Ca^{2+} ion concentration vs time graph for SR 10, 5 and 3 at 90°C from bulk precipitation test.

This result is in accordance with several research published in literature [26, 70, 81, 169]. In a comparable study by Mavredaki et al [81], a turbidity meter was used to track the formation of $CaCO_3$ in the bulk solution at SR ranging from SR 1.5 – SR 55 and 80°C. The study found that as expected the kinetics of $CaCO_3$ precipitation increased as SR increased, due to the higher concentration of scaling ions in the solution at the higher SR, which accelerated the formation of $CaCO_3$. The research also showed that bulk precipitation is possible even at very low SR as there was evidence for $CaCO_3$ precipitation even at SR 1.5 and SR 2.5. It is important to note that a probable reason for no evidence of $CaCO_3$ precipitation in the static jar test at SR 3 and 50°C whilst there was evidence for bulk precipitation at SR 1.5, is due to the higher temperature of 80°C in which the turbidity test was performed, as temperature is considered to accelerate the kinetics of $CaCO_3$ formation [81].

The limitation of the studies from literature mentioned earlier is that they do not provide any insight into the growth-rate of $CaCO_3$ in the bulk solution at low SR, whilst in the static jar test the growth-rate was assessed by applying a linear fit to the calcium ion concentration versus time results obtained from AAS. An important

implication of quantifying the growth-rate of $CaCO_3$ in the bulk solution is the need to learn more about the distinction between bulk precipitation kinetics and surface deposition kinetics at low SR. This would be useful for the development of a reliable model for predicting scale formation at low SR conditions [170].

6.4.2 Effect of temperature on the kinetics of bulk precipitation at low SR.

The results presented in Chapter 4, section 4.1.2, illustrate that an increase in temperature led to a notable increase in the growth-rate of $CaCO_3$ in the bulk solution at all the SR examined, due to the higher change in the calcium ion concentration with time observed as the temperature increased from 50^{o}C to 90^{o}C.

The influence of increased temperature on the growth-rate of $CaCO_3$ was evaluated by applying a linear fit to the calcium ion concentration versus time graph after the induction period and before the stablisation of the calcium ion concentration. The result showed that the growth rate increased as temperature increased for all the SR investigated as summarised in Figure 6. 6. This result is in accordance with several studies in literature indicating that an increase in temperature accelerates the rates of calcite scale formation [26, 69, 72, 143, 171, 172]. The faster kinetics observed at the higher temperature are attributed to the inverse solubility relationship between temperature and $CaCO_3$ precipitation [173, 174].

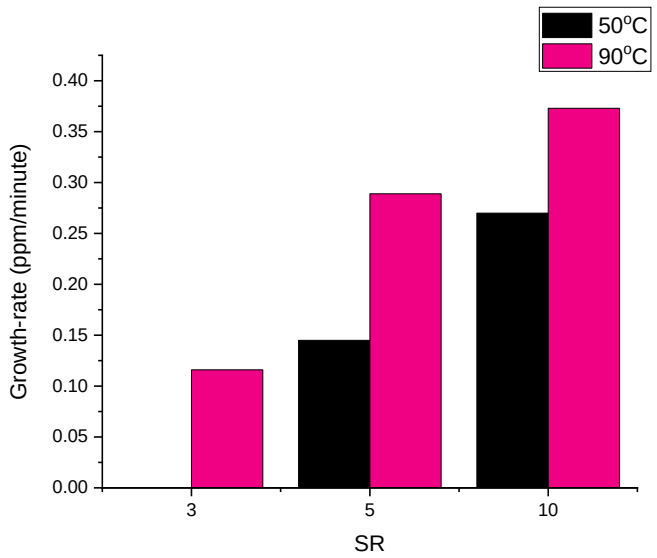

Figure 6. 6 – Growth-rate vs SR for bulk precipitation at two different temperatures.

The previous research reported in literature has been focused on quantifying bulk precipitation at higher SR, i.e. above SR 10. However, this study provides insight into the kinetics of bulk precipitation at SRs below SR 10[48]. These results also

showed that the difference between the growth-rate of $CaCO_3$ in the bulk solution was more significant at a lower temperature (50^oC) compared to a higher temperature (90^oC). For instance, at 50^oC, there was no evidence for $CaCO_3$ precipitation at SR 3, a growth rate of 0.14ppm/min was obtained at SR 5, whilst at 90^oC, there was evidence for $CaCO_3$ precipitation at both SR 3 and SR 5, although the brine composition was lower at the higher temperature for the same SR. The brine compositions used in this study for the 50^oC and 90^oC experiments are presented in Chapter 3, Table 3.1 and Table 3.2 respectively. These results suggests that at higher temperatures, there is a greater tendency for $CaCO_3$ to precipitate in the bulk at low SR due to kinetic effects.

A better understanding of the effect of temperature on the induction time, and growth-rate of $CaCO_3$ formation in the bulk solution is useful for the design of kinetic models for predicting scale formation. It can also support the understanding of the mechanisms and kinetics of scale deposition on surfaces, by helping to determine whether homogenous nucleation in the bulk solution is expected or if the crystallisation process is controlled exclusively by heterogeneous nucleation on the surface. This would be useful in the development of strategies to mitigate the risk of scale formation in low SR solutions. [26, 175].

6.5 Kinetics of $CaCO_3$ surface deposition at low SR

The beadpack setup and the *in-situ* visualisation cell were used to study the kinetics of $CaCO_3$ deposition at low SR. The growth-rate of $CaCO_3$ in the beadpack was calculated from the change between the initial and final calcium ion concentration Δ ($C_{ao} - C_a$) and the residence time in the pack. The equation for this calculation is provided in the appendix, whilst the growth-rate of $CaCO_3$ in the *in-situ* visualisation cell was determined from the slope of the graph showing the average size of crystal with time, by applying a line of best fit to the graph. The results for the average size of crystals deposited on the surface with time was obtained from the MATLAB program developed in this study, the protocol for image processing is explained in the methodology chapter, section 3.5.2.

The result showing the growth-rate of $CaCO_3$ at 50^oC and SR 10, 5 and 3 with the *in-situ* visualisation cell is presented in Figure 6. 7. The slope for the graph of the average size of crystals with time at SR 10 was divided into 3 sections to better quantify the growth-rate of $CaCO_3$ at different stages during the experiment. The first section (0 – 60minutes) corresponds to a period of both nucleation and growth, this is because the results for the number of crystals with time, as shown in Chapter 4, Figure 4.7, reveals that the number of crystals was increasing with time within

this duration. Section B, (60 – 180minutes) is assumed to be a period of only crystals growth, as there was no further increase in the number of crystals at this point. However, the average size of crystal continued to increase. Therefore, the slope of the graph in the section was used as the growth rate of $CaCO_3$ at this condition. Section C (180 – 240minute) is assumed to be the equilibrium point as average size of crystals was observed to increase very slowly with time until the end of the experiment.

At SR 5, the average size of crystals was observed to increase slowly with time throughout the duration of the experiment. This is due to the low concentration of scaling ions in the solution at this condition, and at SR 3 there was no evidence for crystal growth, this can be attributed to the very low concentration of scaling ions at this condition which did not support the growth of $CaCO_3$. Nonetheless, In general, the results demonstrate that the growth-rate of $CaCO_3$ generally increased as SR increased at 50°C.

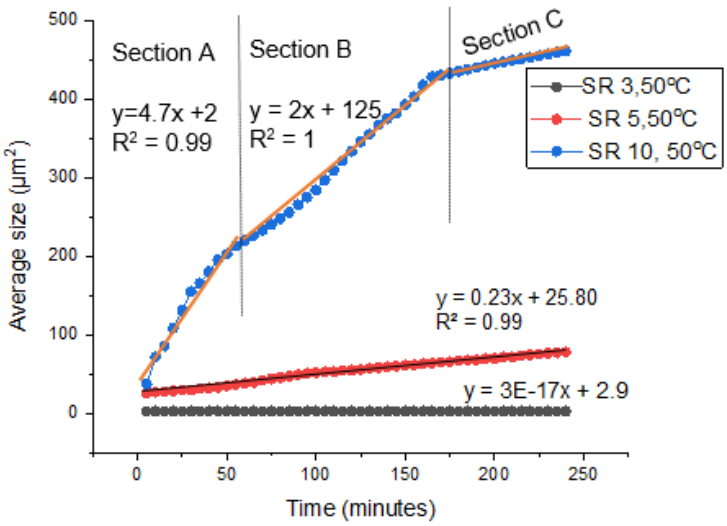

Figure 6. 7 - Comparing the average size of crystals formed on the surface with time and their growth-rates SR 10, 5, and 3 at 50°C, section A corresponds to a period of both nucleation and growth of $CaCO_3$, section B relates to a period of only crystal growth and section C shows a period of stabilisation in the growth of the $CaCO_3$ on the surface.

In line with the results obtained at 50°C, the data obtained from the study of the effect of SR (SR 8, 4 and 2) on the kinetics of $CaCO_3$ deposition with the *in-situ* visualisation cell at 79°C , is presented Figure 6. 8. The slope for the average size of crystals with time at SR 8, was also split into 3 sections. Section A (0 - 55minutes) relates to the period of both nucleation and growth, Section B (55 - 125minutes), the crystal growth stage, and Section C (125 – 240minutes) the equilibrium point, due to the very slow increase in the average size of crystal with time.

At SR 4 and SR 2, the average size of crystals was observed to increase slowly with time following a linear trend throughout the duration of the experiment. However, as expected the kinetics was faster at SR 4. Overall, the results shows that the growth-rate increased as SR increased at 79°C, this is due to the higher concentration of scaling ions in the solution as SR increased, which is the driving force for $CaCO_3$ deposition on the surface.

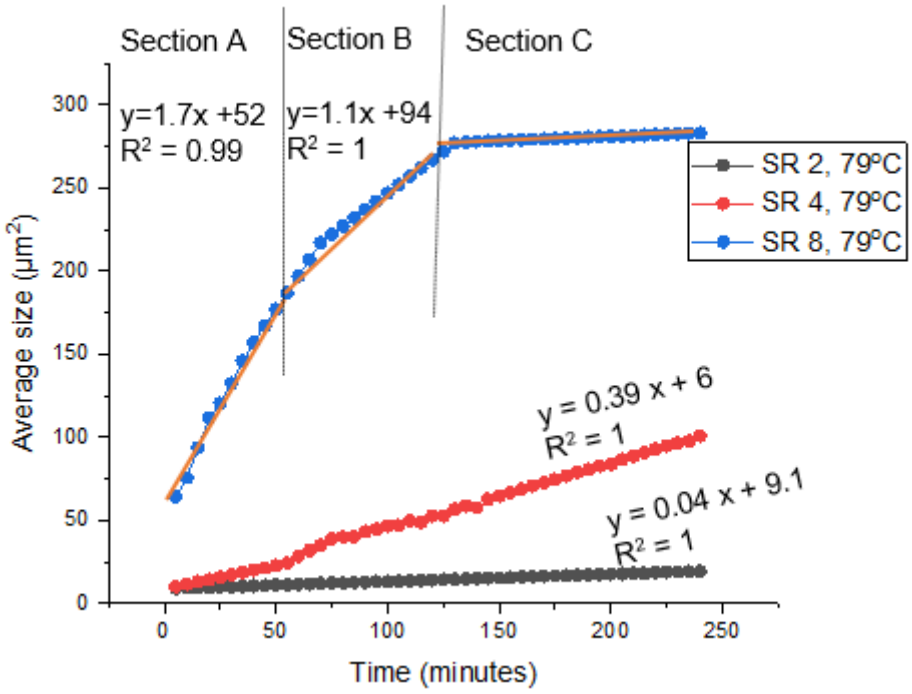

Figure 6. 8 - Comparing the average size of crystals formed on the surface with time and their growth-rates for SR 8, 4 and 2 at 79°C, section A corresponds to a period of both nucleation and growth of $CaCO_3$, section B relates to a period of only crystal growth and section C shows a period of stabilisation in the growth of the $CaCO_3$ on the surface.

Table 6. 4 – Provides a summary of the linear equations and growth-rate of $CaCO_3$ deposition as a function of SR obtained from the *in-situ* visualisation cell tests at 50°C and 79°C.

Table 6. 4 - Growth-rate of calcium carbonate as a function of SR from the *in-situ* visualisation cell tests.

	50°C			79°C	
SR	Linear equations	Growth-rate (µm²/min)	SR	Linear equations	Growth-rate (µm²/min)
SR 10	Y = 2x + 106	2.00	SR 8	Y = 1.1x + 136	1.1
SR 5	Y = 0.23x + 26	0.23	SR 4	Y = 0.39x + 6	0.39
SR 3	-	-	SR 2	Y = 0.04x + 9	0.04

The graphs representing the effect of SR on the growth-rate of $CaCO_3$ in the *in-situ* visualisation cell at 50°C and 79°C are shown below in Figure 6. 9 and Figure 6. 10 respectively.

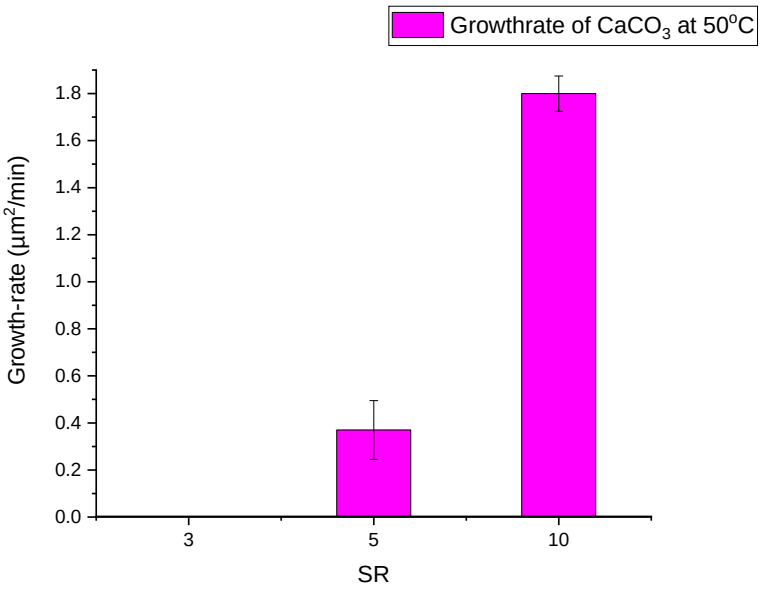

Figure 6. 9 - The *in-situ* visualisation cell results for the effect of SR on the growth-rate of $CaCO_3$ at 50°C.

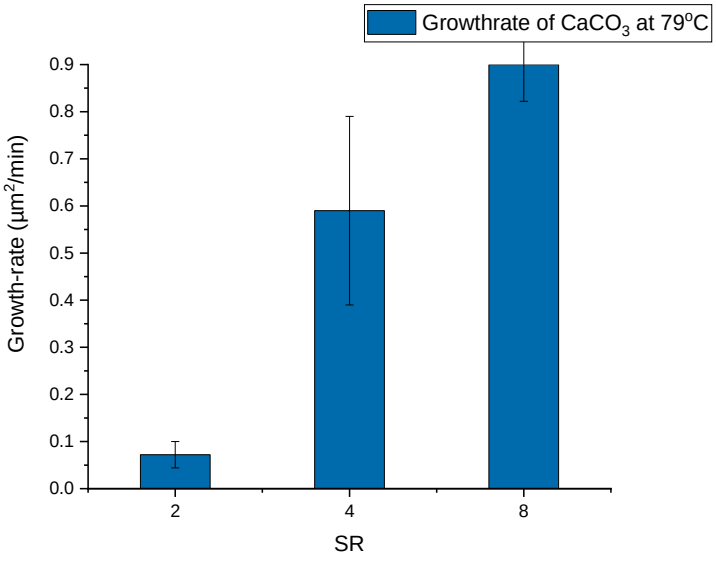

Figure 6. 10 - The *in-situ* visualisation cell results for the effect of SR on the growth-rate of $CaCO_3$ at 79°C.

In agreement with the findings from the *in-situ* visualisation cell, the data from the study of the effect of SR on the kinetics of $CaCO_3$ deposition with the beadpack also showed that the growth rate of $CaCO_3$ increased as SR increased at 50°C, this is summarised in Table 6. 5 and illustrated in Figure 6. 11.

Table 6. 5 - Growth-rate of calcium carbonate as a function of SR from the beadpack test at 50°C.

SR	Growth-rate (ppm/min)
SR 10	2.70
SR 5	0.73
SR 3	0.47

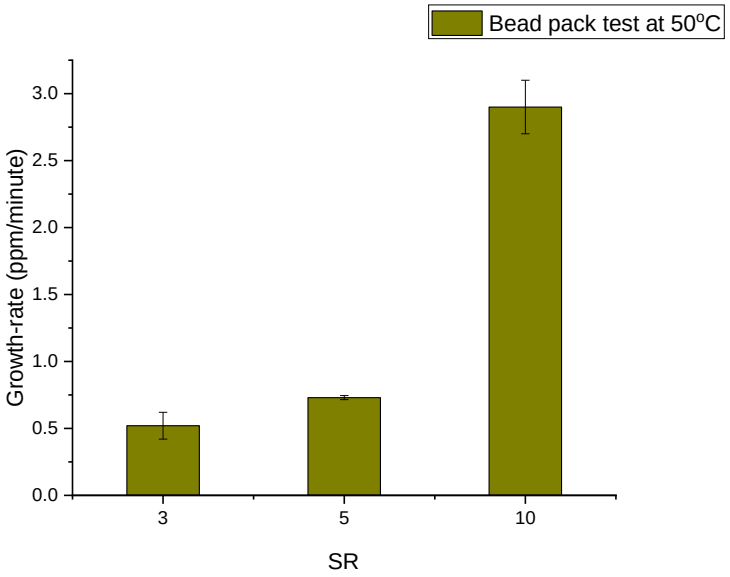

Figure 6. 11 - The beadpack results for the effect of SR on the growth-rate of $CaCO_3$ at 50°C.

The results from the *in-situ* visualisation cell illustrates the difference between the growth-rate of $CaCO_3$ deposition on the surface is larger at a lower temperature (50°C), compared to a higher temperature (79°C). For example, at 50°C, the difference between the growth-rate of $CaCO_3$ at SR 3 and SR 10 is 2μm^2/min, whilst at a higher temperature of 79°C, the difference between the growth-rate at SR 2 and SR 8 is 1.06μm^2/min. This highlights the effect of a higher temperature in accelerating the kinetics of $CaCO_3$ surface deposition. This finding is in agreement with several research published in literature [69, 72, 176]. For instance, In study by Norah et al[177], the dynamic tube blocking rig was used to evaluate the kinetics of $CaCO_3$ deposition as a function of temperature (20 – 130°C) and pH of (6.0 – 8.3), which is reflective of field conditions , the study found that an increase in temperature significantly increased the kinetics of $CaCO_3$ deposition especially at downhole conditions with a pH 6. These findings indicates that at a higher temperature, there is greater possibility of obtaining measurable data on the kinetics of $CaCO_3$ surface deposition at low SR conditions.

The data from both the beadpack and the *in-situ* visualisation cell also reveal that an increase in the SR led to an increase in the growth-rate of $CaCO_3$ on the surface. These results agree with several published pieces of research in literature

[25, 35, 104]. For instance, Feth et al [34] investigated the kinetics of $CaCO_3$ deposition on a stainless steel sample. The experiment was conducted with a rotating disk electrode (RDE) at SR 12.5, SR 31.6 and SR 100 and temperatures of 24^oC and 70^oC. The kinetics of $CaCO_3$ deposition were determined by carrying out mass gain measurements of the scale deposits at different time intervals. The analysis of the scale deposition data identified that, as expected, the growth-rate of $CaCO_3$ on the surface increased as SR increased, due to the higher concentration of scaling ions in the solution at the higher SR which is the driving force for $CaCO_3$ formation [26]. The drawback of this research is that it is focused on quantifying the kinetics of $CaCO_3$ deposition at a higher SR (i.e. above SR 12), and does not provide any insight into the kinetics of $CaCO_3$ deposition at SR below 12.

In addition, it was also mentioned that the mass of $CaCO_3$ deposited on the stainless steel sample was low in comparison to the mass of $CaCO_3$ precipitation in the bulk solution at the same temperature. This is unanticipated, as literature suggests that $CaCO_3$ is more likely to deposit on the surface than to precipitate in the bulk solution [35, 119]. The lower amount of scale deposited on the surface in comparison to the bulk solution was attributed to the low surface area (3.8cm^2) of the stainless steel sample in the RDE, which did not provide sufficient area for $CaCO_3$ deposition to take place. This indicates that the presence of a low surface area minimises the amount of the deposition which can occur on the surface. However, in contrast to this low surface area, the surface area available in the beadpack is 184cm^2. This significantly higher surface area is expected to facilitate the deposition of a larger amount of scale, which would help to better quantify $CaCO_3$ deposition in low SR brines.

This study illustrates the effect of SR on the growth-rate of $CaCO_3$ on the surface at low SR conditions, which is important because surface crystallisation is the main cause of blockages in pipelines, impacting safe hydrocarbon operations and leading to deferred production. The crystals formed in the bulk solution are normally transported and whilst they might collect in strainers, their impact on operations is generally limited.

The two techniques also provide complementary insights into the kinetics of $CaCO_3$ deposition on the surface, whilst the *in-situ* visualisation cell can help to determine how the crystals would grow on the surface of the pipelines with time before blockages occur, the beadpack can support in evaluating the change in the ionic composition of the brine with time due to scale formation, which can be useful for tracking the SR of the brine. Therefore, the use of more than one technique is valuable for generating reliable data on the mechanisms and kinetics of $CaCO_3$ deposition at low SR conditions.

A better understanding of the kinetics of surface deposition at low SR can serve as the building block for the development of a reliable kinetic model for predicting scale formation at these conditions. This kinetic model would be beneficial for identifying when inhibition treatments are required to maximise productivity and injector availability [25, 35].

6.5.1 Growth-rate of $CaCO_3$ on the surface as a function of area-to-volume ratio (A/V)

The results presented in Table 6. 6, illustrates the effect of A/V on the kinetics of $CaCO_3$ deposition at SR 10, 50^{o}C at a constant flowrate of 20ml/hr. The A/V in the beadpack was varied by changing the diameter of stainless-steel bead used for the surface deposition test. The experiment with an A/V ratio of 455.5m^{-1} was conducted with 0.009m diameter beads and 0.006m diameter beads was used for the test with an A/V of 852.46m^{-1}.

Table 6. 6 - The effect of A/V on the kinetics of $CaCO_3$ deposition at SR 10 and 50^{o}C

Diameter of stainless-steel beads(m)	Area/volume (m^{-1})	Surface area (m^2)	(C_{ao} - C_a) ppm	Growth-rate (ppm/min)	Deposition rate (ppm/m^2/min)
0.009	455.45	0.0078	39.91	1.3	284
0.006	852.46	0.0046	42.18	1.5	192

The results shows that an increase in the A/V from 455.5m^{-1} to 852.46m^{-1}, resulted in only a little increase in the amount of $CaCO_3$ deposited on the surface, as the difference between the initial calcium ion concentration (C_{ao}) and equilibrium calcium ion concentration (C_a) only increased from 39.91ppm to 42.18ppm respectively. The slight increase in the growth-rate of $CaCO_3$ from 1.3ppm/min to 1.5ppm/min can be attributed to an increase in the degree of heterogeneous nucleation on the surface as the A/V ratio increased. This is because the experiment was performed at low SR conditions and heterogeneous nucleation controls the crystallisation process [35]. It is suspected that if the experiment was conducted at a higher SR i.e. above SR 70, homogenous nucleation in the bulk solution would be favoured over heterogeneous nucleation on the surface [97, 146]. Therefore, at higher SR, it is expected that an increase in the A/V would not result in an increase in the growth-rate of $CaCO_3$ on the surface.

The results in Table 7.6 also shows an increase the growth-rate (ppm/min) as the A/V increased in-spite of the reduction in the surface area in the pack (m^2) i.e. from 0.0078m^2 to 0.0046m^2, suggesting that the effect of increasing the A/V outweighs the effect of increasing the surface area in the pack. This finding demonstrates the

effect of A/V should be considered for the development of a reliable kinetic model for predicting scale deposition at low SR.

Furthermore, the small increase noticed in the growth-rate (in ppm/min) of $CaCO_3$ is not consistent with the deposition rate (in ppm/m^2/min) results. A notable drop in the deposition rate was observed as the A/V increased. This is unanticipated, as an increase in A/V is expected to enhance the tendency for nucleation to take place on the surface, due to the increase in the contact area for deposition to occur. A plausible explanation for the reduction in the deposition rate observed is that there is only a finite amount of scaling ions (i.e. the Ca^{2+} and CO_3^{2-} ions) passing through a specified surface area in the pack at any given time, which implies that there is a limit to the amount of deposition that can take place regardless of the magnitude of surface area present in the pack. Therefore, as the A/V increased, it would get to a point where there is no further deposition, thereby causing a reduction in the deposition rate per area in a given time.

The limitations of the body of work in literature on the kinetics surface deposition of $CaCO_3$ is that there is no attention given to assess the effect of A/V on the kinetics of $CaCO_3$. A similar study on the effect of A/V on the formation of iron calcium carbonate revealed that when the A/V ratio was increased from 7.9cm^2 to 31cm^2 in the presence of calcium ions, this resulted in a notable increase in the formation of corrosion products [178]. This result is not comparable to the findings from the beadpack test, as the A/V increased by a factor of 4 in comparison to the beadpack test in which the A/V increased only by a factor of 2.

A deeper understanding of the impact of A/V on the kinetics of inorganic scale formation is important because it could help to better predict the amount of scale deposition expected in a given area per unit time. This would provide greater clarity on where scale is expected to form in a pipeline and help to determine whether inhibition is required to manage the scale deposition issues.

6.5.2 Effect of surface roughness on the kinetics of $CaCO_3$ deposition on the surface

The results illustrating the effect of surface roughness on the kinetics of $CaCO_3$ deposition are given in Table 6. 7, indicating that the kinetics of $CaCO_3$ deposition increased as the surface roughness increased for the stainless-steel materials. However, the PTFE material did not support the deposition of scale, although it had the highest roughness. This is not surprising due to the unreactive and hydrophobic nature of the surface of the PTFE material.

Table 6. 7 - The effect of surface roughness on the kinetics of $CaCO_3$ deposition at SR 10, 50°C

Material	Type	Roughness (nm)	Growth-rate (ppm/min)
Stainless steel	Smooth stainless steel bead	41	0
	Etched stainless steel bead	57	2.8
PTFE	PTFE bead	460	0

The findings observed in this study are in accordance with several published works in literature [37, 179-181]. For instance, the research by Keysar et al [138] on the effect of surface roughness on the crystallisation of calcite on mild steel demonstrated that an increase in the surface roughness led to an increase in the number of nucleation sites on the surface which favoured the adhesion of $CaCO_3$ to the surface. Amthal et al [37] also assessed the effect of surface roughness on the crystallisation of inorganic scale on an aluminium surface, by using a once through flow cell. The findings from this study showed that the roughness of a surface evidently influenced the kinetics of scale deposition, as there was an increase in the quantity of scale deposited when the surface roughness was increased.

In contrast to the results obtained from the previous studies mentioned, the work by Liu et al [101] on the role of surface roughness on the adhesion of $CaCO_3$ to a stainless steel surface, which was performed under static conditions, reported that there is no direct correlation between surface roughness and scale deposition, as there was no notable difference between the fouling rates of the samples with the highest and lowest surface roughness. However, the relationship between surface roughness and adhesion of $CaCO_3$ to the surface was associated with the corrosion resistance capabilities of the surface. It was suggested that, as the tendency for the surface to corrode increased, the ability for scale to adhere to that surface also grew, due to the increase in the contact area of the sample. The increase observed in the kinetics of $CaCO_3$ deposition as the surface roughness increased for the stainless steel material can be attributed to the increase in the number of hooking sites which provide a better opportunity for nucleation to take place on the surface [162].

Overall, the findings from this study shows that when the surface roughness of the stainless steel material was increased from 41nm to 57nm there was a notable

increase in the growth-rate of $CaCO_3$ on the surface. However, there was no evidence for $CaCO_3$ deposition on the PTFE material which had the highest value of surface roughness, this is attributed to the low surface energy of the PTFE material which did not favour the nucleation of scale on the surface. The data from this research also demonstrates that the beadpack is a suitable technique for evaluating the effect of surface roughness on the kinetics of $CaCO_3$ deposition at low SR. One implication of understanding the effect of surface roughness on the ability for $CaCO_3$ to nucleate onto different surfaces is to support the design of suitable materials or effective surface modifications which would be beneficial for minimising scale deposition issues in the oil and gas industry [162].

6.5.3 The growth-rate of $CaCO_3$ on the surface as a function of flowrate.

In this section, the results obtained from the study of the effect of flowrate on the growth-rate of $CaCO_3$ on the surface with the *in-situ* visualisation cell and the beadpack are discussed.

6.5.3.1 Effect of flowrate on the growth-rate of $CaCO_3$ study with the *in-situ* visualisation cell

Flowrate is regarded as one of the main factors that accelerates the kinetics of $CaCO_3$ deposition on the surface [36, 104, 141, 142]. The results showing the effect of increasing the flowrate from 20 – 30ml/min on the growth-rate of $CaCO_3$ deposition at SR 10, 5 and 3, and 50^oC from the *in-situ* visualisation cell are presented in Figure 6. 12.

The results obtained from the study of the effect of SR on the kinetics of $CaCO_3$ deposition i.e. SR 10, 5 and 3, at 50^oC and 20ml/min has been discussed earlier in section 6.5. However, these results are compared with the results obtained for the same SRs (i.e. SR 10, 5 and 3), but at a faster flowrate of 30ml/min to illustrate the effect of flowrate on the kinetics of $CaCO_3$ deposition.

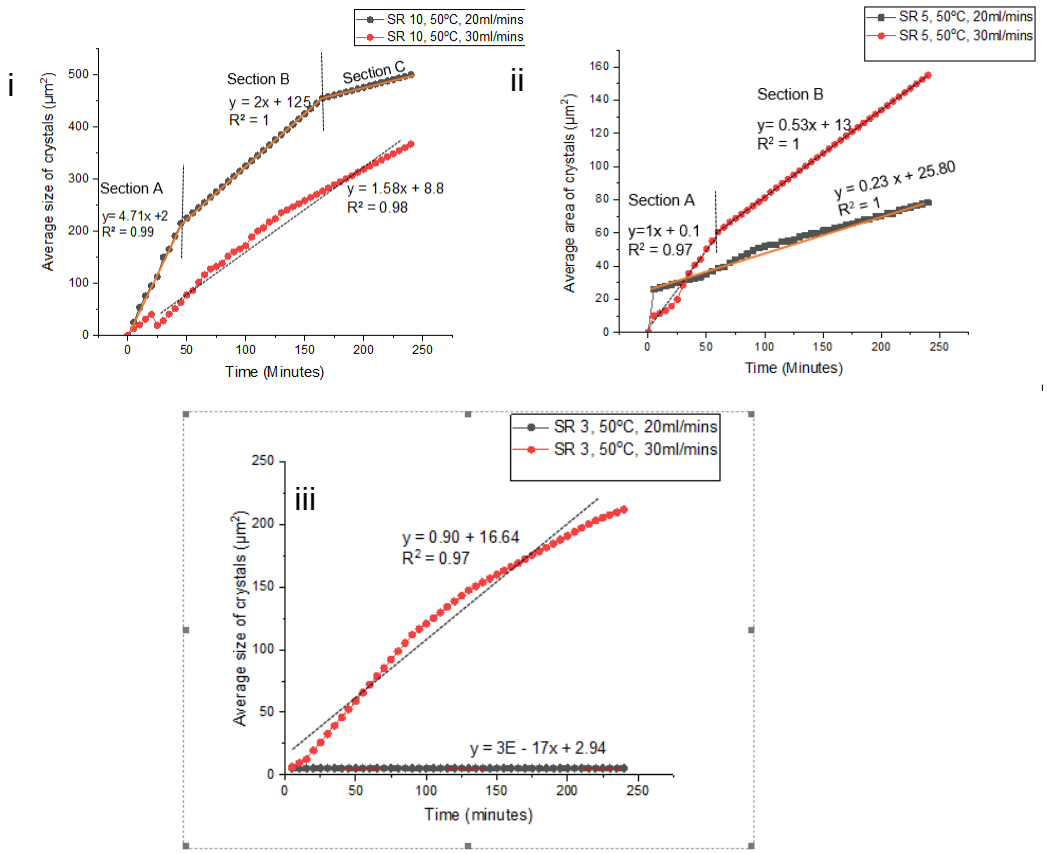

Figure 6. 12 - Comparing the effect of flowrate of on the growth-rate of $CaCO_3$ with time at (i) SR 10, (ii) SR 5 and (iii) SR 3. section A corresponds to a period of both nucleation and growth of $CaCO_3$, section B relates to a period of only crystal growth and section C shows a period of stabilisation in the growth of the $CaCO_3$ on the surface.

The results showed that when the flowrate was increased from 20ml/min to 30ml/min there was a general increase in the overall kinetics of $CaCO_3$ deposition on the surface. The data obtained from the study of the effect of flowrate on the growth-rate of $CaCO_3$ is summarised in Table 6. 8.

Table 6. 8 - Effect of flowrate (20 and 30ml/min) on the growth-rate of $CaCO_3$ at SR 10, 5 and 3 at 50°C.

SR	Flowrate (ml/min)	Growth-rate (µm²/min)	R^2
SR 10	20	2.00	0.99
	30	1.58	0.98
SR 5	20	0.23	0.99
	30	0.52	0.99
SR 3	20	0.00	1.00
	30	0.90	0.97

At SR10, the growth rate of $CaCO_3$ was 2µm²/min at the lower flowrate of 20ml/min and 1.58 µm²/min at the higher flowrate of 30ml/min, the slightly higher growth-rate observed at the lower flowrate might seem unexpected. This can be attributed to

the inverse relationship between nucleation rate and crystal growth [69]. The number of crystals that nucleated on the surface at the higher flowrate was significantly more than the number of crystals deposited at the lower flowrate (i.e., 55 crystals deposited at 30ml/min and only 15 crystals deposited at 20ml/min). Nevertheless, the kinetics were still faster at the higher flowrate as the surface coverage of the crystals was notably greater than at the lower flowrate (Figure 6. 13).

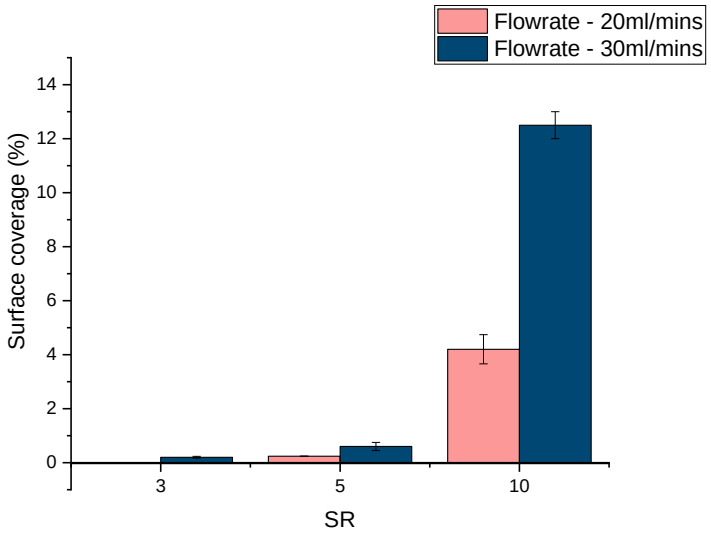

Figure 6. 13 - Effect of flowrate on the surface coverage of $CaCO_3$ at 50°C, showing an increase in surface coverage as flowrate increased.

Figure 6.13, also illustrates that as the flowrate increased, the surface coverage of $CaCO_3$ on the surface increased at the higher SR (i.e. SR 10) compared to the lower SR (i.e. SR 3), this result may be explained by the fact that at a higher SR, more scaling ions are being transported to the surface where the reaction is taking place at a faster rate. Therefore, the scaling ions (Ca^{2+} and CO_3^{2-}) are consumed and replaced simultaneously, thereby, facilitating the kinetics of $CaCO_3$ surface deposition at the higher SR.

Furthermore, contrary to expectations, the results also shows that the growth-rate of $CaCO_3$ was higher at SR 3 compared to SR 5, i.e. $0.9\mu m^2$/min at SR 3 compared to a growth-rate of $0.52\mu m^2$/min at SR 5, 30ml/min. The growth-rate is expected to be higher at SR 5, due to the higher concentration of scaling ions in the solution. However, the higher growth-rate observed at the lower SR is attributed to the limited amount of $CaCO_3$ crystals deposited on the surface at SR 5 and SR 3, which makes it difficult to effectively differentiate the kinetics of $CaCO_3$ deposition at these conditions.

This results suggests that the *in-situ* visualisation cell is not suitable for effectively quantifying the kinetics of $CaCO_3$ deposition at SR 5 and SR 3 at 50°C. A possible explanation for this might be the absence of a high A/V in the *in-situ* visualisation

which did not support the deposition of a quantifiable amount of $CaCO_3$ crystals on the surface at SR 3 and SR 5.

6.5.3.2 Effect of flowrate on the growth-rate of $CaCO_3$ study with the beadpack

In line with the results obtained from the *in-situ* visualisation cell, the findings from the study of the effect of flowrate with the beadpack setup, Figure 6.6 also revealed that when the flowrate was increased from 20ml/hr to 60ml/hr, the difference between the initial calcium ion concentration and equilibrium calcium ion concentration ($\Delta C_{ao} - C_a$) also increased from 42.2 ppm to 61.1 ppm respectively. This suggests an increase in the kinetics of $CaCO_3$ deposition due to increased flowrate.

The increase in the formation of $CaCO_3$ noticed at the higher flowrate is not reflected in the deposition rate (ppm/m^2/min) as shown in Table 6. 9. A possible explanation for this is because the surface area of beads in the pack for the test conducted at the higher flowrate was considerably greater than the surface area of beads in the pack at the lower flowrate. In addition, as there is a limit to the amount of deposition that can take place at a specified flowrate, after the maximum amount of deposition has occurred a further increase in the A/V would result in a reduction in the deposition rate per area over time. Therefore, as the surface area is appreciably higher at the higher flowrate compared to the lower flowrate, this resulted in a lower surface deposition rate at the higher flowrate.

Table 6. 9 - Effect of flowrate on the kinetics of $CaCO_3$ deposition results using the beadpack at SR 10 and 50°C.

Flowrate (ml/hr)	Diameter of bead (m)	Number of beads	Surface area (m^2)	A/V (m^{-1})	Residence time (minute)	(C_{ao} - C_a) ppm	Growth-rate (ppm/min)	Growth-rate (ppm/m^2/min)
60	0.006	214	0.0242	1085	23.4	61.1	2.6	107.44
20	0.006	69	0.0078	852.46	27.5	42.18	1.5	192.31

These results demonstrate that increasing the flowrate plays an important role in driving the process of scale formation in low SR conditions, probably because an increase in flowrate enhances the transportation and diffusion of the scaling ions onto the stainless-steel surface for scale formation to take place [104, 142]. Furthermore, increased flowrate also encourages effective mixing of the cation and anion brine which promotes the chance of successful collisions between the scaling ions and the surface, thereby facilitating the process of $CaCO_3$ deposition.

The findings from this research are in line with previous work by Muryanto et al [36] who investigated the effect of flowrate on the growth-rate of $CaCO_3$. The growth-rate of the crystals was determined by measuring the increase in the mass of scale deposited on the surface with time at different flowrates. The results suggested that the growth rate of $CaCO_3$ increased as flowrate increased. A different study by Durate et al [141] on the effect of water flowrate on $CaCO_3$ deposition in production tubing also mentioned that flowrate directly influences the formation of $CaCO_3$ and an increase in flowrate causes more dramatic fouling issues. Durate research demonstrates that an increase in flowrate increases the kinetics of $CaCO_3$ deposition and this should be taken into consideration for the development of a reliable kinetic model for predicting $CaCO_3$ deposition at low SR conditions.

6.5.4 Comparing the effect of A/V to the effect of flowrate on the kinetics of $CaCO_3$ deposition on the surface.

The results presented in Figure 6. 14 show the effect of A/V and flowrate respectively on the growth-rate of $CaCO_3$. The analysis identified that increasing the flowrate from 20 – 60ml/hr, at a similar A/V led to a notable increase in the growth-rate of $CaCO_3$ from 1.5ppm/min to 2.6ppm/min. However, increasing the A/V from 455.5m^{-1} to 852.5m^{-1} at a constant flowrate led to only a slight increase in the growth-rate of $CaCO_3$ from 1.3ppm/min to 1.5ppm/min. These results are summarised in Table 6. 10.

Table 6. 10 - Comparing the results for the effect of increasing flowrate to increasing A/V on the kinetics of $CaCO_3$ deposition.

Parameter	Values	Surface area (m^2)	Growth-rate (ppm/min)	Deposition rate (ppm/m^2/min)
Flowrate (ml/hr)	20	0.0078	1.5	192.3
	60	0.0242	2.6	109.7
Area to volume ratio (m^{-1})	455.45	0.0078	1.3	284
	852.46	0.0046	1.5	192

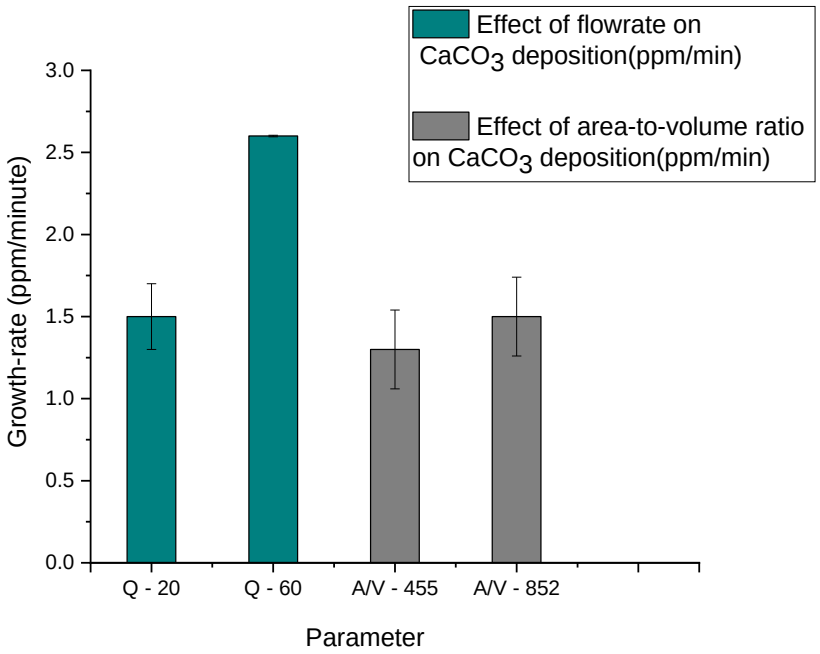

Figure 6. 14 - Comparing the effect of increasing flowrate (Q) to increasing area-to-volume ratio A/V on the growth-rate (ppm/min) of $CaCO_3$ at SR 10 and 50°C.

Increase in flowrate produced a greater increase in the growth-rate (ppm/min) than an increase in A/V. This data suggests that increasing the flowrate is a more dominant factor than increasing A/V in driving the formation of $CaCO_3$ on the surface. A possible explanation for this might be that increasing the flowrate encourages effective mixing of brine and the transportation of the ions to the surface, thereby promoting the likelihood for $CaCO_3$ deposition to occur. Even though increasing the A/V is expected to promote a greater degree of heterogeneous nucleation due to the presence of a greater surface area, it is suspected that increasing the flowrate better supports the chance of $CaCO_3$ nucleation and growth on the surface by enhancing a more effective collision between the scaling ions and the surface.

In contrast to the trend observed of the effect of increasing the flowrate and A/V on the growth-rate (in ppm/min) of $CaCO_3$, a marked reduction in the deposition rate (in $ppm/m^2/min$) is observed as the flowrate and A/V increased as shown in Figure 6. 15. This is related to different surface areas present in the pack during the surface deposition test, as shown earlier in Table 7.9.

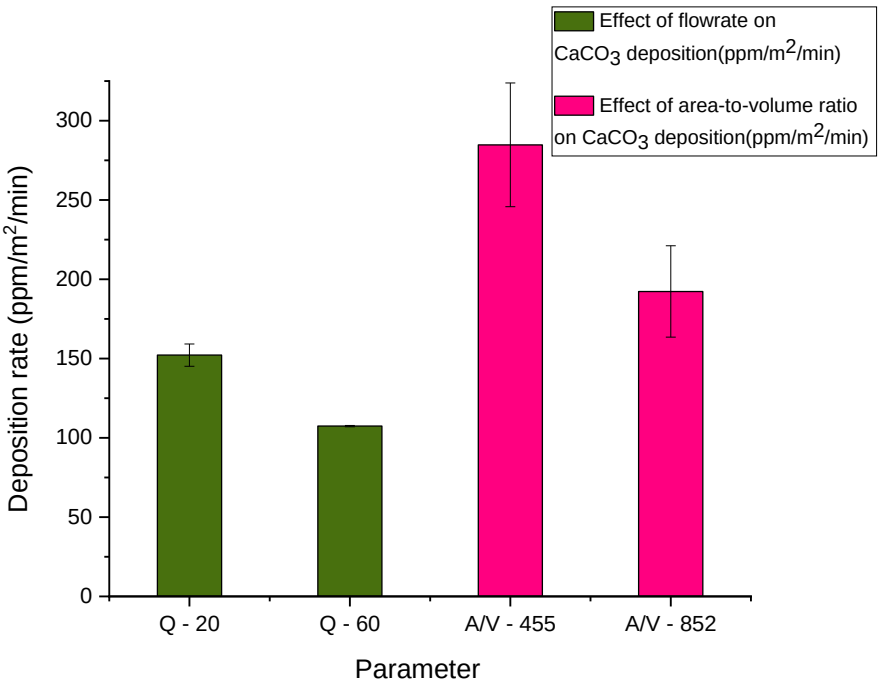

Figure 6. 15 - Comparing the effect of increasing flowrate (Q) to increasing area-to-volume ratio A/V on the deposition rate (ppm/m^2/min) of $CaCO_3$ at SR 10 and 50^{o}C.

The previous studies conducted in this area have been focused on assessing the effect of flowrate on the deposition of $CaCO_3$ [36, 141, 142, 166]. However, no research attention has been given to understanding the differences between the effect of A/V and flowrate on the kinetics of $CaCO_3$ deposition. This study provides new insights into the impact of flowrate in contrast to A/V on the kinetics of surface deposition in low SR brines.

The findings from this study indicate that potentially flowrate could have a greater influence on the kinetics of surface deposition over A/V, and should be taken into account during the development of a reliable model for predicting scale deposition at low SR. The results also demonstrate that this current topic requires further investigations over a broader range of A/V and flowrate conditions to promote a better understanding of the relationship between A/V and flowrate on the growth-rate of $CaCO_3$.

6.6 Mechanisms of $CaCO_3$ precipitation on the surface at low SR

The mechanisms of $CaCO_3$ deposition are the procedures which can talk place either individually or simultaneously, depending on factors such as SR, temperature and flowrate to bring about the deposition of $CaCO_3$ on the surface. These processes include the nucleation and crystal growth stages as discussed in Chapter 2. An understanding of the mechanisms of $CaCO_3$ deposition at low SR

is essential because scaling issues at these conditions are insidious and are not easily detectable until blockage has occurred, this can led to serious safety and operational issues which has significant financial implications for oil and gas companies.

A lack of in-depth knowledge on the deposition mechanisms creates uncertainty in discerning the most effective method of tackling the scaling issues at low SR conditions. A deeper insight into the mechanisms of $CaCO_3$ deposition at low SR would also help to identify more clearly whether nucleation or growth inhibitors would be suitable for managing the deposition issues. [92, 119]. According to the previous research on the mechanisms of $CaCO_3$ formation on surfaces, the deposition process begins with the movement of the scaling ions from the bulk solution to the boundary layer interface. Afterwards, the integration of the of the scaling ions onto the crystal lattice takes place [182]. Therefore, it is assumed that the mechanism of $CaCO_3$ is caused by either:

(1) The transportation of the scaling ions from the bulk solution to the membrane interface.

Or,

(2) The incorporation of the scaling ions on the crystal or a combination of both processes as illustrated by Figure 6. 16.

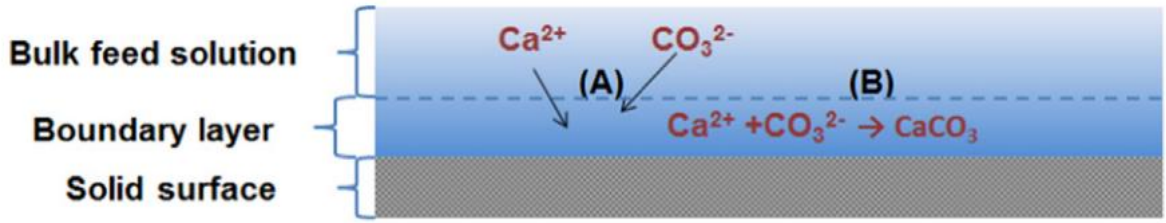

Figure 6. 16 – A representation of the steps involved in the deposition $CaCO_3$ on the surface [182].

In addition, Nonyes and Whitney's [55] study on the mechanisms of crystal growth revealed that it is the diffusion of the scaling ions onto the crystal lattice that drives the crystallisation process on the process. This observation is in alignment with the findings by Beaunier et al [108]. In the study a model for the nucleation of $CaCO_3$ was developed which was later improved by Euvrard et al [183]. The aim of the research was to investigate the nucleation and growth of $CaCO_3$ on the surface by using image analysis software to process the SEM images from the deposition test, and to obtain information on the number and average size of crystals formed. The study found that the nucleation process can be categorised into instantaneous or progressive. It was explained that there is a specified number of active sites per surface area on a given sample and the tendency for nucleation to occur on the

surface is directly proportional to the quantity of nucleation sites present on the surface.

Furthermore, it was also suggested that the actual surface area was likely to increase due to the integration of new crystals onto the surface of pre-precipitated crystals; this is described as the extended surface area, $S_{ext}(t)$, which is represented in equation 7.13 and equation 7.14.

Instantaneous nucleation

$$S_{ext}(t) = -\ln\big(1 - S(t)\big) = \frac{MK_1N_0t}{\rho} \qquad 7.13$$

Progressive nucleation

$$S_{ext}(t) = -\ln\big(1 - S(t)\big) = \frac{MK_1N_0At^2}{\rho} \qquad 7.14$$

$S_{ext}(t)$ is the extended surface area, S(t) is the actual covered surface area, A is the nucleation rate, K_1 is the lateral growth-rate (mol/μm/s), M is the molar mass of $CaCO_3$ (100g/mol), ρ is the density of the crystals (ρ = 2.71 x 10^{-12}g/μm^3 for calcite), N_o is the number of active nucleation site (corresponds to the number of crystals deposited). Instantaneous nucleation takes place when $S_{ext}(t)$ is proportional to time, and progressive nucleation occurs when $S_{ext}(t)$ is proportional to (t^2) [92, 108, 119]. A schematic representation of these two types of nucleation is presented in Figure 6. 17.

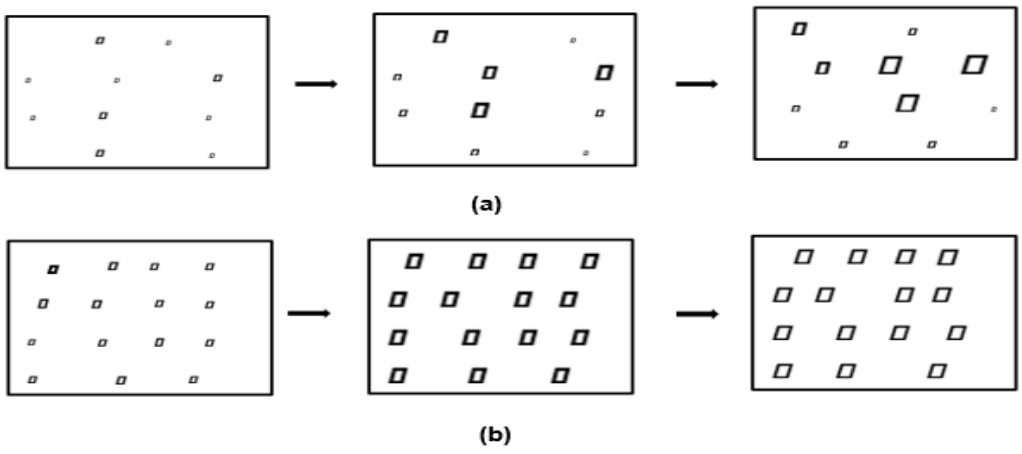

Figure 6. 17 - Progressive nucleation is represented by (a) - where new crystals continues to deposit on the surface throughout the crystallisation process, whilst (b) corresponds to instantaneous nucleation, where all the crystals nucleate at the same time before crystal growth takes place.

Instantaneous nucleation refers to the crystallisation process whereby all the crystals nucleate at the same time and the crystal growth process takes place afterwards, whilst in progressive nucleation, the nucleation and crystal growth processes occur simultaneously. In this type of nucleation, the crystals nucleate and grow, but new crystals continue to nucleate throughout the duration of the scale deposition process. In accordance with literature, instantaneous nucleation is commonly experienced at high SR and progressive nucleation is more probable at low SR [184, 185].

In the experimental results presented in Chapter 4, Figure 4.12 shows the graph for the surface coverage of $CaCO_3$ crystals with time for SR 10, 5 and 3 at 50^oC respectively from the *in-situ* visualisation cell experiment. These results were fitted into the Beaunier model to assess the mechanisms controlling the nucleation process, and the results obtained from the analysis are presented in Figure 6. 18.

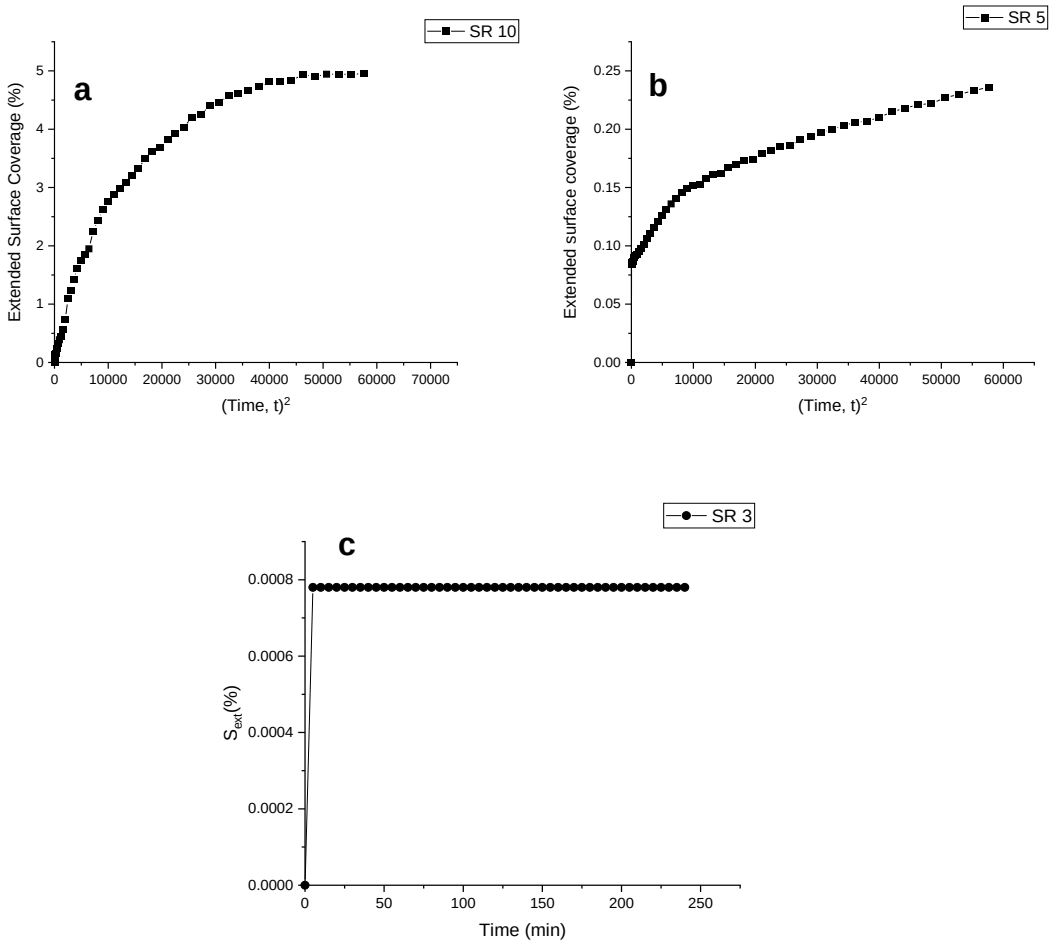

Figure 6. 18 – Extended surface coverage graph versus t^2 for (a) SR 10, (b) SR 5 and (c) SR 3 at 50^oC.

The findings from this investigation showed a parabolic relationship between extended surface coverage (S_{ext}) and t^2 at SR 10 and SR 5, which is contrary to

expectations. A linear relationship was expected because progressive nucleation is assumed to control the formation of $CaCO_3$ deposition on the surface at low SR [97, 122]. Moreover, at SR 3 there was a little initial increase in the S_{ext} value with time, but afterwards there was no change in the S_{ext} for the entire duration of the test. This is because the crystals which formed at this condition did not grow, suggesting that the *in-situ* visualisation cell is not a suitable technique for assessing the mechanisms of $CaCO_3$ deposition at very low SR. This can be attributed to the absence of a high surface area in the *in-situ* visualisation cell. The findings from the analysis revealed that the results from S_{ext} versus t^2 graph did not support Beaunier's model for progressive nucleation at all the SR investigated, i.e. SR 10, SR 5 and SR 3, indicating that this model is not suitable for assessing the mechanisms of $CaCO_3$ at very low SR.

Nonetheless, progressive nucleation can still be assumed for SR 10 at 50^{o}C, based on the results obtained from the *in-situ* visualisation cell for the number and average size of crystals deposited on the surface with time, as shown in Figure 6. 19. The data shows that within the first 90minute of the experiment, the number of crystals and the average size of crystals increased simultaneously with time before stabilisation in the number of crystals was attained after 90minutes. Thereafter, the crystal growth process continued until the end of experiment. This depicts the progressive nucleation process at SR 10, this finding is in line with previous studies reported in literature [97, 108]. However, at SR 5 and SR 3, the number of crystals deposited on the surface was not sufficient to determine the mechanism controlling their crystallisation process. This can be attributed to the presence of a low area-to-volume ratio (A/V) in the *in-situ* visualisation cell which did not encourage the generation of a substantial amount of deposition at these very low SR condition.

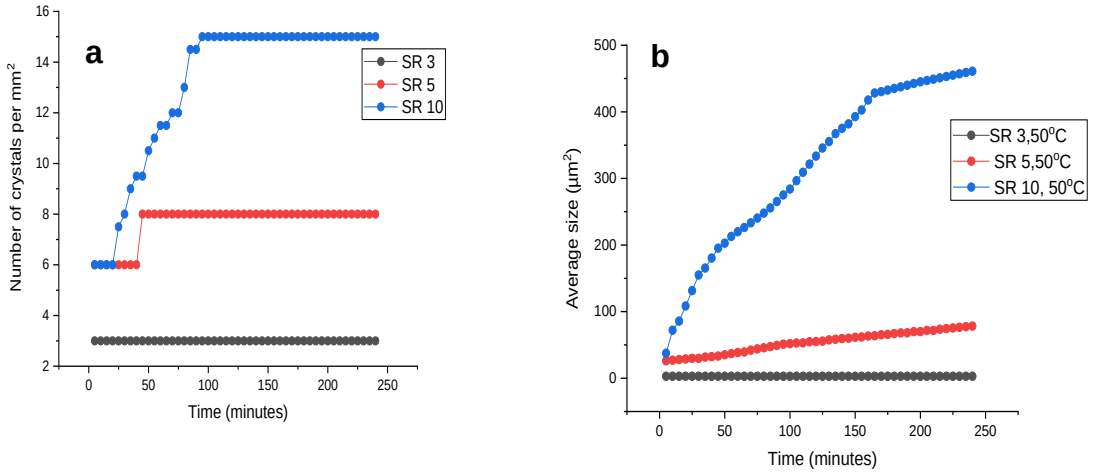

Figure 6. 19 – Effect of SR 10, 5 and 3 on (a) number of crystals deposited on the surface with time and (b) average size of crystals formed on the surface with time at 50^{o}C.

An important implication of understanding the mechanisms of $CaCO_3$ deposition at low SR is to assist in evaluating whether nucleation or growth inhibitors would be effective for mitigating scale deposition issues at low SR[92].

6.7 Comparing the kinetics of $CaCO_3$ precipitation in the bulk to the surface at low SR.

The results presented in Table 6. 11, compares the kinetics of $CaCO_3$ precipitation in the bulk solution to its deposition on the surface at SR 10, 5 and 3 at 50^{o}C.The analysis identified that for all the SR investigated, the growth-rate of $CaCO_3$ deposition on the surface was noticeably higher compared to its precipitation in the bulk solution.

For instance, at SR 10, the growth-rate of $CaCO_3$ was observed to be 10 times faster on the surface compared to the bulk solution, at SR 5, the growth-rate of $CaCO_3$ was 5 times faster on the surface compared to bulk solution and at SR 3, the growth-rate of $CaCO_3$ was estimated to be 0.47ppm/minute on the surface, whilst there was no evidence for $CaCO_3$ formation in the bulk, these results are summarised in Figure 6. 20. This data provides an insight into the extent to which the presence of a surface impacts the kinetics of $CaCO_3$ deposition on the surface in contrast to the bulk solution. These results are in alignment with several published works in the literature [25, 34, 35, 81, 97].

Table 6. 11 - Comparing the growth-rate of $CaCO_3$ in the bulk solution from the static jar test to the surface from the beadpack test at SR 10, 5 and 3 at 50^{o}C

Saturation ratio (SR)	Surface deposition (ppm/minutes)	Bulk precipitation (ppm/minutes)
SR 10	2.70	0.27
SR 5	0.73	0.15
SR 3	0.47	0.00

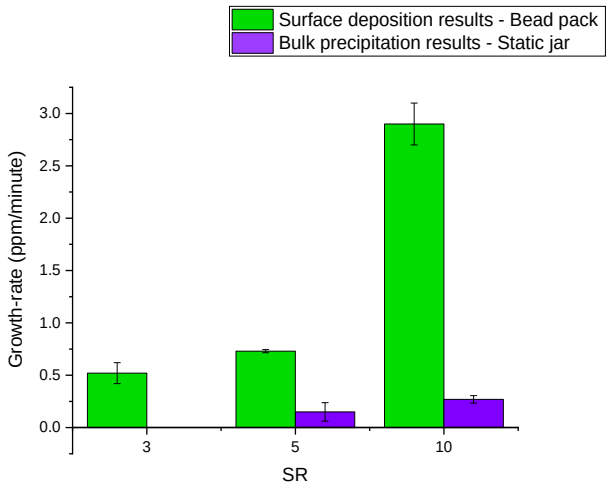

Figure 6. 20 - Comparing the growth-rate (ppm/min) of $CaCO_3$ in the bulk solution from the static jar test to the surface from the beadpack test at SR 10, 5 and 3 at 50ºC.

In addition, the results obtained at SR 3 shows that $CaCO_3$ surface deposition occurred, even though there was no precipitation in the bulk solution. This finding is consistent with the data obtained from comparing the induction time for surface deposition to bulk precipitation, presented in section 6.3, the analysis identified that at SR 3, the induction time surface deposition was significantly shorter compared to bulk precipitation. This implies that surface deposition can take place without the influence of homogenous nucleation in the bulk solution. This result also reflect those of Sanni et al[119], who found at SR 10, SR 15 and SR 25, surface scaling occurred without the precipitation of $CaCO_3$ in the bulk solution, this suggests that at low SR, the mechanism controlling the deposition of $CaCO_3$ is surface crystallisation.

A possible explanation for the faster kinetics observed on the surface in contrast to the bulk solution at low SR is because it requires less energy for $CaCO_3$ deposition to take place on the surface in comparison to its precipitation the bulk solution and the crystals preferentially take the pathway that requires less energy [55, 146]. This study helps to quantify the degree to which surface deposition occurs faster compared to bulk precipitation and provides a better clarity on the distinction between the two processes in low SR brines. In addition, this work demonstrates the capability of the beadpack in generating a measurable data on the kinetics of $CaCO_3$ deposition at low SR.

The findings from this study illustrates that a reliable model for predicting scale formation should not be solely based on thermodynamic calculations from bulk solution analysis, rather, surface parameters such as surface roughness, surface energy, and surface modifications should be incorporated into a kinetic model for accurate scale prediction. A better understanding of the kinetics of $CaCO_3$ deposition on the surface in relation to its precipitation in the bulk solution at low

SR is useful for understanding the distinction between $CaCO_3$ precipitation in the bulk solution and its deposition on the surface. This can support in the design of optimal facilities for accurately predicting the kinetics of $CaCO_3$ deposition in the oil and gas industry [25].

6.7.1 Synergy between the effect of saturation ratio (SR) and effect of flowrate on the kinetics of $CaCO_3$ deposition at low SR

Several reports in literature have shown that an increase the saturation ratio (SR) and flowrate increases the kinetics of $CaCO_3$ deposition on the surface [36, 77, 102, 119]. However, an understanding of the synergy between these two parameters is lacking. In this study, the synergy between the effect of SR and the effect of flowrate on the surface coverage of $CaCO_3$ was explored. The surface coverage value was used because it accounts for the effect of SR and flowrate on both the kinetics of $CaCO_3$ nucleation and growth on the surface.

This test was conducted to determine whether it is the SR or the flowrate that plays a dominant role in accelerating the kinetics of $CaCO_3$ deposition on the surface. The experiement was performed with the *in-situ* visualisation cell at SR 10, 5 and 3 at 50^{o}C and a flowrate of 20 and 30 ml/mins.

The findings from this investigation show that it is only at SR 10 that a substantial amount of deposition was observed on the surface, as illustrated in Figure 6. 21. At, SR 10, when the flowrate increased from 20 – 30 ml/mins there was a notable increase in the surface coverage of $CaCO_3$ on the stainless steel surface. A plausible explanation for this is, an increase in flowrate encourages a more effective mixing of the cation and anion brine which favours the deposition of more $CaCO_3$ on the surface in comparison to a lower flowrate [36].

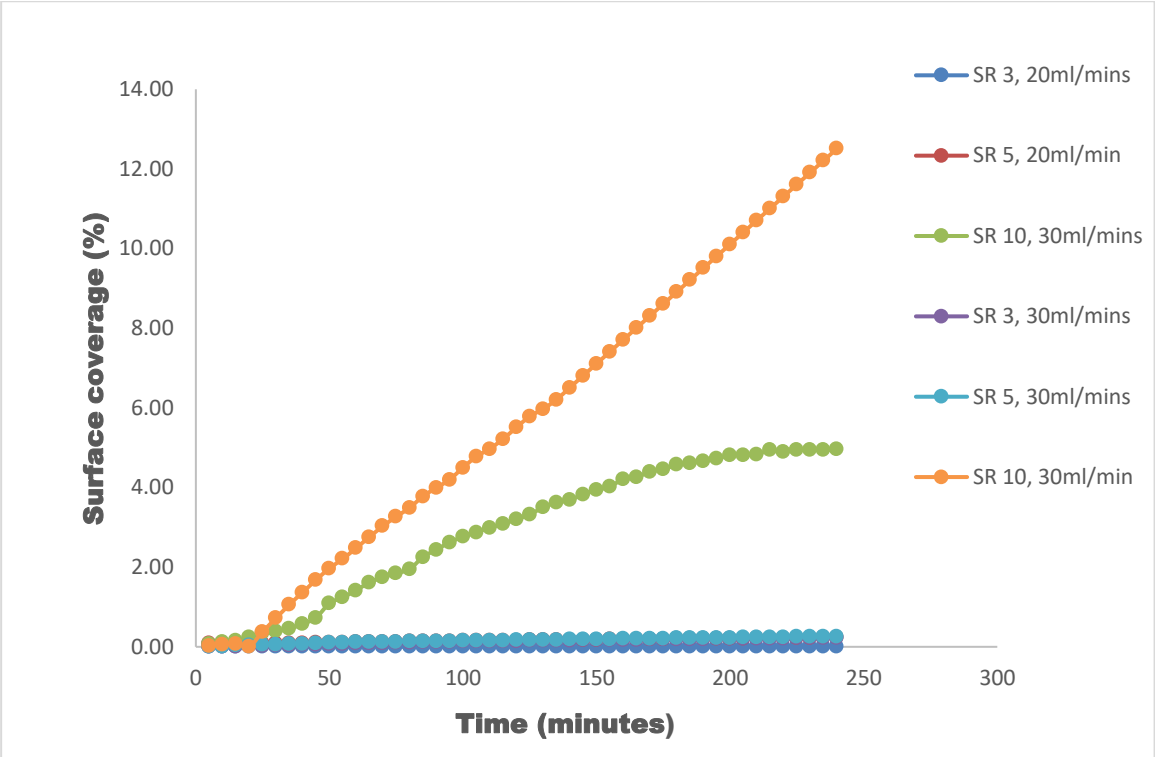

Figure 6. 21- Synergy between effect of SR and effect of flowrate on the surface coverage of $CaCO_3$ at SR 10, 5 and 3 at 50°C.

However, at SR 5 and SR 3, the amount of $CaCO_3$ deposited on the surface was insufficient to extrapolate for a long duration of time. This can be attributed to the low area-to-volume ratio (A/V) available in the flow cell, making it difficult to obtain an appreciable amount of deposition at low SR (i.e SR 5 and SR 3). This results suggests that the *in-situ* visualisation cell is not suitable for effectively understanding the synergy between the effect of SR and the effect of flowrate at low SR.

Therefore, to have a better insight into the relationship between the role of different parameters such as SR, flowrate or temeprature on the kinetics of $CaCO_3$ deposition at low SR. The use of an appriopriate technique with a high A/V which can support the generation of a considerable amount of deposition at low SR is essential.

Chapter 7 – Conclusion and Recommendations for Future work

7.1 Conclusion

This study set out to understand the mechanisms and kinetics of $CaCO_3$ precipitation in the bulk solution and its deposition on the surface at low SRs, which would serve as the framework for the development of a reliable kinetic model for predicting scale deposition at low SR. This chapter provides a summary of the main conclusions from this study based on the results discussed in the previous chapters. The chapter is divided into four distinct sections in relation to the objectives of this work.

7.1.1 Factors influencing $CaCO_3$ formation in the bulk solution and on the surface at low SR

This study has shown the effect of saturation ratio, temperature, and flowrate on the mechanism and kinetics of $CaCO_3$ precipitation in the bulk solution and its deposition on the surface at low SR. The influence of these factors on the induction time and growth-rate of $CaCO_3$ was also determined. The findings from investigation of the impact of these factors are summarised as follows.

- The results from the study of the effect of SR on the kinetics of $CaCO_3$ precipitation in the bulk solution conducted with the static jar at low SR, illustrated generally that, as the SR increased the induction time for $CaCO_3$ precipitation reduced except for the results obtained at SR 3 and SR 5 at 90^{o}C, where the induction time was the same. Overall, the growth-rate of $CaCO_3$ in the bulk solution also increased as SR increased, which is attributed to the higher concentration of scaling ions present in the solution as SR increased.

- The findings from this work also demonstrate that temperature is one of the main factors which accelerate the precipitation of $CaCO_3$ in the bulk solution at low SR, as the induction time for $CaCO_3$ precipitation generally reduced as temperature increased (apart from SR 10). The growth-rate of $CaCO_3$ in the bulk solution also increased as temperature increased, which can be attributed to the inverse solubility relationship between the precipitation of $CaCO_3$ and temperature. Hence, as the temperature increased the solubility of $CaCO_3$ reduced.

- The study of the effect of temperature on the growth-rate of $CaCO_3$ in the bulk solution revealed that at a lower temperature, there was a larger difference between the growth-rate of $CaCO_3$ at the lower and higher SR compared to a higher temperature. This highlights the role of a higher temperature in accelerating the kinetics of $CaCO_3$ precipitation at low SR. This finding indicates that at a high temperature there is a better chance of obtaining measurable data on the kinetics of $CaCO_3$ precipitation in the bulk at low SR conditions.

- This study also shows a strong influence of the SR on the nucleation and growth of $CaCO_3$ on the surface in low SR brines, demonstrated by an increase in the surface coverage of crystals on the stainless-steel material as SR increased across all SR and temperature combinations.

- The effect of flowrate on the kinetics of $CaCO_3$ deposition on the surface was evident, as an increase in flowrate resulted in a notably higher surface coverage of $CaCO_3$ crystals deposited on the stainless-steel material at all the SR investigated. A possible explanation for this is that a higher flowrate promotes the contact between the fluid and the surface, thereby enhancing the likelihood for the surface crystallisation of $CaCO_3$ to take place. A higher flowrate also encourages effective mixing of the anion and cation brine, which facilitates the reaction between the scaling ions leading the formation of $CaCO_3$.

- The surface deposition results obtained from the *in-situ* visualisation cell at SR 5 and 3 showed a very low amount of deposition, which is challenging to extrapolate for a long duration of time, this makes it difficult to effectively assess the mechanisms and kinetics of $CaCO_3$ deposition in these conditions with this setup. This suggests that the *in-situ* visualisation cell is not suitable for effectively quantifying the kinetics of $CaCO_3$ deposition at very low SR in short time periods with low fluid volumes.

7.1.2 The development of a new technique for studying the kinetics of scale deposition at low SR

The beadpack design which was adopted from the sand pack technique was developed to better assess the kinetics of $CaCO_3$ deposition on the surface due to the limitations of the *in-situ* visualisation cell and the static jar setup in effectively quantifying the kinetics of $CaCO_3$ at low SR i.e., SR 5 and SR 3. The major findings

from the surface deposition test performed with the beadpack are summarised as follows.

- The beadpack was able to provide measurable data on the kinetics of $CaCO_3$ deposition at all the SR examined including SR 5 and SR 3, without the influence of homogenous nucleation. This is attributed to the presence of a high area-to-volume ratio in the pack which favoured the deposition of a substantial amount $CaCO_3$ on the surface within an acceptable time frame in the laboratory.

- The beadpack is an effective means of providing reproducible information relating to surface deposition rates in low SR environments, which could help in the design of an accurate kinetic model for predicting scale deposition at low SR. This scale prediction tool will be useful to better identify when treatments are needed to maximise productivity and reduce cost associated with conservatism in hydrocarbon and carbon capture, utilisation and storage (CCUS) operations.

7.1.3 Comparing the kinetics of bulk precipitation to surface deposition at low SR.

The results from the bulk precipitation test conducted with the static jar setup was compared with the results from the surface deposition tests performed using the beadpack, to have an insight into the degree to which the presence of a surface impacts the kinetics of $CaCO_3$ formation in comparison to mere bulk precipitation. The key findings from this analysis as summarised as follows.

- This study has shown that the induction time for $CaCO_3$ surface deposition is shorter in the beadpack compared to the bulk precipitation induction time for SR 5 and SR 3. This is attributed to the presence of high area-to-volume ratio (A/V) in the beadpack, as it requires less energy for crystals to nucleate on the surface in comparison to its precipitation in the bulk solution at low SR.

- This study revealed that at low SR, $CaCO_3$ deposition on the surface can take place solely due to heterogeneous nucleation and without the influence of pre-precipitated crystals in the bulk solution.

- This study also found that the growth-rate of $CaCO_3$ was 10 times faster at SR 10 in the beadpack compared to the static jar test and 5 times faster for

SR 5. Moreover, at SR 3, whilst there was no evidence for $CaCO_3$ precipitation in the bulk solution, the growth-rate of $CaCO_3$ was estimated to be 0.47ppm/min on the surface.

- The results from the study indicate that the presence of a high area–to-volume ratio appreciably accelerated the growth-rate of $CaCO_3$ on the surface in comparison to its precipitation in the bulk solution at low SR.

7.1.4 The sensitivity of the beadpack to different parameters such as surface roughness, area-to-volume ratio, and flowrate.

The effect of surface roughness, area-to-volume ratio and flowrate on the kinetics of $CaCO_3$ deposition on the surface were assessed with the beadpack to determine the sensitivity of the newly developed design to different experimental parameters. The main outcomes from the investigation are summarised as follows.

- The study revealed that for stainless materials, a slight increase in the surface roughness of the material led to a pronounced reduction in the induction time for $CaCO_3$ deposition and a significant increase in the growth-rate of $CaCO_3$ on the surface.

- The increase in the kinetics of $CaCO_3$ deposition observed as the surface roughness increased for the stainless-steel materials, was attributed to the higher surface energy of the material and an increase in the contact area available on the surface as the roughness increased, which enhanced the tendency for $CaCO_3$ to nucleate on the surface.

- The results also showed no evidence for $CaCO_3$ deposition on the surface of the PTFE material which had the highest value of surface roughness. This was attributed to the hydrophobic nature of the material as well as its lower surface energy which does not favour the deposition of $CaCO_3$.

- The investigation of the effect of A/V on the kinetics of $CaCO_3$ deposition with the beadpack showed that an increase in the A/V led to a slight increase in the growth-rate (ppm/min) of $CaCO_3$ on the surface; a possible explanation for this is that the presence of a higher A/V in the pack induced a greater degree of heterogeneous nucleation on the surface.

- The analysis also revealed a reduction in the deposition rate of $CaCO_3$ ($ppm/m^2/min$) as the A/V increased. A possible explanation for this is because there is only a fixed amount of scaling ions passing through a specified area per unit time. Therefore, a considerably higher A/V in proportion to the amount of scaling ions in the solution would cause a reduction in the deposition rate per unit area with time.

- The findings from the beadpack test also showed that flowrate has a significant impact on the kinetics of $CaCO_3$ deposition on the surface, as an increase in flowrate led to a notable increase in the growth-rate of $CaCO_3$. This is because a higher flowrate assists the transportation and diffusion of the scaling ions onto the surface for surface deposition to take place.

7.2 Summary of Novelty

The novelty factors of this research are outlined as follows:

The beadpack design was developed as it is able to better quantify the kinetics of $CaCO_3$ deposition at low SR within a shorter time frame due to the availability of a high area-to-volume ratio (A/V) in the pack.

- The effect of A/V on the kinetics of $CaCO_3$ deposition was investigated with the beadpack and the results provided evidence for instantaneous nucleation at a high A/V and progressive nucleation at lower A/V.

- The findings from the beadpack test demonstrated that heterogeneous nucleation of $CaCO_3$ on the surface was possible without the influence of homogenous nucleation in the bulk solution at low SR conditions.

- The effect of surface roughness on the kinetics of $CaCO_3$ deposition was assessed with the beadpack. The result revealed that for stainless steel materials, a slight increase in their surface roughness led to a notable increase in the kinetics of $CaCO_3$ deposition on the surface, whilst the PTFE material which had the highest surface roughness did not support the deposition of $CaCO_3$.

- The induction time for $CaCO_3$ surface deposition was shorter in the bead pack compared to the bulk precipitation induction time from the static jar test for SR 5 and SR 3; this is attributed to the presence of a high A/V in the beadpack.

- The growth-rate of $CaCO_3$ deposition on the surface was compared to its precipitation in the bulk solution. Analysis identified that at SR 10, the growth-rate of $CaCO_3$ was 10 times faster on the surface from the beadpack test compared to the bulk solution from the static jar test and 5 times faster for SR 5. In addition, whilst there was no evidence for $CaCO_3$ precipitation in the bulk solution at SR 3, the growth-rate of $CaCO_3$ was estimated to be 0.47ppm/min on the surface.

- A new MATLAB algorithm was developed to better asses the number, average size and surface coverage of the crystals deposited on the surface from the *in-situ* visualisation cell experiments at low SR.

- A new setup was also developed for the bulk precipitation test at 90^oC, consisting of a hot plate and beaker with a condenser attached; the condenser is connected to a chiller which is used to circulate cold water at 12^oC to prevent evaporation of the solution during the test.

- The findings from the bulk precipitation tests illustrated that increasing the SR and temperature (from 50^oC to 90^oC) led to an increase in the kinetics of bulk precipitation and growth rate of $CaCO_3$ in low SR solutions.

7.3 Relevance of the research to academia and industry

This study has shown that scale formation is detectable and measurable at very low SR within a reasonable time frame in the laboratory when a suitable technique is used. Prior to this study, the kinetics of scale deposition at low SR have been difficult to quantify effectively within an acceptable time frame with the current techniques used, which include the static jar setup, the dynamic tube blocking rig and the *in-situ* visualisation cell. However, in this work, the newly developed beadpack design was able to provide reproducible data on the kinetics of $CaCO_3$ deposition at very low SR in less than 4 hours, which is attributed to the presence of a high area-to-volume ratio (A/V) in the pack.

The findings from the beadpack design also contribute to the existing body of knowledge by providing new insights into the role of A/V in increasing the degree of heterogeneous nucleation on the surface at low SR, thereby causing a slight increase in the kinetics of $CaCO_3$ deposition on the surface. This information can be beneficial for the development of a reliable kinetic model for predicting scale deposition at low SR. The results from the study of the effect of A/V on the kinetics

of $CaCO_3$ deposition also showed evidence for instantaneous nucleation at high A/V and progressive nucleation at lower A/V. This insight on the mechanisms of $CaCO_3$ crystallisation should be useful in the design of efficient inhibition systems for managing scale deposition issues at low SR conditions.

The findings reported from this study have demonstrated that surface roughness in isolation is not the decisive factor that drives the kinetics of $CaCO_3$ deposition on the surface, as there was no deposition of $CaCO_3$ on the PTFE material which had the highest value of surface roughness, whilst for the stainless steel materials, the kinetics of $CaCO_3$ deposition increased as their surface roughness increased, indicating that the type of the material should be seriously considered. This knowledge can help in the design of surface coatings and modifications for effective management of scaling issues in the oil and gas industry.

In addition, this work has also shed new light on the variation between the induction time and growth-rate of $CaCO_3$ in the bulk solution and on the surface at low SR. The results illustrate that there is a clear distinction between the kinetics of $CaCO_3$ precipitation in the bulk solution and its deposition on the surface at low SR. This implies that the conventional practice in the oil and gas industry, (where the scale prediction software used accounts for only the thermodynamics of bulk precipitation without consideration for surface deposition or kinetics) should be extended to use a different scale prediction tool to predict the kinetics of bulk precipitation and surface deposition.

Overall, this present study provides a suitable technique which can be used to obtain quantifiable data on the kinetics of $CaCO_3$ deposition at low SR. This new technique can be probed further to investigate the kinetics of $CaCO_3$ deposition at much lower SR (below SR 3), which would be more relevant for the oil and gas industry. This work also lays the ground for further research which could help in the development of a reliable kinetic model for predicting scale deposition at low SR. This would minimise the uncertainty experienced when estimating the scaling tendencies at low SR and significantly reduce the cost associated with conservatism in design of barriers to tackle scaling issues.

7.4 Recommendations for future work

The work conducted in this research can serve as the building blocks for the development of a reliable kinetic model for predicting the kinetics of $CaCO_3$ deposition at low SR. The newly developed beadpack design could also be probed further to pursue a deeper understanding of the mechanisms and kinetics of $CaCO_3$ deposition at low SR. Therefore, in this chapter, recommendations for future work are proposed to build on this work.

The following recommendations are suggested for future research.

7.4.1 Matching $\frac{VT}{A}$ in the *in-situ* visualisation cell and the beadpack to field conditions

The findings from the study have demonstrated that the results from the beadpack setup and *in-situ* visualisation are complementary. The two different setups provide unique insights into the crystallisation process of $CaCO_3$ at low SR. However, the surface deposition tests conducted using these techniques were performed under laminar flow conditions and low shear rate. This is not representative of the turbulent flow conditions and high shear rate experienced in the oil and gas industry. Therefore, to make the experimental conditions more comparable to the severe physical conditions in the industry, further research should focus on matching (VT/A) and the brine chemistry from field conditions to laboratory conditions.

Where V(m^3) is the volume of *in-situ* visualisation cell or pore volume in the beadpack, T(s) is the residence time of the *in-situ* visualisation cell or beadpack as a function of flowrate and A(m^2) is the area of sample in the *in-situ* visualisation cell or surface area of the beads in the beadpack: VT/A, represents the volume of brine passing through a specified surface area per unit time. Table 7.1 provides an example of the experimental conditions which could be used to match VT/A in the beadpack and the *in-situ* visualisation cell.

Table 7. 1 - Experimental conditions for matching VT/A in the beadpack and the *in-situ* visualisation cell.

Beadpack			*In-situ* visualisation cell	
Parameter	**Symbol**	**Value**	**Parameter**	**Value**
Area of bead	A (m^2)	0.018	Area of sample (m^2)	0.00031
Pore volume	V (m^3)	0.0000078	Volume of the visualisation cell (m^3)	0.000011
Residence time	T (s)	1404	Residence time (s) at (40.4 ml/min)	16.60
	(V * T)/A	0.59	(V * T)/A	0.59

The results from the two different techniques can be assessed to determine if consistent information is obtained on the mechanisms of $CaCO_3$ nucleation and growth. The outcome from this analysis could potentially provide a better insight into the mechanisms and kinetics of $CaCO_3$ deposition in low SR brines, as the experimental conditions better reflect the extreme conditions encountered during oilfield operations.

7.4.2 The development of a reliable model for predicting the kinetics of $CaCO_3$ deposition on the surface at low SR.

This study has demonstrated that in comparison to the common techniques used for studying the kinetics of $CaCO_3$ deposition in the laboratory, such as the static jar, dynamic tube blocking rig and the *in-situ* visualisation cell. The newly developed beadpack technique is more suitable for effectively quantifying the kinetics of $CaCO_3$ surface deposition at low SR within a reasonable timeframe in the laboratory.

Nonetheless, there is still a need for the development of a reliable kinetic model for predicting scale deposition on the surface at low SR. The previous studies published in literature has been focused on developing models for predicting the likelihood for bulk precipitation to take place in the presence of seed crystals [44, 65, 186] with no consideration for the kinetics of scale deposition on the surface at low SR.

Therefore, to build on this work, further experimental work can be undertaken with the beadpack design to generate more data at a series of different low SR

conditions (i.e. below SR 3). This would be beneficial for the development of a reliable kinetic model for predicting scale deposition at low SR. This can be achieved by plotting the graph of SR/$\sqrt{G}$ against $\sqrt{G}$ where G represents the growth-rate of $CaCO_3$ in (ppm/m^2/s), this graph is illustrated in Figure 7.1. The growth-rate of $CaCO_3$ can be determined as a function of the change in the calcium ion concentration (effluent) with time due to the deposition of $CaCO_3$ on the surface and the surface area in the beadpack.

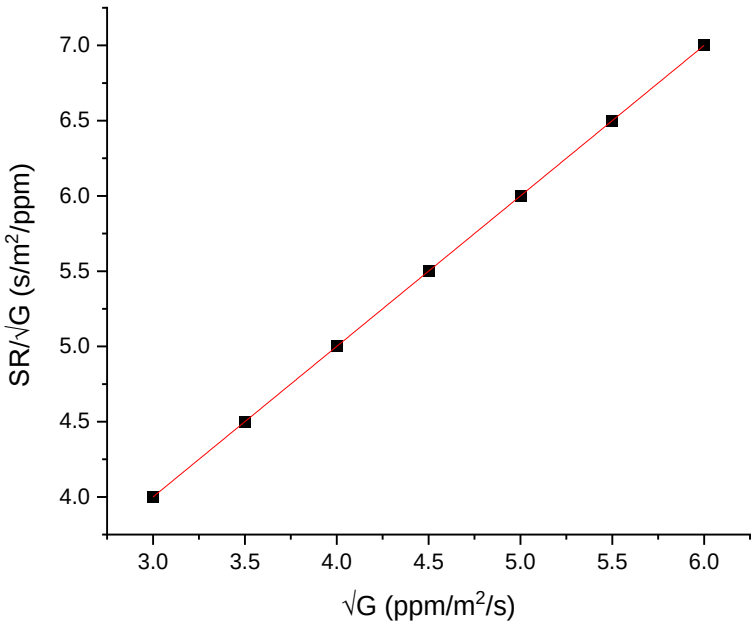

Figure 7. 1 - $CaCO_3$ growth-rate data for low SR plotted to determine the mass transfer constant K_d, from the slope of the graph and surface reaction constant K_r from the intercept.

7.4.3 Improving the beadpack design

The beadpack used in this study is made from a polycarbonate material which can be used for surface deposition tests up to 140^{o}C and is appropriate only for low pressure tests. Further modifications are recommended to improve the heat and pressure resistance properties of the beadpack, such as the use of borosilicate glass which can withstand up to 525^{o}C and 30psia. This would enable surface deposition tests to be performed at high temperatures and high pressure (HT/HP), which is more comparable to the conditions experienced in deep-sea environments.

Surface deposition experiments conducted at HT/HP would also help to generate more quantifiable data at very low SR (below SR 3). This would be useful for the

development of a reliable kinetic model for predicting scale deposition at low SR for the oil and gas industry.

7.4.4 Inhibition studies

Further studies can be conducted with the beadpack to determine the Minimum Inhibitor Concentration (MIC) that would be effective for reducing scale formation at Low SR conditions, by injecting different scale inhibitors such as Polyphosphino carboxylic acid (PPCA) which is a conventional inhibitor for $CaCO_3$ deposition, or green scale inhibitors such as polyacrylates (PA) at different dosages.

Assessment of the effect of different inhibitors on $CaCO_3$ deposition kinetics would also be useful for providing guidance on the type on inhibitors (i.e. whether nucleation or growth inhibitors) suitable for managing the threat of $CaCO_3$ deposition at low SR. A better understanding of dosage and type of inhibitor effective for low SR solutions would also be beneficial for the development of a reliable model which accounts for the role of inhibitors on the mechanisms and kinetics of $CaCO_3$ deposition on the surface.

7.4.5 Effect of coatings and use of glass for surface deposition tests

The effect of materials such as smooth and etched stainless steel and PTFE (Polytetrafluoroethylene) beads on the kinetics of $CaCO_3$ deposition was explored in this study. However, to have a deeper insight into the effect of substrate nature and surface energy on $CaCO_3$ deposition, further research could be undertaken to investigate the effect of different coatings (such as gold, bronze, and copper) on the mechanisms and kinetics of $CaCO_3$ deposition in low SR brines at different flow conditions.

In addition, it would be worthwhile to conduct beadpack experiments with glass beads. The findings from this test could be compared to the results from the bulk precipitation test performed with a glass beaker, to have a better understanding of the variation between $CaCO_3$ deposition on the surface in contrast to its precipitation in the bulk, as well as the role of surface area on the kinetics of $CaCO_3$ formation at the same SR, temperature and in the presence of the same substrate.

A better insight into the effect of substrate nature and coatings on $CaCO_3$ deposition would support future design of efficient materials for minimising $CaCO_3$ deposition issues in the oil and gas industry.

References

1. C.F.E. The impact of the Ukraine war on global energy markets. 2022 [cited 2022 October 2022]; Available from: https://www.cer.eu/sites/default/files/insight_NB_14.7.22.pdf.

2. bp. bp Statistical Review of World Energy. 2022 [cited 2022 27/10/2022]; Available from: https://www.bp.com/content/dam/bp/business-sites/en/global/corporate/pdfs/energy-economics/statistical-review/bp-stats-review-2022-full-report.pdf.

3. Shamoon, A., et al., Environmental impact of energy production and extraction of materials-a review. 2022.

4. Administration, U.S.E.I. International energy outlook 2021. 2022 [cited October 2022; Available from: https://www.eia.gov/outlooks/ieo/introduction/sub-topic-01.php.

5. Demadis, K.D., et al., Industrial water systems: problems, challenges and solutions for the process industries. 2007. 213(1-3): p. 38-46.

6. Devold, H., Oil and gas production handbook: an introduction to oil and gas production. 2013: Lulu. com.

7. England, W.A., Secondary Migration and Accumulation of Hydrocarbons: Chapter 12: Part III. Processes. 1994.

8. Geographic, N. Petroleum. 2022 [cited 2022 27/10/2022]; Available from: https://education.nationalgeographic.org/resource/petroleum.

9. Education, E. Oil and gas reservoir. 2022 [cited 2022 27/10/2022]; Available from: https://energyeducation.ca/encyclopedia/Oil_and_gas_reservoir.

10. Alvarado, V. and E.J.E. Manrique, Enhanced oil recovery: an update review. 2010. 3(9): p. 1529-1575.

11. Ahmed, T., Reservoir engineering handbook. 2018: Gulf professional publishing.

12. Kokal, S. and A.J.W.P.C.O.P. Al-Kaabi, Enhanced oil recovery: challenges & opportunities. 2010. 64: p. 64-69.

13. Vishnyakov, V., et al., Primer on enhanced oil recovery. 2019: Gulf Professional Publishing.

14. Hocott, C.R., Enhanced oil recovery: What of the future ?, in The Future Supply of Nature-made Petroleum and Gas. 1977, Elsevier. p. 389-396.

15. Dai, C., Formation damage during chemical flooding, in Formation Damage During Improved Oil Recovery. 2018, Elsevier. p. 275-304.

16. Frenier, W.W. and M. Ziauddin, Formation, removal, and inhibition of inorganic scale in the oilfield environment. 2008: Society of Petroleum Engineers Richardson, TX.

17. Kelland, M.A., Production chemicals for the oil and gas industry. 2016: CRC press.

18. Brooks, J., H. Lu, and M. Barber. Kinetic Turbidity Test Method for Scale Inhibitor Evaluation on Multifunctional Scales. in CORROSION 2021. 2021. OnePetro.

19. Contreras, V., et al., Experimental analysis of inorganic scale deposition in pipes: Mesoscale flow loop development and case study. 2022. 209: p. 109776.

20. Loureiro, J.B., et al. Large Scale Pipe Flow Experiments for the Evaluation of Non-Chemical Solutions for Calcium Carbonate Scaling Inhibition and Control. in SPE International Oilfield Scale Conference and Exhibition. 2022. OnePetro.

21. Chen, T., et al. Understanding of the Co-Deposition of Calcium Sulphate and Calcium Carbonate Deposition in ESP. in CORROSION 2021. 2021. OnePetro.

22. Kan, A.T. and M.B. Tomson, Scale Prediction for Oil and Gas Production, in International Oil and Gas Conference and Exhibition in China. 2010, Society of Petroleum Engineers: Beijing, China. p. 29.

23. Zhang, P., K. Allan, and B. Hugh. Selection of Calcium Carbonate Scale Critical Values for Deepwater Production. in SPE International Symposium on Oilfield Chemistry. 2015. OnePetro.

24. Mackay, E.J. and M.M. Jordan, Impact of brine flow and mixing in the reservoir on scale control risk assessment and subsurface treatment options: case histories. 2005.

25. Fujah-Sanni, A., et al. Enhancing Capability to Reduce Scale Management Cost in Hydrocarbon Production and CCUS Projects Through Developing an Understanding of Bulk and Surface Scaling Kinetics at Low Saturation Ratios. in SPE International Oilfield Scale Conference and Exhibition. 2022. OnePetro.

26. Chen, T., Q. Wang, and F. Chang, $CaCO_3$ Scale Risk Assessment - Thermodynamics vs Kinetics, in CORROSION 2016. 2016, NACE International: Vancouver, British Columbia, Canada. p. 14.

27. Abdel-Aal, N., K. Satoh, and K. Sawada, Study of the adhesion mechanism of $CaCO_3$ using a combined bulk chemistry/QCM technique. Journal of Crystal Growth, 2002. 245(1): p. 87-100.

28. Tantayakom, V., et al., Scale inhibition study by turbidity measurement. Journal of colloid and interface science, 2005. 284: p. 57-65.

29. Söhnel, O. and J.J.J.O.C.G. Mullin, Precipitation of calcium carbonate. 1982. 60(2): p. 239-250.

30. Spanos, N. and P.G. Koutsoukos, Kinetics of Precipitation of Calcium Carbonate in Alkaline pH at Constant Supersaturation. Spontaneous and Seeded Growth. The Journal of Physical Chemistry B, 1998. 102(34): p. 6679-6684.

31. Spanos, N. and P.G.J.T.J.o.P.C.B. Koutsoukos, Kinetics of precipitation of calcium carbonate in alkaline pH at constant supersaturation. Spontaneous and seeded growth. 1998. 102(34): p. 6679-6684.

32. Teng, H.H., et al., Thermodynamics of calcite growth: baseline for understanding biomineral formation. 1998. 282(5389): p. 724-727.

33. Morizot, A. and A.J.S.J. Neville, Using an electrochemical approach for monitoring kinetics of $CaCO_3$ and $BaSO_4$ scale formation and inhibition on metal surfaces. 2001. 6(02): p. 220-223.

34. Setta, F.-A., A. Neville, and H.J. Chen, A surface kinetic scaling model for CaCO 3 on a stainless steel surface (316 L). NACE - International Corrosion Conference Series, 2012. 1: p. 285-303.

35. Chen, T., A. Neville, and M. Yuan, Calcium carbonate scale formation—assessing the initial stages of precipitation and deposition. Journal of Petroleum Science and Engineering, 2005. 46(3): p. 185-194.

36. Muryanto, S., et al., Calcium carbonate scale formation in pipes: effect of flow rates, temperature, and malic acid as additives on the mass and morphology of the scale. 2014. 9: p. 69-76.

37. Al-Gailani, A., et al., Role of temperature, roughness and pressure in crystallization fouling from potable water on aluminium surface. 2021. 23: p. 100911.

38. Burn, S., et al., Desalination techniques—A review of the opportunities for desalination in agriculture. 2015. 364: p. 2-16.

39. Vazirian, M.M., et al., Surface inorganic scale formation in oil and gas industry: As adhesion and deposition processes. Journal of Petroleum Science and Engineering, 2016. 137: p. 22-32.

40. Duggirala, P.Y.J.C.D.I.C.I.S.C.d.E., Concepción, Chile, Mayo, Formation of calcium carbonate scale and control strategies in continuous digesters. 2005.

41. Schaschke, C., A dictionary of chemical engineering. 2014: OUP Oxford.

42. Ferguson, R.J. mineral scale prediction and control at extreme TDS. in International Water Conference. ESWP, Orlando, FL, USA. 2011.

43. Baugh, T.D., et al., A Fast and Information-Rich Test Method for Scale Inhibitor Performance, in Offshore Technology Conference. 2012, Offshore Technology Conference: Houston, Texas, USA. p. 10.

44. Wiechers, H., P. Sturrock, and G.J.W.R. Marais, Calcium carbonate crystallization kinetics. 1975. 9(9): p. 835-845.

45. Oddo, J., J. Smith, and M. Tomson. Analysis of and solutions to the $CaCO_3$ and $CaSO_4$ scaling problems encountered in wells offshore Indonesia. in SPE Annual Technical Conference and Exhibition. 1991. OnePetro.

46. Stamatakis, E., et al., An improved predictive correlation for the induction time of $CaCO_3$ scale formation during flow in porous media. Journal of Colloid and Interface Science, 2005. 286(1): p. 7-13.

47. Khormali, A., et al., Experimental analysis of calcium carbonate scale formation and inhibition in waterflooding of carbonate reservoirs. 2016. 147: p. 843-850.

48. Sanni, O., et al., Development of a novel once-through flow visualization technique for kinetic study of bulk and surface scaling. 2017. 88(10): p. 103903.

49. Civan, F., Reservoir formation damage. 2015: Gulf Professional Publishing.

50. Van Hook, A., Crystallization: theory and practice. 1961: Reinhold Publishing Corporation.

51. Harouaka, K., et al. The Effect of Surface Material on the Mechanics of Calcium Carbonate Scale Deposition. in SPE International Oilfield Scale Conference and Exhibition. 2018. OnePetro.

52. Kügler, R.T., K. Beißert, and M. Kind, On heterogeneous nucleation during the precipitation of barium sulfate. Chemical Engineering Research and Design, 2016. 114: p. 30-38.

53. Coulson, J.M. and J.F. Richardson, Coulson & Richardson's Chemical Engineering. V. 5. Solutions to the Problems in Chemical Engineering from Volume 2. 2002: Butterworth-Heinemann.

54. Myerson, A.S., Concluding remarks. Faraday Discussions, 2015. 179(0): p. 543-547.

55. Mullin, J.W., Crystallization. 2001: Elsevier.

56. Zhao, J., et al., A review of heterogeneous nucleation of calcium carbonate and control strategies for scale formation in multi-stage flash (MSF) desalination plants. 2018. 442: p. 75-88.

57. Söhnel, O. and J. Garside, Precipitation: basic principles and industrial applications. 1992: Butterworth-Heinemann.

58. Söhnel, O. and J.W. Mullin, Precipitation of calcium carbonate. Journal of Crystal Growth, 1982. 60(2): p. 239-250.

59. Amor, M.B., et al., Influence of water hardness, substrate nature and temperature on heterogeneous calcium carbonate nucleation. Desalination, 2004. 166: p. 79-84.

60. Piucco, R.O., et al., A study of frost nucleation on flat surfaces. 2008. 32(8): p. 1710-1715.

61. Garside, J. and M.J.J.o.c.g. Larson, Direct observation of secondary nuclei production. 1978. 43(6): p. 694-704.

62. Wauquier, J.-P., Petroleum Refining: Crude oil, petroleum products, process flowsheets. Vol. 1. 1995: Editions Technip.

63. Roos, Y.H. and S. Drusch, Phase transitions in foods. 2015: Academic Press.

64. Zhang, Y. and R. Dawe, The kinetics of calcite precipitation from a high salinity water. Applied Geochemistry, 1998. 13(2): p. 177-184.

65. Nancollas, G.H. and M.M. Reddy, The crystallization of calcium carbonate. II. Calcite growth mechanism. Journal of Colloid and Interface Science, 1971. 37(4): p. 824-830.

66. Robertson, J.O. and G.V. Chilingar, Environmental aspects of oil and gas production. 2017: John Wiley & Sons.

67. Kelland, M.A., Production chemicals for the oil and gas industry. 2014: CRC press.

68. Sanni, O., et al. Study of surface deposition and bulk scaling kinetics in oilfield conditions using an in-situ flow rig. in CORROSION 2015. 2015. OnePetro.

69. Charpentier, T.V. and A. Neville. Controlling the Kinetic Versus Thermodynamic Growth of Calcium Carbonate Scale in the Bulk and on Surfaces. in CORROSION 2016. 2016. OnePetro.

70. Bello, O., Calcium Carbonate Scale Deposition Kinetics on Stainless Steel Surfaces. 2017, University of Leeds.

71. Williams, H., et al., Scale Dissolver Application Under HP/HT Conditions - Use of a HP/HT "Stirred Reactor" for *In-Situ* Scale Dissolver Evaluations, in SPE International Symposium on Oilfield Scale. 2005, Society of Petroleum Engineers: Aberdeen, United Kingdom. p. 13.

72. Amiri, M., J.J.P.s. Moghadasi, and technology, The effect of temperature on calcium carbonate scale formation in Iranian oil reservoirs using OLI ScaleChem software. 2012. 30(5): p. 453-466.

73. Dyer, S.J. and G.M. Graham, The effect of temperature and pressure on oilfield scale formation. Journal of Petroleum Science and Engineering, 2002. 35(1): p. 95-107.

74. Kitano, Y.J.B.O.t.C.S.O.J., A study of the polymorphic formation of calcium carbonate in thermal springs with an emphasis on the effect of temperature. 1962. 35(12): p. 1980-1985.

75. Mejri, W., et al., Effects of temperature on precipitation kinetics and microstructure of calcium carbonate in the presence of magnesium and sulphate ions. 2014. 52(25-27): p. 4863-4870.

76. Andritsos, N., A.J. Karabelas, and P.G. Koutsoukos, Morphology and Structure of $CaCO_3$ Scale Layers Formed under Isothermal Flow Conditions. Langmuir, 1997. 13(10): p. 2873-2879.

77. Walker, P. and R. Sheikholeslami, Assessment of the effect of velocity and residence time in $CaSO_4$ precipitating flow reaction. Chemical Engineering Science, 2003. 58(16): p. 3807-3816.

78. Yang, Q., et al., Investigation of Calcium Carbonate Scaling Inhibition and Scale Morphology by AFM. Journal of Colloid and Interface Science, 2001. 240(2): p. 608-621.

79. Chen, T., et al., Calcium carbonate scale formation—assessing the initial stages of precipitation and deposition. 2005. 46(3): p. 185-194.

80. Sanni, O., et al. $CaCO_3$ Scale Surface Nucleation and Growth Kinetics in a Once-Through in situ Flow Rig as a Function of Saturation Ratio (SR). in CORROSION 2016. 2016.

81. Mavredaki, E. and A. Neville. Prediction and evaluation of calcium carbonate deposition at surfaces. in SPE international oilfield scale conference and exhibition. 2014. OnePetro.

82. Frota, T., et al., Assessment of scale formation in the column of an oil and natural gas producing well: A case study. Brazilian Journal of Petroleum and Gas, 2013. 7: p. 15-29.

83. Ghizellaoui, S. and M. Euvrard, Assessing the effect of zinc on the crystallization of calcium carbonate. Desalination, 2008. 220(1): p. 394-402.

84. Chen, T., A. Neville, and M. Yuan, Assessing the effect of Mg^{2+} on $CaCO_3$ scale formation–bulk precipitation and surface deposition. Journal of Crystal Growth, 2005. 275(1): p. e1341-e1347.

85. Østvold, T. and P. Randhol. Kinetics of $CaCO_3$ scale formation. The influence of temperature, supersaturation and ionic composition. in International Symposium on Oilfield Scale. 2001. Society of Petroleum Engineers.

86. Reddy, M.M. and G.H. Nancollas, Calcite crystal growth inhibition by phosphonates. Desalination, 1973. 12(1): p. 61-73.

87. Chen, T., et al., Following the Formation of $CaCO_3$ Scale Formation by in situ WAXS. Journal of Optoelectronics and Advanced Materials, 2007. 9.

88. Saksono, N., et al., Effects of pH on calcium carbonate precipitation under magnetic field. 2009. 13(2): p. 5.

89. Reddy, M.M. and G.H. Nancollas, The crystallization of calcium carbonate: I. Isotopic exchange and kinetics. Journal of Colloid and Interface Science, 1971. 36(2): p. 166-172.

90. Han, J. and K.J.C.R. Burgess, Fluorescent indicators for intracellular pH. 2010. 110(5): p. 2709-2728.

91. Carballo-Paradelo, S., et al., Direct determination of V, Ni, and Co in emulsified fuel oil samples by electrothermal atomic absorption spectrometry (ETAAS). 2009. 30: p. 129-138.

92. Sanni, O.S., et al., Evaluation of laboratory techniques for assessing scale inhibition efficiency. Journal of Petroleum Science and Engineering, 2019. 182: p. 106347.

93. Seeger, T.S., et al., Magnesium and calcium determination in desalted crude oil by direct sampling graphite furnace atomic absorption spectrometry. Fuel, 2019. 236: p. 1483-1488.

94. Akin, G.W. and J.V. Lagerwerff, Calcium carbonate equilibria in solutions open to the air. II. Enhanced solubility of $CaCO_3$ in the presence of Mg^{2+} and SO_4^{2-}. Geochimica et Cosmochimica Acta, 1965. 29(4): p. 353-360.

95. Lin, Q., et al., Interactions between octenyl-succinic-anhydride-modified starches and calcium in oil-in-water emulsions. 2018. 77: p. 30-39.

96. Chen, T., A. Neville, and M.J.C.E.S. Yuan, Influence of Mg^{2+} on $CaCO_3$ formation—bulk precipitation and surface deposition. 2006. 61(16): p. 5318-5327.

97. Sanni, O.S., Calcium carbonate surface/bulk scaling mechanisms and kinetics in a once-through in-situ flow visualization rig. 2016, University of Leeds.

98. Banerjee, S., et al., Process parameter optimization in lathe turning operation to improve the surface roughness and reduce the cutting force using Taguchi method. 2017. 4(8): p. 1-8.

99. Agrawal, G., et al., Wettability and contact angle of polymeric biomaterials, in Characterization of Polymeric Biomaterials. 2017, Elsevier. p. 57-81.

100. Orkoula, M.G., et al., Wettability of $CaCO_3$ surfaces. 1999. 157(1-3): p. 333-340.

101. Liu, Y., et al., Investigation of adhesion of $CaCO_3$ crystalline fouling on stainless steel surfaces with different roughness. International Communications in Heat and Mass Transfer, 2011. 38(6): p. 730-733.

102. Tzachristas, A., et al. Scale Formation and Wetting of Surfaces: A Microfluidics Investigation. in CORROSION 2021. 2021. OnePetro.

103. Østvold, T. and P. Randhol. Kinetics of $CaCO_3$ Scale Formation. The Influence of Temperature, Supersaturation and Ionic Composition. in International Symposium on Oilfield Scale. 2001.

104. Raheem, K., et al. Surface Precipitation and Growth Kinetics of Calcium Carbonate ($CaCO_3$) Scale Using a Novel Capillary Flow Rig. in CORROSION 2021. 2021.

105. Guo, S., et al., Effect of substrate on nucleation rate of two-dimensional colloidal crystals. 2019. 19(6): p. 3215-3221.

106. Wang, H., et al., Formation of $CaCO_3$ Deposits on Hard Surfaces Effect of Bulk Solution Conditions and Surface Properties. 2013. 5(10): p. 4035-4045.

107. Gabrielli, C., et al., Nucleation and growth of calcium carbonate by an electrochemical scaling process. Journal of Crystal Growth, 1999. 200(1): p. 236-250.

108. Beaunier, L., et al., Investigation of electrochemical calcareous scaling: Nuclei counting and morphology. Journal of Electroanalytical Chemistry, 2001. 501(1): p. 41-53.

109. Morizot, A.P., A. Neville, and J.D. Taylor, An assessment of the formation of electrodeposited scales using scanning electron and atomic force microscopy. Journal of Crystal Growth, 2002. 237-239: p. 2160-2165.

110. Han, Y.S., et al., Factors affecting the phase and morphology of $CaCO_3$ prepared by a bubbling method. Journal of the European Ceramic Society, 2006. 26(4): p. 843-847.

111. Neville, A., T. Hodgkiess, and A.P. Morizot, Electrochemical assessment of calcium carbonate deposition using a rotating disc electrode (RDE). Journal of Applied Electrochemistry, 1999. 29(4): p. 455-462.

112. Morizot, A., A. Neville, and T. Hodgkiess, Studies of the deposition of CaCO3 on a stainless steel surface by a novel electrochemical technique. Journal of Crystal Growth, 1999. 198-199: p. 738-743.

113. Howick, L.C., Book reviews - The formation and properties of precipitates. Analytical Chemistry, 1967. 39(14): p. 80A-81A.

114. Wang, Z., A. Neville, and A. Meredith. How and why does scale stick-Can the surface be engineered to decrease scale formation and adhesion? in SPE International Symposium on Oilfield Scale. 2005. OnePetro.

115. Euvrard, M., C. Filiatre, and E. Crausaz, A cell to study *in-situ* electrocrystallization of calcium carbonate. Journal of Crystal Growth, 2000. 216(1): p. 466-474.

116. Duchene, A., A. Neville, and M. Euvrard, An *In-Situ* Flow Cell To Highlight Different Mechanisms Of $CaCO_3$ Inhibition By Green And Non Green Polymers, in OTC Brasil. 2011, Offshore Technology Conference: Rio de Janeiro, Brazil. p. 11.

117. Li, L., et al., Microfluidic Control of Nucleation and Growth of $CaCO_3$. Crystal Growth & Design, 2018. 18(8): p. 4528-4535.

118. Nancollas, G.H., The growth of crystals in solution. Advances in Colloid and Interface Science, 1979. 10(1): p. 215-252.

119. Sanni, O., et al., $CaCO_3$ Scale Surface Nucleation and Growth Kinetics in a Once-Through *in-situ* Flow Rig as a Function of Saturation Ratio (SR). 2016.

120. Söhnel, O. and J.W. Mullin, Interpretation of crystallization induction periods. Journal of Colloid and Interface Science, 1988. 123(1): p. 43-50.

121. Eroini, V., Kinetic study of calcium carbonate formation and inhibition by using an in-situ flow cell. 2011, University of Leeds.

122. Sanni, O., et al. Using a Real-Time Visualisation Technique for the Assessment of Surface Scale Kinetics and Mechanisms of Inhibition. in SPE International Oilfield Scale Conference and Exhibition. 2016.

123. Bahun-Wilson, K.A., Transport and Adsorption Properties of Carboxylated Carbon Nanotubes for Enhanced Scale Inhibitor Squeeze Lifetime Performance. 2018, University of Leeds.

124. Aliaga, D., et al., Barium and calcium sulfate precipitation and migration inside sandpacks. 1992. 7(01): p. 79-86.

125. Jamialahmadi, M., H.J.I.J.O.O. Muller-Steinhagen, Gas, and C. Technology, Mechanisms of scale deposition and scale removal in porous media. 2008. 1(1-2): p. 81-108.

126. Katritsis, D., et al., Wall shear stress: theoretical considerations and methods of measurement. 2007. 49(5): p. 307-329.

127. Chhabra, R.P. and J.F. Richardson, Non-Newtonian flow in the process industries: fundamentals and engineering applications. 1999: Butterworth-Heinemann.

128. Van Loon, A.T., Analytical atomic absorption spectroscopy: selected methods. 2012: Elsevier.

129. Robinson, J.W.J.A.C., Atomic absorption spectroscopy. 1960. 32(8): p. 17A-29A.

130. Kitamura, M., Controlling factor of polymorphism in crystallization process. Journal of Crystal Growth, 2002. 237: p. 2205-2214.

131. Raheem, K., et al. Surface Precipitation and Growth Kinetics of Calcium Carbonate ($CaCO_3$) Scale Using a Novel Capillary Flow Rig. in CORROSION 2021. 2021. OnePetro.

132. Hu, Z. and Y.J.P.t. Deng, Synthesis of needle-like aragonite from calcium chloride and sparingly soluble magnesium carbonate. 2004. 140(1-2): p. 10-16.

133. Yang, Q., et al., Investigation of induction period and morphology of $CaCO_3$ fouling on heated surface. 2002. 57(6): p. 921-931.

134. Kim, W.-S., et al., Polymorphic change of calcium carbonate during reaction crystallization in a batch reactor. 2004. 43(11): p. 2650-2657.

135. Amor, M.B., et al., Influence of water hardness, substrate nature and temperature on heterogeneous calcium carbonate nucleation. 2004. 166: p. 79-84.

136. Charpentier, T., et al. Evaluation of anti-fouling surfaces for prevention of mineral scaling in sub-surface safety valves. in SPE International Oilfield Scale Conference and Exhibition. 2014. OnePetro.

137. Law, K.-Y.J.T.J.O.P.C.L., Definitions for hydrophilicity, hydrophobicity, and superhydrophobicity: getting the basics right. 2014, ACS Publications. p. 686-688.

138. Keysar, S., et al., Effect of Surface Roughness on the Morphology of Calcite Crystallizing on Mild Steel. Journal of Colloid and Interface Science, 1994. 162(2): p. 311-319.

139. Hwang, B.J., et al., Nucleation and growth mechanism of electropolymerization of aniline on highly oriented pyrolytic graphite at a low potential. 2001. 13(1): p. 37-44.

140. Triantou, D., et al., Influence of electrochemical copolymerization conditions of 3-methylthiophene and biphenyl on the morphology and nanomechanical properties of the films. 2015. 132(38).

141. Silva, D.J., K.S. Sorbie, and E.J. Mackay. Introduction of Kinetic Effects into the Thermodynamic Modelling of $CaCO_3$ Scale Precipitation. in SPE International Oilfield Scale Conference and Exhibition. 2018. OnePetro.

142. Moghadasi, J., et al., Scale Formation in Oil Reservoir and Production Equipment during Water Injection (Kinetics of $CaSO_4$ and $CaCO_3$ Crystal Growth and Effect on Formation Damage), in SPE European Formation Damage Conference. 2003, Society of Petroleum Engineers: The Hague, Netherlands. p. 12.

143. Neville, A. and A.J.C.E.S. Morizot, A combined bulk chemistry/electrochemical approach to study the precipitation, deposition and inhibition of $CaCO_3$. 2000. 55(20): p. 4737-4743.

144. Peyvandi, K., A. Haghtalab, and M.R. Omidkhah, Using an electrochemical technique to study the effective variables on morphology and deposition of $CaCO_3$ and $BaSO_4$ at the metal surface. Journal of Crystal Growth, 2012. 354(1): p. 109-118.

145. Söhnel, O. and J.W. Mullin, A method for the determination of precipitation induction periods. Journal of Crystal Growth, 1978. 44(4): p. 377-382.

146. Liu, X.J.T.J.O.C.P., Heterogeneous nucleation or homogeneous nucleation? 2000. 112(22): p. 9949-9955.

147. Graham, A.L., et al., How minimum inhibitor concentration (MIC) and sub-MIC concentrations affect bulk precipitation and surface scaling rates. 2006. 21(01): p. 19-25.

148. Chien, W.-C., et al., Heterogeneous nucleation rate of calcium carbonate derived from induction period. 2007. 46(20): p. 6435-6441.

149. Gomez-Morales, J., J. Torrent-Burgues, and R.J.J.O.C.G. Rodriguez-Clemente, Nucleation of calcium carbonate at different initial pH conditions. 1996. 169(2): p. 331-338.

150. Lundager Madsen, H.E., Theory of long induction periods. Journal of Crystal Growth, 1987. 80(2): p. 371-377.

151. Lioliou, M.G., et al., Heterogeneous nucleation and growth of calcium carbonate on calcite and quartz. 2007. 308(2): p. 421-428.

152. Koutsoukos, P.G., P.D. Natsi, and Z. Amjad. Nucleation and Crystal Growth of Calcium Carbonate in the Presence of Zn. in AMPP Annual Conference+ Expo. 2022. OnePetro.

153. Olsson, L.-F., Induction time of precipitation of calcium carbonate, in Studies in Physical and Theoretical Chemistry, H. Nomura, F. Kawaizumi, and J. Yarwood, Editors. 1995, Elsevier. p. 349-352.

154. Chien, W.-C., C.-C. Lee, and C.Y. Tai, Heterogeneous Nucleation Rate of Calcium Carbonate Derived from Induction Period. Industrial & Engineering Chemistry Research, 2007. 46(20): p. 6435-6441.

155. Koutsoukos, P.G. and C.G.J.J.O.t.C.S. Kontoyannis, Faraday Transactions 1: Physical Chemistry in Condensed Phases, Precipitation of calcium carbonate in aqueous solutions. 1984. 80(5): p. 1181-1192.

156. Flaten, E.M., M. Seiersten, and J.-P. Andreassen, Induction time studies of calcium carbonate in ethylene glycol and water. Chemical Engineering Research and Design, 2010. 88(12): p. 1659-1668.

157. Cheong, W.C., P.H. Gaskell, and A. Neville, Substrate effect on surface adhesion/crystallisation of calcium carbonate. Journal of Crystal Growth, 2013. 363: p. 7-21.

158. Eroini, V., et al. Preventing Scale Formation Using Modified Surfaces. in CORROSION 2011. 2011.

159. Bohnet, M., Influence of the Transport Properties of the Crystal/Heat Transfer Surface Interfacial on Fouling Behavior. Chemical Engineering & Technology, 2003. 26: p. 1055-1060.

160. Epstein, N. Fouling in heat exchangers. in International Heat Transfer Conference Digital Library. 1978. Begel House Inc.

161. Eroini, V., et al., Preventing Scale Formation Using Modified Surfaces, in CORROSION 2011. 2011, NACE International: Houston, Texas. p. 15.

162. Wang, Z., A. Neville, and A. Meredith, How And Why Does Scale Stick - Can The Surface Be Engineered To Decrease Scale Formation And Adhesion?, in SPE International Symposium on Oilfield Scale. 2005, Society of Petroleum Engineers: Aberdeen, United Kingdom. p. 8.

163. Zettler, H., et al., Influence of surface properties and characteristics on fouling in plate heat exchangers. 2005. 26(2): p. 3-17.

164. Oliveira, R., Understanding adhesion: A means for preventing fouling. Experimental Thermal and Fluid Science, 1997. 14(4): p. 316-322.

165. Kazi, S.N., G.G. Duffy, and X.D. Chen, Mineral scale formation and mitigation on metals and a polymeric heat exchanger surface. Applied Thermal Engineering, 2010. 30(14): p. 2236-2242.

166. MacAdam, J. and S.A. Parsons, Calcium carbonate scale formation and control. Re/Views in Environmental Science & Bio/Technology, 2004. 3(2): p. 159-169.

167. Bargir, S., et al., The use of contact angle measurements to estimate the adhesion propensity of calcium carbonate to solid substrates in water. Applied Surface Science, 2009. 255(9): p. 4873-4879.

168. Martins, A., et al. Large Scale Laboratory Tests for Calcium Carbonate Scaling in Sliding Sleeve Valves. in SPE International Oilfield Scale Conference and Exhibition. 2020. OnePetro.

169. Waly, T., et al., The role of inorganic ions in the calcium carbonate scaling of seawater reverse osmosis systems. 2012. 284: p. 279-287.

170. Pääkkönen, T.M., et al. Crystallization fouling of $CaCO_3$-effect of bulk precipitation on mass deposition on the heat transfer surface. in Proceedings of International Conference on Heat Exchanger Fouling and Cleaning VII, Austria. 2009.

171. Wang, Q., T. Chen, and F. Al-Dawood. New Understanding on Calcium Carbonate Scaling Kinetics. in CORROSION 2019. 2019. OnePetro.

172. Morse, J.W., R.S. Arvidson, and A.J.C.R. Lüttge, Calcium carbonate formation and dissolution. 2007. 107(2): p. 342-381.

173. Oddo, J.E. and M.B.J.J.o.P.T. Tomson, Simplified calculation of $CaCO_3$ saturation at high temperatures and pressures in brine solutions. 1982. 34(07): p. 1583-1590.

174. Proctor, S. Scale Dissolver Development and Testing for HP/HT Systems. in International Symposium on Oilfield Scale. 2000. OnePetro.

175. Xu, B., et al. Influence of Calcium and Bicarbonate Ions on the Kinetics of $CaCO_3$ Formation at High Temperature in the Absence and Presence of Scale Inhibitors. in SPE International Oilfield Scale Conference and Exhibition. 2014. OnePetro.

176. Putri, P.Y., et al., Effect of temperature on precipitation rate of calcium carbonate produced through microbial metabolic process of bio materials. 2016. 18(2): p. 103-108.

177. Aljeban, N., et al. Systematic calcium carbonate scale risk evaluation from downhole to topside flowline. in SPE Asia Pacific Oil & Gas Conference and Exhibition. 2020. OnePetro.

178. Jacklin, R., et al. Iron Calcium Carbonate Formation in CO_2 Environments – Effects of A/V Ratio in Autoclave Experiments. in AMPP Annual Conference + Expo. 2022.

179. Packham, D.E.J.I.J.O.A. and adhesives, Surface energy, surface topography and adhesion. 2003. 23(6): p. 437-448.

180. Hartshorn, S.R., Structural adhesives: chemistry and technology. 2012: Springer Science & Business Media.

181. Delollis, N.J.J.N.Y.M.-G.r., Handbook of Adhesive Bonding. 1973.

182. Julian, H., et al., Numerical study of $CaCO_3$ scaling in submerged vacuum membrane distillation and crystallization (VMDC). Journal of Membrane Science, 2018. 559: p. 87-97.

183. Euvrard, M., et al., Kinetic study of the electrocrystallization of calcium carbonate on metallic substrates. Journal of Crystal Growth, 2006. 291: p. 428-435.

184. Bukuaghangin, O., The kinetics of barium sulphate scale formation and inhibition in the bulk solution and on surfaces. 2017, University of Leeds.

185. Barber, M., Calcium Carbonate Crystallization Kinetics in Relation to Surface Scale Formation in Oil and Gas Pipelines. 2018, University of Leeds.

186. Tai, C.Y., et al., Interpretation of calcite growth data using the two-step crystal growth model. 2006. 61(16): p. 5346-5354.

187. Plummer, L. and E. Busenberg, The solubilities of calcite, aragonite and vaterite in CO_2-H_2O solutions between 0 and 90°C, and an evaluation of the aqueous model for the system $CaCO_3$-CO_2-H_2O. Geochimica Et Cosmochimica Acta - GEOCHIM COSMOCHIM ACTA, 1982. 46: p. 1011-1040.

Appendix

SR Calculation

The value of saturation ratio was determined from the concentration of calcium ion measured is calculated as follow;

$$\mathrm{SR} = \frac{\left[\gamma_{i\,[Ca^{2+}]}\mathrm{Ca}^{2+}\right]\left[\gamma_{i\,[CO_3^{2-}]}\mathrm{CO}_3^{2-}\right]}{\mathrm{K}_{\mathrm{SP}[\mathrm{CaCO}_3]}} \quad (1.0)$$

Where γ_i is the activity coefficient, Ksp is the solubility product, Ca^{2+} and CO_3^{2-} is concentration of calcium and carbonate ion respectively, the unit for these concentrations is moles/litre.

The carbonate ion concentration is determined from the total carbonate concentration (A).

$$\mathrm{A} = \mathrm{H}_2\mathrm{CO}_3 + \mathrm{HCO}_3^- + \mathrm{CO}_3^{2-} \quad (1.1)$$

From the carbonic reaction in equation (1.1)

$$\mathrm{HCO}_3^- = \frac{[\mathrm{H}^+][\mathrm{CO}_3^{2-}]}{\mathrm{K}_2} \quad (1.2)$$

From carbonic reaction in equation (1.2)

$$\mathrm{H}_2\mathrm{CO}_3 = \frac{[\mathrm{H}^+][\mathrm{HCO}_3^-]}{\mathrm{K}_1} \quad (1.3)$$

Substituting equation (1.2) and (1.3) into equation (1.1)

$$\mathrm{A} = \mathrm{CO}_3^{2-}\left(\frac{(\mathrm{H}^+)^2}{\mathrm{K}_2}\right) + \frac{[\mathrm{H}^+][\mathrm{CO}_3^{2-}]}{\mathrm{K}_2\mathrm{K}_1} + \mathrm{CO}_3^{2-} \quad (1.4)$$

Rearranging equation (1.4) the carbonate ion concentration becomes.

$$\mathrm{CO}_3^{2-} = \mathrm{A}\,\frac{1}{\left(1 + \frac{(\mathrm{H}^+)^2}{\mathrm{K}_2\mathrm{K}_1} + \frac{\mathrm{H}^+}{\mathrm{K}_2}\right)} \quad (1.5)$$

Where, A is equivalent to the $NaHCO_3$ concentration, H^+ is a function of the pH of the solution, and K_1 and K_2 are the first and second dissociation constant of carbonic acid [187].

Bead pack dimensions calculations

Residence time calculation for bead pack

$$\text{Residence time} = \frac{\text{Voidage x Pack volume}}{\text{Flowrate}} \quad (1.8)$$

Voidage = 0.46

Flowrate = 20ml/hr = 5.55 x$10^{-9}$$m^3$/s

Pack volume = 0.00001696m^3

Residence time = (0.46 x 0.00001696)/ 5.55 x10^{-9} = 1405.7(s) = 23.4 minutes.

Equation for growth rate (r_a) of $CaCO_3$ calculation for the bead pack

$$\text{Residence time} = \frac{C_{ao} - C_a}{r_a} \quad (1.9)$$

Growth-rate of $CaCO_3$ calculation at SR 10, 50°C with the beadpack

$$= \frac{218.84 - 153.83}{23.4} = 2.7\text{ppm/ min} = \ 1.96\ x\ 10^{-2}\frac{mg}{s}/m^2$$

Growth-rate of $CaCO_3$ calculation at SR 5, 50°C with the beadpack

$$= \frac{136 - 118.2}{23.4} = 0.73\text{ppm/ min} = \ 1.73\ x\ 10^{-6}\frac{mg}{s}/m^2$$

Growth-rate of $CaCO_3$ calculation at SR 3, 50°C with the beadpack

$$= \frac{133.86 - 122.86}{23.4} = 0.47\text{ppm/ min} = \ 1.12\ x\ 10^{-6}\frac{mg}{s}/m^2$$

Converting ppm to mg/s/m^2

Converting from 65ppm or mg/l to mg/m^3 = 65,000mg/m^3

Converting from mg/m^3 to mg/s = 65000mg/m^3 x flowrate (5.55 x $10^{-9}$$m^3$/s)

= 3.61 x 10^{-4}mg/s

Converting from mg/s to mg/s/m^2 = (3.61 x 10^{-4} mg/s) / surface area (0.0184m^2)

= 1.96 x 10^{-2}mg/s/m^2.

The equations used to determine the other parameters associated with the bead pack are presented as follows;

$$\text{Void space} = \frac{\text{Volume of void}}{\text{Volume of bed}} \quad (2.0)$$

$$\text{Volume of void} = \text{Volume of bed} - \text{Volume of beads} \quad (2.1)$$

$$\text{Volume of bed} = \frac{\pi(D^2)}{4} x\ L \quad (2.2)$$

$$\text{Volume of beads} = \frac{4\pi r^3}{3} x\ \text{Number of beads} \quad (2.3)$$

$$\text{Superficial velocity} = \frac{\text{Volumetric flowrate}}{\text{Cross sectional area}} \quad (2.4)$$

$$\text{Surface area of bead} = 4\pi r^2 \text{ x Number of beads} \quad (2.5)$$

Theoretical calculations for change in calcium ion concentration in the outlet of the bead pack

Diameter of beads = 3mm

Number of stainless-steel beads in the pack = 712

Diameter of beads in the pack = 3 x 712 = 2136mm = 213.6cm

Growth rate of calcium carbonate for SR 10, 50^{o}C at 10ml/mins = 8.37 x10^{-13}kg/s

Diameter of sample for the visualization cell = 1cm

Growth-rate of calcium carbonate with 213.6cm = 8.37 x10^{-13} x 213.6 = 1.79 x 10^{-10}kg/s

Calculation for ΔCa for the bead pack

$$\text{Volume (V)} = \frac{Q(\Delta Ca)}{r_A} \text{ (Equation 1)}$$

Where

V is the volume of the bead pack (m^3) = 1.694 x 10^{-5}

Q is the volumetric flowrate (m^3/s) = 1.67 X 10^{-7}

r_A the growth-rate of $CaCO_3$ for SR 10, 50^{o}C =1.79 x 10^{-10}kg/s

ΔCa = (v x r_A)/Q = 1.82 x 10^{-8}kg

Convert ΔCa from kg to mol

Moles = Mass/ Molar mass

Molar mass of $CaCO_3$ = 0.1kg/mol

Moles = 1.82 $x10^{-8}$ (kg)/ (0.1 kg/mol)

= 1.82 x 10^{-7}moles

ΔCa in the outlet of the bead pack is = 1.82 x 10^{-7}moles

Converting to ppm

1ppm = mg/l

Total volume of brine used for test (flowrate is 10ml/mins, the test was for 4hrs) = 2400ml

Convert from ml to l = 2.4l

I.e. there was a change of 1.82 x 10^{-8}kg in 2.4 in the calcium ion concentration from the bead pack

Converting from kg to mg = 0.0182mg/2.4l

Change in calcium ion in ppm = 0.0182/2.4 = 0.00758ppm

In–situ visualisation cell dimensions and calculations

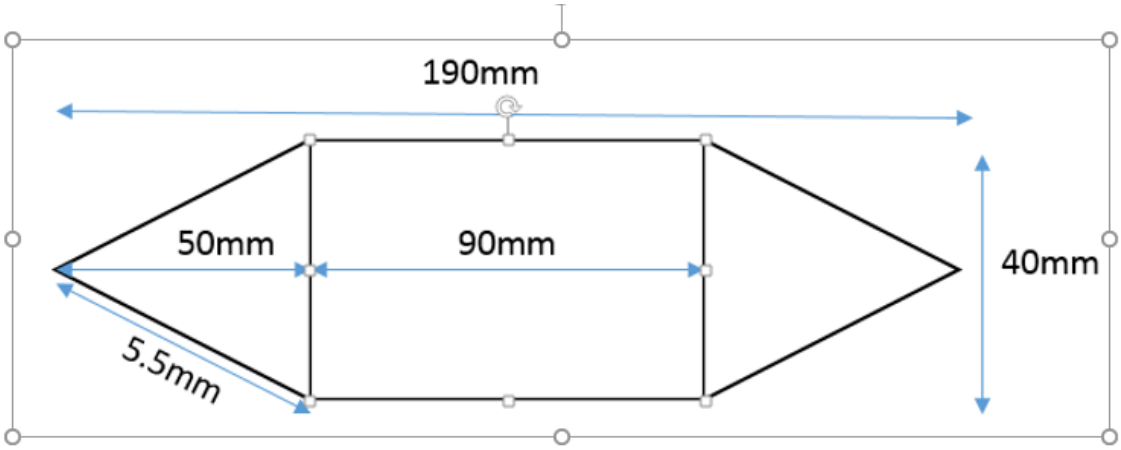

Volume of *in-situ* visualisation cell calculation

Rectangular shape = (90mm X 40mm) = 3600 mm^2

2 Triangles = 2(0.5 *40mm X 50mm) = 2(1000) = 2000mm^2

Total area = 3600 +2000 = 5600mm^2

Volume = 5600 * 2 = 11200mm^3 = 11.2ml

Volume of cell (V_C) = 11.2ml = 1.12 $x10^{-5}$ m^3

Theoretical calculations for change in calcium ion concentration in the outlet of the *in-situ* visualisation cell

Growth-rate calculation

The average area of crystal formed at SR 10, 50^{o}C and 10ml/min, from *in-situ* visualisation cell at 240minutes (14400s) = 58.76μm^2

Calculating growth rate in μm^3/s for 100um diameter = (58.76 x 58.76$^{0.5}$)/time = (450.229)/14400

= 0.031μm^3/s

Convert from 0.031μm^3/s to m^3/s = 3.1 x 10^{-20}m^3/s

Convert the growth rate from m^3/s to kg/s = (Area in m^3/s) x (Density of $CaCO_3$)

Density of $CaCO_3$ = 2700kg/m^3

Growth rate in kg/s = 3.1 x 10^{-20} m^3/s X 2700kg/m^3 = 8.37 x 10^{-17}kg/s

Area of the whole stainless-steel sample of radius 10000 μm

= 4 x π x 5000^2 = 3.14 x 10^{8}um^2

Imaging area (radius 100μm) = 4 x π x 50^2 = 3.14 x 10^{8}um^2 = 3.14 x10^4

Whole area of stainless steel/ imaging area= 3.14 x 10^{8}um^2/3.14 x10^4 = 10000

Growth rate for the whole area of the stainless-steel sample = 8.37 x 10^{-17}kg/s x 10000

= 8.37 x 10^{-13}kg/s

Calculation for ΔCa for *in-situ* visualisation cell

$$\text{Volume (V)} = \frac{Q(\Delta Ca)}{r_A} \quad \text{(Equation 1)}$$

Where

V is the volume of the *in-situ* visualisation cell (m^3) = 1.28 x 10^{-5}

Q is the volumetric flowrate (m^3/s) = 1.67 X 10^{-7}

r_A the growth-rate of $CaCO_3$ in the *in-situ* visualisation cell (m^2/s) for SR 10 = 8.37 x 10^{-13}kg/s

ΔCa = (v x r_A)/Q = 6.41 x 10^{-11}kg

Convert ΔCa from kg to mol

Moles = Mass/ Molar mass

Molar mass of $CaCO_3$ = 0.1kg/mol

Moles = (6.41 x 10^{-11}kg)/ (0.1 kg/mol)

= 6.41 x 10^{-10}moles

ΔCa in the outlet of the *in-situ* visualisation cell is = 6.41 x10^{-10}moles

Converting to ppm

Convert from kg to mg = 6.41 x 10^{-5}mg in 2.4l (because the flowrate was 10ml/min and the duration of the test was 4hrs)

ΔCa in mg/l = (6.41 x 10^{-5}/2.4)

MATLAB code for processing the images from the *in-situ* visualisation cell.

```
image = imread ('SR350C.jpg');
imshow(image)
%%
g=rgb2gray(image);
imshow(g)
%%
imhist(g);
%%
binaryimage=g<70;
imshow(binaryimage);
%%
binaryimage = (~binaryimage);
imshow(binaryimage)
%%
[L,num]= bwlabel(binaryimage);
%%
area = regionprops(binaryimage,"Area");
%%
areaValues = zeros(1,6);
for i = 1:6
areaValues(1,i) = area(i).Area;
end
meanArea = mean(areaValues);
%% Surface Coverage
nWhite = nnz (binaryimage);
nBlack = numel (binaryimage) - nWhite;
srfc = nWhite/nBlack;
```

Procedures for processing the images from the *in-situ* visualisation cell with the MATLAB algorithm developed in this study.

In this section, a step-by-step guide of how the images from the *in-situ* visualisation cell experiments were processed using the new MATLAB algorithm to obtain information on the number of crystals, average size of crystals and surface coverage of the crystals deposited on the surface is presented.

- Upload the image from the *in-situ* visualisation cell into MATLAB
- Click new script.
- To show the uploaded image in the MATLAB software, input the code 'image = imread ('Picture5.jpg');imshow(image)' , (where 'picture 5' is the uploaded image) into the workspace. Afterwards, click 'run section', this command would show the uploaded image, an illustration of this is shown in the image below.

- To convert the image into greycolor, input the code 'g=rgb2gray(image);imshow(g) into the workspace and, click 'run section', this command would show the image in greycolor, an illustration of this is shown in the image below.

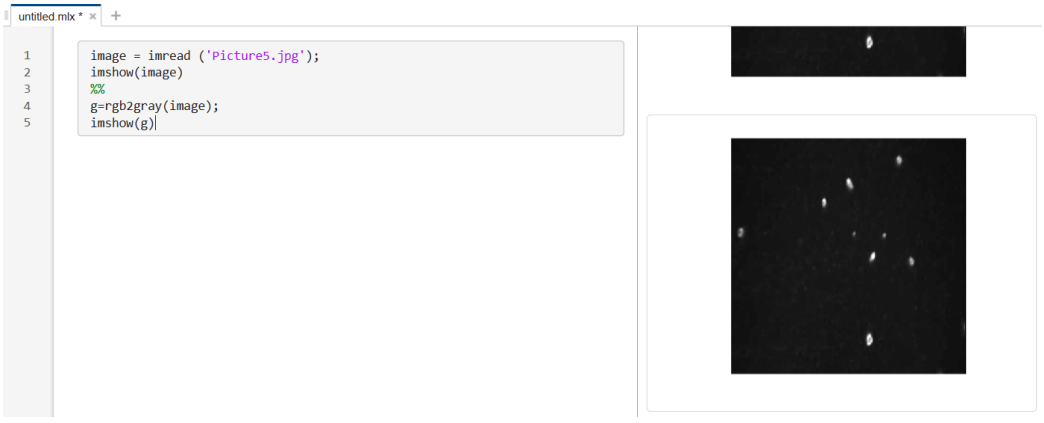

- To convert the image data into a grey scale, input the code 'imhist(g);' into the workspace and, click 'run section', this function is used to convert the image into binary by initially changing the image data into a grey scale from 0 – 255, an illustration of the greyscale is presented in the image below.

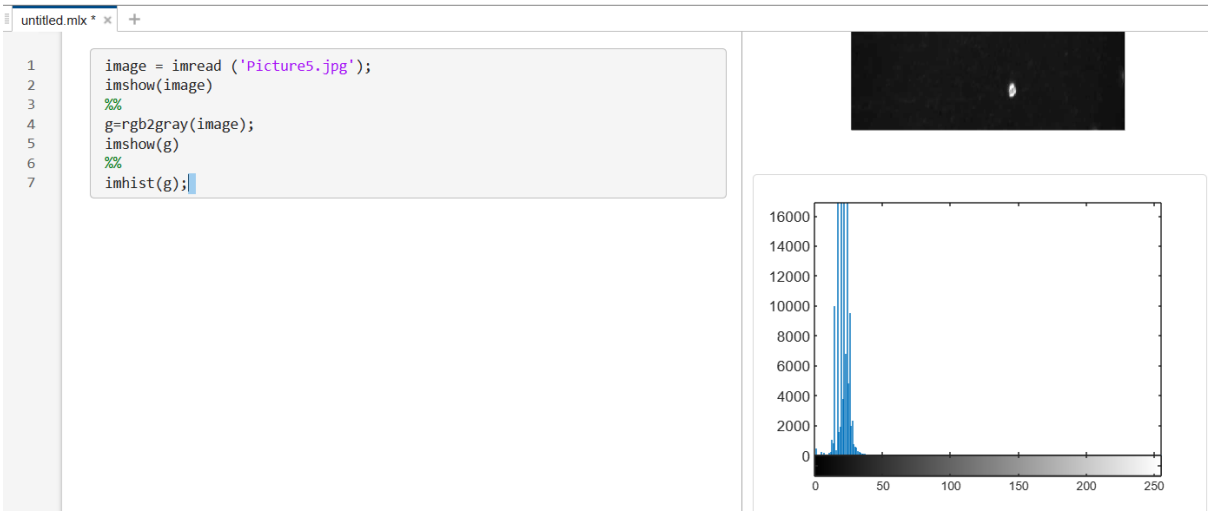

- To convert the image into binary (i.e. black and white), input the code 'binaryimage=g<50;imshow(binaryimage);'into the workspace, g<50 was used because the histogram plot shows that the region for the black background is less than 50.

  Afterwards, 'click run section', This command converts the image to a binary form, with the crystals in black and the background in white, an illustration of this is shown in the image below.

- To reverse the image generated in the previous section, with the crystals now in white and the background in black, input the code 'binaryimage = (~binaryimage);imshow(binaryimage)' into the workspace and, click run section, an illustration of this is shown in the image below.

- To determine the number of crystals in the image, input the code '[L,num]= bwlabel(binaryimage);' into the workspace and, 'click run section', this command would count the number of crystals in the image and present it in the workspace on the left side of the screen, an illustration of this is shown in the image below.

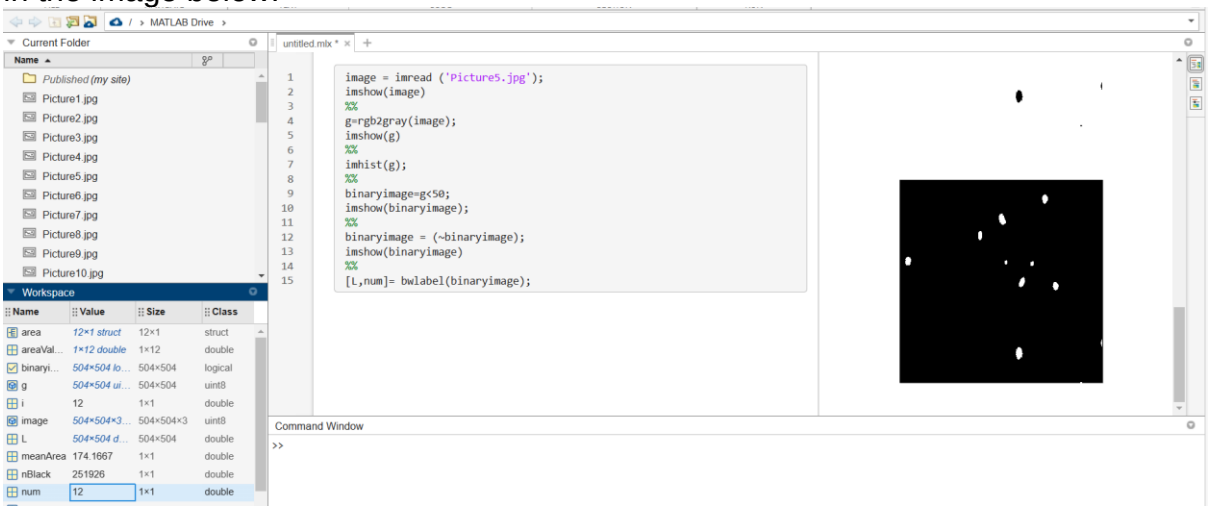

- To determine the average size of crystals in the image, Input the code 'area = regionprops(binaryimage,"Area");%%areaValues = zeros(1,6);for i = 1:6 areaValues(1,i) = area(i).Area; end meanArea = mean(areaValues); into the workspace, where, n represents the number of crystals obtained earlier and click 'run section', this command would determine the average area of the crystals and present the value in the workspace, an illustration of this is shown in the image below.

- To calculate the surface coverage of crystals in the image, Input the code ‘nWhite = nnz (binaryimage);nBlack = numel (binaryimage) - nWhite; srfc = nWhite/nBlack; into the workspace and click ‘run section’, this command would determine the surface coverage of the crystals and present the value in the workspace, an illustration of this is shown in the image below.

- The data obtained for the number, average size and surface coverage of the crystals with time can be plotted on excel and be used for further analysis.

Surface roughness values for the smooth and etched stainless beads

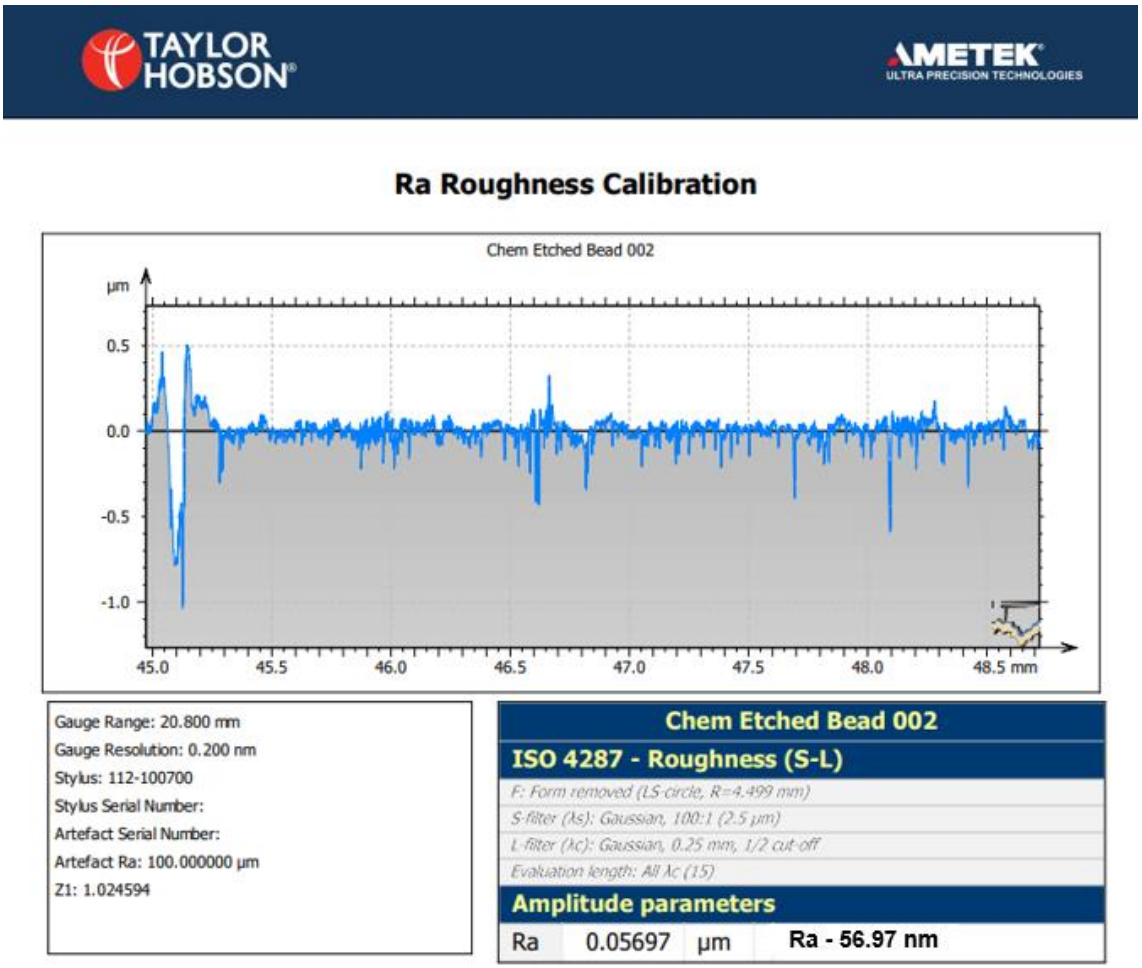

Figure A. 1 - Surface roughness for the etched stainless steel beads measured with the Talysurf Novus equipment, showing a value of 57nm.

Ra Roughness Calibration

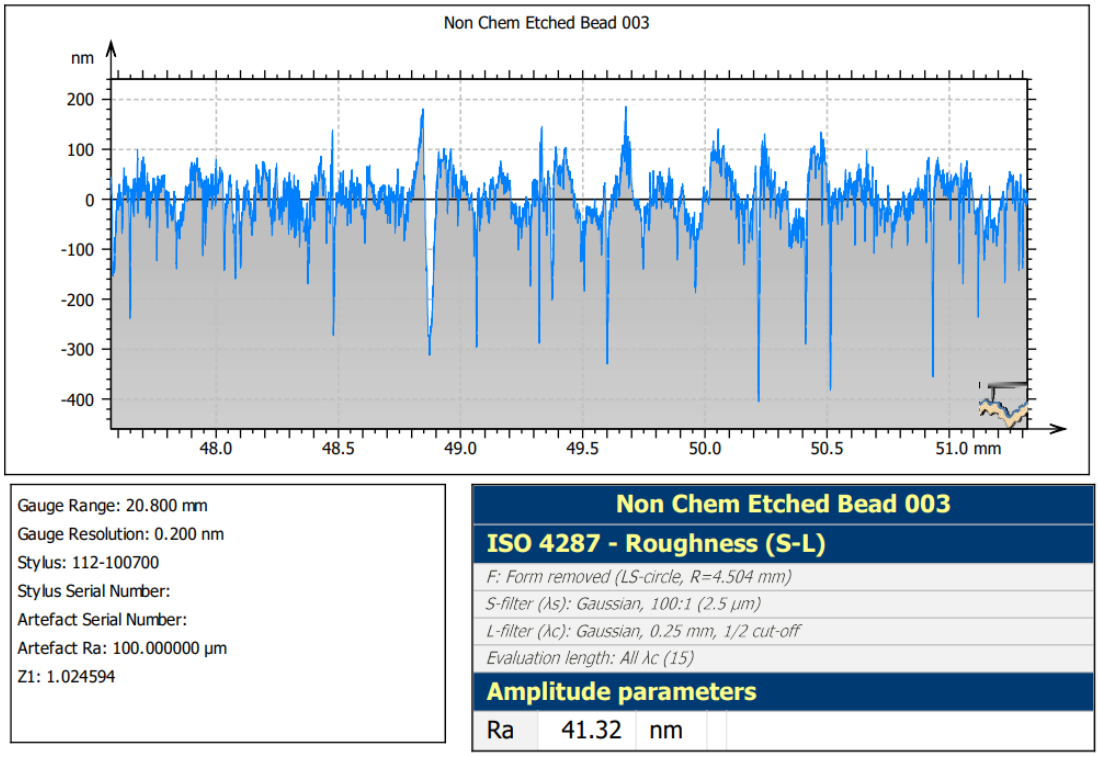

Figure A. 2 - Surface roughness for the smooth or non-etched stainless steel beads measured with the Talysurf Novus equipment, showing a value of 41.32nm.